



KNOWLEDGE SYSTEMS, INC.

**Best Practice Procedures for
Predicting Pre-Drill
Geopressures in Deep Water
Gulf of Mexico**

6/11/2001

CONFIDENTIAL

*This report is provided to DEA Project 119 Project Participants under the terms of the
DEA Project 119 Participation Agreement and is thereby subject to restrictions of
confidentiality and non-disclosure to third parties.*

DEA Project 119

Manual



Best Practice Procedures for
Predicting Pre-Drill
Geopressures in Deep Water
Gulf of Mexico

6-112001

CONFIDENTIAL

This report is the property of Knowledge Systems, Inc. and is not to be distributed outside the company without the express written permission of Knowledge Systems, Inc.

6-112001-110

Abstract

Corporate Offices

Knowledge Systems, Inc.
P. O. Box 1279
Stafford, Texas 77497-1279
Phone: 281-879-1400
Fax: 281-879-1499
E-mail: sales@knowsys.com

European Office

Knowledge Systems, Inc.
P.O. Box 274 Paradis
5856 BERGEN
Norway
Phone: +47 55 92 45 62
Fax: +47 55 92 45 62
E-mail: sales @knowsys.com

Please visit the Knowledge Systems' website at <http://www.knowsys.com>

Information in this document is subject to change without notice, and does not represent a commitment on the part of Knowledge Systems. The software described in this document is furnished under a license agreement or non-disclosure agreement. It is against the law to copy the software on any medium except as specifically allowed in the license or non-disclosure agreement.

© Copyright Knowledge Systems, 1989-2001. All rights reserved. *DrillWorks* is a registered trademark of Knowledge Systems, Inc. *PostScript* is a registered trademark of Adobe Systems, Inc. *Windows* is a trademark of Microsoft Corporation

Document Information

Title: Best Practice Procedures for Predicting Pre-Drill Geopressures in Deep Water Gulf of	
Description:	
Author(s): Saad Saleh, Selim Shaker	
Reviewer(s): James W. Bridges, Terry Miller (editor-kellner)	
Creation Date: 6/8/2001 12:07 PM	Last Date Modified: 6/11/2001 1:46 PM
Approved By:	Approval Date: 6/08/01
Will be sent to: DEA 119 participants	
Sources Used: (can be other documents used as sources)	
Project Number:	Document Number: 2001-00015



Corporate Offices

Knowledge Systems, Inc.
12000
Corporate Center, Suite 2000
Dallas, TX 75244
Tel: (214) 424-1000
Fax: (214) 424-1001

Corporate Office

Knowledge Systems, Inc.
12000
Corporate Center, Suite 2000
Dallas, TX 75244
Tel: (214) 424-1000
Fax: (214) 424-1001

Knowledge Systems, Inc. is a leading provider of software solutions for the financial services industry.

Knowledge Systems, Inc. is a leading provider of software solutions for the financial services industry. We have over a decade of experience in providing software solutions for the financial services industry. Our software solutions are designed to help financial institutions improve their operational efficiency and reduce their costs. We have a proven track record of success in providing software solutions for the financial services industry. Our software solutions are designed to help financial institutions improve their operational efficiency and reduce their costs. We have a proven track record of success in providing software solutions for the financial services industry.

Document Information

Document Title	Knowledge Systems, Inc. - Corporate Office
Document ID	KS-CORP-001
Document Type	Corporate Office
Document Status	Active
Document Date	2000-01-01
Document Author	Knowledge Systems, Inc.
Document Reviewer	Knowledge Systems, Inc.
Document Approver	Knowledge Systems, Inc.

Table of Contents

1	Introduction	1
1.1	Summary of DEA 119 Activities and Results.....	3
1.1.1	State of the Art in Pore Pressure Estimation Study.....	3
1.1.2	Best Practice for Processing Seismic Data for Geopressure Analysis Study	4
1.1.3	State of the Art in Fracture Gradient Estimation Study	4
1.1.4	Pre-Drill Overburden Estimation	5
1.1.5	Velocity-Effective Stress Relations	5
1.1.6	Construction of Deep Water Database.....	6
1.1.7	Construction of a DEA 119 Project Website	6
1.1.8	Development and Evaluation of Various Methods and Models.....	6
1.1.8.1	Conventional Analysis	6
1.1.8.2	New Pore Pressure Prediction Models	7
1.1.8.3	Neural Networks	7
1.1.8.4	Basin Modeling	7
1.2	How to Use This Manual	8
1.2.1	Procedures for Geopressure Prediction: Chapters 2-6	8
1.2.1.1	Chapter 2 – Inventory Available Data.....	8
1.2.1.2	Chapter 3 – Determine Prediction Strategy Based on Data Inventory	8
1.2.1.3	Chapter 4 – Single Well Analysis	8
1.2.1.4	Chapter 5 – Basin Analysis	9
1.2.1.5	Chapter 6 – Combining Uncertainties to Determine Certainty of Prediction.....	9
1.2.2	Geopressure Reference – Appendices A – F.....	9
1.2.2.1	Appendix A – New Models for Pore Pressure Estimation in the Gulf of Mexico	9
1.2.2.2	Appendix B – State of the Art in Pore Pressure Estimation	10
1.2.2.3	Appendix C – Seismic Prediction of Geopressure: Some Basic Principals and the Best Practice Methodolgy.....	10
1.2.2.4	Appendix D – State of the Art in Fracture Gradient Estimation	10
1.2.2.5	Appendix E – Pre-Drill Overburden Estimation	10
1.2.2.6	Appendix F – Velocity – Effective Stress Relation.....	10
2	Inventory Available Data.....	11
2.1	Introduction.....	11
2.2	Data Requirements for a Single Well Prediction	12
2.3	Additional Data Requirements for Prediction Using Geopressure Basin Modeling ..	12
2.4	Evaluation of Seismic Velocity Data for Geopressure Prediction	15
2.4.1	Guidelines for Generating Interval Velocities from Seismic Data.....	15
2.4.1.1	Scenario 1 – Offset Well(s) Available – Calibrated Dataset	15
2.4.1.2	Offset Well(s) Available - Un-calibrated Dataset	15
2.4.1.3	No Offset Well(s) Available within the Coverage of the Seismic Dataset	16
2.4.1.4	Seismic Quality Evaluation "Quick Checks"	16
2.5	Data that Can Be Used for Geopressure Prediction	18
2.5.1	Geological Age and Formation Information	18
2.5.2	Conventional Wireline Data	19
2.5.3	Special Wireline Data	19
2.5.4	Measurement While Drilling Data – MWD.....	19
2.5.5	Logging While Drilling Data – LWD, FEL.....	19
2.5.6	Text Based and Lower Precision Data	20
2.6	Evaluating Data Quality.....	23
2.6.1	Evaluation of Geologic and Structural Data	24

2.6.2	General Sources of Errors and Anomalies	26
2.6.3	Sources of Error in Sonic Log Data	27
2.6.3.1	Checklist for Sonic Data Quality Control.....	28
2.6.3.1.1	Wellbore Environment - Drilling Fluids	29
2.6.3.1.2	New Casing Interval and Bit Size Changes.....	30
2.6.3.1.3	In Situ Stress Effects on Compressional Sonic	30
2.6.3.1.4	Other Effects	30
2.6.4	Log Normalization	31
2.6.5	Missing Data/Questionable Data/Unusable Data.....	31
2.6.6	Rating the Quality of Data	32
2.6.7	Quality Assessment of Offset Wells Calibration Data.....	34
2.6.7.1	Evaluating the Quality of RFT Data.....	34
2.6.7.2	Mud Weight Data	38
2.6.7.3	Gas Shows	39
2.6.7.4	Well Flow and Kick	39
2.6.7.5	Apply a Weighting Scheme to Grades	39
2.6.8	Discussion of Geopressure Indicators.....	40
2.6.8.1	RFT Data	40
2.6.8.2	Mud Weight Data	40
2.6.8.3	Kicks, Well Flows and Lost Circulation	40
2.6.8.4	Gas Shows	41
3	Determine Geopressure Prediction Strategy	43
3.1	Overpressures and High Overpressures	43
3.2	When to Use Basin Modeling for Geopressure Prediction?.....	44
3.3	Geopressure Prediction Without Basin Modeling.....	46
4	Single Well Analysis	47
4.1	Introduction.....	47
4.2	Procedures.....	48
4.2.1	Data Quality Assessments.....	48
4.2.2	Assess Prospect Geologic Setting	48
4.2.3	Analyze Offset Well Data	48
4.2.3.1	Determining OBG Profile and Correcting for Prospect Water Depth	49
4.2.3.1.1	Offset Density Data.....	49
4.2.3.1.2	OBG from Prospect Interval Velocity Data	54
4.2.3.1.3	Using Offset Sonic Data.....	55
4.2.3.2	Determining Adjustment Factor for Seismic Interval Velocities	56
4.2.3.3	Identify Top of Pressure Transition.....	59
4.2.3.4	Develop a Normal Compaction Trend.....	60
4.2.3.5	Identify Unloading	65
4.2.3.5.1	Procedure to Predict Unloading	65
4.2.3.5.2	Example of Unloading	68
4.2.3.6	Identify Centroid Effect.....	72
4.2.3.6.1	Procedure for Centroid Analysis	72
4.2.3.6.2	Example of Centroid Effect.....	74
4.2.3.7	Calibrate Conventional Models.....	80
4.2.3.8	Apply New DEA 119 Models to Offset Wells	80
4.2.4	Prospect Well Analysis.....	80
4.2.4.1	Seismic Data Only ("Quick-Look" Method).....	81
4.2.4.2	Develop Quasi-Calibration from Offset Well Data	82
4.2.4.3	Apply Calibrated Conventional Models	85
4.2.4.4	Apply New DEA 119 models.....	85



5	Geopressure Basin Analysis	89
5.1	Geopressure Basin Modeling Overview	89
5.2	Case Study in the Auger Basin	93
5.2.1	Basin Stratigraphy.....	94
5.2.2	Structure Segments	95
5.3	Geopressure Calibration in the Auger Basin.....	95
5.3.1	Definitive Geopressures and Stratigraphy	96
5.3.2	Synthetic Well Data	96
5.3.3	Single Well Calibration	96
5.4	3-D Framework.....	98
5.4.1	Adding Boundary and Infill Wells.....	98
5.4.2	Using Parameters Transfer.....	98
5.4.3	Using Pore Pressure/porosity Misfit Maps	98
5.4.4	Fine-tuning the 3-D Framework	99
5.5	Specifying the Main Geological Framework	100
5.6	Viewing Results in 3-D.....	101
5.7	Testing the Predictive Effectiveness of the Model.....	102
5.8	Pore Pressure Monitoring in Real-Time	103
5.9	Integration of Geophysical Data in the Geopressure Basin Model	103
5.9.1	Use of Seismic Velocity to Make Pseudo-wells	103
5.9.2	Sequence Boundaries.....	104
5.9.3	Fault Juxtaposition.....	106
5.9.4	Seismic Facies	106
5.9.5	Using Seismic Data to Enhance the Accuracy of the Geopressure Basin Model.....	107
5.10	Modeling Salt Tectonics	108
6	Integrating Uncertainty in Prediction	109
6.1	Introduction.....	109
6.2	Overview of Monte Carlo Simulation.....	109
6.3	Using Monte Carlo Simulation for Geopressure Prediction.....	110
6.3.1	How to use the Simulator.....	111
6.3.2	Example 1: Uncertainty in Pore Pressure Analysis from Seismic Data	112
6.3.3	Example 2: Processing of Wireline Sonic Data	112
7	Index	119
8	Appendix	123
A.	New Models for Pore Pressure Estimation in the Gulf of Mexico	123
B.	State of the Art in Pore Pressure Estimation.....	123
C.	Best Practice for Processing Seismic Data for Geopressure Analysis	123
D.	State of the Art in Fracture Gradient Estimation	123
E.	Pre-Drill Overburden Estimation	123
F.	Velocity – Effective Stress Relations.....	123

..... 1

..... 2

..... 3

..... 4

..... 5

..... 6

..... 7

..... 8

..... 9

..... 10

..... 11

..... 12

..... 13

..... 14

..... 15

..... 16

..... 17

..... 18

..... 19

..... 20

..... 21

..... 22

..... 23

..... 24

..... 25

..... 26

..... 27

..... 28

..... 29

..... 30

..... 31

..... 32

..... 33

..... 34

..... 35

..... 36

..... 37

..... 38

..... 39

..... 40

..... 41

..... 42

..... 43

..... 44

..... 45

..... 46

..... 47

..... 48

..... 49

..... 50

..... 51

..... 52

..... 53

..... 54

..... 55

..... 56

..... 57

..... 58

..... 59

..... 60

..... 61

..... 62

..... 63

..... 64

..... 65

..... 66

..... 67

..... 68

..... 69

..... 70

..... 71

..... 72

..... 73

..... 74

..... 75

..... 76

..... 77

..... 78

..... 79

..... 80

..... 81

..... 82

..... 83

..... 84

..... 85

..... 86

..... 87

..... 88

..... 89

..... 90

..... 91

..... 92

..... 93

..... 94

..... 95

..... 96

..... 97

..... 98

..... 99

..... 100



1 Introduction

This manual of best practice is one of several work products from a two year joint industry project conducted for the purpose of developing an improved methodology for prediction of pre-drill pore pressures and fracture gradients for oil and gas wells drilled in deep water (wells in water depths greater than 1500 ft). The joint industry project was conducted under the auspices of the Drilling Engineering Association as DEA 119 and was funded by 22 oil and gas operating and service companies. The official project sponsor was Chevron USA. The primary objective of the project was to develop an improved methodology that can be used by drilling engineers and geoscience professionals to improve drilling operations, safety and reduce drilling costs for wells drilled in the deep water. Based on the consensus of participants, the project was limited to the Gulf of Mexico and geologically similar areas in other parts of the world. Virtually all the well data submitted by project participants was from the Gulf of Mexico. A strong argument can be made that the results are broadly applicable to geologically similar regimes in other parts of the world, i.e. deltaic basins with reservoirs in relatively young geologic strata that have undergone fairly rapid deposition.

The DEA 119 Project has involved a variety of activities to include surveys of present industry methods, collection of data and detailed analysis for over 100 deep water GOM wells, and the development and evaluation of a number of new models and methods. These project activities are summarized in the next section of this manual and documented in detail in the appendices. The primary objective of this manual is to distill the results of these analyses and studies into a step-by-step best practice for the prediction of geopressures for wells to be drilled in deep water. The manual is organized into two primary parts –

- Best practice guidelines
- Geopressure reference material consisting of documentation of project activities for the background behind the guidelines.

As used in this manual, “geopressure” is a broad term that refers to the various components and expressions of pressure that naturally exists in the geologic environments where petroleum reservoirs are found. The geopressure components include pore pressures, fracture pressures and overburden pressures. For drilling operations, these pressures are most often expressed in the form of a gradient that can be compared with the drilling mud density referred to at the wellsite in units of pounds per gallon (ppg).

Probably the most important geopressure to predict prior to drilling a well is the pore pressure, which is the pressure exerted by pore fluids on the surrounding grains of formation material. When the pore pressure is normal or hydrostatic, drilling operations are easy and typically trouble free (unless there are wellbore stability problems, a subject of separate study). The drilling is more challenging and prone to problems when the pore pressure is anomalous, in that it is higher or lower than the normal predicted hydrostatic pressure for a depth of interest. Pore pressure might be abnormally high in areas where impermeable rocks such as shales form as compacted sediments, or low in areas where fluids have been drained such as near a depleted hydrocarbon reservoir.

The accurate prediction of pore pressures and fracture gradients prior to drilling has long been a difficult and challenging problem. Responsibility for this important element of well planning varies from company to company and case to case -- often residing with the drilling engineer, but sometimes with the geologist, geophysicist, or the petrophysicist. In all cases, the drilling engineer is the target client for this prediction. An accurate prediction of pore pressures and fracture gradients is required for the drilling engineer to make an efficient well plan in terms of casing design, mud weights, drilling time and safety. The impact of sometimes inaccurately predicted pore pressures in wells drilled in shallow water has not been as evident as in deep water drilling where wells are more expensive and problems can be more spectacular.

Pore pressure predictions are more critical in deeper water because both the fracture and overburden gradients, which are based on the depth below the Kelly bushing, increase more slowly with total depth as the water depth increases. Consequently, the operating safety margin between pore pressure and fracture gradient decreases as the water depth increases. This factor is illustrated in Figure 1-1 where a geopressure analysis of an identical well at two different water depths is computed. The well on the left drilled in zero water depth has a relatively wide margin between the pore pressure and fracture gradient and can be drilled with only two casing strings. When the same well is moved to a water depth of 5000 ft, the margin between the pore pressure and fracture gradient is much smaller, and four casing strings are required to drill the well to the same depth below the sea floor. With the lower formation strength safety margin, pore pressures that would be manageable at the more shallow depth can cause a multitude of difficulties in deep water. Problems can range from "shallow water flows" that make it very difficult to even set the surface casing to situations where the well cannot be completed at all, and an expensive sidetrack is required. Accordingly, there is a somewhat urgent need to have the availability of an improved prediction of pore pressures for wells to be drilled in the deep water and to have, at the very least, more knowledge and control of the prediction process.

The responsibility for geopressure prediction varies by company, but there is general agreement that more accurate geopressure predictions can lower costs, reduce problems and improve the safety of drilling operations. While these objectives are the primary responsibility of the drilling engineer, this manual of best practice procedures should be useful to drilling engineers, geophysicists, geologists and petrophysicists and all others who are involved in geopressure prediction.



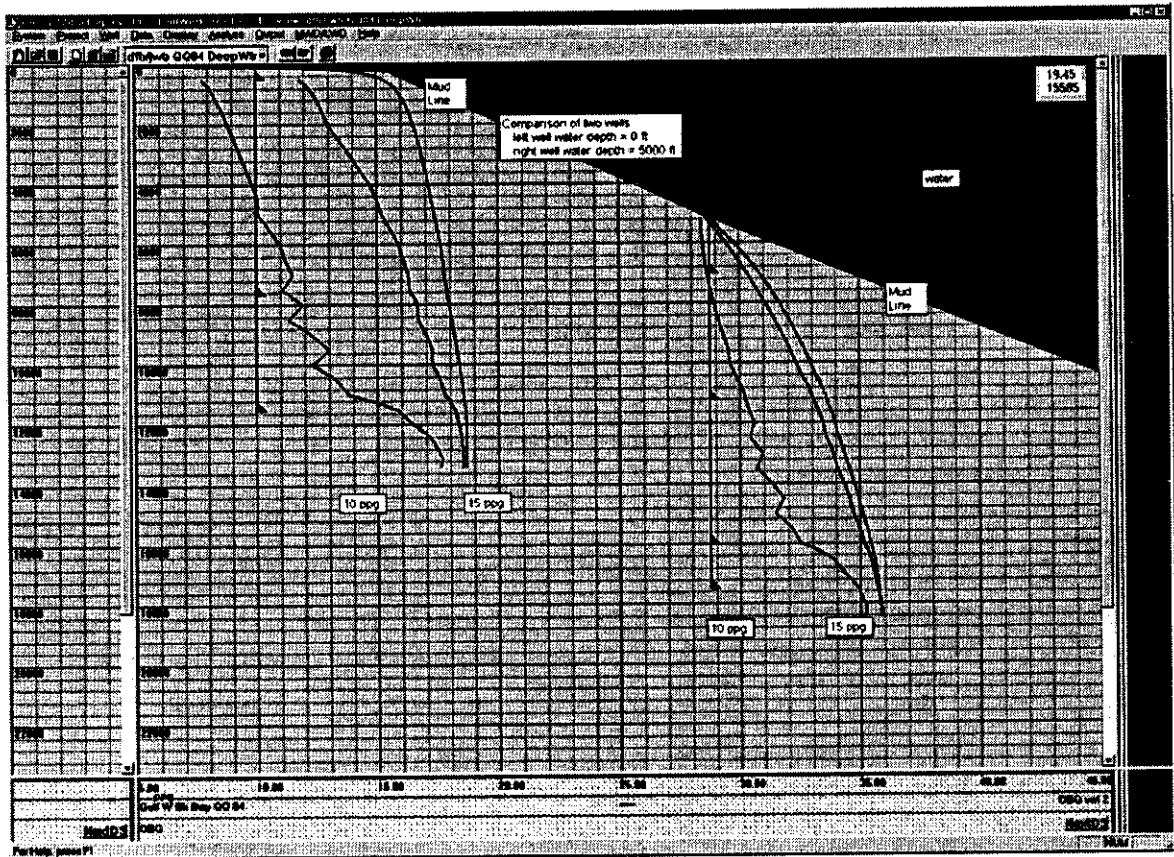


Figure 1-1 Identical Well Drilled at Two Water Depths Illustrates Deep Water Drilling Challenge

1.1 Summary of DEA 119 Activities and Results

The DEA 119 Project to Develop an Improved Methodology for Pre-Drill Pore Pressure and Fracture Gradient Prediction for Deep Water Wells began in early 1999 and the first phase was completed in April 2001. The project centered on the collection of data for more than 100 wells in the deep water Gulf of Mexico and the utilization of that data to develop and test new and improved models and methods. This manual is one of the primary work products from the project. In addition, the project has completed a number of significant tasks that are summarized below. A second project phase is planned to further utilize the unique and valuable database that has been built.

1.1.1 State of the Art in Pore Pressure Estimation Study

A survey was made of the current state of the art in pore pressure prediction in terms of the models, methods and assumptions used by the industry today. The methods were categorized into two general approaches –

- Direct Methods
- Effective Stress Methods
 - Vertical Methods
 - Horizontal Methods
 - Other

The methods were then discussed in terms of pore pressure indicators to include acoustic and resistivity data.

Dr. Glenn Bowers, a recognized expert in the field, was the primary research person for this part of the project. A total of 15 methods were documented and discussed and a list of 36 references was included. All of this was documented in DEA 119 Report No. 1 which is included in Appendix B of this manual and can also be downloaded from the DEA 119 password protected website www.knowsys.com/DEA_119_Prop.html

1.1.2 Best Practice for Processing Seismic Data for Geopressure Analysis Study

A study was undertaken to determine the best practice methodology for processing seismic data for the specific purpose of estimating geopressures. This is important because most seismic processing is carried out for the purpose of exploration with the focus of investigation at the deeper depths where petroleum reservoirs are typically located.

Such processing often obscures seismic characteristics that are indicative of geopressures below the mudline at shallower depths. In addition, unless there is special processing, the analyses typically do not have sufficient resolution to support geopressure analysis required for drilling operations.

Basic principals of seismic prediction of geopressure were documented, and a guide to seismic velocity analysis for geopressure work with a step-by-step data processing checklist is included.

Dr. Nader Dutta, a recognized expert in the field, was the primary research person for this part of the project. The complete report can be found in Appendix C of this manual and can also be downloaded from the DEA 119 password protected website www.knowsys.com/DEA_119_Prop.html.

1.1.3 State of the Art in Fracture Gradient Estimation Study

A survey was made of the current state of the art in fracture gradient prediction in terms of the models, methods and assumptions used by industry today. The methods were divided into the following categories

- Minimum Stress
- Hoop Stress
- Fracture Methods
- Direct Methods

The methods and the underlying assumptions were discussed along with expected results of the different methods. Comments on the quality of data produced by the methods were also disclosed.

Dr. Glenn Bowers produced the report, and it can be found in Appendix D of this manual and can also be downloaded from the DEA 119 password protected website www.knowsys.com/DEA_119_Prop.html

1.1.4 Pre-Drill Overburden Estimation

The overburden stress at any given depth is a function of the density of the overlaying sediments and therefore cannot be known at the pre-drill stage. This critical element, which is fundamental to both pore pressure and fracture gradient estimation, must be inferred from indirect or empirical methods. This report documented an investigation into

- Methods using depth only
- Methods that combine depth and compaction models
- Methods that use acoustic data

Approximately 17 different methods were evaluated and the results compared to the definitive overburden gradient of 12 wells in the Deep Water Database to determine which methods were most effective. The measure of effectiveness of the various methods was graded by the variance of the gradient produced by the method from the definitive overburden gradient. Based on this study, a new velocity/density transform was developed that provided superior results to the ones currently used by industry. This transform was distributed in programmatic form as a PREDICT UDP (User Defined Program) at DEA 119 Workshop No. 1.

Steve Hobart, a Principal Geopressure Consultant for Knowledge Systems was the primary research person for this part of the project. All of this work was documented in DEA 119 Report No. 4 which can be found in Appendix E of this manual and can also be downloaded from the DEA 119 password protected website www.knowsys.com/DEA_119_Prop.html

1.1.5 Velocity-Effective Stress Relations

A survey was done of the three possible ways to approach effective stress calculations using velocity data:

- Direct methods
- Indirect methods
- Trend-line methods.

Steve Hobart produced the report, and it can be found in Appendix F of this manual and can also be downloaded from the DEA 119 password protected website www.knowsys.com/DEA_119_Prop.html

1.1.6 Construction of Deep Water Database

Central to the project has been the construction of a database of pressure related data from over 100 wells in the deep water, virtually all in the Gulf of Mexico (four wells are from West Africa and the North Sea). Of the 100-plus wells, 44 were contributed by project participants and the balance from other sources including the MMS (also a project participant that was helpful with data provision) and Geophysical Development Corp. Purchased data was used for some wells considered essential. The kind of data available for each well varies – for all wells a fairly complete suite of log data is available. Actual pressure data in the form of RFTs is available for more than half the wells, checkshot data is available for many, geological data for a few and daily drilling reports for several.

The well data has been categorized, scrutinized and analyzed in various different ways and various subsets of the data have been used for different project phases. All of the wells have been completely analyzed for geopressures at least once and many have been analyzed multiple times. The final analysis phase involved analyzing each well with all the kinds of data available, matching the results with pressure indicators, and producing a definitive pore pressure and fracture gradient profile for the well. That definitive gradient was then assigned a confidence factor from 1 to 10 based on how close the computed result matched the pressure indicators. In the evaluation of new methods and models described in this report, the wells with a high confidence factor were most useful in the testing. The database is a primary asset from this project and plans are to ultimately make it available for use on the project website.

1.1.7 Construction of a DEA 119 Project Website

A password protected website has been built that contains status and project reports in Adobe PDF format. It is planned for the website to eventually contain all the data from well analyses such that it can be accessed by project participants. The address of the website is www.knowsys.com/DEA_119_Prop.html.

1.1.8 Development and Evaluation of Various Methods and Models

Following construction of the project database, a major effort was devoted to the development and evaluation of various methods and models for geopressure prediction. These models or methods relied primarily on seismic velocity data or its surrogate, acoustic data.

1.1.8.1 Conventional Analysis

Each well in the database has been analyzed using conventional models as documented herein. The analysis used all the available data for the well. For example, if a well had resistivity, sonic, and checkshot data, conventional analyses were performed to determine a pore pressure and fracture gradient for the well with each of these data. The results were calibrated against each other, RFTs (when available), and mud weight data. The overburden gradient was generated using the density log when available and the new method documented in DEA 119 Report No. 4 (Appendix E of this manual) when density

data was not available. The acoustic data was typically evaluated using both straight and curved (Bowers) trend lines. The resistivity data was corrected for temperature.

The results from these various analyses were then reviewed by a project committee of geopressure experts to determine the “definitive” pore pressure and fracture gradients for that well along with a confidence factor from 1 to 10 that was subjectively assigned by the committee. The results with higher confidence factors were then used for evaluating and training other methods and models.

1.1.8.2 New Pore Pressure Prediction Models

More than 10 new theoretically and empirically based models have been generated from various porosity/effective stress relationships in the literature. The theoretical models have been tested against a set of 20 wells that have definitive pressure profiles considered to be of the highest quality. Several of the theoretical models consistently predicted pressures for these wells more accurately than do the standard models used by industry today.

In parallel with the theoretical models, the empirical models developed from regression analyses used training sets of 10 and 20 wells. Both linear and non-linear regression methods were used to produce over 40 new models. Several of these empirical models have accurately predicted pore pressures more accurately than the theoretically-based models.

1.1.8.3 Neural Networks

Given the capabilities of neural network technology, it was anticipated that a neural net would be an effective way to predict geopressures, given a good set of training data that covered a diverse area. A lot of effort was put into this phase of the project, but the results were less favorable than anticipated. As a consequence, this area of investigation was dropped.

Much time was expended to put together good training sets of data and then optimizing the parameters to be used in training. In the final analysis, all data was referenced to depth below mudline, water depth was used as a key training factor as was interval velocity and the effort was directed to find effective stress as opposed to pore pressure. As mentioned above, the results were inconclusive and were also inferior to results produced by the new models.

1.1.8.4 Basin Modeling

The other methodology that was evaluated was the use of basin modeling to predict geopressures. There was a learning curve associated with this area of investigation as there has been for each of the others. The initial effort attempted to take virtually all 100-plus GOM wells in the DEA 119 database and put them into a basin model. The results from this effort were not successful. Given more geological input, it was realized that the GOM deep water is comprised of many sub-basins, most of which are enclosed by salt bodies of one sort or another. Based on this realization, it was decided to use a sub-basin approach where there were several available wells that could be used for calibration of the model.

The Auger Basin was selected for evaluation. The basin extends between GC 142 (South of the shelf margin) in the northeast to the GB 602 (deep salt ramp) in the southwest. It was chosen because of its unique geological setting and good quality data from six wells was available.

The evaluation plan was to use five of the six wells to calibrate the basin model, and then test the model for its ability to predict geopressures for the sixth well. The results from this investigation were very good, with the prediction matching the known definitive values by +/- 0.25 ppg. Based on these good results, even though anecdotal, it was concluded that basin modeling was an effective method for geopressure prediction. The basin modeling software used for this study was DrillWorks/BASIN, a Knowledge Systems software product introduced this year.

1.2 How to Use This Manual

This manual is designed to provide a combination of step-by-step procedures with detailed reference material for the theory behind the procedures. The procedures are contained in Chapters 2 through 6 while the reference material is in six appendices A through F.

1.2.1 Procedures for Geopressure Prediction: Chapters 2-6

1.2.1.1 Chapter 2 – Inventory Available Data

From a broad perspective, the quantity and quality of data available for use play important roles in the process of predicting pre-drill geopressures. Chapter 2 of the manual tabulates the data required as well as the data desired for geopressure prediction and provides guidelines for the evaluation of the quality of this data.

This chapter provides guidelines for grading the data that is available with a confidence factor. This confidence factor can then be used for risk analysis and combining uncertainties as discussed in Chapter 6.

1.2.1.2 Chapter 3 – Determine Prediction Strategy Based on Data Inventory

Chapter 3 of this manual provides some guidelines for making the decision whether or not to perform the basin analysis. There are a number of considerations that go into this decision and they are discussed in this chapter. The concepts of “overpressure” and “high overpressure” are introduced. The possibility of high geopressure warrants a more extensive effort to predict geopressure.

1.2.1.3 Chapter 4 – Single Well Analysis

Chapter 4 provides procedures for performing the analysis of a single well. Single well analysis is required whether it is the sole approach or it will be part of a basin analysis, where single wells must be analyzed to calibrate the basin model. Many of the new results, methods and models resulting from the DEA 119 project are presented in this

chapter. Concepts such as the “Centroid” effect and “Unloading” are also discussed with examples.

1.2.1.4 Chapter 5 – Basin Analysis

Chapter 5 provides guidelines and the step-by-step procedures involved in performing a basin analysis. This chapter includes details of the analysis of the Auger Basin that was performed as part of the DEA 119 project.

1.2.1.5 Chapter 6 – Combining Uncertainties to Determine Certainty of Prediction

Chapter 6 pulls everything together by illustrating one method of combining the uncertainties in the data with uncertainties in the model to produce a prediction that includes a most likely prediction along with a high and low prediction based on a specified probability.

1.2.2 Geopressure Reference – Appendices A – F

The appendices described below contain important technical details generated in the course of the DEA 119 Project. Essentially all the best practice procedures presented herein were distilled and derived from the materials and information contained in the appendices.

1.2.2.1 Appendix A – New Models for Pore Pressure Estimation in the Gulf of Mexico

One of the major accomplishments of the DEA 119 Project has been the development of a number of new models and transforms for computing pore pressure from velocity and other data. The primary project objective was to develop an improved methodology for pre-drill pore pressure prediction. Pre-drill implies that only seismic velocity site-specific data is available for use, so the primary focus of this exercise was to produce new models that can be used with velocity data. Since there was actually very little seismic velocity data available with the wells in the database, sonic logs and check shots were used as surrogate seismic velocity data.

More than 50 new models were developed and tested against data in the database. The models included some that were based purely on linear and non-linear regression and some that were based on theoretical principles and concepts. In all cases, regression was used to optimize the model coefficients. Typically the regression models were “trained” with data from 20 wells where there was high confidence in the results such that a “definitive” pore pressure profile could be used for calibration. The models were then tested against approximately 80 additional wells and were graded by those with the lowest average absolute error. All of this data is contained in a number of well-organized EXCEL spreadsheets and a summary of this work is included in Appendix A: DEA 119 Report No. 6 by Dr. Saad Saleh.

1.2.2.2 Appendix B – State of the Art in Pore Pressure Estimation

This reference, DEA 119 Report No. 1 by Dr. Glenn Bowers, is summarized in Section 1.1.1. It is a survey of the common industry practices and some comments on the normal trend curve assumed for velocity and its relevance to deep water geopressure predictions.

1.2.2.3 Appendix C – Seismic Prediction of Geopressure: Some Basic Principals and the Best Practice Methodolgy

DEA 119 Report No. 2 by Dr. Nader Dutta, as summarized in Section 1.1.2 is included as an important reference. This report focuses on the basics of seismic velocity concepts and analysis as they relate to geopressure.

1.2.2.4 Appendix D – State of the Art in Fracture Gradient Estimation

DEA 119 Report No. 3 by Dr. Glenn Bowers as summarized in Section 1.1.3 is a discussion of the methods and underlying assumptions in current industry practices for fracture gradient estimation.

1.2.2.5 Appendix E – Pre-Drill Overburden Estimation

DEA 119 Report No. 4 by Steve Hobart as summarized in Section 1.1.4 is a thorough documentation of methods of estimating this fundamental element of pore pressure prediction.

1.2.2.6 Appendix F – Velocity – Effective Stress Relation

DEA 119 Report No. 5 by Steve Hobart, a Principal Geopressure Consultant of Knowledge Systems, Inc. is a survey of direct and indirect methods.

2 Inventory Available Data

From a broad perspective, *quantity* and *quality* of data available for use are the primary considerations in the process of predicting pre-drill geopressures. This chapter tabulates the data required as well as the data desired for geopressure prediction and provides guidelines for the evaluation of the quality of this data.

In simple terms, if there are sufficient data available, building a basin model to predict geopressures at new well locations produces the best results. The basin model provides a powerful way to correlate results from offset wells drilled in the area and considers a broad range of pressure mechanisms such as hydrocarbon maturation, thermal expansion, as well as the lateral movement of formation fluids as affected by sealing and non-sealing faults. If there are not sufficient data available for basin modeling, then the recourse is to perform a single well analysis.

This chapter also provides guidelines for grading the data that is available with a confidence factor. This confidence factor can then be used for risk analysis and combining uncertainties as discussed in Chapter 6.

2.1 Introduction

Usually one of the most time consuming and difficult tasks in making a geopressure prediction is to pull together all the required data. A good prediction requires a combination of geophysical, petrophysical, geologic and drilling data. The prediction process requires judgment and flexibility to be able to work with the data available to make a prediction. In companies where each of these disciplines is represented by a separate department, there are sometimes organizational issues that make this process cumbersome. This chapter includes a list of desirable data for a single well analysis and the additional data required for a basin analysis. These lists are sometimes called wish lists, because all the desired data are rarely available.

Beyond the availability of the data is its variable quality. A significant part of this chapter is devoted to evaluating or grading the quality of the available data. It is dangerous to assume that data is accurate without questioning the way it was obtained and processed. This is particularly true with seismic velocity data, which is often the only indicator of porosity/compaction/geopressure in the area where a new exploration well is planned. This data can be problematic both from the standpoint that velocity data processing is typically driven by exploration requirements that are focused on locating reservoirs in deep depths and not within the more shallow sections where pressure transition zones and other problems occur. In addition, many drilling engineers may not be acquainted or comfortable with the “mysteries” of geophysics.

Regarding both data quantity and quality, this chapter attempts to provide a guide or framework for grading the data to be used for geopressure prediction. This is a difficult and highly subjective area, so these guidelines must be viewed as a starting point. However, this approach can be valuable once consistent guidelines are established within a company. The uncertainty analysis procedure that is outlined in Chapter 6 of this manual can be used to evaluate the potential variability of a geopressure prediction such that more intelligent planning is possible.

2.2 Data Requirements for a Single Well Prediction

Figure 2-1 shows a typical checklist of the data required for the prediction of geopressures for a single well. The geologic maps and seismic cross sections that show structure are very important to help determine the possibility of hydrodynamic effects and/or unloading. These are factors that can result in “high overpressures” as discussed in Chapter 3 of this manual.

Some of the required data is useful to make a quantitative prediction of geopressures, i.e. a density log can be used to calculate an overburden gradient and a sonic log or seismic interval velocity profile can be used to compute an effective stress or pore pressure. Other data is useful to make a qualitative prediction of the likelihood of overpressure. For example, there is a wealth of information in the daily drilling reports and mud logs from offset wells that may indicate when and where pressure events occurred. The serious geopressure analyst should make use of all the available data to help the prediction process. A later section in this chapter will discuss the significance of various types of data to the geopressure prediction process.

2.3 Additional Data Requirements for Prediction Using Geopressure Basin Modeling

The checklist in Figure 2-1 contains most of the data required for geopressure basin modeling and to make a prediction for a new well location. The wells to be used for model calibration obviously need the same data as required for a single well prediction. Some of the additional data required for a basin geopressure analysis are listed below:

- Stratigraphic column for the basin with geologic ages for all the formations.
- Lithology for the stratigraphy with emphasis on the applicable compaction relationships, including vertical and horizontal porosity.
- A minimum of three wells for calibration that are representative of the geologic extent of the basin that will be modeled. Three is a minimum number, and better results will usually be obtained with additional wells to better define the basin extent. This is especially true when there are multiple pressure compartments as defined by faulted and complex geologic structures.
- For each calibration well, a definitive pore pressure gradient and porosity profile are required. In addition, the formation tops corresponding to the basin stratigraphic column are required.
- For situations where the minimum numbers of calibration wells are not available, “pseudo-wells” can be utilized at selected seismic CDP locations to provide more basin definition. A definitive pore pressure and porosity profile with depth is also required as well as the formation tops for each pseudo-well. The analyst should realize that these pseudo-wells are inferior to actual wells so that the model results may be more uncertain.

Figure 2-1 Typical Data Checklist for Single Well Analysis

Well Name: _____ **Location:** _____

Well Spud Date: _____ **Depth Units:** _____

Coordinates: Latitude _____ **Longitude** _____

Country: _____ **Water Depth:** _____

Kind of Data	Desired Medium	Primary Well	Offset #1	Offset #2	Offset #3
Area geologic description	text				
Seismic interval velocities	digital				
RMS seismic velocities	digital				
Air Gap	value				
Water Depth	value				
Well TVD relative to RKB	value				
Well MD relative to RKB	value				
Well temperature profile (regional if individual well data is not available)	digital or tabular				
Well Shale CEC profile (regional if individual well data is not available)	digital or tabular				
Stratigraphy/Formation Tops/Unconformities	digital or tabular				
Survey data, incl TVD	digital				
Gamma ray log data	digital				
Resistivity log data	digital				
Sonic log data	digital				
SP log data	digital				
Bulk density log data	digital				
Neutron porosity log data	digital				

Kind of Data	Desired Medium	Primary Well	Offset #1	Offset #2	Offset #3
Caliper log data	digital				
D exponent log data	digital				
Gas log data	digital				
RFTs or MDTs	tabular				
LOTs or FITs (including plots)	tabular /graphic				
Mud Weights / ECDs	tabular				
Casing depth and size	tabular				
Kicks w/ mud weight to kill	text				
Mud log data incl. Dxc, gas data and lithology	paper log				
Description of any Drilling Problems	text				
XRD or FTIR Mineralogy	Tabular or text				
Mud resistivity and mud salinity	Tabular or text				
Formation water salinity	Tabular or text				
Geologic maps that show structure	Maps				
Seismic Cross Sections	Paper Display				

Other Checklist Data:

- Location of all significant faults and other geologic features such as salt bodies.

2.4 Evaluation of Seismic Velocity Data for Geopressure Prediction

The accuracy of pre-drill pore pressure prediction is a function of the accuracy of the interval velocity and the assumed normal compaction trend (for conventional methods). Often the pressure analyst is provided with stacking velocities from the basic depth/velocity analysis that has been performed for evaluation of the exploration prospect. Much caution is in order when using this data, because its value for geopressure analysis is questionable. This data is typically interpreted with focus on the exploration prospect at deep depths with little focus on the shallower sections where considerable pressure transitions might occur. This can result in unacceptable errors in the predicted geopressures. This section contains guidelines and criteria for processing seismic velocity data so that it is more suitable and accurate for geopressure prediction..

When drilling engineers or well site geologists travel to a location, they may be provided with a “Seismic Collage or Paste-Up”. This paste-up usually includes 2-D slices through the proposed location, one or two 3-D or pseudo-3-D block views, and a series of structure contour maps.

An experienced well site field geologist can visualize, extract and “predict” a variety of information from these basic presentations. Knowledge of how structure influences, or is a product of, abnormal pressure can help determine if a prospect will be sited within a likely zone of instability or abnormal pressure. For example, wells sited at or proximal to hinge lines in compacting and deforming basins will likely exhibit abnormal pressure from one or more sources or mechanisms.

2.4.1 Guidelines for Generating Interval Velocities from Seismic Data

There are several different scenarios to be considered when evaluating the quality of seismic data for geopressure prediction. These are discussed below.

2.4.1.1 Scenario 1 – Offset Well(s) Available – Calibrated Dataset

- At least one offset well is available for calibration. In this case, there should be information directly related to the true rock velocity. The depths of the major formation tops are more accurate than those determined from seismic data interpretation.
- In the best case, the given interval velocity has already been calibrated with log data. This data can be used without any adjustment and its quality can be ranked as good.

2.4.1.2 Offset Well(s) Available - Un-calibrated Dataset

- Use available sonic logs, checkshots, or VSPs to calibrate and adjust the interval velocity functions at the well locations.
- Correlate these calibrated functions to the interval velocity function at the target location.

- Make necessary adjustments before using in the pore pressure analysis.

An interval velocity calibrated this way will be considered of good quality.

2.4.1.3 No Offset Well(s) Available within the Coverage of the Seismic Dataset

The analyst has to look at all necessary quality control data plots to assure the quality of the interval velocity before a pore pressure analysis, because quite a few practices in seismic data processing that are considered good or neutral for seismic imaging may have negative effects on pore pressure analysis.

The following specific plots should be viewed and examined closely by an experienced geophysicist:

- The pre-stack depth migrated line sections passing through the target location.
- The interval velocity at and near the target location.
- The typical QC panels of pre-stack depth migration, such as velocity analysis, semblance, un-stacked but move-out-corrected gathers, and a short pre-stack depth migrated stacked section.
- Even though stacking velocity is not the one that we use for pore pressure analysis, QC plots for stacking velocity, such as velocity spectra, semblance, NMO-corrected gathers, stacked sections and brute-stacked sections are sometimes useful.
- An interpreted depth section will be very helpful if to verify the interval velocity by doing seismic forward modeling.

The usability rating of this seismic data will be a result of the outcome of these quality checks.

2.4.1.4 Seismic Quality Evaluation "Quick Checks"

Some measures and checks to evaluate the quality of the interval velocity are within the capability of the engineer, geologist or analyst (provided that rock properties and basic structural effects are known). Note that generalized velocity ranges are included in the guidelines below, so care must be taken to consider local variables such as formation ages, internal matrix chemistries and geometries. Also, fluid content and fluid properties, and the presence of local phenomena such as volcanics or evaporates should be noted. Some of the following are quality checks that the engineer or geologist can make, while others are questions that can be asked of the geophysicist providing the data.

- Are there any velocities too high or too low for the known rock velocities at the area? Make every effort to relate seismic interval velocities to anticipated rock velocities. Be aware that these velocity guidelines are general and may vary locally with formation age, anisotropy, stress orientation and other factors:
 - Velocity > 10,000 fps where Shale is generally 6,000 – 16,000 fps; Salt is 15,000 fps; Limestone is 21,000 fps; Dolomite is 23,000 fps; Quartz is 18,000 fps.
 - Sandstone: (unconsolidated = <17,000 fps; semi-consolidated = 18,000 fps and consolidated = 19,000 fps).

- ❑ Are there enough velocity functions at and around the target location so that the spatial variation can be verified?
- ❑ Are the velocity functions smooth enough spatially to make geologic sense?
- ❑ Do we have artifacts? Or “outlying” data?
- ❑ Do the QC plots show the quality assuring features such as the flattening of the events in an NMO-corrected gather?
- ❑ What were the criteria for picking velocity data?
- ❑ Have the necessary pre-processing procedures been done? How good are the results? Was de-multiple processing done? Were datum static and residual static corrected?
- ❑ The following steps will help improve the confidence level in the velocity data:
 - Use data from a location with very mild structure to construct a local interval velocity function.
 - Use this constructed velocity function to correlate other velocity functions.
- ❑ Finally, the interval velocity can be verified with better assurance by constructing a synthetic gather with the velocity model, and then using it to compare with the corresponding real gather to see if the velocity is acceptable.

	Vertical	Lateral	Comment
Low resolution Spec data and standard	0-2 Hz (400-500 ms)	~1 mile	Constant pressures in 500-800 foot interval; smeared geology
Closer picks and QC Reprocessed lines	0-4 Hz (200-400 ms)	~1000 feet	250-400 foot interval; improved geological resolution
High Resolution Seismic amplitudes (AI) at Every seismic trace	(8,10)-(50-60) Hz (10-20 ms)	~100 feet	100-200 foot interval; improved geologic resolution
Frequency gap	4,(8-10)Hz		Need a prior model based on well data and integration with other geological data (facies)

Table 2-1 Velocity Resolution from Seismic Data

Table 2-1 shows important criteria about the relationship of frequency to depth resolution. Do not expect to predict a 100 ft pressure ramp using low and medium resolution data.

The reader is encouraged to read the materials in Appendix C for more detailed coverage of this important subject.

2.5 Data that Can Be Used for Geopressure Prediction

Experienced geopressure analysts will utilize any relevant data to enhance the prediction process. This section lists the wide variety of information that is generally available from the location or prospect selection to the post-well reporting phase. Geopressure prediction is a challenging task and the more indicators that are considered, the more accurate the prediction will be. Some of this data can be used to quantify a prediction value while others have qualitative value. Both are important.

Prior to starting the development of a prospect, it is necessary to prepare to manage the information that can be gathered and extracted from the records available. It is important to have a software tool that can manage the large amounts of varied data involved. A general overview of the process is as follows:

- Set up the pre-drill data and information repository for the new well in pore pressure software with the capacity to handle multiple databases and wells.
- Input the relevant seismic interval velocities.
- Input the anticipated well path to include kick-off depth, MD vs. TVD profile.
- Determine location data for reference information (LAT/LONG, surface coordinates/XY) for seismic line(s) and prospect well.
- Determine water depth, rig floor elevation and air gap (elevations at mean tide).
- Input water depth vs. TVD profile (if the well ins highly inclined)
- Use estimated or measured temperature at mud line (usually 40F).
- Obtain an estimated or measured temperature profile (maximum reading thermometers on WL logs).
- Review all of the available data for completeness, quality and record the acquisition dates.
- "Mine" the written annotations and descriptions on the logs for any information that might be useful to interpret initial pressure modeling and computed results that may fall outside of the expected or anticipated results.

2.5.1 Geological Age and Formation Information

This can be an actual formation name (such as Wilcox or Vicksburg), Paleo-fossil name (analyst to research age and/or provenience) or a seismic reflector designation. Related data may be substituted such as depths and bases of major lithological units and structural events defined as follows:

- Unconsolidated shale top (assume mud-line)
- Pseudo-plastic shales (poorly consolidated usually evident on sonic and neutron)
- Sand packet(s) onset
- Salt/Evaporite event top and base if known
- Carbonate stringers onset or emplacement of significant beds (seismic reflector)
- Unconformities - emplacement of any major (regional) events

- ❑ Faults - emplacement of any major (regional); dip and strike relative to well(s) or basin
- ❑ Relevant structural information and anticipated hydrocarbon columns
- ❑ Location of anticipated well path intersections with faults and unconformities
- ❑ Structural emplacement of well in seismic section and/or seismic structural collage

2.5.2 Conventional Wireline Data

- ❑ Sonic-conventional - calibration and training data
- ❑ Array acoustic – for shear and compressional wave
- ❑ Long-spaced sonic
- ❑ Sonic (compressional-wave)
- ❑ Sonic (shear-wave)
- ❑ Neutron (DPRS)
- ❑ Resistivity
- ❑ Conductivity
- ❑ Gamma ray-natural
- ❑ Gamma ray-spectral

2.5.3 Special Wireline Data

- ❑ RFT/SFT – pressure testing tools; calibration and training data
- ❑ MDT/RCT – pressure testing and reservoir characterization tools; calibration and training data
- ❑ IMAGELOGS such as STAR or MRIL –formation characterization tools; structural verification especially faults and fractures and more
- ❑ DIPLOGS – bedding and formation characterization tools; structural verification and dip orientation; valuable for stress field orientation by examination of well bore eccentricity azimuthally displayed by the multi-arm calipers

2.5.4 Measurement While Drilling Data – MWD

- ❑ MWD Direction (DS) directional orientation tool for BHA
- ❑ MWD Gamma (DGS) direction and basic lithology tool
- ❑ MWD Gamma Resistivity(DGR) direction, basic lithology and formation characterization tool (fluid, porosity and permeability characterization).

2.5.5 Logging While Drilling Data – LWD, FEL

- ❑ Gamma/Resistivity basic lithology and formation characterization tool (basic fluid characterization sensor suite); abnormal pressure detection

- ❑ Gamma/Resistivity/Neutron basic lithology and formation characterization tool (basic hydrocarbon and fluid characterization sensor suite); abnormal pressure detection; rock density and porosity measurements
- ❑ Gamma/Resistivity/Neutron/Sonic lithology and formation characterization tool (basic hydrocarbon and fluid characterization sensor suite); abnormal pressure detection; rock density and porosity measurements
- ❑ Gamma/Resistivity/Neutron/Sonic lithology and formation characterization tool plus caliper
- ❑ Gamma/Resistivity/Neutron/Sonic lithology and formation characterization tool plus Mechanical sub plus Annular Temperatures and Pressure and (possibly EMW).

2.5.6 Text Based and Lower Precision Data

Many of these paper logs can be digitized, if necessary, to create the more portable ASCII or other digital file formats for importing into the pressure prediction and modeling software.

- 1 Seismic Sections** – Used by the experienced analyst to determine structural emplacement for the prospect well or study wells. Also, used to locate well(s) in relationship to structural styles or features. Can be used to indicate most likely geopressure mechanisms and types of drilling hazards to be anticipated.
- 2 Composite Logs** – Wireline, LWD/MWD, Geological Interpretive log, Total Gas, Chromatographic Break Down, Show Zones, Cores, Open-Hole Tests (Drill Stem and Production Tests), fluid recoveries. Composite logs are uncommon domestically but are standard international wellsite and analytical tools A variety of data can be mined from these presentations.
- 3 Geological Logs** – From wellsite geologist: Fossil assemblages, diagenetic indicators; interpretive lithology; show evaluation; porosity estimates and style; detailed secondary and ancillary mineral suites (diagenetic indicators).
- 4 Mud Logs**– ROP (Inst/Avg), Total Hydrocarbons (Units/%), Chromat Breakdown (C1, C2, C3, IC/NC4, IC/NC5), Hydrocarbon Indicator, Porosity (basic), Show Qualifiers (basic), Cut/Stain/ Fluorescence, Percent Lithology, Interpretive Lithology (sometimes), Lithology Descriptions, Rock Type (shale, sandstone, siltstone, carbonates, evaporites, coal, conglomerate, etc.), Index Minerals (pyrite, Glauconite, 2ndary calcite/aragonite, Micas), Basement Definitions and rock type(s), fossils (basic species identification).
- 5 Drilling Fluid Reports** – Mud Type, mud weight, gas cut/water cut, chlorides, PV/YP, API WL, HTHP WL, pH, Ions (calcium, Potassium, chlorides, KCl, NaCl, Others): These should supercede log header as the principal source of mud weight data.
- 6 LWD/MWD Logs** – Real-Time Logs (low data density and data which is error prone); Gamma (basic), resistivity (electro magnetic or other), conductivity (resistivity inverse); MW annulus, Pressure annulus, Temperature annulus, tool

temperature, sonic (caliper estimated compensation), neutron density, neutron porosity, neutron-gamma derived lithology indicators (Schlumberger-Anadrill).

- 7 Engineering Mud Logs** – Drilling Exponents (d-Exp, DC's Exp, A Exp, Sigma, Pore Pressure Est., Fracture Gradient Est., Rock Densities (Shale Density or Shale Bulk Density), Overburden Estimation (sometimes), Circulating Temperature In/Out, Relative Flow Out (absolute sometime), torque, trip properties (abnormal fill, torque/drag, bridging, reaming, fill on bottom, trip gas, Swab-Surge), connection gas, trip gas (short trip gas, dummy trip gas), well flow (SIDPP/CASP), lost circulation (MW/Depth), ECD (supercedes MW).
- 8 Engineering Morning Reports** – Compilations or syntheses of all wellsite daily reports; basic overview of daily wellsite operations; a ready source of basic data.
- 9 Drill Bit Reports** –Can derive formation abrasivity indices from individual bit run data and determine suitability of bit run for derivation of pseudo-drilling exponent type variables (poor bit to formation match can negate these models as can forgetting to correct derived Pore Pressure trend lines for “jump shifts” due to use of diamond or PDC bits and for hole sizes less than 12.25”).
- 10 Casing Reports** – Limited value but a useful reference for past casing seat or casing setting depths; usually an indicator of problem formation depths; cross-check records for LOT depths, hole size and mud type change depths.
- 11 Pressure Tests:** Leak-Off Tests (LOT), Formation Integrity (FIT) and Pressure Integrity Tests (PIT), EMW or PSI values (important to distinguish between full LOT and FIT/PIT).
- 12 Wireline Logs** – Sonic Logs (normal, long-spaced, array acoustic shear-wave, BHCS), SP, Gamma (conventional natural Gamma or spectral), Resistivity, Conductivity, Caliper (single or multi-arm), Neutron Porosity, Neutron Density, Neutron Fluids identification, Magnetic Resonance Imaging Log (MRIL, STAR).
- 13 Elevations** – Kelly Bushing/Rotary Kelly Bushing Datum (KB/RKB), Rotary Table (RT- not all rigs have a RT – especially older GOM and small footprint rigs), Drill Floor (DF), Air Gap (AG), Water Depth (WD), Mean Sea Level (MSL – usually taken between mean high and low tide), Sub-Sea, Mud Line (ML and variants BML or Below Mud Line), Measured Depth (MD – long hole measured depth from pipe tally, geograph depth or other depth measurement device such as Wireline cable), True Vertical Depth (TVD – calculated depth compensated for hole angle or deviation – this is the depth to be used in all hydrostatic, pore pressure, fracture pressure, overburden calculations, etc.).
- 14 Directional Data Reference Tables and Plots:** The sources of directional survey data are mechanical or electronic and are listed here in order of increasing preference and general accuracy (MWD most accurate):
 - Single shot series – “TOTCO” (least accurate – subjective for fractional angles and tend to be inaccurate due to lack of basic tool maintenance)
 - Multi-shot series - more accurate - subjective for fractional angles; surveys must agree; may also be suspect due to lack of basic tool maintenance)

- Wireline run side entry sub – preferred to above but may have inherent error related to cable stretch and ROP effects similar to MWD (verify surveys are corrected for ROP ranges and compensated for line stretch)
 - MWD DGS or MWD DS - Measurement while drilling directional with gamma survey or Directional Service only - preferred survey
 - MWD directional data presentation in the Gulf of Mexico compensated for "Grid Correction" in calibration tables entered into the tool - most preferred survey
- 15 Geographical Location** – Latitude and Longitude, Northing/Easting; specify survey system datum type: SAD, GPS, NAD, others)
- 16 LWD Data:** All MWD data should be verified as corrected for ROP, pipe stretch and compression effects, labeled as real-time only or variously as real-time and/or memory log data replacements. In some cases, an either/or situation exists where it might be useful to differentiate real-time only from memory mode data.
- 17 Mud Logging Data:** Domestically, the mud logging information may provide the only detailed record of the actual geology and lithology drilled. Generally presented as percent lithologies, occasionally as an interpretive log, may include written sample descriptions. The following are the primary information of use to the pressure analyst that originates with the mud logger.
- D-exp or Dcs – uncorrected drilling exponent, or corrected for mud weight or ECD effect (should plot both to help visualize amount of over-under balance)
 - ROP (rate of penetration in feet per hour and/or minutes per foot)
 - WOB weight on bit
 - RPM rotary table revolutions per minute
 - Mud Weight in/out
 - Mud temperature in/out
 - Drill gas (Total and/or Compensated for ROP and hole volume)
 - Connection (CG), trip (TG), short-trip (STG), dummy trip (DTG) gas levels
 - Gas Chromatography (C1, C2, C3, IC4/NC4 and IC5/NC5)
 - Equivalent Circulating Density (ECD)
 - Torque
 - CEC or cation exchange capacity
 - Hydrocarbon Show intervals
 - Bit Records with ROP performance
 - General mud properties
 - Continuous Chlorides in/out plots
 - Well control pressures from Shut-in events(shut in drill pipe and casing pressures)

- Density Log whether Bulk Density or "sink or swim" measurement technique; differentiate between "bulk scale" density (preferred) or "sink and swim (too subjective; lots of operator error; requires experience)
- Relative (%) flow out or absolute flow measurement (such as Foxboro magnetic flow meters, sonic or Doppler devices)

18 Numerical data: Formatted in any of the following file structures: ASCII, LAS, WITS, and DrillWorks/PREDICT.

2.6 Evaluating Data Quality

Quantifying uncertainty in log measurements and other data, which are relevant to petrophysical rock properties and eventually to geopressures can be a difficult endeavor. The complexity of the task comes from the following:

- Log responses are directly affected by tool make, type, timing or measurements, and wellbore conditions.
- It is difficult to judge the balance of high quality data (but limited) to low quality data (but plentiful). In most cases, a greater quantity of noisy data may be better than a few good data points.

In assessing the quantity and quality of data, there will typically be less data available in the shallow depths versus the data intensive regions near the reservoir. Data quality is also depth related, as more kinds of complementary measurements will be taken at the deeper depths.

The objectives from data quality verification and assessment are:

- Reduce risk of drilling failure.
- Reduce drilling cost.
- Assess the uncertainty in well construction design to more closely predict pore and fracture pressures with the least possible uncertainty.
- Recognize outlier data that are separated by one or two standard deviation from the rest of the population. Outlier data can have a major impact on the spatial correlation of variables and modeling.

The subject of uncertainty in log-derived petrophysical data is of concern to a wide cross section of disciplines in the petroleum industry. Practical guidelines to minimize potential pitfalls in geostatistical reservoir characterization must be advanced by service and operation companies. Assessing data quality is the first step in any geostatistical study. The basic tasks of assessing data quality include:

- Review statistical behavior of the data.
- Determine relationship between well and seismic data.
- Recognize anomalies early in the study.
- Generate histograms of reservoir and seismic parameters based on an assumption of normal distribution.
- Examine histograms for outliers.

- Recognize lithological regional “trends”.
- Use cross plots to identify “outlier” wells or data.

2.6.1 Evaluation of Geologic and Structural Data

It is strongly recommended that the analyst plot several of the major raw log data curves to identify missing data locations and/or major data shifts that could indicate faults, unconformities, gas effects, pressure seals, and depth of various pressure phenomena such as unloading, abnormal secondary cementation, or sealing effects. The following section provides comments on detailed information sources that can be mined by an experienced pressure analyst. The analyst should become familiar with these guidelines as they can save significant time trying to explain why some data may not fit the expected results. These guidelines also provide hints on how to manipulate some of the lithology effect exponents.

- 1 Useful, visual data grouping criteria are structural unconformities, age-related unconformities, faults, fracture fields, major depositional-environmental changes (continental to marine or transgressive/regressive event horizon) and so-called “log jump shifts”.
- 2 Abnormal pressure indicators may be classified into broad groups and can be determined by “mining” or close examination of the “raw data” plots recommended above such as mud and geological logs or sample descriptions. Other indicators can be:
 - Mineralogical - authigenic glauconite and micas, pyrite, quartz, euhedral quartz and calcite crystals.
 - Physical - slickensides, fracturing, gouge deposits, salt and pyrite castes in samples, etched quartz grains (acid gas migration), chlorite rings, grain deformation, cross-grain fracturing.
 - Drilling indicators - Change in hole fill, cuttings shape and size, torque, bit bounce, drill-string vibration effects, Drill on/off; change in relative gas background including connection and trip gasses; measured or relative flow out changes (increase/decrease/surging), rotary or motor stalling (hole unloading).
 - Geochemical/diagenesis - such as changes in shale CEC/MBT, chlorides changes in mud and on influx events. Not all gas increases are wholly hydrocarbon events as some are driven by water flows where gas is entrained, but may not be the real problem. Transformation of clay or shales from montmorillonites to illites or mixed-layer clay minerals; presence or indication of micas and mica family alteration (glauconite \leftrightarrow clays \leftrightarrow micas); changes in ferrous or iron mineral families; changes in clay color and texture as indicators of beginning stages of “ion” exchange or leaching between adjacent formations or secondary minerals content in matrix; anhydrite \leftrightarrow gypsum transform causes depletion or expulsion of excess water molecules under specific conditions (revisit the old concepts of Bowen Type or Solution-Phase-ternary-solution plot diagrams).
 - Geothermal - formation temperature gradient changes as evidenced by plotting trend from wire-line BHT data (max reading thermometers) or by plotting

MWD/LWD measured temps (ideally tool temp vs annular or the delta of the two) and supplemented by delta mud TPOT-TPIN.

- Structural faults or fracture swarms are usually located at specific stress or "flex" points in large geological features such as synclines/anticlines; flanks and roof of diapiric features such as salt domes or mobile shale events such as diapiric shale intrusions;
- 3 Major causes of regional stresses and/or stress fields as inferred from seismic or by "experiential" overview of raw data plots generated in visualization exercises should also be noted for comparison to mapped and contoured data. This was done for wells in this project to "test" for geopressure relationships to temperature and mud weight. Test case temperature contour isopach maps at 5,000, 10,000 and 15,000 ft. were plotted for comparison to mud weight and pressure comparison or correlation. This data would initially be considered more appropriately in gradient form at some depth of interest where 1.3° F/100 ft. is generally considered an indication of abnormal conditions. A standard normal temperature gradient reference line (1.0° F/100 ft) is used to help visualize any deviation from that line as either questionable data or as a candidate for comparison to other measured events. Elevated geothermal gradients will generally be observed in the vicinity of diapiric structures such as salt domes, boundaries of mobile shale masses and diapirs, centroids, flanks of anticlines, limbs synclines or folded structures, axial points and lines within active collapsing basins or structures (down-warping).
 - 4 Salt or Evaporite Sections - Geophysical Salt Survey mapping data makes a perfect reference compliment to interpreting several of the study area data and the contoured DEA 119 datasets, particularly the temperature and mud weight contour maps. A salt contour map should be made available for planning a new or prospect location where minimal offset data is available.
 - 5 Geologic age and structural effects on Logs: Major unconformities can be related to age, faulting, or erosion; by catastrophic events such as landslides/slope edge failure, turbidite scouring, uplift/down-warping, or volcanism – all of which manifest as wholesale shifts or "jump shifts" in most logging suites though not necessarily to the same extent. Gamma, resistivity and neutron logging tools are sensitive to volcanic events: Gamma logs may read higher than background, sonic logs may read faster velocities, may cycle-skip at bed boundaries, may exhibit "ringing" at bed boundaries and neutron logs may indicate higher than background densities and much lower porosities. Carbonate events cause similar responses except that Gamma reads much lower than for volcanic events. Resistivity logs will generally read very high though exceptions might imply high iron (especially magnetite or other conductive minerals); diplogs may also be affected as well as directional tools relying on magnetometers using magnetic field and major dip changes corrections (older rocks of Jurassic or Permian age may show dip and field reversal).
 - 6 Faults – like age related events, these will cause logs to respond as appropriate for the emplaced age of the faulted formations; fault boundaries may show up on MWD logs, sonic logs and more or less on Gamma logs with characteristically exhibited curve shapes and responses. Some companies have started to maintain example reference databases of these effects.

- 7 Salinities (CHL) – salinities or resistivities will change as a function of the age of rocks below an unconformity or similarly within fault emplacement; however, in some cases, water salinities in the fault zone itself can be enigmatic especially in continental marine or shelf marine environments where salt and fresh water formations are present for long geologic periods (fresher is not necessarily younger and vice versa); the rule of thumb is the older the formation, the higher the salinities.

2.6.2 General Sources of Errors and Anomalies

It may be helpful to have an understanding of the source of errors and anomalies that reduce the data quality. Problem sources can be attributed to the following:

- 1 Selection of inappropriate tools for the mud system in the hole. Also, poor selection of standoffs, centralizers, weights, pad sets, snorkels, hydraulic arms for wall contact tools.
- 2 Ignoring maximum logging speed recommendations for wireline or excessive ROP for MWD (control drill as needed to gather quality data).
- 3 Adverse hole conditions such as washed out intervals, junk in the hole, deviated well or depth locations of severe doglegs, bridging zones, etc.
- 4 Faults, unconformities, evaporites, coals, pyrite, bentonitic or swelling shale intervals, glauconite, show zones: all of which may affect the performance accuracy of one or more tools.
- 5 Not making the appropriate corrections for heavy weight muds (+12.0 ppg barite weighted muds) needed to correct neutron density affects some resistivity logs and sonic.
- 6 Poor communication between service company engineer and operators on wellsite.
- 7 Mud weights may be erroneously reported as homogeneous when they should have been gas cut; wireline data is affected by gas in formation (gas effect) as is the mud weight if it has entrained gas. Mud log or any of the daily reports from the well such as engineering, mud engineer or IADC daily reports may provide insights to mud weight history.
- 8 Mud weight curves derived from Wireline Log headers are minimally derived curves (weak data density). Some of the pressure prediction models require a particular data density or coverage which is derived by extrapolating between the few log header points; this may not be a valid operation. Determine if the well was incrementally weighted up or done in a step-wise manner. Was the well drilled to a basic plan or drilled for kicks? If the latter, a smooth interpolated mud weight curve is invalid and is not accurately representative of actual well conditions. It reflects poor drilling practices and an unplanned “knee jerk” response to formation conditions.
- 9 Mineral Effects on Wireline Data
 - Radioactivity – carnotite/uranium enriched or “hot” mineral sands cause elevated Gamma log values and high geothermal gradients (Gulf Coast Area)
 - Volcanic ash – bentonitic shales; swelling, water wet, elevated Gamma values

- Phosphates – fossil shell phosphatic/chiton or phosphate source rocks; elevate Gamma values
 - Lime/calcite concentration – limy shales need sonic correction applied (add 10 μ /ft to all limy shale values to re-fit to the trend or pore pressure estimate will be too high).
 - Barite and Boron – affect Neutron Logs; heavy barite muds require corrections to logs and boron is present in some Texas Coastal Plain/Gulf Coast formation fluids; deeper, older formations or those sourced from the land based rocks may reflect the same properties.
 - Mica – can affect several logs (such as Gamma, spectral Gamma and Neutron); unfortunately, as clays undergo diagenesis, growth of orthogenic mica is an indicator of this process so it is both useful and damaging to preserving the data trend; large additions of mica LCM (muscovite and Biotite) may also affect these wireline data as well as mask formation events, plug RFT tools, MWD tools and down hole motors – all of which can result in data gaps as tools power down.
 - Pyrite – may cause perturbations in Sonic, MWD and other nuclear and/or magnetic field type logs (such as EMI/FMI, MRIL, EWR-MWD); typically this shows up as “spiking” or very occasionally as cycle skipping on logs.
- 10** RFT points may not correspond to a predicted or log generated pressure curve, which is more common than expected given an understanding of the difficulty of getting a good RFT measurement in unconsolidated or highly permeable formations. Success may be determined by proper selection of pad type (soft, hard or articulated), standoff capabilities (bow spring or articulating arm), proper choice of snorkel, and experience of operator.
- RFT quality is affected by caliper (check on logs); it is difficult to take a measurement when the hole diameter precludes setting a pad or tool (check tool set pressures to determine if seal failures may be recouped by changing pad and arm configuration to allow for higher set pressures and greater extension).
 - Depth control on the RFT measurements: Check Gamma trace markers with another Gamma log (always run a Gamma ray log for correlation and depth checking).
 - Effect of structure or Centroid effect
 - RFT/MDT/RCT service companies should provide a summary table on the header or tail of the logs with a minimum annotation to include all pressures, times and duration of tests, set pressure, and basic observations such as tight, poor seal, seal failed, tool failed.

2.6.3 Sources of Error in Sonic Log Data

Sonic log measurements are strongly affected by wellbore conditions (unlike seismic data measurements). Sonic logging tools make “in situ” wellbore measurements of rock velocities. Wellbore properties and geometries can have profound affects on these measurements.

The observed compressional sonic velocity recorded with conventional sonic devices is affected by hole size, formation and/or filtrate water salinity, dissolved gas, borehole and formation temperature, pore pressure, low saturation biogenic free gas, and the presence of hydrocarbons. The magnitude of this effect may not be well appreciated by users of borehole sonic logs. These factors can have a significant affect upon measured interval transit times and our ability to interpret sonic logs for porosity or upon ties to seismic velocities or amplitudes. These factors can affect interval transit times by 10 or more microseconds in unconsolidated sandstones, limy intervals, dirty sands with siltstone/shale streaks or stringers, inter-bedded rhythmic or laminated shales and sandstones or shales and limestones (depending on relative bulk volumes of shale or limestone the sonic may be biased slower or faster).

Conventional sonic equations such as the Wyllie time average or the Raymer-Hunt travel time equation provide little insight to the influences these environmental factors may have upon conventional sonic logs. A clear understanding of environmental effects provides a rationale for the analyst to correct sonic logs for these influences. This leads to more accurate interpretation of sonic logs for porosity, fluid content and improved ties with seismic and checkshot velocities.

There are a multitude of natural and mechanical events that can effect measurements from sonic tools. Inherent tool noise and some sensor cross-talk can be calibrated out or minimized. The single most important noise reduction device is a correctly grounded logging skid and cable system. Choosing appropriate filters in acquisition software will take care of most other noise effects. Some log quality control manuals go into detail using examples of many types of repeating log problems such as spiking, cycle skipping and lack of sensitivity. An experienced, conscientious wireline or MWD operator will automatically account for and correct or minimize these problems. Log QC is best served by becoming aware of the types of log artifacts most common to your area and service company.

2.6.3.1 Checklist for Sonic Data Quality Control

The geopressure analyst should be aware of the following factors that can affect the quality of sonic data:

- Wellbore Environment
 - Drilling fluid effect
 - Tool eccentricity
 - Hole caliper single or multi-arm
 - Hole rugosity
 - Logging speed
 - Casing interval
 - Multiple casing
 - Tool scaling
 - Directional wellbore effects

- Wellbore damage
- Formation anisotropy (deviated beds, dipping beds)
- In Situ Stresses

Some of these factors are discussed in detail below:

2.6.3.1.1 Wellbore Environment - Drilling Fluids

Shale can experience significant damage from water base drilling fluids. Field evidence suggests that the effect of drilling fluid damage on sonic velocity can be profound. As damage increases, the DT (sonic interval) decreases relative to the undamaged rock (away from the wellbore). Up to 30% change in DT is possible with severe formation damage. Therefore, it is important to understand **that damage to shale** may cause the following effects:

- Sonic tool tends to read slower travel time (micro sec/ft) than normal.
- Density log will read too low causing OBG to be underestimated.

If a formation damage effect on sonic tool measurements is suspected, the following checks are useful:

- Check caliper, almost all current sonic logs are run with a caliper (either single or multi-arm)
- Check departure of shallow and deep or medium and deep induction curves on resistivity logs (if available). Look for indications of drill fluid invasion or filter-cake effect, and for deep invasion beyond the usual skin damage zone. Determine if the invasion is from whole mud, filtrate or in the case of oil muds (native state, MSO or synthetics), if the “salt or activation phase” has infiltrated. Decreasing activity or electrical stability values on the mud reports for oil muds is a clue to this mechanism.
- Compare sonic to seismic data. If it is observed that the sonic is reading about 20% higher than seismic travel time, this may be an indication of shale damage during drilling. Damage can take several forms such as hole washout, shale-clay expansion, filtrate invasion or in the case of some drilling fluids, desiccation.
- If the seismic data is consistently lower than the sonic, then there is indication of shale damage or shale properties changed during drilling by one or more of the mechanisms discussed.
- If MWD logs are available, compare the MWD sonic to WL sonic. The MWD sonic should have little effect from shale damage. The MWD tool measures shale sonic travel time before major damage occurs to the shale. However, be aware that high ROP’s may make real-time sonic log comparisons invalid (use Memory Log where possible). This is especially so when comparing real time Gamma logs to WL logs.
- Sonic reading in sand usually does not get affected by damage from drilling fluid, however sands may wash out, thus increasing hole gauge, salt water to fresher water transitions, mineralogical effects in sands may affect the sonic log.

- Oil base mud does not have any effect on sonic reading in shale or sand except as described below.
- Shale damage may be diagnosed by comparing log responses if the same shale interval is logged twice (few days apart) or the mechanical effects if the hole swells or caves in (fill on bottom or bridging).
- Occasionally, oil muds, iron hematite or similar minerals used as weight materials may cause “spiking” on sonic logs (Shell and Mobil have been fond of these additives, so be cautious with older records).

2.6.3.1.2 New Casing Interval and Bit Size Changes

After running a casing string, the new drilling interval has entirely new environmental effects on subsequent logging runs. Therefore, it is expected that sonic data may show an abrupt transition from the old logging interval to the new one. The transition may be a sharp change in sonic trend usually referred to as a “jump shift”. This is generally more prominent in hole size changes at or below 8.25” in diameter.

- New logging tool may be run if the hole size changes dramatically (check notes and serial numbers on log headers).
- New mud system – operator may displace the mud system at a casing point especially in the production intervals or when changing from straight hole to deviated hole.
- New lithology, age or geological context – casing is set for a variety of reasons which may be related to many engineering decision points or be run for geological reasons alone.

2.6.3.1.3 In Situ Stress Effects on Compressional Sonic

Sonic speed in rock is known to be influenced by rock stress. Plona et al (2000) presented a new sonic tool technology to identify stress-induced anisotropy and thus providing a tool to determine or model stress orientation(s) through or around a wellbore. They showed that both the intrinsic and stress-induced anisotropy are clearly distinguishable using a dipole sonic tool. Anisotropy arises from structural effects such as fractures or layering of thin zones or local biaxial or triaxial tectonics stress within the formation. Acoustic anisotropy in a rock can be divided into two broad categories: Intrinsic and stress-induced.

The stress anisotropy may cause a 20% change in the shear sonic velocity but may cause a lower change in the compressional velocity.

2.6.3.1.4 Other Effects

If the well is deviated or there are dipping beds, the effect of anisotropy is manifested in 20 to 25% difference in the DT vertical versus DT horizontal. Greater than 40 degrees in well deviation or bed inclination is the beginning of significant anisotropy effect in layered shale, although not so much for sand.

2.6.4 Log Normalization

Anomalous or outlier log values from several wells presented a significant challenge to the DEA project team. This is common with the pressure prediction processes, and some comments are offered to help develop judgment in dealing with anomalies. There are typically two possibilities concerning the source of such anomalies:

- The outlier values may indicate a valid condition such as major change in lithology trend or structural feature such as a non-sealed fault. This might cause the analyst to use the outlier data to “seed” another population of data points representing outlier conditions such as new lithology or emplacement outside of the defined structural bounds for the study.
- The outlier data is simply bad data that should be either corrected or taken out.

The process of log normalization is outlined in a recent paper by Sheir (2001). Much of the following discussion has benefited from Sheir’s paper.

The objective of the normalization process is to reduce systematic meaningless noise within the data and recognize some random noise due to tool and rock changes. Environmental sources of systematic errors are mud filtrate invasion and filter cake, sidedbed effects, objects and/or material in the wellbore with magnetic susceptibility or electrical conductivity. Sheir contends that approximately 20% of porosity logs require adjustments and virtually all SP, Gamma ray, and GNT-type neutron curves require adjustment.

Available methods for normalization are listed below (Sheir, 2001)

- Statistical method (all wells)
- Visual comparison method (selected wells)
- Pick a well and compare

The reader is encouraged to consult the references for additional information on this method. In general all methods of log normalization utilize the following approaches:

- Shifting curves (scaling factors)
- Trend surface Analysis (detect regional changes or gradients)
- Histograms
- Cross Plot

2.6.5 Missing Data/Questionable Data/Unusable Data

Rarely does a well have a complete set of well logs from surface seismic well logs from surface to total depth. Well logs are often adversely affected by borehole conditions. The traditional solution is to empirically derive the missing data. Some of the familiar approaches are:

- Estimating compression wave velocity from resistivity (Faust, 1951)
- Estimating density from compression wave velocity (Gardner, 1974)
- Estimating shear wave velocity from compression velocity using lithology specific coefficients (Castagna, Greenber, and Chesser, 1992)

- Estimating compression travel time from density and neutron logs (Chesser)

2.6.6 Rating the Quality of Data

The following is a discussion of how to rate the quality of available data with examples and a grading scheme is presented to assign a confidence factor to the data. Flowcharts are presented to facilitate and show the integrated nature of the quality assessment and verification process.

As the following section is quite detailed the reader may wish to refer to it later as the need arises.

Figure 2-2 Quality Assessment of Geopressure Analysis Data

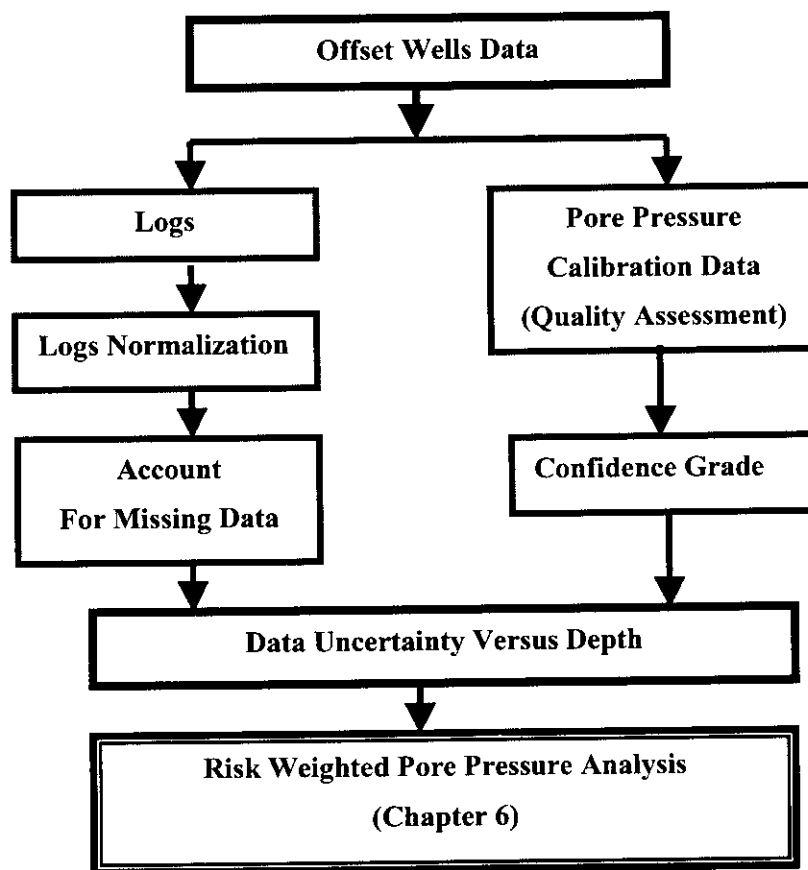
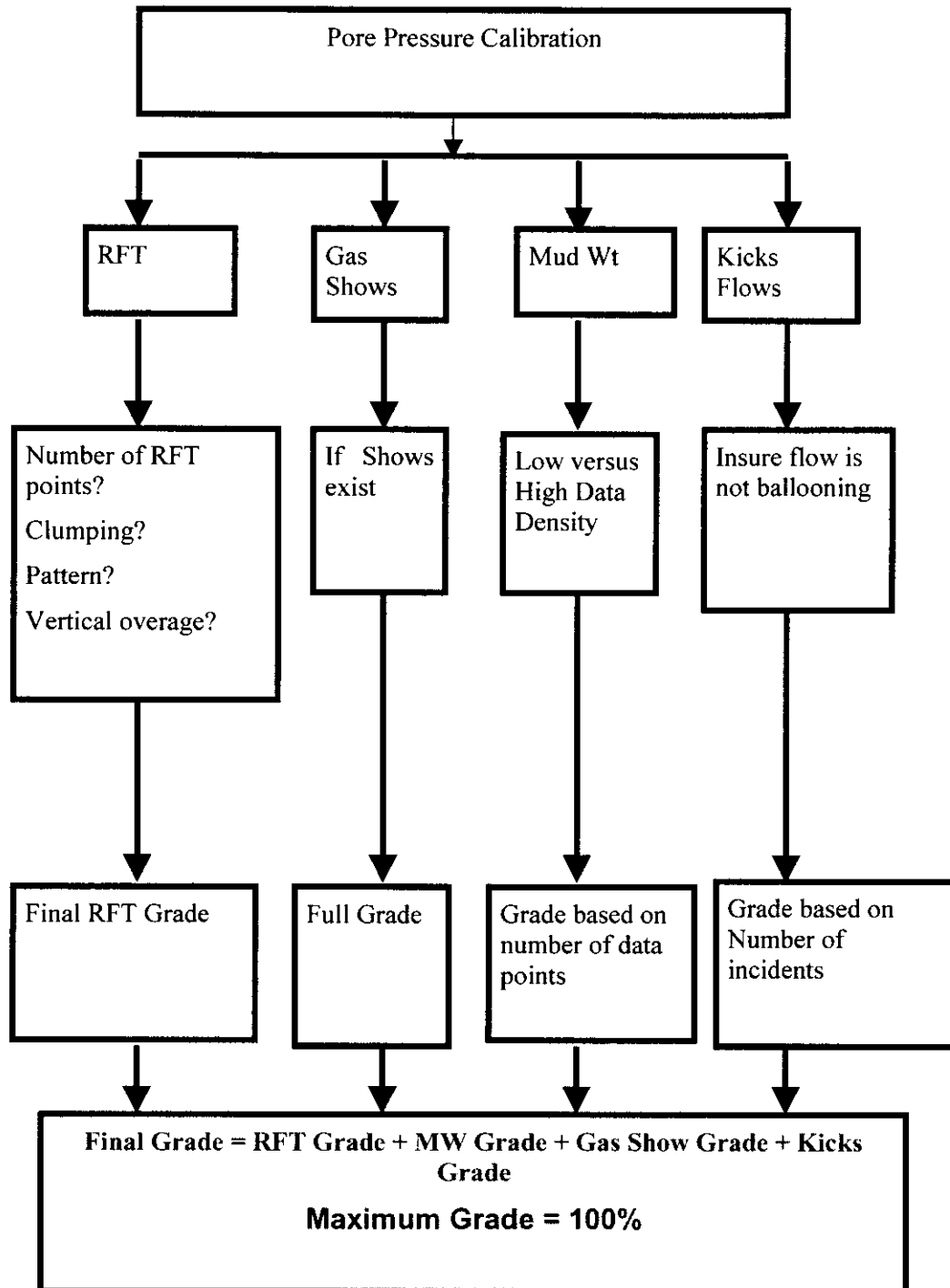


Figure 2-3 Offset Wells Calibration Data



2.6.7 Quality Assessment of Offset Wells Calibration Data

Offset wells are utilized to calibrate models for a prospect pore pressure prediction. Only a few known pressure points are required to calibrate a model, although providing a complete pore pressure profile for the logged intervals in all calibration wells is an optimum requirement. The verification of calibrated models along an entire well or well series is also an important part of the basin geopressure analysis (Chapter 5).

The following pore pressure indicators share common features - all of them can be strong quantitative measurements of pore pressure:

- RFT data
- Mud weight data
- Gas Shows
- Kicks and well flow

Methods to quantify the quality of each of these kinds of calibration data are discussed below and a weighting scheme to grade data quality is presented.

2.6.7.1 Evaluating the Quality of RFT Data

The rationale for grading RFT points is as follows:

- RFT measurements are affected by the tool and wellbore conditions
- If RFT measurement is taken in shale this almost certainly will give very low pressure in comparison to sand pressure. The reason for this is that shale's low permeability will not allow complete pressure transmission to the RFT tool.
- In some cases, RFT points are affected by poor seal between the tool and formation wall allowing leakage of drilling fluids.

The following is an objective, although somewhat arbitrary, way of rating the quality of RFT data points. Consider the following attributes:

- Vertical Coverage
- Number of RFT points
- Clumping
- Pattern
- Deviation of values from some reference such as mud weight trend

The following discussion gives the reasoning for RFT rating criteria:

1 Vertical Coverage

Vertical coverage (Figure 2-4) is important to validate a greater portion of the pressure profile.

Rating Scheme:

$$G_v = 10 * (1 - e^{-\lambda * (D_t - D_b) / 500})$$

Where: Gv Vertical Coverage Grade
 λ = 0.5
 D_t Top TVD of the pressure profile
 D_b Bottom TVD of the pressure profile

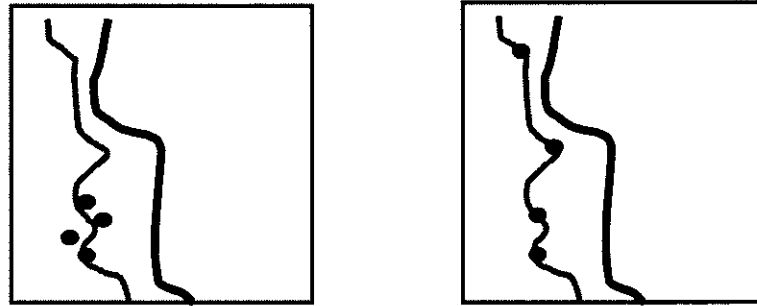


Figure 2-4 Comparison of Poor Vertical Coverage and Spacing on Left and Better Vertical Spacing shown on Right

- 2 Number of RFT points: Providing a grade for the RFT point is simple based on the fact that high quantity or “number” of RFT points will help to confirm pore pressure. Few greatly divergent RFT points is difficult to ascertain the representation of pore pressure.

$$G_n = 10 * (1 - e^{-\lambda * N})$$

Where G_n Grade points for the number of RFT points
 λ = 0.3
 N Number of RFT points

NOTE: Notice that RFT point count above 15 adds little value to the RFT grade. This is simply due to the fact that more points will not delineate the pressure any further (given good vertical coverage).

3 RFT Clumping

Figure 2-5 shows that clumping is not desired and has less value compared to uniformly distributed RFT points. In order to assess the “degree of clumping”, the moment of RFT points is introduced to gauge the functional uniformity of vertical distribution.

The clumping effect may be rated based on one or combination of the following suggested methods:

- Moment concept
- The Standard deviation method

Moment Concept: The moment of RFT points is introduced to gauge the functional uniformity of vertical distribution. The method is founded on the concept of computing a “moment” of each RFT point around an arbitrary horizontal axis. Similar to the definition of a moment in Mechanics, an RFT point moment is defined as the product of an assigned RFT value times its moment arm. An arbitrary horizontal axis (depth) is used as a reference to compute the depth distance to each RFT point depth.

The suggested mathematical equation to assign a numerical value to clumping grade is as follows:

$$G_c = 10 * [1 - e^{(-\lambda * \text{abs}(1 - MR))}]$$

Where	G_c	Clumping Grade
	λ	an exponent
	abs	Absolute Value
	MR	Moment Ratio

Moment Ratio = Moment of Actual RFT points / Optimum Moment

Moment of Actual RFT points = Sum of Moment of ALL RFT points

Moment of an RFT point = Moment Arm length * an arbitrary value given to the RFT point

Optimum Moment = Moment of RFT points if they are equally distributed vertically

The arbitrary value of an RFT point is NOT the value of the measurements (in ppg or psi). It is simply a number that rates the importance of that RFT point or group of points. For example, if we consider the upper half of RFT points are more correct than the bottom half, then we may elect to give the upper points value greater than the bottom RFT as follows:

Upper RFT points value = 1.0

Bottom half of the RFT points value = 0.5

If the RFT points all given the same weight regardless of their position, we may chose to give them the value of 1.0.

Standard Deviation Method: This method is based on the following procedure:

- The vertical depths between consecutive RFT points are computed
- The standard deviation of the of the depths differences is computed
- If the standard deviation is zero, this indicates that the RFT points are equally distributed with the same vertical distance separating them. In this case an optimum vertical distribution is achieved and a full grade is given.
- In the case the RFT points are not uniformly distributed on the vertical depth scale, the standard deviation will be more than zero. A maximum possible value of standard deviation will approach the maximum vertical distance between the shallowest and deepest RFT points depths.
- A clumping grade is given to the RFT points based on a certain criteria utilizing the standard deviation as an input.

NOTE: If we have only one or two RFT points, then a Clumping Rating shall not be applied.

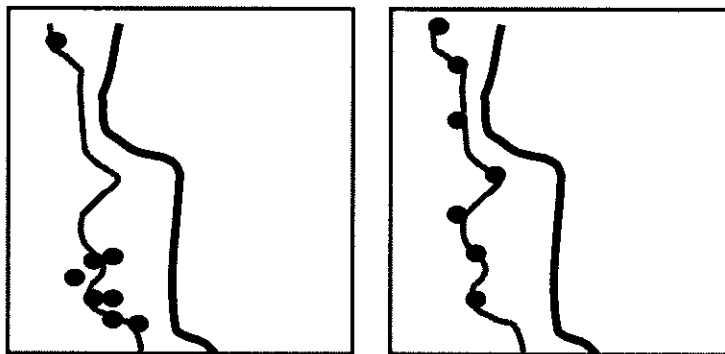


Figure 2-5 Clumping Pattern of RFT Points on Left Compared with Optimally Distributed Points Shown on Right

4 RFT Pattern

RFT pattern refers to the pressure differences between RFT points which may indicate problematic measurements or the discrete nature of a reservoir unit or sub-unit. Often, we can see RFT points showing ± 2 ppg in variation over a small vertical distance. In other cases, RFT points exceed the mud weight used. RFT points which exceed mud weight should not necessarily be considered as bad measurements.

A measurement of the lateral (horizontal dispersion) of RFT points is rated as a function of the standard deviation of the RFT points. Suggested equation is in the form:

$$G_p = A e^{-\lambda} * STDEV$$

Where

Gp	RFT pattern grade
λ	= an exponent
STDEV	Standard deviation of RFT points

Perhaps the standard deviation by itself is not a good measure of the pattern rating. An improved measure is the normalized STDEV which is written as follows:

$$\text{STDEV Ratio} = \text{STDEV} / \text{TVD Vertical Coverage}$$

Where TVD vertical coverage refers to the vertical depth covered by RFT points.

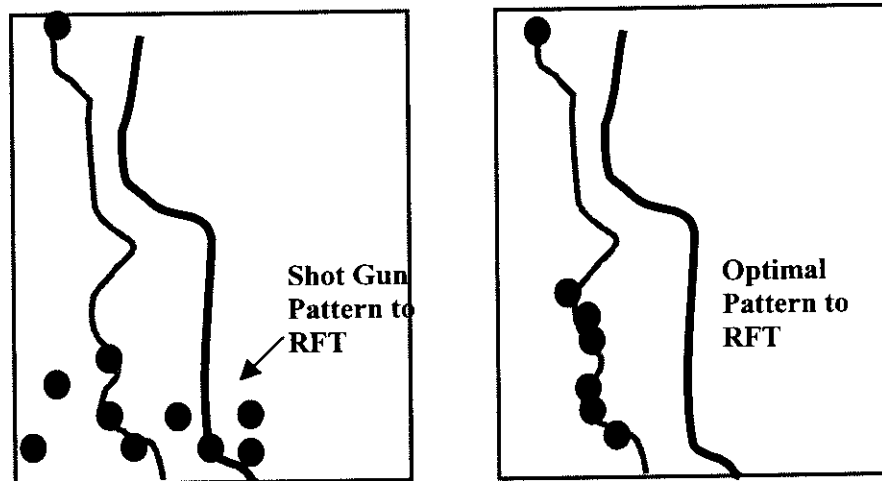


Figure 2-6 Illustration of Shot Gun Pattern Rating of RFT Points on Left and Optimal Pattern on Right

2.6.7.2 Mud Weight Data

Mud weight data can be of four distinct categories:

- Log Headers (casing point to casing point)
- Mud weight data available from daily API/AAODC report, drilling, mud log and MWD reports
- Foot by Foot mud weight data (MWD) which may include annular pressure
- Mud Log MWIN/MWOT continuous sensor plot (usually a formatted engineering log) and can be presented as part of a LAS/ASCII file.

The best data quality is the MWD data, which accurately incorporates wellbore condition (flow, cuttings, etc) during the drilling process. Any of the four categories may be found

in the database. Therefore, to provide a numerical grade to mud weight data, the rating system is based solely on the number of available data points.

$$G_{mw} = A * [1 - \text{EXP}(- \lambda * N)]$$

Where,

G _{mw}	Mud Weight grade
λ	an exponent
N	Number of MW data points
A	constant

Notice that the mud weight data points function allow an asymptotic approach to maximum grade value at about 200 points. This indicates that data points beyond 50 add little resolution (or value) to the calibration of pore pressure.

2.6.7.3 Gas Shows

The value given to gas shows is based on simple criteria:

If the mud logging service provides gas shows, then full maximum value is given. Otherwise, the value is zero.

2.6.7.4 Well Flow and Kick

If proper data is taken and analyzed in a kick or well flow incident, the confidence in pore pressure estimate derived from this information is very high. In fact, one pore pressure value from kick or well flow may be valued higher than two or three RFT measurement. The grade given to kicks or well flow can be measured by a similar equation used for mud weight data.

2.6.7.5 Apply a Weighting Scheme to Grades

The weighting scheme is required to adjust the maximum value that can be allocated for any given indicator of pore pressure. This project adopted a weighting scheme that allocated a maximum value to RFT values of 42% of total possible grade (100%). The mud weight data was rated up to 35%. The remaining (27%) was shared by the kicks and gas shows.

The sum of all the possible grades to gives the final confidence grade in the calibration data. This grade can be used for the following purposes:

- As a rough measure of the confidence in the estimated pore pressure profile in the “Definitive Pore Pressure” assigned to the offset well.
- As a weighting factor for calculation of “Uncertainty Adjusted” error in the predicted pore pressure.

2.6.8 Discussion of Geopressure Indicators

2.6.8.1 RFT Data

RFT data is one of the most difficult to acquire accurately as indicated by the nature of the many "scatter or shotgun patterns" common to the data plots. Many times, the tight spacing is caused by the effort to get a valid pressure test in less than optimum conditions for a point of interest. All points are usually plotted without any attempt to qualify them. Only the RFT engineer or geologist (if present) will retain a feel for the testing program.

When taking RFT' measurements in laminated formations where intercalated limes or shales form perfect (competent) seals, the variation in formation pressures can be dramatic (from normal to overpressured), even over short intervals of one to two feet. In some cases the scatter pressures accurately reflect true formation pressures, yet create a statistical problem for use in modeling and calibration.

2.6.8.2 Mud Weight Data

The best source of mud data is the daily mud reports. The second best data quality is the MWD or Mud Logging data, which accurately incorporates wellbore condition (flow, cuttings, etc) during the drilling process. Generally, the MWD software relies on a data feed from the Mud Logging Database for basic mud properties. A standalone mud logging operation relies on the mud logger to generate the APL and other calculated data derived from mud weight. Often, this data is of questionable quality for many reasons including lack of understanding or training of the mud logger in drilling fluid mechanics. Any of these categories may be found in the database but the analyst should not assume they are correct.

Mud weight is only a good dataset if it was incrementally altered in response to well bore behavior and not to a set of pre-defined requirements.

2.6.8.3 Kicks, Well Flows and Lost Circulation

Well flows or kicks can result from drilling into pressured formations or reduced mud densities caused by surface water additions or by down hole influxes of formation water.

- Location of a kick or flow indicates the depth at which mud weight became too low for effective well control or formation fluid is pressured (both indicate onset of possible abnormal pressures).
- Some have argued that kicks may also indicate the onset of one of the first effects of drilling into a seal containing excessive amounts of fluids generated by shale diagenesis. These fluids typically contain high or concentrated chloride levels and are being injected into an underlying sand (typical Gulf Coast style condition). Watch the temperature profile if available from MWD tools or do progressive plots of wireline BHT data as the well is logged. Watch for decreased or surging well flow when drilling and beware of alternate "loss and gain" conditions.

- If the available data includes a shut-in pressure (shut-in drill pipe pressure-SIDPP and/or Casing Pressure - CASP or ideally Initial pressures/ISIDPP/ICASP, and Final pressures/FSIDPP/FCASP then the data can be used to definitively calibrate and verify further analyses.

2.6.8.4 Gas Shows

- Gas shows marked on mud logs should be used to set a mental flag reserved to enhance interpretation of the modeled results and processes.
- An experienced analyst can use the magnitude of the event, duration and curve characteristics to enhance and help evaluate, verify or calibrate a pressure.
- A lost circulation mud weight can also be of value if the depth of loss can be located with certainty, since the lost mud weight can be converted to an effective hydrostatic at that depth (gradient estimation derived). Similarly, a gas cut mud weight and a known uncut mud weight can be used to estimate a formation pressure. Often early returns of gas peaks or Total Gas background shifts will “lag back” to the vicinity of lost circulation zone(s).
- A gas cut or Halliburton mud weight which will also allow an estimate for formation pressure (more gas cut points, the better). Mud reports should be evaluated to see if gas-cut mud returns were associated with salinity (chlorides) changes.

References

- Sheir, Dan, Personal communication, April 25, 2001.
- Greene, K., “Normalizing Technique Helps Plot Pressure from Logs”, *Oil & Gas Journal*, October 23, 1978. pps 147-156.
- Ham, H.H., “A Method of Estimating Formation Pressures from Gulf Coast Well Logs”, *Transactions Gulf Coast Association, Geological Society*, 1996, Vol. 16 pp. 185-197.
- Plona, T.J., Kane, M.R., Sinha, B.K., Walsh, J. and Vilorio, O., “Using Acoustic Anisotropy”, 41st SPWLA Symposium, June 2000.
- Hornby, B.E. and Robert O’Connor R., “Determination of Very Slow Gas-bearing Formation Velocities using Borehole Sonic and Borehole Seismic Measurements”
- Plona, T.J., Sinha, B.K., Kane, M.R., Winkler, K.W., and Frignet, B., “Stress-induced Dipole Anisotropy: Theory, Experiment and Field Data”, SPWLA Symposium, 1999.
- Faust, L.Y., “Seismic Velocity as a Function of Depth and Geologic Time”, *Geophysics*, 1951, Vol 16, pps 192-206.
- Catagna, J.P. and Backus, M.M., “Offset-dependent Reflectivity – Theory and Practice of AVO Analysis”, *Investigations in Geophysics*, No. 8, S.E.G.
- Greenberg, M.L. and Castagna, J.P., “Shear-wave Velocity Estimation in Porous Rocks: Theoretical Formulation”, *Geophysical Prospecting*, Vol. 40, 195-209.



3 Determine Geopressure Prediction Strategy

The geopressure prediction strategy depends on a number of factors with the primary ones having to do with the availability of quality data, appropriate software tools, and of course, adequate time and budget. This is a crucial part of the planning process for a well and deserves serious consideration. There are a number of “train wrecks” where safety and cost problems vividly illustrate the results of inadequate attention to this important area.

The data and requirements recommended in this manual may be considered by some readers to be excessive, and indeed may be excessive for routine wells on the continental shelf. One should weigh the costs of obtaining these data against the potential costs incurred from unforeseen drilling problems. Problem costs on a five million dollar well do not get the attention and scrutiny that they do on a fifty million dollar well. For wells in the deep water where drilling costs are measured in the tens of million of dollars and daily costs for drilling rigs approach several hundreds of thousand dollars, it can be very shortsighted to attempt to economize on the important planning effort required to predict geopressures. While such tasks as re-processing seismic velocity data for better resolution or the team effort required to build a geopressure basin model are costly in time and money, these items can make the difference between success and failure in drilling a well in the deep water.

As a benchmark from a non-related but comparable industry, the long established architectural and engineering planning costs for the construction of a new building are typically in the range of 10% to 15% of the total cost of construction. Applying this rate to the construction of a deep water well that will cost \$25 million, \$2.5 to \$3.75 million should be spent on the planning process. This translates into 17,000 to 25,000 planning hours or 2100 to 3100 planning days. Given the lean staffs that characterize the oil and gas industry today, this time is not typically spent. There needs to be a better recognition of these issues and their importance to the industry.

This chapter attempts to provide guidance for the selection of a strategy to predict the geopressures required to plan a well in the deep water. The concepts of overpressures and high overpressures are introduced, with some guidelines to help determine when high overpressures might be anticipated. The possibility of high overpressures impacts the strategy significantly as this factor can justify more extensive efforts to predict overpressures than would otherwise be the case. Given the proven superiority of predictive results, a basin approach to geopressure prediction is clearly preferable, so the strategy on the surface seems very simple. However, as discussed in earlier chapters, the data requirements for a basin analysis are demanding and not always available for a rank exploration well.

3.1 Overpressures and High Overpressures

Dr. Glenn Bowers introduced the concept of “overpressures” and “high overpressures” in an important paper titled “Determining an Appropriate Pore-Pressure Estimation Strategy” presented at the 2001 Offshore Technology Conference. High overpressures can be defined as those where the pressures in the shales are not in equilibrium with the pressures in the adjacent sands. These high overpressures are typically a result of some

source such as thermal expansion, hydrocarbon generation or charged sands *in addition* to the overpressures caused by undercompaction. Overpressures, on the other hand, are the pressures from undercompaction that can be readily quantified at a given depth using various models that compare actual and normal compaction in shales as measured by some porosity or effective-stress indicator such as seismic interval velocity. High overpressures require a high pressure prediction technique that is more involved than the traditional overpressure prediction techniques. These techniques are discussed in some detail in Chapter 4 of this manual as they relate to concepts most often referred to as Unloading or the Centroid theory.

Serious drilling problems can develop when high overpressures occur in wells where only overpressures have been anticipated. More than once, these problems have resulted in the loss of a well. Shallow water flows are a classic example of high overpressures.

Some guidelines from Bowers' paper are included in Chapter 4 to help identify those cases where high overpressures are possible. For those cases, there are obvious justifications for more planning than for the well expecting only overpressures. For example, the expectation of high overpressures can help justify the cost and effort required for basin modeling of geopressures as basin modeling considers most of the pressure sources that produce high overpressures.

3.2 When to Use Basin Modeling for Geopressure Prediction?

If there is sufficient data available, the best results are produced by building a basin model to predict geopressures at new well locations. The basin model provides an effective way to correlate results from offset wells drilled in the area. Additionally, the pressure mechanisms such as hydrocarbon maturation and thermal expansion as well as the lateral movement of formation fluids as affected by sealing and non-sealing faults are considered by basin modeling. If there is not sufficient data available, then the only recourse is to perform a single well analysis using offset wells (if available) for calibration. It should be noted the basin analysis also requires a single well analysis for the wells that will be used to calibrate the basin model.

While basin analysis has proven to be a superior way to predict geopressures at a proposed well location, the amount of varied data required to perform such an analysis is extensive. Further, the construction of a geopressure basin model requires more geological expertise than the typical drilling engineer possesses, so a team effort is usually required for success.

The model scope must be properly sized or it will be difficult to calibrate. For example, in the DEA 119 Project, the first attempt to use basin modeling for geopressure prediction involved attempting to build a model of the entire deep water section of the Gulf of Mexico as shown in Figure 3-1. As more geologic knowledge came to bear on the effort, it was realized that the Gulf of Mexico includes a number of mini-basins, most of which are embedded or surrounded by salt, as shown in Figure 3-2.

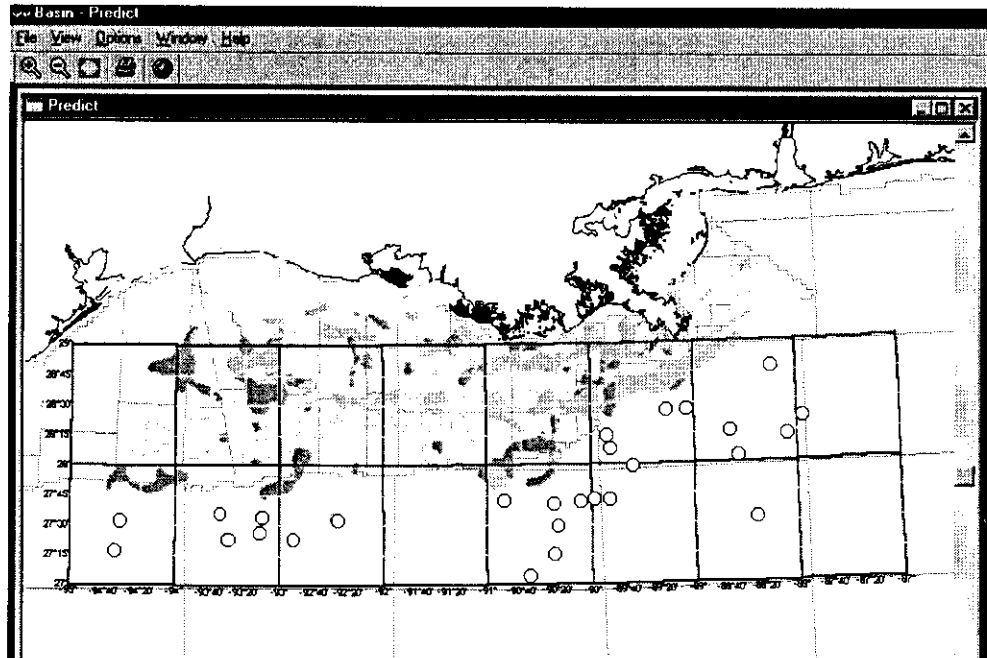


Figure 3-1 The geology of entire Gulf of Mexico deep water area is too variable for a single basin model.

It was then decided to select a well-defined mini-basin to evaluate the effectiveness of basin modeling for geopressure prediction. The Auger Basin was selected because it is a well-known basin in the GOM and also because several wells were available in the database that had definitive data suitable for calibration and prediction.

The process for construction of a geopressure basin model is summarized in Chapter 5 of this manual. Once a model is built and properly calibrated, the steps required to make a geopressure prediction at a new proposed well location are quite easy.

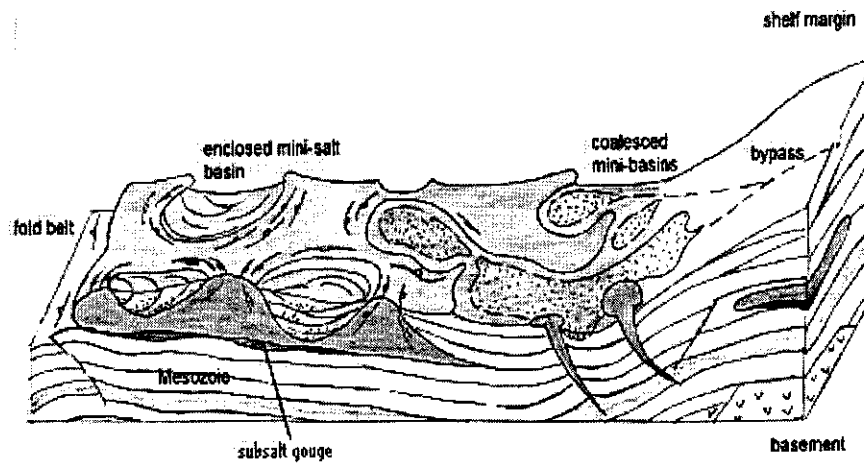


Figure 3-2 Schematic diagram illustrating GOM geologic provinces

3.3 Geopressure Prediction Without Basin Modeling

When there is insufficient data for constructing a geopressure basin model, the alternative is to make a prediction using the data at hand. In the case of a rank exploration well in a new area, typically the only data available is seismic interval velocity data at the proposed well location. To emphasize the points made in Chapter 2, every effort should be made to verify that the data has been prepared in accordance with the recommended guidelines in Chapter 2 and Appendix C. The other important consideration repeated again here for emphasis is to make every effort to determine whether overpressures or high overpressures are to be expected. The steps and data required for geopressure prediction for a single well are contained in Chapter 4 of this manual. Chapter 6 presents the Monte Carlo simulation for using velocity profiles from multiple-shot points around a proposed well location to obtain a prediction.

4 Single Well Analysis

4.1 Introduction

This chapter is written to guide drilling engineers and geoscientists through the maze of different considerations in geopressures (overburden and pore pressure) prediction for wells in deep water. New methods and models developed under the DEA 119 project are introduced where appropriate with guidelines for their application.

The process of geopressure analysis for a single well can be organized into four major steps:

- ❑ Review and input data inventory into geopressure software, then make a data assessment and verification as described in Chapter 2.
- ❑ Access geologic setting of prospect for geologic impacts such as structure, salt proximity, fault blocks or mini-basin. Review seismic cross-sections to determine if dipping beds or structures require consideration of Centroid Effect. Identify faulted or uplifted effects. Develop calibration parameters based on offset wells data analysis utilizing compaction trend methods, new models and/or overburden stress.
- ❑ If there is a Centroid Effect, extrapolate sand pore pressures along fluid gradient from shale pressures profile.
- ❑ Compute shale pore pressure profile.

Geopressure analyses typically assume that a pore pressure measured in a sand should equal that in an adjacent shale. Accordingly, most geopressure models are designed to determine geopressures in shales by analyzing changes in porosity and density with depth as measured by various downhole sensors utilized with wireline and MWD/LWD tools.

However, as documented in several recent technical papers and confirmed by the DEA 119 project data analyses, there are situations where this is not the case. Dipping beds and other geologic structures can result in hydrodynamic effects in which sand is pressured significantly higher or lower than the adjacent shales. These cases can be explained with a concept called the Centroid Effect and examples are discussed herein.

Somewhat related to the Centroid Effect is the theory of Unloading. The source of high excess geopressures can be caused by factors other than undercompaction, such as geologic uplift and erosion, internal fluid generation from hydrocarbons, or thermal expansion effects. These features can result in high overpressure as defined in Chapter 3.

Some examples of these concepts are presented in this chapter with guidelines for when to consider them. The examples are taken from the DEA 119 database. It should be stressed that there are few “text book” examples to illustrate one concept on an isolated basis.

4.2 Procedures

The above listed major steps or phases to undertake a pore pressure analysis represent a global approach. The following provides more detailed guidelines on how to perform the subtasks within those steps.

4.2.1 Data Quality Assessments

The reader is referred to Chapter 2 of this manual for a detailed discussion of available data and how to assess the quality. The basic understanding of the data should be focused on the following issues:

- Quality of velocity data at the prospect location. Match seismic and checkshot data of offset wells to determine corrections needed to prospect's seismic data.
- Should the estimated seismic interval velocity that did not show a velocity reversal be adjusted to accommodate known velocity reversals observed at certain formations in the offset wells?

4.2.2 Assess Prospect Geologic Setting

Understanding the geology and geologic setting of a prospect can provide a large amount of information about how to develop offset calibration data and conduct a pore pressure analysis. Much of this information would be developed as a part of a Basin Analysis if this step is undertaken as discussed in Chapter 3. If not, the pore pressure analyst should consider the geologic setting of the prospect area when selecting and assessing offset well data to make sure that depositional settings (sediment sources and rate), the proximity to salt bodies, etc are as similar as possible. Determining geological structure elements, specifically sand bodies with large relief, is important in deciding which part of the section to match pressure data and in developing calibration points.

The analysis of a centroid effect is not limited to the prospect well data, however. The same analysis should be done on the offset wells to properly define the definitive pore pressure. The definitive pore pressure is used to calibrate the conventional models and selection of new DEA 119 models for subsequent use in the prospect analysis. This will be discussed in detail in the offset well analysis section.

4.2.3 Analyze Offset Well Data

Analysis of offset wells is the most time consuming part of the pore pressure prediction process. The ultimate objective is to provide key parameters for the prospect's well analysis. The following analysis should be performed:

- Determining OBG for the prospect
- Determining adjustment factor(s) for seismic data
- Identify top of pressure transition
- Develop compaction trend
- Identify unloading

- ❑ Identify centroid effect
- ❑ Calibrate conventional models
- ❑ Apply the new DEA 119 models

A detailed discussion of the above list is presented below.

4.2.3.1 Determining OBG Profile and Correcting for Prospect Water Depth

The overburden pressure can be derived from several options listed and discussed in Appendix E of this manual. Therefore, the reader is referred to Appendix E for additional details.

Overburden for the prospect well can be determined from two sources:

- ❑ Offset well density data
- ❑ Calibrated seismic or sonic velocity to density transforms.

There are three types of data that may be used to develop an OBG to the prospect. Identify the available data in order to select a procedure. They are listed according to a suggested order of priority – perform the first one that applies:

- ❑ Offset density data
- ❑ Prospect interval velocity data
- ❑ Offset Sonic data

4.2.3.1.1 *Offset Density Data*

- 1 Convert density log data depth reference to depth below the mudline.
- 2 Insert shallow density data using ODP (Ocean Drilling Program) data and the best-fitting interpolation equation (recommended procedure is given later in this section).
- 3 Insert values of 2.16 into any identified salt intervals.
- 4 Integrate the densities to obtain overburden pressures (recommended procedure later in this section).
- 5 Compute the prospect's water column pressure.
- 6 Add the water column pressure to the overburden pressures.
- 7 Convert the pressures to gradient units.
- 8 Extrapolate the OBG as necessary such that an OBG can be computed to the anticipated total depth of the prospect well.

Recommended Procedure for Adding Missing Density Data

The following procedure is intended to integrate log data and shallow sediments density data to obtain the OBG for a well. Typically, a density log is not available for the entire column of sediments. Common practices to fill in the missing density data are:

- Using average density value
- Using linear interpolation between the top of the log and an assumed surface value at the mud line.

In both cases significant error can arise with subsequent errors in pore pressure estimates and fracture gradient. It is not uncommon to have more than 4000 ft of vertical depth below the mudline without direct measurements of bulk density from density logs or sonic-derived density values. Seismic data at shallow depths are not reliable for such estimates.

For shallow density values, published data from the Ocean Drilling Program (ODP) whose data are archived by Texas A&M University, can be used to fit an interpolation scheme. Figure 4-1 shows the integrated OBG profile utilizing shallow sediments density (per area or basin) and limited density log data.

Integrating the Densities to Calculate the Overburden Pressure

The overburden is simply the weight of materials above the depth of interest. This can be obtained by integrating the density data or approximated by summing the average densities of finite thicknesses of sediments. Because the density typically increases non-linearly with depth, the layer thicknesses should be no more than 50 ft at depths below the mudline less than 3000 ft. Layer thicknesses can be increased to 100 ft or more at greater depths once densities changes more slowly with depth.

$$\text{Overburden stress} = \sum (D_i - D_{i-1}) * [(\rho_{bi} + \rho_{bi-1}) / 2] \dots\dots\dots \text{EQN (4.1)}$$

Where D_i depth below the mudline of the bottom of the i^{th} layer
 ρ_{bi} bulk density at depth i below the mudline

For example, let us assume a bulk density of 2.17 g/cc at 3000 feet and a density of 2.19 g/cc established at 3100 feet. The pressure contributed by the layer extending from 3000 to 3100 feet is considered to be the same as that contributed by a layer with an average density of $(2.17 + 2.19) / 2 = 2.18$ g/cc. The total contribution of the layer to the overburden is calculated by converting the average density to psi/ft using the appropriate conversion factor and then multiplying that gradient by the thickness.

$$((2.17 \text{ g/cc} + 2.19 \text{ g/cc}) / 2) * 0.4335 \text{ (psi/ft) / (g/cc)} * (3100 \text{ ft} - 3000 \text{ ft}) = 94.5 \text{ psi}$$

The pressure due to seawater column is computed in a similar manner, an average density of 1.03 g/cc for the seawater is a reasonable value to use.



Once the overburden stress in reference to depth below mudline is computed, the effect of water depth is included by simply adding water pressure to overburden stress at each depth point. The overburden gradient (OBG) is then calculated by converting the pressures to gradient.

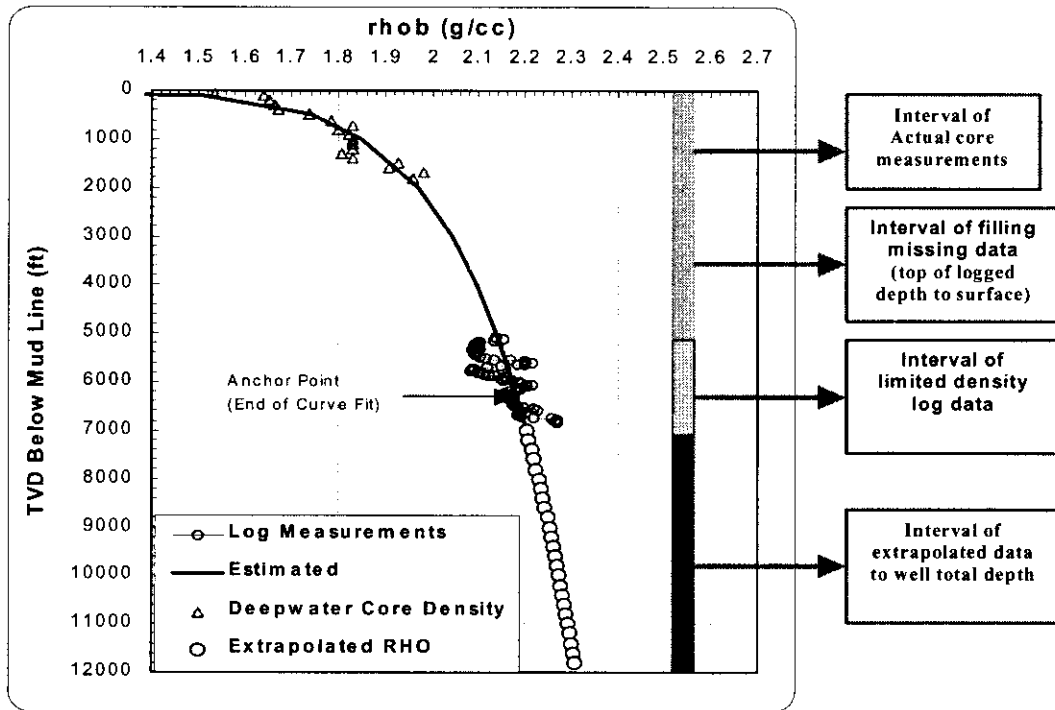


Figure 4-1 Integrated Density Profiles

Three Fitting Equations for Missing Density Data:

Missing data is typically from mudline to the top of the density log. In addition, if the density log interval is short, density data below the logged interval must be extrapolated. To fit an equation between the mudline and top of logging interval, three possible fitting equations may be used, namely:

- An exponential equation of the form

$$\text{Rho} = \text{Rho}_s - (\text{Rho}_s - \text{Rho}_m) e^{-k \cdot \text{ML}} \dots\dots\dots(\text{EQN 4.2})$$

Where: Rho density at a given depth below the mudline
 Rho_s density of the shale solids, e.g. 2.6 – 2.8 g/cc
 Rho_m density at the mudline, e.g. 1.3 – 1.5 g/cc

- e base of (natural) logarithms
- k empirical compaction constant, e.g. 0.000085 ft⁻¹
- ML depth below the mudline, ft

□ A power fitting equation of the form:

$$\text{Rho} = A * \text{ML}^N \dots\dots\dots(\text{EQN 4.3})$$

- Where:
- Rho fitted bulk density of sediments
 - ML total vertical depth below mud line
 - N an exponent
 - A an empirical coefficient

N can be estimated from the following: Using the anchor point coordinates (rho_d, ML_d):

$$N = [\log(\text{rho}_d/A)] / [\log(\text{ML}_d)] \dots\dots\dots(\text{EQN 4.4})$$

The table below is a guide to using this equation:

Variable	Value	Comment
Rho _{ml}	1.5 gm/cc	Fixed density value at the mudline
Rho _{deep}	2.5 to 2.68	Variable value to accommodate the state of stress in the formation at depth.
n	0.00023	This exponent can be varied until best match is obtained.

□ Two-parameter Exponential Equation (Miller, 2001):

Miller suggested using the following equation to match shallow sediments density data in a two-step process:

First: Compute the porosity from the following equation to match known shallow core data (Ocean Drilling Program , ODP, public domain database)

$$\phi = \phi_a + \phi_b \exp(-\kappa * \text{ML}(1/N)) \dots\dots\dots(\text{EQN 4.5})$$

- Where:
- $\phi_a + \phi_b$ mudline porosity
 - ML depth below mudline in feet



κ and N are empirically determined parameters that provide a reasonable fit to the data.

Second: Compute the bulk density (ρ_b) as follows:

$$\rho_b = \rho_s (1 - \phi) + \rho_w \phi \quad \dots\dots\dots(\text{EQN } 4.6)$$

Where: ρ_s average density of the sediment grains (2.65 for sands, 2.70 for shales)

ρ_w density of the pore water (1.03 gm/cc)

Approximate values for the parameters are shown in the table below:

	ϕ_a	ϕ_b	κ	N
Shale	0.09	0.69	0.00086	1.15
Medium Shale	0.12	0.60	0.00086	1.12
Siltstone	0.20	0.38	0.00088	1.08

NOTE: The process of integrating all data (shallow, missing data, extrapolated data, and logged data) assumes that the missing density data are in normally pressured sediments. This may be not correct if there is only a short logged interval and the data is extrapolated to greater depths where undercompaction is expected. In this case, the integrated density profile will yield higher than actual overburden stress.

If you have used the Miller equations of estimating densities, the effect of over pressure can be approximated by simultaneously increasing ϕ_a and decreasing ϕ_b by the same amount until the approximate sediment density equals the log density at the top of the log.

Example: Evaluation of the Three Fitting Equations

Figure 4-2 shows the performance of the three fitting equations on well GB 602. The power law equation (EQN 4.2) has a better fit to shallow data than the others. However, if the same equation is used to extrapolate for density values below the logged interval, then EQN 4.1 is best.

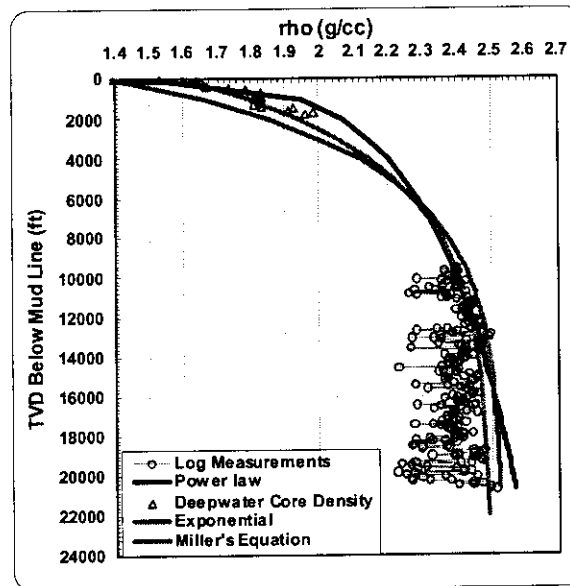


Figure 4-2 Illustration of Three Fitting Equations to Density Data

4.2.3.1.2 OBG from Prospect Interval Velocity Data

Convert the velocity data to synthetic density data using the DEA 119 transform:

- 1 Calculate porosities from the interval velocities: $\phi = (1 - V / V_m)^{1/x}$
 - ϕ porosity
 - V seismic interval velocity
 - V_m matrix velocity, 14913 ft/sec
 - x 2.19
- 2 If porosity is less than 40%, calculate densities: $\rho_b = \phi \rho_f + (1 - \phi) \rho_m$
 - ρ_b bulk density, g/cc
 - ρ_f pore fluid density, 1.03 g/cc worked well in DEA 119 study
 - ρ_m matrix density, 2.60 g/cc worked well in DEA 119 study
- 3 If porosity is greater than 40%, supply missing density values according to the interpolation scheme described above.
- 4 Integrate the densities to obtain overburden pressures
- 5 Extrapolate the OBG as necessary such that an OBG can be computed to the anticipated TD of the prospect well.

4.2.3.1.3 Using Offset Sonic Data

Convert to synthetic density data using steps 1-3 of prospect interval velocity data procedure outlined above.

- 1 Depth shift the composite density dataset by the difference in water depths between the offset and prospect wells.
- 2 Integrate the shifted densities. Add the prospect's water column pressure (if not done in step 3 of interval velocity conversion).
- 3 Convert the pressure to gradient units
- 4 Extrapolate the OBG as necessary such that an OBG can be computed to the anticipated TD of the prospect well.

Example: Overburden No 2 (The effect of salt sections)

The presence of salt in the sedimentary column presents a unique feature to the overburden gradient calculation. Salt is non-porous and has a uniform density of 2.16 g/cc. When it is ascertained that the well penetrates salt, the density for the salt-filled interval should be set to 2.16 g/cc.

There are several ways to identify the presence of a salt body. To a geophysicist, salt can be recognized due to the lack of coherent primary reflectors within a thick section. In addition, the characteristic "dome" shape, or intrusive character, of many salt bodies, with associated draping and drag deformation of the pierced formations helps to provide structural evidence of the presence of a salt body. Finally, petrophysical logs can also readily signal the presence of salt: uniformly low Gamma ray intensity, high resistivity, consistent bulk density log values of 2.03 – 2.06 g/cc, -2% Neutron porosity or sonic transit time of 67 microseconds per foot.

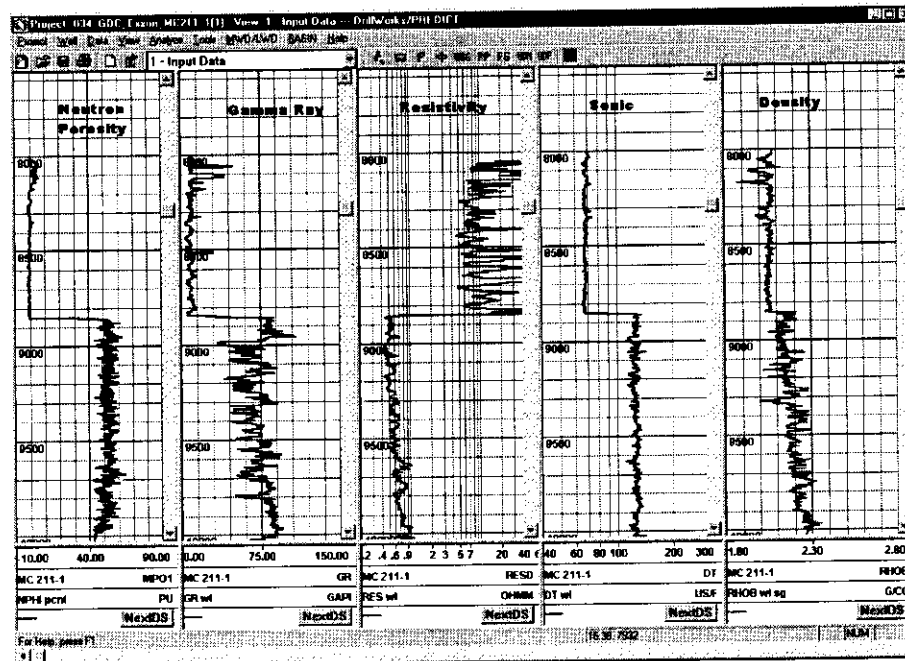


Figure 4-3 Sample Sub-salt data from DEA 119 database

4.2.3.2 Determining Adjustment Factor for Seismic Interval Velocities

In general, the seismic interval velocities on a well should closely match the check shot results and the sonic log porosity trend. This naturally assumes that all three sets of data have been converted to a common basis, such as interval Δt 's or interval velocities. However, a problem can arise because seismic interval velocities are affected by anisotropy and noise as a result of the horizontal separation between the acoustic source, the receiver and the resultant non-vertical reflection path.

If we assume that check shot data that has been converted into interval Δt 's or interval velocities will provide an accurate representation of the corresponding seismic interval Δt 's or interval velocities with the associated anisotropic effects removed, then it should be possible to improve the quality of the seismic data by making it agree more closely with the checkshots. A relatively simple way to do this is to ratio the seismic values up or down by trial-and-error until the misfit between the seismic data and the check shot data is minimized. The required seismic correction factor should definitely be less than 10%, and, hopefully, less than 5%. This technique should be regarded as a fairly quick way to generate a reasonable solution to the problem. It is not meant to be scientifically rigorous.

Although checkshot data is preferred because it most closely mimics results that would be expected from fully normalized seismic data, it is not always available. If there is no checkshot data available or if it is incomplete, then it is possible to apply the technique

mentioned in the preceding paragraph to sonic log data. When sonic logging data is used, it is probably best to try to match the seismic interval velocities or interval Δt 's with the sonic log shale porosity values, usually the filtered sonic shale points, rather than the raw sonic data. Again, the idea is to ratio the seismic data up or down to improve the overall fit between the seismic and the sonic.

In practice, seismic, sonic and check shot data may all be available on an offset well, but, only seismic data will be available on the prospect. If the prospect is geologically similar to its offset, then it may be reasonable to determine the required seismic correction factor on the offset and then apply it to the seismic data on the prospect.

In the figures below, a 7% correction factor was applied to the seismic data to improve its fit with the check shot and the sonic shale porosity trend. The 7% figure was derived through trial-and-error. In Figure 4-4 the data was converted to interval Δt 's. In Figure 4-5 the same data was converted to interval velocities. In both figures, the black line represents "uncorrected" seismic interval Δt or interval velocity, the red represents the filtered shale points from the sonic log, and the yellow represents the check shot data converted to interval Δt 's or velocities. In both figures, the 7% correction factor resulted in an improved fit of the seismic data to the sonic and the check shot, particularly in the deeper sections. The 7% correction factor was later used in adjusting the seismic interval velocities on a geologically similar offset.

In actual practice, it may not be possible to obtain a good fit in the shallower sections, so it is better to concentrate on improving the fit in the deeper sections. The misfit in the shallower sections can be largely attributed to water depth changes along the seismic line and to systematic errors in processing the shallow seismic data.

Check shot to seismic velocity calibration is used to determine the magnitude of the necessary anisotropy compensation. The seismic velocity data is adjusted to remove the systematic bias that arises from the differences between the check shot velocity and seismic velocity data. The determined anisotropy factor is then applied to the seismically derived time-to-depth function at the proposed well location. Failure to apply anisotropy correction can result in a biased depth prediction of pressures (Wilhelm, R., et al., 1998)

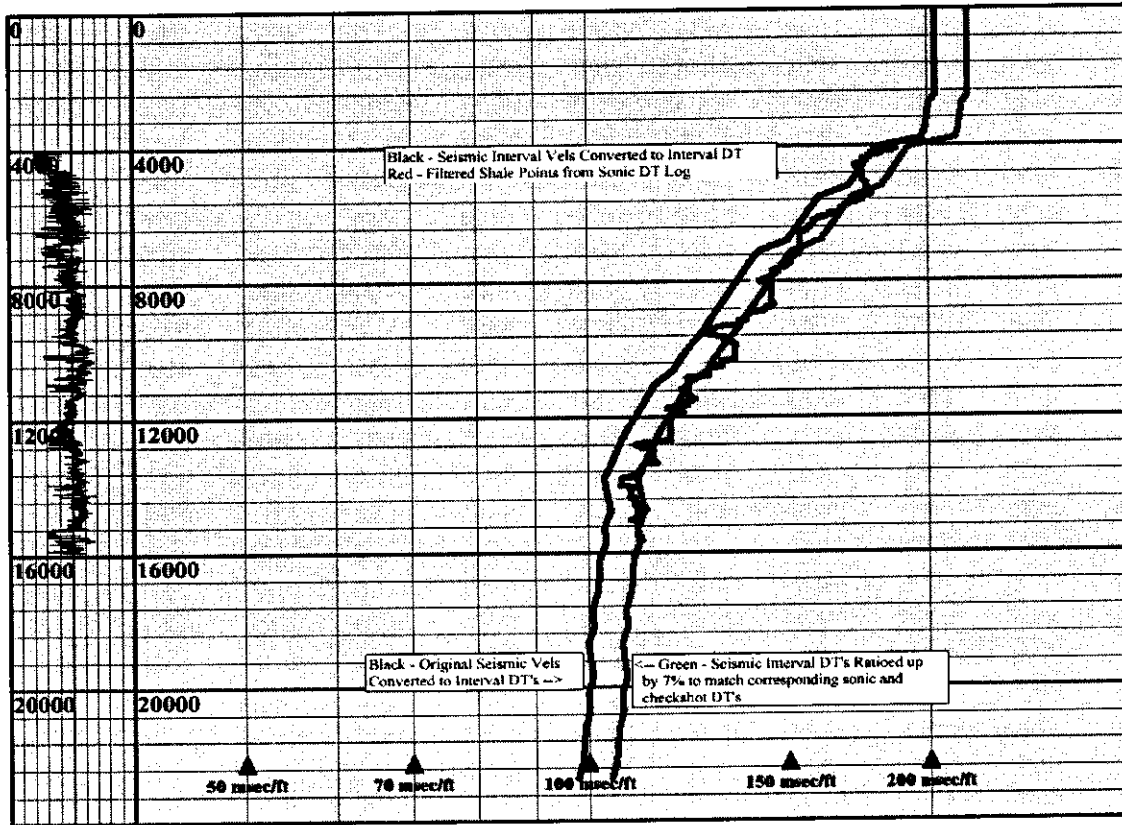


Figure 4-4 Illustration of Adjusting Seismic Interval Velocities to Match Checkshot Data



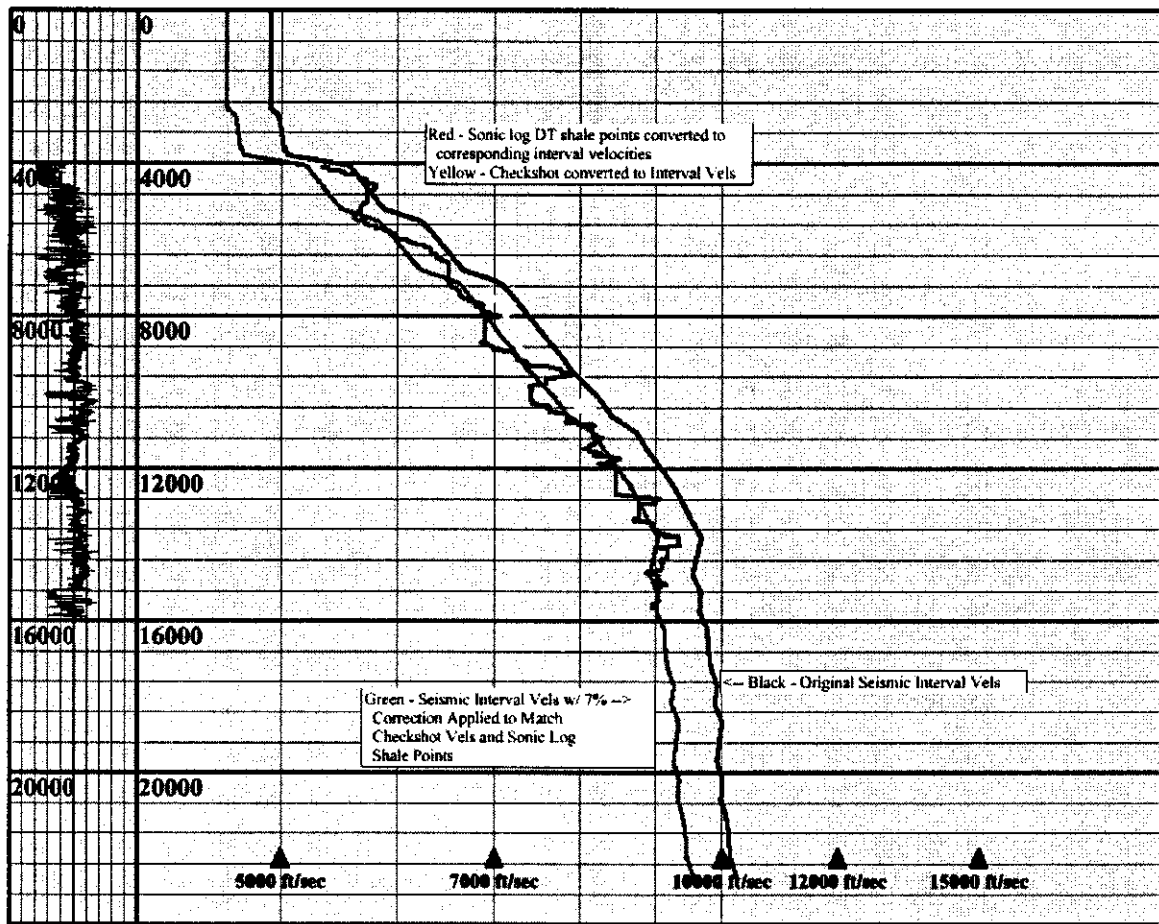


Figure 4-5 Interval Velocities

4.2.3.3 Identify Top of Pressure Transition

Seismic data cannot detect the top of a transition zone accurately. However, offset well data can locate the top of pressure transition zone much more accurately. Therefore, it is recommended that the top is defined from offset data and correlated with the seismic profile. Typically, the transition zone may coincide with distinct geologic markers that can be projected to seismic data. If the seismic data does not reflect the velocity reversal that is expected at the top of the transition zone, a “forced velocity reversal” may be considered to adjust the seismic data. The top of the transition zone can be used as the marker depth to adjust a velocity reversal on seismic data. It is possible however, that the undercompaction and overpressures may start immediately below the mudline in deep water sediments. Therefore, velocity reversal may not be apparent.

The transition from hydrostatic to over-pressured interval in the GOM areas can vary from a few hundred to several thousand feet in thickness. However, drilling experiences in the Plio-Pleistocene formations of the deep water GOM (water depth greater than 1000 ft) have shown that in these areas, the transition zone is usually not well developed, and the pore pressures are usually higher than hydrostatic pressure at shallow depths and continue to build up gradually with depth, with occasional occurrences of pressure reversal.

4.2.3.4 Develop a Normal Compaction Trend

Different analysis may require different types of compaction trends. The compaction trend may be classified as:

- Effective stress-velocity compaction trend (Bowers, 1994)
- Sonic (or seismic) velocity or interval time versus depth below the mudline.

In general what we term the Bowers' normal compaction trend is preferred. Calibration of a compaction trend from offset wells is a critical step of data analysis. This analysis should be focused on the following :

- 1 Establish the compaction trend for all available offset wells
- 2 Study compaction trends variations. If the compaction trends are different, then it is not readily apparent which compaction trend to use for the offset well. However, we must realize that the compaction trend is strongly influenced by the lithology. If an offset well can be characterized by a lithology indicator such as percentage of shale, or sand-shale ratio, then the compaction trend can be correlated to the lithology indicators.
- 3 Develop correlation of compaction trends versus lithology indicators (% clay for example) is difficult to construct, yet it is one of the most vital information required in rigorous pore pressure analysis. If such correlation can be established from offset wells, then a predicted "lithology class" for the prospect is possible with today's advancement in seismic interpretations.

Figure 4-6 illustrates the possible ranges of the Virgin Curve (velocity-effective stress cross plots) from offset well analyses. Such variations may also be considered in the modeling of uncertainty in the prediction of pore pressure. The effect of uncertainty in the effective stress caused by the uncertainty in the compaction trend is graphically displayed in Figure 4-6 Part A. In contrast, the uncertainty in seismic or sonic velocity can create uncertainty in the effective stress when the compaction trend is known as shown in part B. Of course, if both uncertainties are combined the resulting range of potential effective-stress prediction is even larger.

Examples:

The following well examples are presented to emphasize the effect of lithology variations on the normal trend estimates from well to well (even though they are in the same minibasin) and even lithology variations (versus depth) in the same well on the effective stress-velocity compaction trend.

The compaction trend for Well GC 260 (Figure 4-7) lies approximately on the “average” compaction trend for the GOM. This average was established by Bowers (1994). The triangular data points represent shale points and the circular ones represent sand points. Well GC 235 exhibited a different compaction trend as shown in Figure 4-8. The data points are scattered and the general trend is slightly twisted from the “average” trend shown as a solid line. The possible explanations for the marked distinct trends are as follows:

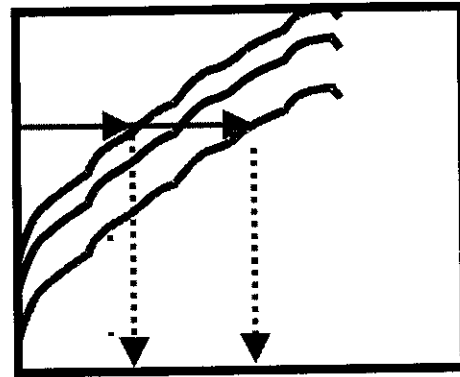
- 1 Gamma ray log as a lithology indicator for well GC 235 is shown in Figure 4-9. There is a general vertical baseline for the gamma ray with possible shift as indicated. The well is more shale than well GC 235.
- 2 Well GC 235 has a continuous increase in gamma ray readings versus depth. It is also more sandy than well GC 260 as indicated by the spiky signature.
- 3 As a result of the apparent lithology differences between the wells, their compaction trends are different. Well GC 235 has even a significant lithology changes versus depth which contributed to its scattered twisted compaction trend.

In the event the compaction trend is similar, then the same trend can be used to the prospect with confidence.

NOTE: Calibration should be heavily weighted toward those wells in the same mini-basin. This may not necessarily coincide with the wells in the closest physical proximity to the prospect. In the GOM, an accurate map for mini-basins is very useful in this analysis. Even in a single minibasin, lithology can be very different from well to well. Therefore, additional consideration to lithology type or class should be used to match offset to prospect.

Part A
The effect of
uncertainty in
compaction trend
on effective stress
determination

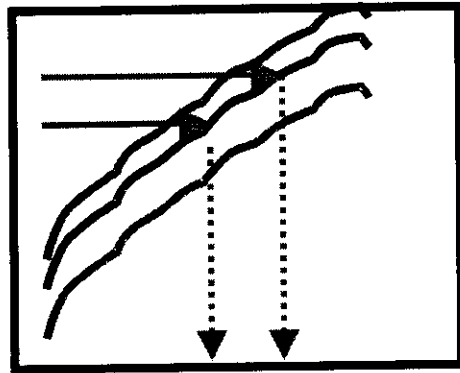
Velocity



Effective Stress

Part B
The effect of
uncertainty in velocity
on effective stress
determination

Velocity



Effective Stress

Figure 4-6 Compaction Trend Variation in Offset Well



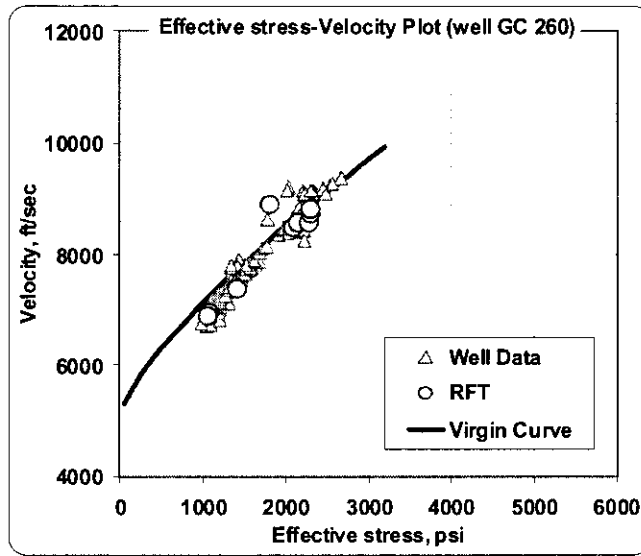


Figure 4-7 Effective Stress-Velocity Plot for Well GC 260

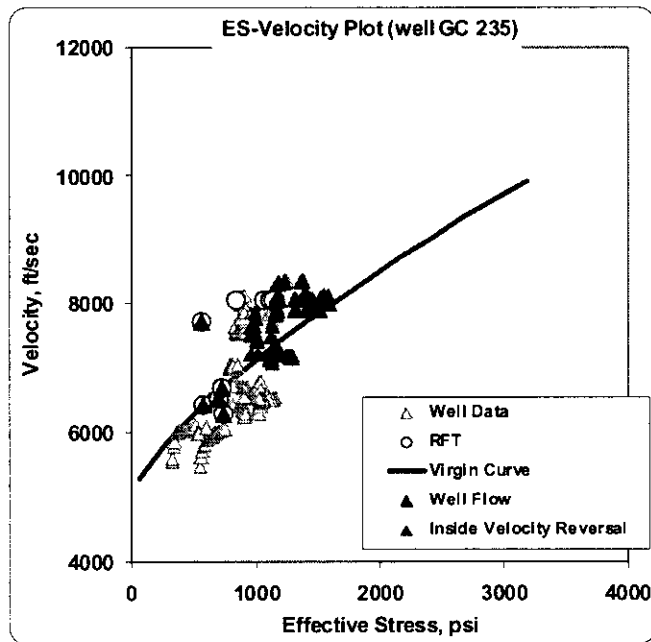


Figure 4-8 Effective Stress-Velocity Plot for Well GC 235

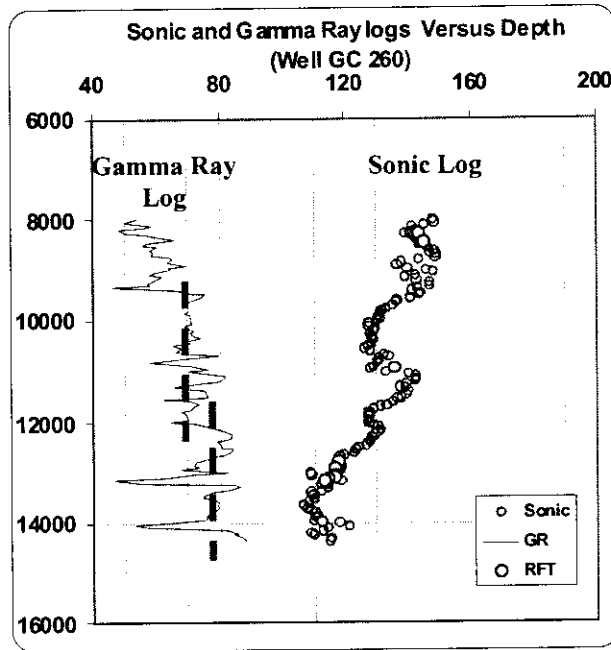


Figure 4-9 Sonic and Gamma ray logs for Well GC 260

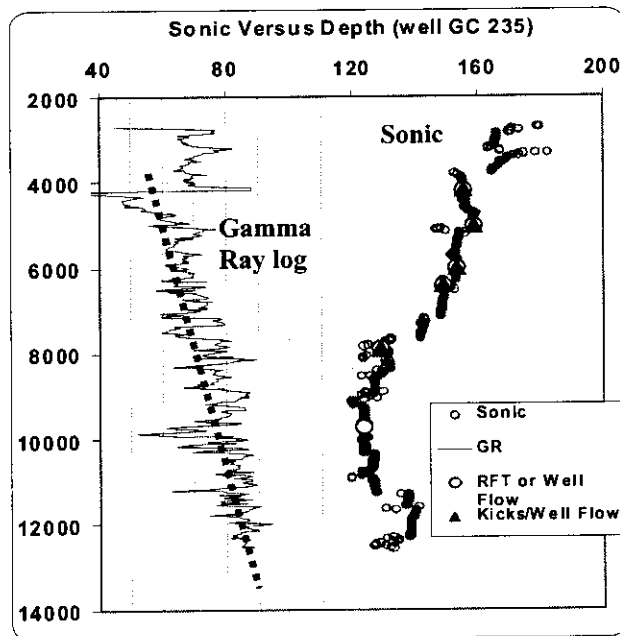


Figure 4-10 Sonic and Gamma ray logs for Well GC 235



4.2.3.5 Identify Unloading

NOTE: The reader may skip this section if unloading is known not to be a problem, which is often the case in the deep water GOM. This section is included for those who have some reason for concern about unloading.

Unloading is the reduction in effective stress due to overpressuring mechanisms other than undercompaction such as fluid expansion, clay diagenesis, and charging from other zones. Therefore, if a zone underwent unloading, the pressure estimation methods will under predict the amount of overpressuring if they do not account for the unloading. Accordingly, identification of unloading is required to adjust the current methods to account for pressure causes other than undercompaction. This may be done by increasing the exponent or shifting the trend line. We must recognize that in the zones that are deemed overpressured due to undercompaction only, the conventional approaches are adequate. Therefore, we may use different models depending on the pressure generation sources (undercompaction versus unloading).

Velocity reversal may “possibly” indicate unloading. However, many velocity reversals are not an indication of unloading. Velocity reversal is in reference to the decreasing velocity below the value at shallower depth. Essentially, velocity reversals can be caused by changes in lithology, unconformities, major faulting and/or unloading. Therefore, Gamma ray and other indicators are important to verify the lithology changes.

Bowers (1994) presented a method to identify unloading and estimate pore pressure in these zones. The essence of the method is the graphical display of effective stress-velocity data to generate the “Virgin Curve”. In the zone of interest, the known pressure points (RFTs, etc.) can be plotted on the same plot. If the selected known pressure points fall on the Virgin Curve, then these points do indicate unloading in this zone. If they fall outside (above) the curve, there is a strong possibility that the zone of interest is unloaded.

In summary, the analyst must determine the proper model (pressure estimation strategy) to be used for pore pressure estimation. If the zone under consideration is undercompacted only (but not unloaded), then conventional methods will be able to predict pore pressure adequately. If there is overpressuring due to unloading effects, then a higher exponent on Eaton equation (up to 5 from the conventional 3 for sonic) is necessary.

Bowers’ method to account for over-pressuring (1994) is also another way to predict pore pressure in unloaded zones.

Based on the above, diagnostics for the recognition of unloading are critical. A procedure for performing these diagnostics is addressed below.

4.2.3.5.1 Procedure to Predict Unloading

The procedure below listed acknowledges Bowers’ approach to diagnose unloading as recently published. Additional measures are included to increase the confidence in the prediction of unloading phenomena:

- 1 Plot the normally compacted sediments effective stress versus velocity. This is called the Virgin Curve. This curve represents the effective stress-velocity path under normal compaction and under-compaction as well. The equation of the velocity under normal compaction is written below (Bowers, 1994):

$$V = 5000 + A * \sigma_{np}^B \dots\dots\dots(EQN 4.7)$$

Where:

V	velocity in ft/sec
A	a constant, a “typical” value for the Gulf Coast = 14.2
B	Exponent, a “typical” value for the Gulf Coast = 0.725
σ	Effective Stress

$$\text{Effective stress } \sigma_{np} = OB - P_{np} \dots\dots\dots(EQN 4.8)$$

Where:

OB	Overburden pressure, psi
P_{np}	Normal Pore pressure, psi

In this particular equation, the pore pressure can be assumed to be a normal saltwater gradient at 8.7 ppg.

- 2 Cross plots:
 - Compute the effective stress in the zone of interest based on known pressure points (kicks, RFTs, etc.) according to EQN-4.8
 - Plot the known pressure points on the velocity-effective stress plot. If the points fall above the Virgin Curve, then the zone (represented by these known pressure points) **may be** unloaded. To verify this conclusion, make additional analyses as shown below.
 - Plot the velocity versus density. Also plot the data points of the zone of interest with a different color to mark the location of these points on the graph. If the plotted data shows that the density is almost constant while the velocity shows a definite decrease, this is a clear indication that the zone is likely unloaded. In this case, effective stress is decreasing while the bulk density is constant. It is critical to filter the density data with a 299-boxcar filter to remove the noise in the data, but also preserve the general trend

- 3 Quick-Look evaluation:
 - Identify velocity reversal zones. Check if there is a lithology change in the velocity reversal zone.
 - Compare sonic, density, and resistivity logs. A clear indication of the need for a high pressure technique is when the sonic and resistivity logs undergo reversals but the density log does not. In this case, the Equivalent Depth method will fail and a high pressure technique is required.



- If the all three logs are showing reversals, then pick a point at the same depth in each reversal and project it vertically upward until it crosses the log again. If the all three logs are crossed at the same depth, then the Equivalent Depth method will work (no unloading). If the density log is intersected at a deeper depth than the other two logs, a high-pressure technique is required.

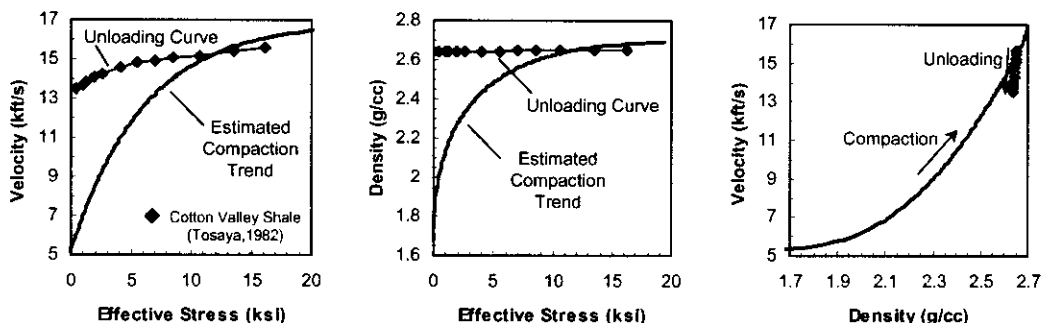


Figure 4-11 Cross Plots for Unloading Diagnostics (after Bowers, 2001)

- 4 Plot effective stress versus vertical depth below the mud line.
 - Effective stress typically increases with depth. In undercompacted sediments, the effective stress increases at a lower rate. If the zone is unloaded, the pore pressure increases at a much higher rate than the overburden. This will cause effective stress to decrease. We must also realize that undercompaction can cause effective stress to decrease with depth without unloading.
 - In undercompacted sediments, shale pore pressure increases a rate equivalent to overburden gradient. If the sediments are unloaded, shale pore pressure increases at a greater rate than the overburden gradient.
- 5 Geologic conditions that may be associated with unloading are:
 - The presence of a seal above the zone of interest such as salt or anhydrite.
 - High temperature gradient in the zone of interest.
 - Depth typically plays a role in the development of unloading. Deep sediments are more compact (less compressible) and less permeable. Therefore, the possibility of constraining pore fluids is higher. Therefore, fluid expansion (one source of unloading) is more likely in deeper, more lithified sediments.
- 6 Compare measured pore pressure in the zone of interest with the estimated pore pressure using the Equivalent Depth method. The Equivalent Depth method underestimates the pore pressure if the fluid expansion mechanism or others are active.
- 7 Check the velocity values for all the data points that fall above the Virgin Curve. If they fall below 8500 ft/sec, unloading is unlikely. The sediments with this velocity

level are probably too soft for unloading to occur. Unloading is more likely if the sediment has a velocity of more than 9500 ft/sec, provided that other indicators are positive.

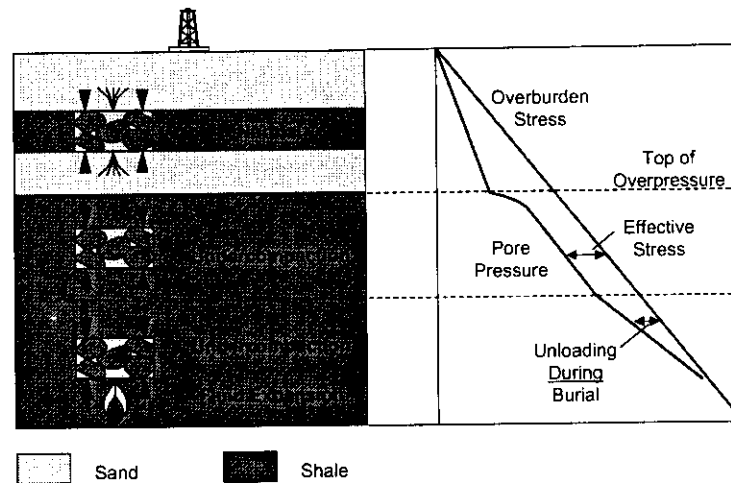


Figure 4-12 The relationship of pore pressure to overburden pressure in undercompacted and unloaded sediments (after Bowers, 2001)

- 8 The Virgin Curve may require adjustment from well to well. Consider the adjustment in the case where a definite trend is established parallel to the Virgin Curve. This indicates that there is a lithology effect.
- 9 Compute the slope of the *excess pore pressure* gradient versus the overburden gradient. If the pore pressure is increasing at a rate approximately equal to the overburden, then this is a possible indication of unloading.
- 10 If all the above indicators are positive, then a compelling case has been made for the occurrence of unloading.
- 11 If we verify that the data points that fall above the Virgin Curve are not caused by unloading, then attention should be focused on other possibilities such as the Centroid Concept, structure or faults. This is discussed in later parts of this Chapter.

4.2.3.5.2 Example of Unloading

The example presented is selected to demonstrate the complexity of the analysis as well as the diversity of possible outcomes. The indicators for the unloading may be shadowed by effects from lithology, depth, and structure.

NOTE: The following is only one example in the GOM which demonstrates the complexities of the analysis. Despite the fact that this example does not show clear unloading, it demonstrates the diagnostic process. It also demonstrates the need to integrate all available data, especially geological data relevant to structure

Unloading Example (Well VK912, Water Depth = 2441 ft)

This well has good RFT vertical coverage. Although there is no mud weight data available, there are density and sonic logs. Figure 4-13 through Figure 4-16 provides the analysis for well VK912. The following are listed reasons for and against the assumption of “unloading” in this well with the final verdict:

Indicator for Unloading:

- ❑ One RFT point (marked) is above the Virgin Curve. This point is suspected to be in unloaded sand since it is departing from the main compaction trend.

Indicators against unloading:

- ❑ The shale pore pressure appears to be parallel to the OBG curve. The effective stress is essentially constant as shown in Figure 4-13.
- ❑ The velocity-effective stress cross-plot does show strong indications of undercompaction but not for unloading. All the RFT points follow the virgin curve except one, marked in the Figures. The Virgin Curve for this well is slightly shifted from the assumed GOM “average” .
- ❑ The velocity reversals are not well established or apparent
- ❑ The velocity at the depth of the suspected RFT point is approximately 9500 ft/sec. This is the extreme low limit of rock velocity that is possible for unloading to occur. Giving this low velocity value, it is unlikely for unloading to occur in a soft sediment such as this point.
- ❑ The conventional pore pressure estimation methods did not underestimate the pore pressure.

Conclusion:

The well appears to be highly undercompacted. There are two separate sand bodies. The bottom-most RFT points shown in the Figures need to be checked for possible errors. A good and quick check would be to compare the RFT pressure to the mud weight pressure at that point. If there are similar, then a seal failure in the RFT tool is suspected.

Perhaps, lithology changes are an important consideration to study. It is very important to gather as much information as possible before drawing any conclusion.

Unloading is not confirmed in the suspected zone. The virgin curve should be adjusted to reflect the well’s lithology. Further consideration should be given to possible structural effect for the sand zone.

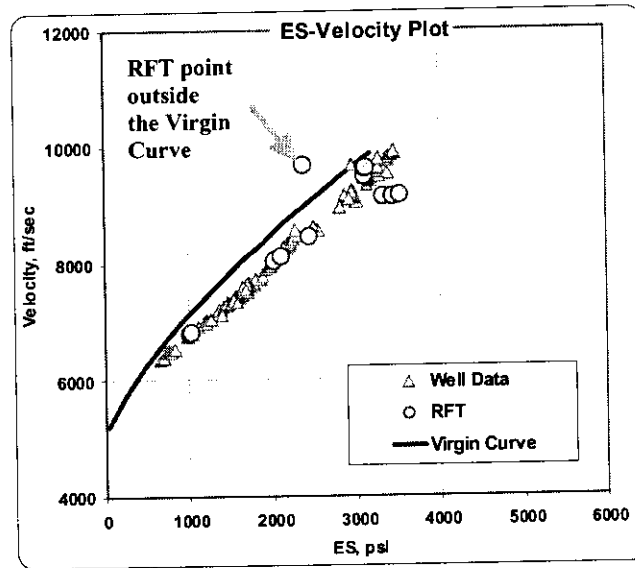


Figure 4-13 Velocity-Effective Stress Cross Plot for Well VK 912 (Unloading Example No. 1)

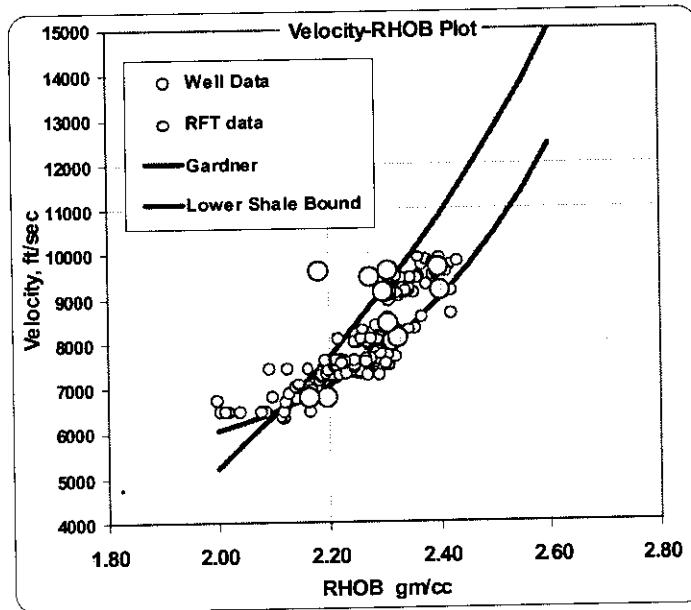


Figure 4-14 Velocity-Density Cross Plot for Well VK 912 (Unloading Example No. 1)



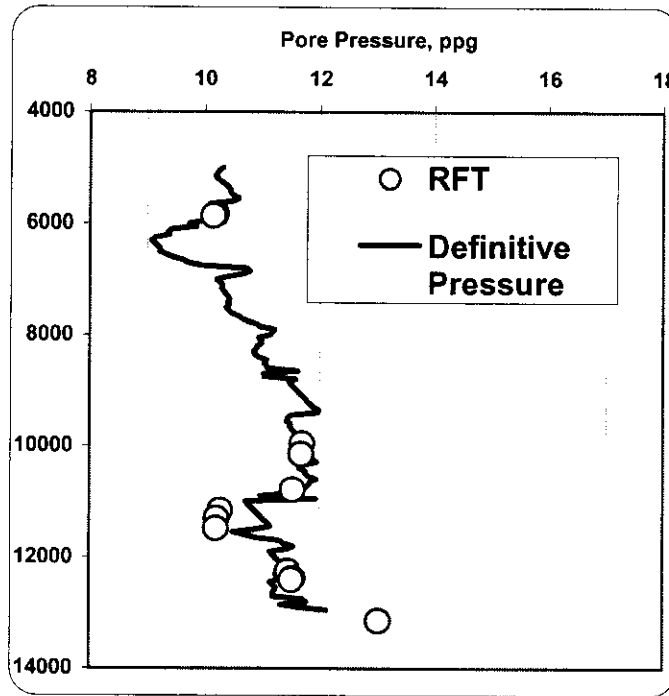


Figure 4-15 Pore Pressure Cross Plot for Well VK 912 (Unloading Example No. 1)

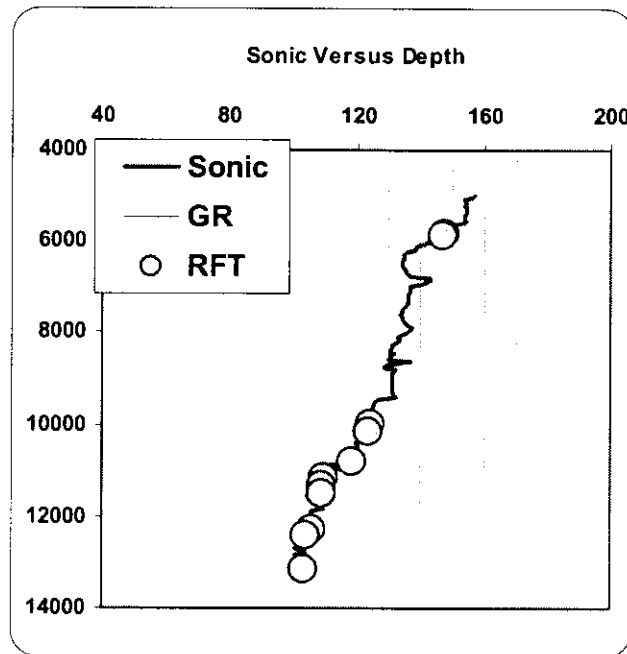


Figure 4-16 Sonic Versus Depth Cross Plot for Well VK 912 (Unloading Example No. 1)

4.2.3.6 Identify Centroid Effect

Structure is defined in this section as the geometry of sand sequence. Thick dipping sand bodies bounded by shale or thin horizontal sand bodies can create different pore pressure estimation strategies or estimation strategy requirements versus the bounding shale formation. Analysis of “structure” is deemed **critical** from offset well data as this gives rise to the following important consideration:

- Understanding whether RFT readings in sand bodies are valid calibrate measurements for prediction of pore pressure in slubs.
- Diagnostics of different sand bodies with no hydraulic connectivity.
- Diagnostics for the Centroid effect are likely to be used in dipping sand formations with high vertical structure.

In dipping sands with high vertical structure and good hydraulic continuity, the centroid effect plays a major role in defining the pore pressure profile in sand and in the overlying or underlying shales. Traugott (1997) defines the centroid as the depth where pore pressure in sand and shale are in equilibrium (Figure 4-13). Traugott (1997) and Stump, et al (1998) stated that the Centroid effect could cause mismatches between estimated pore pressures in sand and those calculated in nearby shales. Calibrating a pore pressure estimation method to match crestal or basal sand pore pressures can cause significant error at other depths (Bowers, 2001). Therefore, it is important to realize that we should not try to match observed pressure in this case.

We must also realize that the concept of the centroid is relatively new to the industry. There is little published information on the subject. The concept is still in the development stage or formulative stage and has been “digested” by few industry professionals.

4.2.3.6.1 Procedure for Centroid Analysis

The systematic process of structure and centroid analysis is outlined below:

- 1 Draw the effective stress versus vertical depth (sub-sea datum is preferred over the kelly bushing) as shown in Figure 4-18 for Well VK912. If the clustered points fall along a straight line with some horizontal separation, then there is good possibility that these different clusters belong to different zones with no hydraulic connectivity. Notice for Well VK912, the RFT points cluster into three distinct groups. The three groups are named A, B, and C. The lines that represent the pore pressure trends of zones A, B, and C are parallel to the normal hydrostatic line. This indicates the pressure in these zones is hydrostatic. However, each zone (A, B, and C) has a different pressure regime.
- 2 Plot the excess pore pressure versus depth. If the excess pressure is constant for a group of points, then this is an indication that they belong to one sand body that is in hydraulic equilibrium. Geologic information should be integrated positively to conclude the structure features.
- 3 Plot the sand RFT points versus depth in terms of pressure and gradient. If the points follow a hydrostatic trend, then this is a good indication of a possible Centroid effect.

- 4 Check the shale pressure and how it intersects the sand pressure profile. If the pore pressure analysis is done correctly, then it should intersect at the midpoint of the hydrostatic column of the sand body.

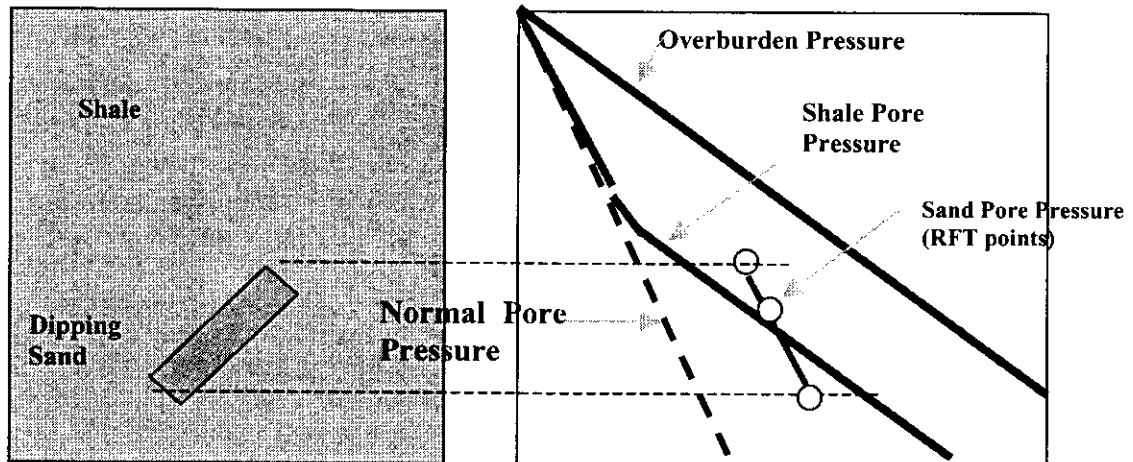


Figure 4-17 Schematic Illustration the Centroid Concept (Traugott, 1997 and Bowers, 2001)

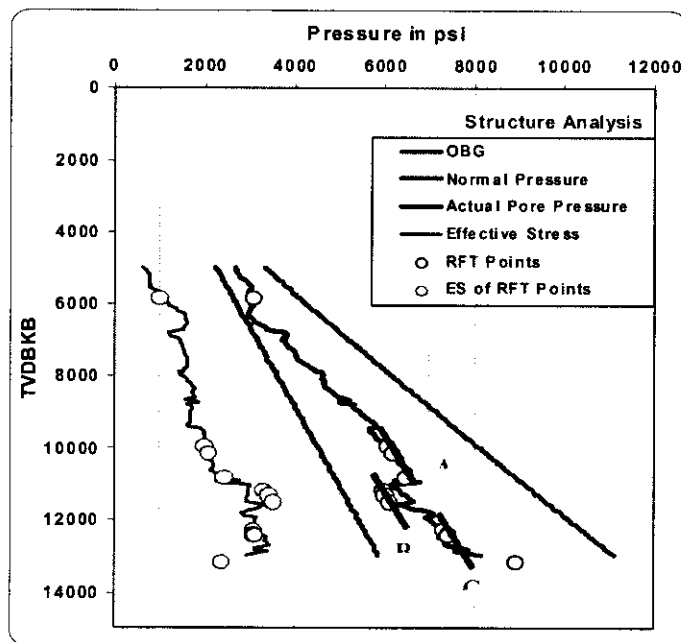


Figure 4-18 Pressure Profile for Shale and Sand Sequence in Well VK 912

4.2.3.6.2 Example of Centroid Effect

It is important to illustrate the concept of the centroid with “real world” example. The example presented shows the complex interactions between lithology, geologic setting and the centroid effect.

Centroid Example: Well GB 543

This well demonstrates a “text book” example of the centroid concept. This well has 21 RFT points with great vertical coverage (600 to 14000 ft). In this example, we will follow the guidelines established earlier for unloading, structure and centroids to show a coherent picture of how to apply all the analytical tools. We will address the complex mechanisms in the following order:

- 1 Unloading analysis
- 2 Structure analysis
- 3 Centroid effect.

Unloading: See Figure 4-19 through Figure 4-23.

Zone A is undercompacted and possibly unloaded. **Zone B** is unlikely to be unloaded. There are some conflicting indicators, some support the unloading possibility, and others do not.

□ **Indicators which support unloading are:**

- Figure 4-19 shows almost all RFT points are located above the Virgin Curve.
- The predicted pore pressure trend is underestimating pore pressure by about 1 ppg in **Zone A**.

At the outset, the density-effective stress plot may support unloading as the RFT points appear to be lined up vertically (See Left cross plot, Figure 4-20). The left plot in Figure 4-20 is done with unfiltered density data and therefore the data scatter is significant. In this case it is not clear whether the RFT points are in a vertical position or not. The density data were filtered with a boxcar-499 and plotted as shown to the right in Figure 4-20. The new definite density trend is not indicative of unloading as initially suspected. This example emphasizes the need to filter the density data.

NOTE: Since compaction trend is applicable to shale and not in sand, the sand data points (the circular points in Figure 4-19) are not expected to follow the same compaction trend for the shale (triangular points)

Indicators which do not support unloading:

- The effective stress is always increasing.
- No clear velocity reversals on the sonic log.

- The velocity values of most RFT points are less than 10000 ft/sec. There is little possibility of unloading to occur at low velocity.

Structure: See Figure 4-21 through Figure 4-26.

- **Zone A** indicates a pressure gradient approaching overburden gradient.
- Define the shale and sand pore pressure trends. This is done in Figure 4-21 which shows that pore pressure for shale and sand zones (RFT points) are assuming different trends or slopes.
- The sand zones are identified by Gamma ray log which indicates if the RFT measurements were taken in sand or shale zones (Figure 4-23).
- The sand zones are further analyzed to check for hydraulic continuity between different sand bodies. This is performed using the following: Figure 4-23, Figure 4-24 and Figure 4-25. Accordingly, the RFT points are classified into two separate zones, **Zone A** and **Zone B**.
- **Zone A** indicates a pressure gradient approaching the overburden gradient
- Hydrostatic **Zone B** is showing that all RFT points follow the hydrostatic gradient.
- Figure 4-25 shows the excess pore pressure in **Zone A** and **Zone B**. The “excess” pore pressure in **Zone A** is continuously increasing which is an indication of pressure discontinuity. This is a result of interbedded shale zones, which provide vertical pressure seals. **Zone B** is showing a constant excess pore pressure that is a direct indication of hydraulic continuity through the sand body.

Centroid Effect:

The following indicators are strong flags for the centroid effect:

- Massive thick sand
- Hydrostatic gradient
- The shale pore pressure intersects the sand pressure profile at the midpoint or Centroid.

Figure 4-26 shows that the shale pore pressure line intersects sand pore pressure at some point approximately a the middle of sand Zone B. The intersection point is a function of the geometry of the sand body and the fluid flow between the shale and sand at the crest and bottom points. It is possible that the intersection occurs at the top, bottom, middle or simply anywhere along the sand body depending on the hydraulic equilibrium in the system.

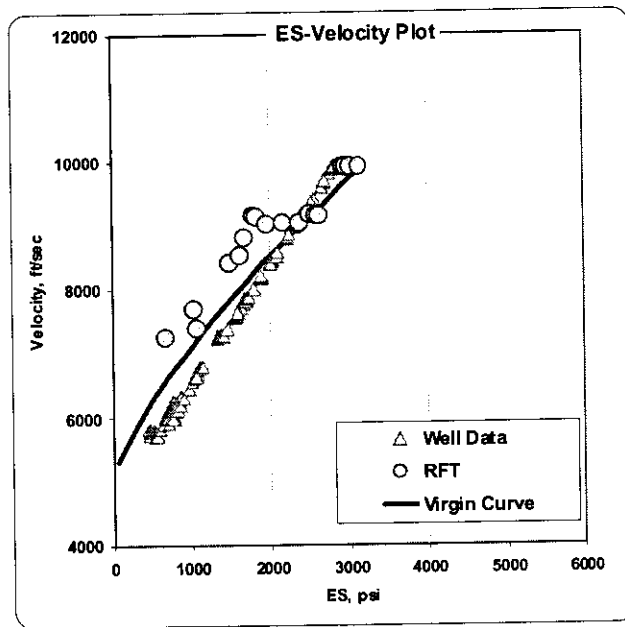


Figure 4-19 Effective-Stress Velocity Cross Plot for Unloading Analysis-Centroid Example No. 1

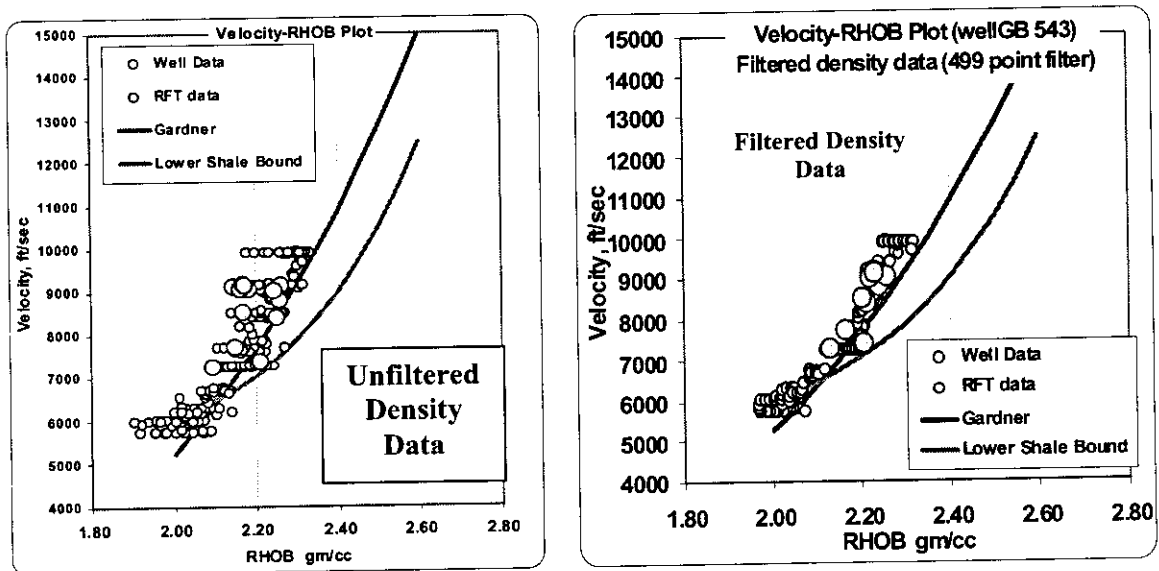


Figure 4-20 Density-velocity Cross Plot for Well GB 543 Unloading Analysis for Centroid Example No.1



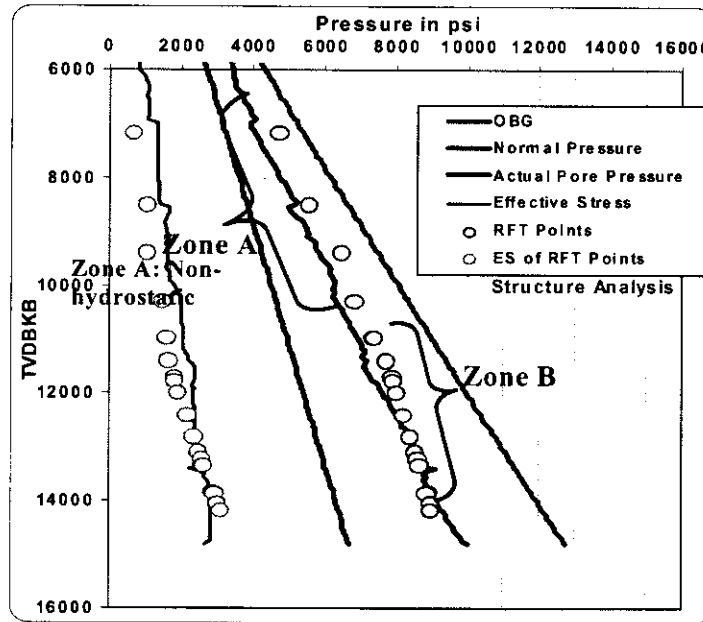


Figure 4-21 Cross Plots for Centroid Example No 1 showing Zones A and B

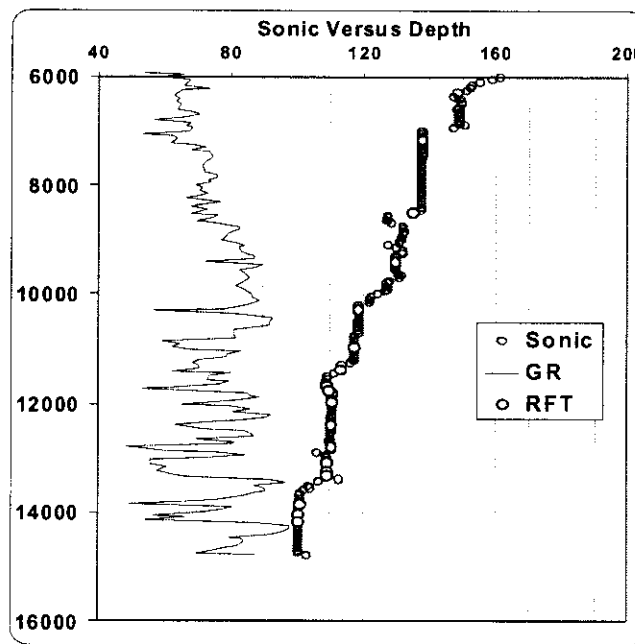


Figure 4-22 Sonic Versus Depth Cross Plot for Well GB 543 Centroid Example No. 1

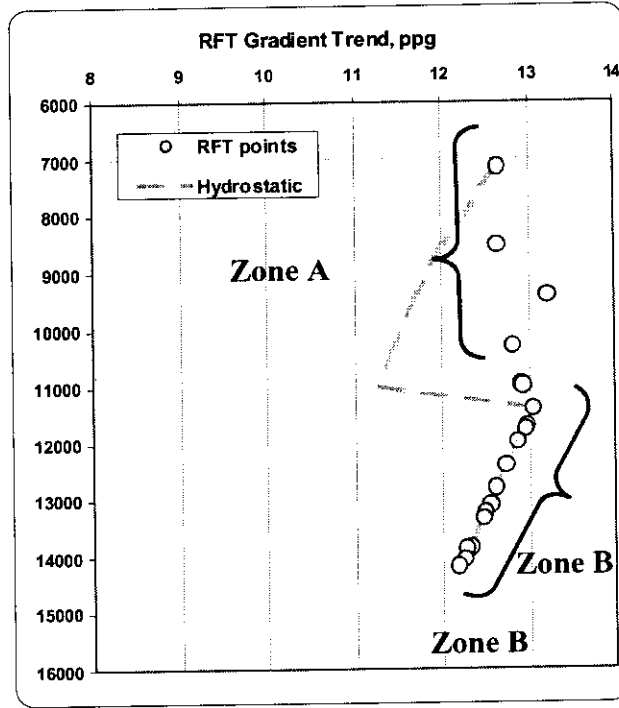


Figure 4-23 RFT Pressure Profile for Centroid Example No 1, Well GB 543

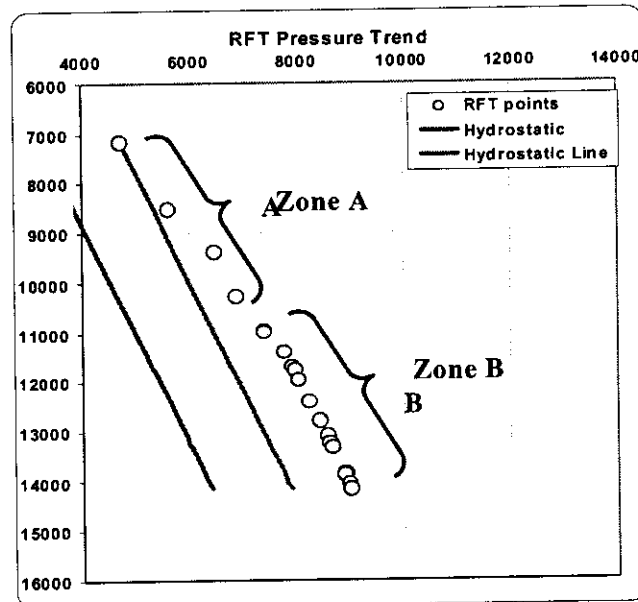


Figure 4-24 Points and Hydrostatic Trend for Centroid Example No. 1 Well GB 453



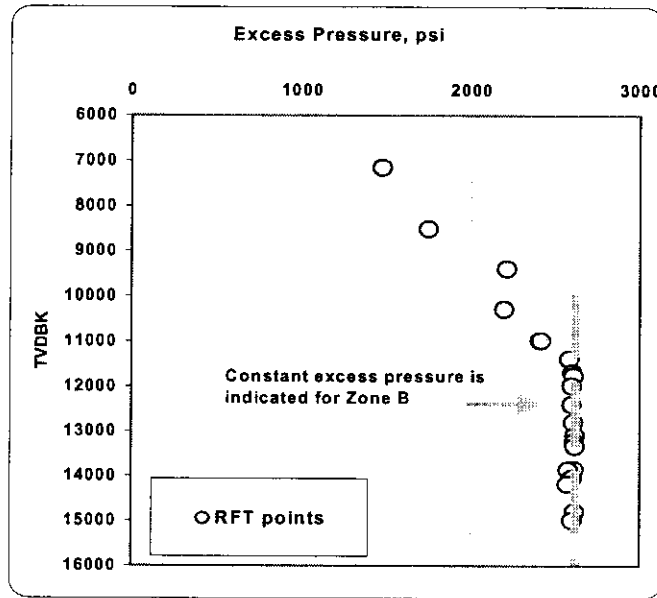


Figure 4-25 Excess Pore Pressure Plot, Well GB 543

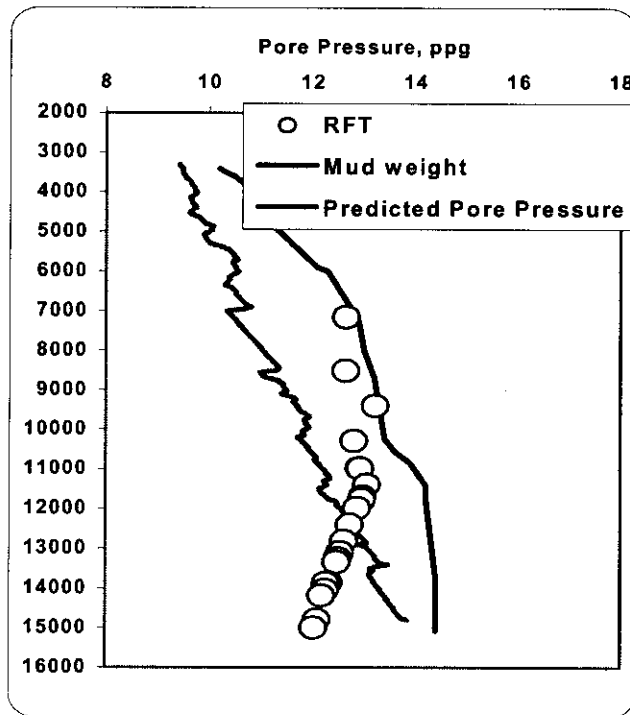


Figure 4-26 Predicted Shale Pore Pressure for Well GB 543

4.2.3.7 Calibrate Conventional Models

Conventional models are the models that utilize a normal compaction trend and the exponent model. The two key input to the exponent models are:

- A compaction trend (velocity versus depth)
- Effective stress exponent

Having established a compaction trend, the analyst must now calibrate the exponent using one or more of the known pore pressure points. After the exponent model is calibrated, it is ready for use on the seismic data of the prospect well.

4.2.3.8 Apply New DEA 119 Models to Offset Wells

The new DEA 119 models are described in Appendix A of this manual. They are all designed to compute pore pressure based on their calibration on DEA 119 GOM database. In essence the steps performed previously to calibrate the exponent model are already done. Since these models are trained to universal data set which capture the entire GOM area, local calibration on a mini-basin scale or even smaller is warranted. This is precisely the reason to perform the calibration of conventional exponent models above.

The objectives of this application are:

- Compare the prediction of the new models with the definitive pore pressure of offset wells
- Select the best model that can be used with greater confidence to the prospect well pore pressure prediction.

4.2.4 Prospect Well Analysis

Having performed the analysis on offset wells, the analyst has:

- Defined the structure
- Defined the compaction trend
- Calibrated conventional models

The analyst is now ready to apply the calibrated conventional models with the ability to define possible uncertainty for the analysis. At this point, it is important to remind the analyst that:

- Definition of compaction trend is not reliable in many cases.
- Calibration data from offset wells may not be sufficient to calibrate the conventional models
- There is still an uncertainty in the application of both the compaction trend and the calibrated models to the prospect well if there is significant structural and lithological diversity.

Therefore, it is imperative that the new tools developed during the course of this project are utilized in conjunction with the standard industry accepted methods.

NOTE: The new models developed in this project are independent of compaction trends (trend lines). They were developed and calibrated based on a universal data set derived from the GOM database. Therefore, these models “carry” with them global averages of compaction features.

Appendix A presents an exhaustive list of all models developed in this project. These models can be classified into the following categories:

- Theoretical models
- Calibrated conventional models
- Empirical models

This section will provide a **list of the top five models**, which have been rated based on an error analysis study. The study utilized the error analysis from 80 wells, all of which have been predicted with over 40 models. The average relative error of the predicted pore pressures is the basis for the model ranking.

We shall proceed with the following sequence of analyses:

4.2.4.1 Seismic Data Only (“Quick–Look” Method)

The Quick-Look method is a simple transform procedure to obtain a pore pressure estimate. The models used require the seismic interval velocity only. No OBG computations or offset calibration are required. The Detailed Analysis procedure utilizes all available models and offset data.

Below is a list of the empirical quick-look models. Variables are explained in Table 4-1 and details of the new models to estimate pore pressure from seismic velocity is given in Appendix A of this manual.

Model	Type	Description
20-J	Exponential	$EXP(2.270 + 0.006282 * \Delta 2)$
20-K	Special Function	$1 / (0.1026 - 0.0005464 * \Delta 2 - (0.0001 * ML))$
20-L	Exponential	$8.7 + 2.4590 * EXP(0.0228 * \Delta 2)$
20-M	Polynomial	$8.7 + 0.1015 * \Delta 2 - 0.0001565 * \Delta 2^2$
20-N	Polynomial	$9.285 + 0.03288 * (DT - (200 * EXP(-0.0001158 * 10^{-5} * ML))) + 0.000831 * (DT - (200 * EXP(-0.001158 * ML)))^2 - 0.000004475 * (DT - (200 * EXP(-11.583 * 10^{-5} * ML)))^3$

Where: $\Delta 2 = DT - 200 * EXP(-0.0001 * ML)$

4.2.4.2 Develop Quasi-Calibration from Offset Well Data

There are two ways to utilize the known pore pressure data from the offset wells:

- Directly calibrating conventional models
- Quasi-calibration for prospect well - extrapolate a known pressure point to the prospect provided that the
 - Pressure point located in a dipping sand body (known elevation differences between prospect and offset wells)
 - Sand body is known to extend to the prospect
 - Fluid content of the sand body is known

The Development of Quasi-calibration for Prospect Well

If we know that a sand extends all the way to the prospect, then we can determine the pressure for the same sand at the prospect. In essence we have a known "quasi-pore pressure point" like an RFT at the prospect.

The process is amplified in the following discussion and example.

Quasi-calibration Example No 1

The pressure at the prospect will be equal to the pressure at the offset minus the hydrostatic pressure exerted by the fluid column in the sand along the vertical distance separating the offset and the prospect.

P_B	=	P_A	$(TVD_B - TVD_A) * \rho_f * C$
Where:		P_B	Pressure at Location B
		P_A	Pressure at Location A
		TVD_B	True vertical depth at B
		TVD_A	True vertical depth at A
		ρ_f	Formation fluid density (.45-.5 psi/ft for water,
		Rho	.33-.35 psi/ft for oil, \approx .12 psi/ft for gas)
		C	Units conversion constant for desired units

In the following example, the pressure is known to be 5,000 psi at 11,000 ft at Location A. If we assume a corresponding depth of 10,000 ft at Location B and a formation fluid density of 0.45 psi/ft, then the sand pressure at Location B will be equal to:

$$P_B = P_A - (TVD_B - TVD_A) * \rho_f * C$$

$$P_B = 5000 - (11000 - 10000) * 0.45$$

$$P_B = 4550 \text{ psi}$$

There may be instances in which more than one fluid exists in the sand. In particular, a fluid column between Location A and Location B may consist of a water column, oil column, and a gas column. This situation can cause significant error in the calculation

because the respective vertical column lengths may not be known with precision. Therefore, in projecting pressures from Location A to Location B, it is often good practice to develop a range of possibilities assuming various formation fluids and vertical fluid column heights.

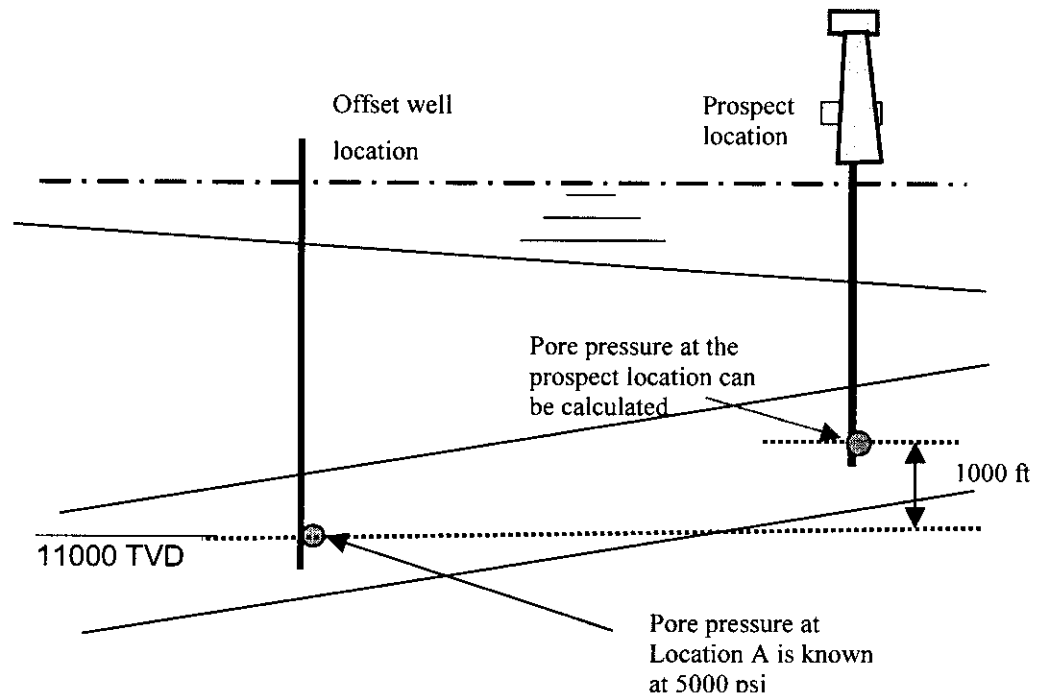


Figure 4-27 The Development of Quasi-calibration Pressure

Quasi-calibration Example No 2

In the following example taken from an actual field situation, the pressure was known at the offset location, but the corresponding formation depth at the prospect wasn't precisely known. Further, the vertical fluid column heights and compositions weren't precisely known. In this example, the preceding formula was applied to a situation in which the horizon depth at the prospect was between 760 ft and 1,510 ft shallower than its corresponding depth at the offset location. Several sidetracks had been drilled at the offset location, so it was possible to determine the water column of 400 ft with a reasonable degree of confidence. However, the composition of the formation fluid above the water column was not known. Therefore, it was necessary to develop a range of equivalent mud weights based on different horizon depths and fluid column heights and compositions. In the example below, an oil column was assumed to lie on top of a 400 ft

water column. A similar calculation can also be performed assuming gas above water (worst case), and a full column of water (best case).

The projected horizon depth at the prospect's location was determined using a seismic cross-section. Seismic cross-sections are generally presented in a two-way-travel time format. The seismic cross-section gives information regarding two-way travel times at various locations. It is possible to determine the approximate vertical distance separating a particular horizon at each of two particular locations by determining the difference in two-way travel times at each respective location. The corresponding depths can be determined indirectly by calculating the two-way time required to reach a certain depth using the seismic interval velocities, sonic logs, or checkshot surveys. A plot of two-way time vs depth was calculated from the seismic interval velocities.

Proposed Location A TWT vs Depth

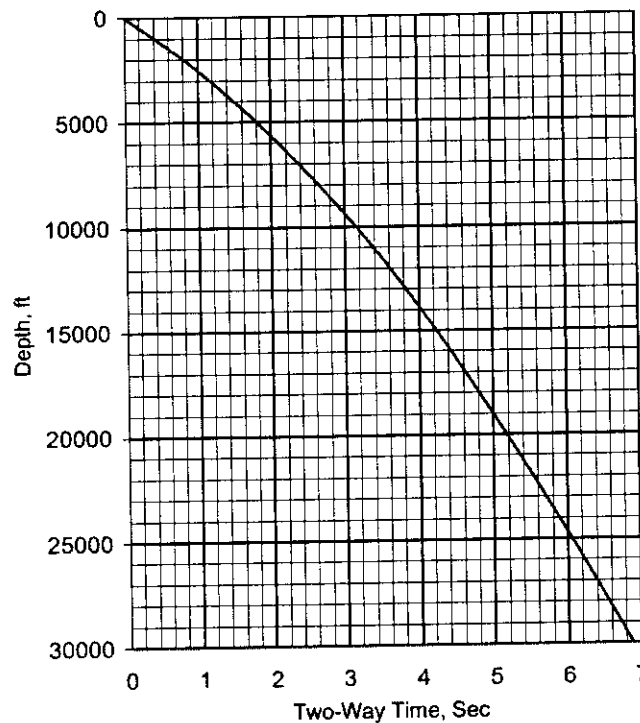


Figure 4-28 Prospect location TWT versus Depth

A plot such as the one above can be developed using the seismic interval velocities at the prospect location and using checkshot, sonic, or seismic at the offset location. The corresponding depths of a particular horizon can then be determined using a plot such as this and the seismic cross section.



In some cases, offset well information may not be available or relevant (eg, the horizons on the offset may not extend all the way to the prospect). In such a case, it is still possible to determine the possible effects of a dipping bed using two-way time vs depth plots, the seismic cross section and the shale pore pressure profiles developed from seismic. The general procedure is as follows:

- 1 Calculate the shale pore pressures from seismic interval velocities. Develop a pressure vs depth profile at each location of interest. Be sure to develop a vertical pressure vs depth profile that passes through each assumed centroid point in the horizon of interest.
- 2 Using the vertical pressure vs depth profiles, calculate the shale pressure at each assumed centroid point in the horizon of interest.
- 3 Calculate the corresponding pressure at the prospect's location based on the assumed vertical fluid column heights. You may want to develop a range of pressures assuming a gas column (high-side pressure case) and a water column (low-side pressure case).
- 4 Calculate the equivalent mud weights at the prospect location from the pressures.

4.2.4.3 Apply Calibrated Conventional Models

If there is a quasi-calibration point in the prospect, then the conventional models should be calibrated to the known pressure point(s). This will re-check the calibration performed in Section 4.2.3.7.

4.2.4.4 Apply New DEA 119 models

Having selected the best models from their testing against the definitive pore pressures of offset wells, the new model(s) can be applied to the prospect. At this point the analyst is advised to apply the calibrated exponent model as well for comparison. The top five models are listed in Table 4-2. The following are important considerations regarding the new models:

- These models require no trend line to draw.
- Experience gained from testing these models on 80 wells from the GOM database can be highlighted as follows:
 - Typically all models agree on the predicted pore pressure within a certain range (0.3 to 0.75 ppg). The agreement of all models is good except at shallow depths (0 to 4000 ft below mudline). This disagreement is a reflection of the uncertainty in the input data which is at its highest level at shallow depths.
 - Best agreement is usually the bottom 50% of the depth interval. This is clearly a manifest of the quality of calibration data in this interval. Shallow calibration data are hard to find. Eventually the lack of good data is reflected in the disagreement at shallow depths. In addition, since the calibration data used for all DEA 119 models are based on sonic logging data, the new DEA 119 models have poor calibration at shallow depths (mudline to approximately 3000 ft below mudline).

- If the models disagree, then a careful study should be done to understand why.
- The potential for radical disagreement between all models is one reason to implement the conventional analysis outlined in the previous section. Experience indicates that the new models in many cases are more reliable than the conventional methods. The conventional trend lines methods can be enhanced with the guidelines presented in this chapter pertinent to determining pore pressure estimation strategy, structure, pore pressure quasi-calibration, etc.

Variable	Description
AG	Air gap, ft
DT	Sonic travel time in micro sec /ft
Delta2	= Observed DT – Normal DT Delta2 = (DT-200*EXP(-0.0001*ML))) Where ML is vertical depth below mud line
ML	Vertical Depth below mud line, ft
OBG	Overburden gradient, ppg
OBGpsi	Overburden stress, psi
TVD	Vertical depth below Kelly bushing
WD	Water depth, ft

Table 4-1 List of Variables Used in Modeling

Rank	Model No.	Description
First	TH-1 Theoretical	Baldwin-Butler porosity effective-stress formulation: $P(\text{psi}) = \text{OBG psi} - 5635 * (1 - \text{phiamoco})^{1.094}$ <p>Where: OBG psi is the overburden stress in psi Phiamoco = porosity derived from Amoco empirical equation given as follows: $\text{Phiamoco} = 1.425 * (1 - (V/15000))$ V is velocity in ft/sec</p>
Second	TH-13 Theoretical	Modified version of Bowers' velocity effective-stress relationship: $P(\text{psi}) = \text{OBG psi} - ((V - 5000)/1.046)^{(1/1.069)}$
Third	BTL-B Improved Conventional	Exponent model with Bowers' curved trend: $P(\text{ppg}) = \text{OBG} - (\text{OBG} - 8.7) * (\text{DT}_{\text{BTL-B}} / \text{DT})^{2.227}$ <p>Modified Bowers' trend Type B: $\text{DT}_{\text{BTL-B}} = 10^6 / (5000 + 14.22 * (0.052 * \text{TVD} * (\text{OBG} - 8.7))^{0.7415})$ </p>
Fourth	20-A Empirical	Multiple Regression Model: $P(\text{in ppg}) = -14.02 + 0.1982 * \text{DT} + 0.02251 * \text{OBG} - 0.0008785 * \text{Delta}^2 + 0.00005647 * \text{WD} + 0.0004002 * \text{ML} - 0.0004483 * \text{DT} * \text{DT} + 0.0005492 * \text{Delta}^2 * \text{Delta}^2 + 0.000002685 * \text{ML} * \text{DT} - 0.000009746 * \text{ML} * \text{Delta}^2 + 0.00003297 * \text{ML} * \text{OBG}$
Fifth	20-G Modified Conventional	Modified Exponent model with water depth term: $P(\text{in ppg}) = \text{OBG} - 0.8509 * ((\text{OBG} - 8.7)^{1.037}) * (\text{WD}^{-0.07403}) * ((200 * \text{EXP}(-0.00006 * \text{ML})) / \text{DT})^{2.571}$

Table 4-2 Top Five DEA 119 Models

References

Traugott, M., 1997, "Pore/Fracture Pressure Determinations in Deep Water", Deep Water Technology, August 1997.

Bowers, G. L., 1994, "Pore Pressure Estimation From Velocity Data: Accounting for Overpressure Other Than Undercompaction", SPE 27488 presented at the SPE IADC Conference, 15-18 February 1994.

Bowers, G. L., 2001, "Determining an Appropriate Pore-Pressure Estimation Strategy to be presented at the Offshore Technology Conference to be held in Houston, TX on April 30, 2001.

Miller, Terry, 2001. Personal communication, Knowledge Systems, Inc. Stafford, Texas



5 Geopressure Basin Analysis

As mentioned earlier in this manual, one of the conclusions from the DEA 119 project is that the optimal way to predict geopressures for a new well location is to construct a geopressure basin model. This chapter provides a description of some of the concepts and procedures involved in geopressure basin modeling. One of the best ways to understand a new concept is through use of an example, and a major part of this chapter is devoted to a description of the geopressure model that was built during the course of the DEA 119 project for the Auger Basin in the Gulf of Mexico. Understanding this case study and observing the ease with which a geopressure prediction is made for a new well location using the calibrated model should be informative.

The geopressure basin model is a productive tool to correlate results from offset wells drilled in the area, and also considers a broad range of pressure mechanisms such as hydrocarbon maturation and thermal expansion as well as the lateral movement of formation fluids as affected by sealing and non-sealing faults. Geopressure basin analysis can also be used in studies not directly relating to drilling such as prospect evaluation, intra-basin communication, fault sealing/non-sealing scenarios and hydrocarbon generation potential.

While geopressure basin analysis has proven to be the superior way to predict geopressures at a proposed well location, a great amount of varied data is required to perform such an analysis; see Chapter 2 for details. Further, the construction and calibration of a geopressure basin model requires more geological expertise than the typical drilling engineer possesses, so a team effort is usually required for success. Once the model is built and calibrated, the drilling engineer can quickly and easily use the model to predict pressures at a proposed well location within the model area.

Successful basin analysis can be performed with MicroSoft/Windows based software typically available for regular use. It is very important to properly limit the model's scope; otherwise it can become too large or there will be difficulties in the calibration process. For the analysis described in this chapter, Knowledge Systems' software products DrillWorks/PREDICT and DrillWorks/BASIN were used.

5.1 Geopressure Basin Modeling Overview

The use of forward modeling and data inversion techniques required to predict geopressures at the basin scale is illustrated schematically in Figure 5-1 and also in Figure 5-2. Each well is modeled with respect to the control parameters and lithologically determined compaction laws to produce synthetic porosity and pore pressure curves. An advanced inversion scheme is then used to reduce to a minimum the misfit between the synthetic and the real data, resulting in a set of calibrated control parameters. Faults and other structural features can be added and different scenarios studied, such as sealing/non-sealing faults. The calibrated formation parameters established for each well are used by the 3-D framework to interpolate between known parameters and those at the proposed well location.

The geopressure basin model can be updated while drilling to provide continuously improving data ahead-of-the-bit. In the pressure while drilling mode, an input stream of data from a MWD/LWD contractor is used to make a data-driven analysis of geopressures in real-time. The results from this evaluation, together with any new geological information such as observed formation top depths or unexpected faults, can be used to update the basin geopressure model. An updated model gives a revised projection of the geopressures to guide the drilling operation from the present drilling depth to TD.

The software used in this study performs a calibration of an individual well and a calibration of the basin. The calibration procedure automatically applies data inversion techniques to minimize the misfit between observed and model data. There is an optimal compromise between data accuracy and the complexity of the model, as the results generated by the model are in direct proportion to the quality of the input parameters. As new data becomes available, the predictive accuracy of the model improves.

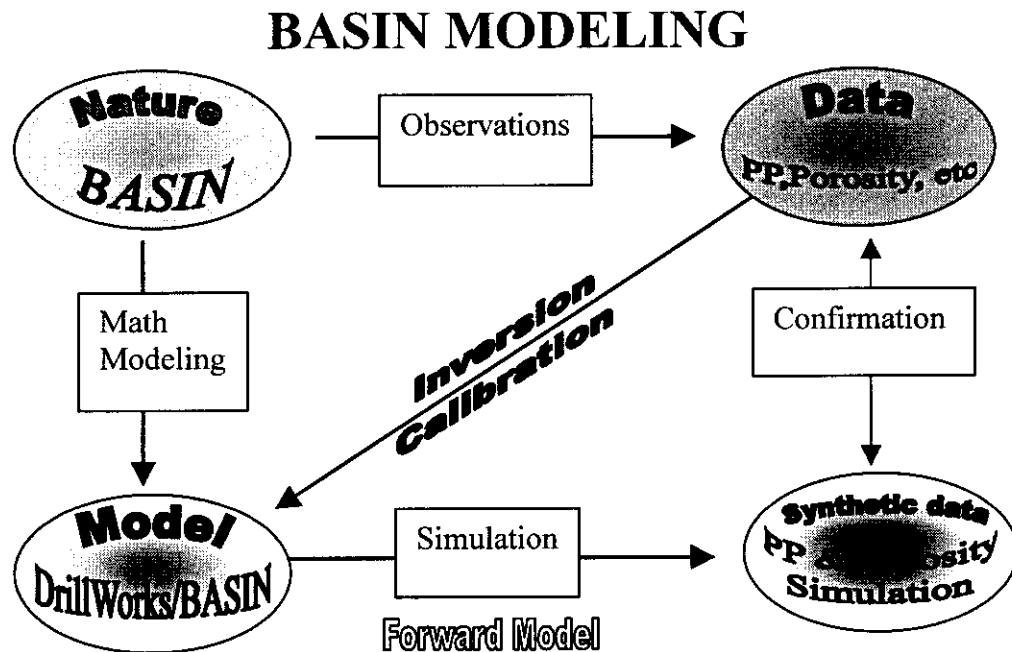


Figure 5-1 Basin Modeling Concept



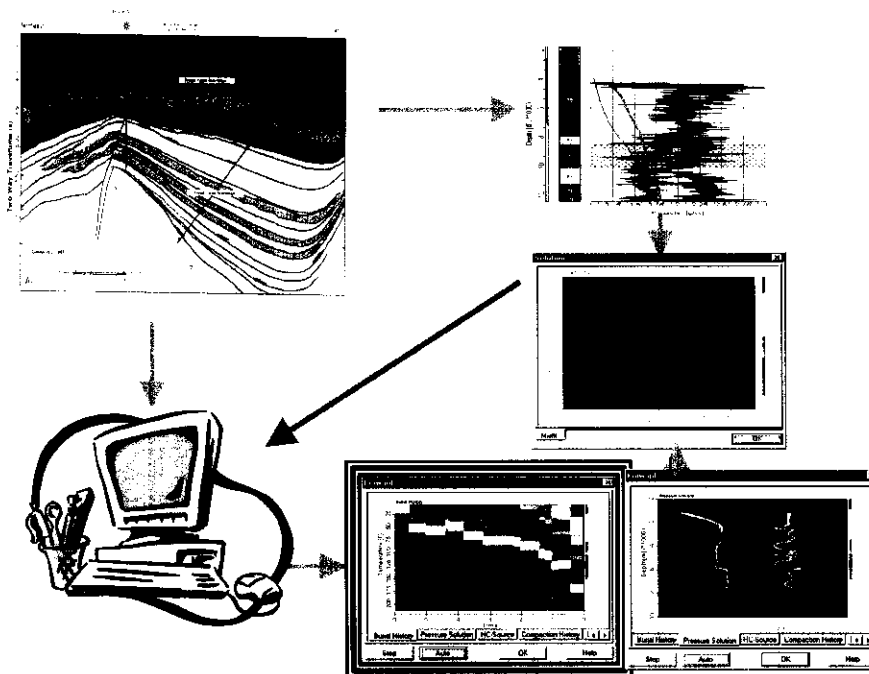


Figure 5-2 Basin Geopressure Modeling Concept from a User's Perspective

Chapter 2 covers in some detail the general data requirements necessary for constructing a geopressure basin model. To supplement this discussion and provide a feel for the details involved in building a geopressure model, some of the software inputs involved in will be described.

A geologic-time based stratigraphic-lithologic column is required to define basin stratigraphy comprising all formation units that exist within the basin area. Each formation unit contains information relating to the geological history of the basin, such as stratigraphic level, geological age and paleo-sea level. In addition, a set of five control parameters are identified for each formation unit to account for the pore pressure through geological time. These control parameters are illustrated schematically in Figure 5-3. The software input dialog screen for the parameters is shown in Figure 5-4.

As a company or user gains experience using geopressure modeling in a particular area like the Gulf of Mexico, default values for these parameters will become familiar. It is important to note that these are not necessarily laboratory-derived values from core data, but should be considered “apparent” values that are used as a starting point for the calibration process. As will be illustrated in the Auger Basin case study, calibration uses definitive pore pressure, porosity and formation tops to adjust these parameters on an iterative basis until there is minimum misfit between the synthetic pore pressure/porosity and the definitive data.

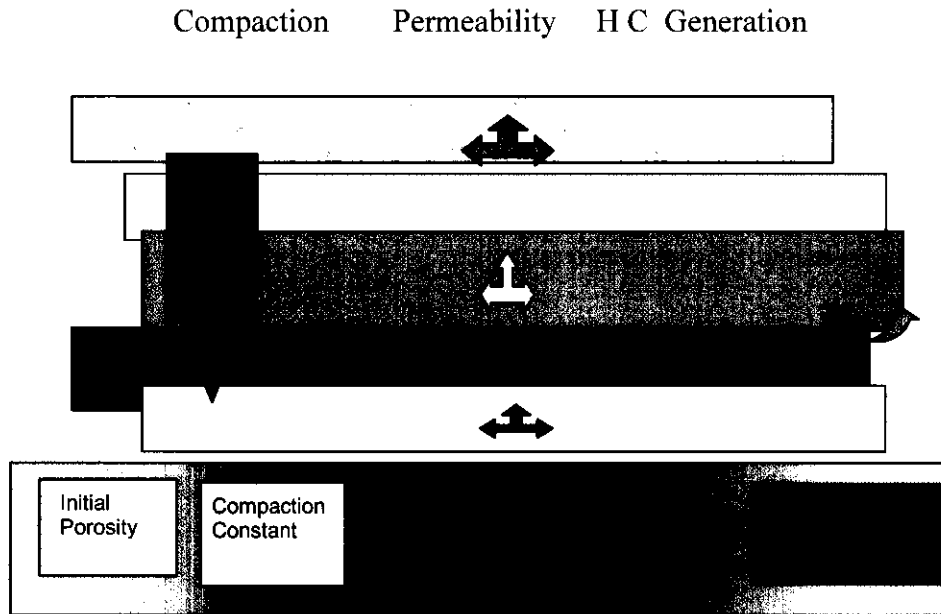


Figure 5-3 Forward Model Parameters

Formation Parameters				
Formation				
Formation Name:	S5	Matrix Density:	2.5	g/cc
Formation Index:	S5	Color:		Paleo Water Depth: 300 ft
Compaction Law:	Clay/Shale	Time Level:	1.4	MY/bpt
Lithology				
Parameters Name	Sand/Sandstone	Left Limit	Right Limit	Steps
Initial Porosity:	0.6	0.4	0.75	70

Compaction Constant: [1/ft]	9.843e-004	3.281e-005	1.963e-003	59

Eff. HC-gener. Potential:	1.e-004	1.e-006	0.1	30

Specific Surface Area:	5.e+006	1.e+006	1.5e+009	64

Eff. Lateral Conduction:	1.e-004	2.e-005	0.1	37

Up	Down	Ok	Cancel	Help

Figure 5-4 Formation Parameters Input Dialog Window

5.2 Case Study in the Auger Basin

The case study carried out in the course of the DEA 119 Project provides a good illustration of the use of basin modeling for geopressure prediction. The Auger Basin was selected for the DEA 119 Project because it is an active and prolific basin in the GOM and also because several wells were available in the database that provided good definitive data. The evaluation was accomplished by building the geopressure basin model *without* using one of the primary wells in the basin. Once the model was built and calibrated, the model was used to predict geopressures for the well that was left out. The geopressures predicted by the model for that well were within +/- 0.25ppg of the known actual pressures.

In the Auger Basin, single well definitive pore pressure analyses were performed on six key wells drilled on different structural styles. They varied from a salt withdrawal mini-basin (Macaroni field), a ramp feature (Habanera field) to a faulted diapiric dome (Auger field). The vertical litho-stratigraphic boundaries separating the different compartments in the basin were assigned based on the age and lithology distribution based on well log correlation.

The model uses five formation parameters for each horizon in each well based on the given lithology, initial porosity, and formation's paleo-water depth. Based on these parameters, the model computes pore pressure and porosity profiles as synthetic data. The system goes through several iterations of the inversion process to fit the synthetic pore pressure/porosity output to the definitive data. During this process, the software adjusts and fine-tunes the five model formation parameters and distributes them spatially to the other wells. The software is capable of eliminating anomalous formation parameter data aggregates by mapping each horizon individually for the entire basin. The model was also able to compensate for the structural effect due to salt withdrawal and invasion, and then manipulate the formation parameters accordingly.

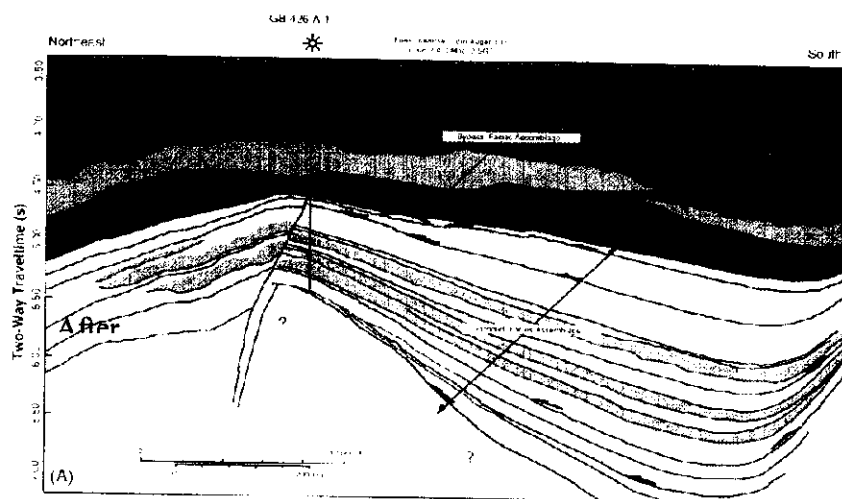


Figure 5-5 Cross section of Auger Basin after Prather et al., 1998.

5.2.1 Basin Stratigraphy

In the Auger Basin, the Plio-Pleistocene (Figure 5-6) section was divided into seven sequences. The low permeability seal beds (shale) represent the cap rock for seven reservoir type beds (sand). They are S₁ to S₇ for the seals and R₁ to R₇ for the reservoir beds (Figure 5-7)

Well correlation was conducted in the entire basin to assign the depth of each unit in the key wells. Based on that correlation, a typical litho-stratigraphic column for the study area was established.

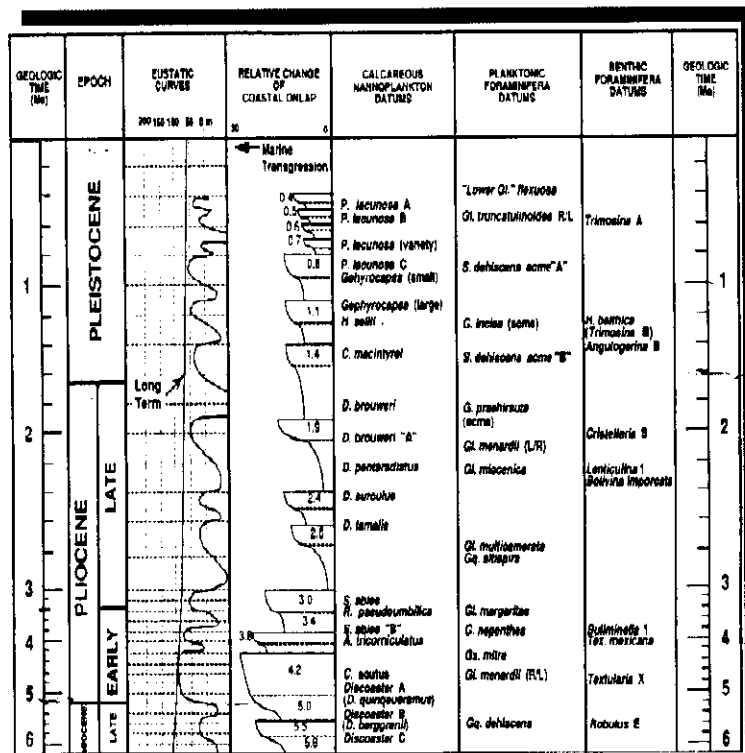


Figure 5-6 Stratigraphic Column of the Plio-Pleistocene of the GOM



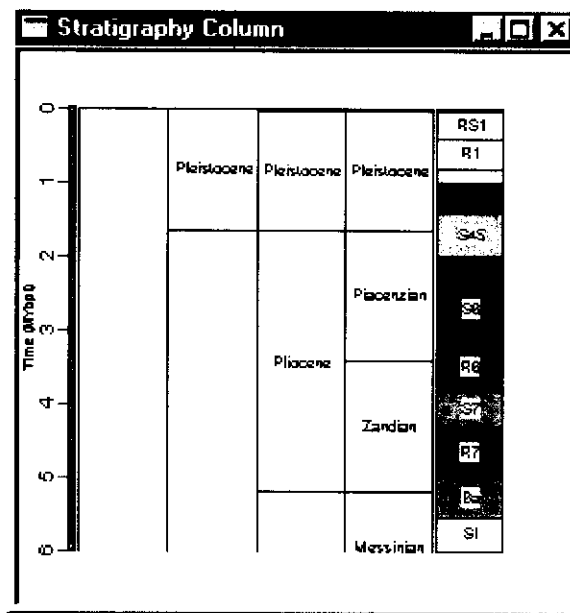


Figure 5-7 Litho-stratigraphic units in Auger Basin used in Geopressure Model

5.2.2 Structure Segments

The Auger Basin is almost completely surrounded by salt walls, which makes it ideal for a geopressure basin study. Downdip from the current flexure trend, the sediments tend to take a ramp shape toward the central salt diapir where the Auger field was initially discovered. Southwest of the Auger field diapir, a large basin was created due to the high rate of salt evacuation in the Macaroni field area. Due to the lack of seismic data in this area, the detailed structural features could not be included. Some of the published maps show three main faults south of GB 300, south of GB 387 and on the crest of the Auger diapiric structure at GB 471. There is also a minor anticlinal feature north of GB 258 and a synclinal feature at the extreme end of the basin west of GB 600 (Figure 5-5).

5.3 Geopressure Calibration in the Auger Basin

Five key wells were chosen for calibration of the formation parameters for the entire basin: GB 258, GB 300, GB 387, GB 516 and GB 602 wells. They represent wells drilled in different geological settings. The sixth well, GB 471-1 was used as a test well to test the validity of the basin model calculations, but was not used to calibrate the model.

5.3.1 Definitive Geopressures and Stratigraphy

The calibration process requires a definitive pore pressure and porosity curve for each calibration well and also requires the depth of each litho-stratigraphic unit. To determine definitive pore pressure and porosity curves for each calibration well, an analysis was made using all available data. Typically, pore pressures were computed from resistivity, sonic and seismic checkshots, if available. These individual pore pressure datasets were calibrated with all pressure indicators to include RFT's, kicks and to a lesser extent, mud weights and the pore pressure that best matched the calibration data was deemed to be the definitive pore pressure for that well.

A similar process was carried out to determine a definitive porosity curve for each well. The depth of the tops of the litho-stratigraphic units were determined from logs such as Gamma ray and seismic cross sections where available. The same process was repeated for the test well, GB-471 so that the definitive values could be used to test the predictive accuracy of the calibrated basin geopressure model.

5.3.2 Synthetic Well Data

In order to generate synthetic pore pressure and porosity using the Forward Model, physical data had to be introduced to the system. For each formation, from S_1 to S_7 and from R_1 to R_7 , the following information was needed:

- Paleo-water depth (Paleo-environment)
- Age of sediments in MY
- Matrix density
- Initial values for the five formation factors with a best estimate and a high and low range, plus the number of step-increments to be used during calibration
- Description of unconformities and faults

5.3.3 Single Well Calibration

The Forward Model generates the synthetic pore pressure and porosity based on the five formation parameters used by the system. By correlating the synthetic data to the actual data for the same well, the misfit between the two can be graphically displayed. (Figure 5-8). The model sends the synthetic data back to the Forward Model (inversion calibration) to adjust the formation parameters in order to narrow the misfit window. This automatic data inversion process between the synthetic and actual data ends when the misfit values become minimal. In the process, all five formation factors for each layer are adjusted at each inversion iteration until there is a close match between the synthetic and definitive pore pressure and porosity for the well (Figure 5-9). All five wells were calibrated in this same way.

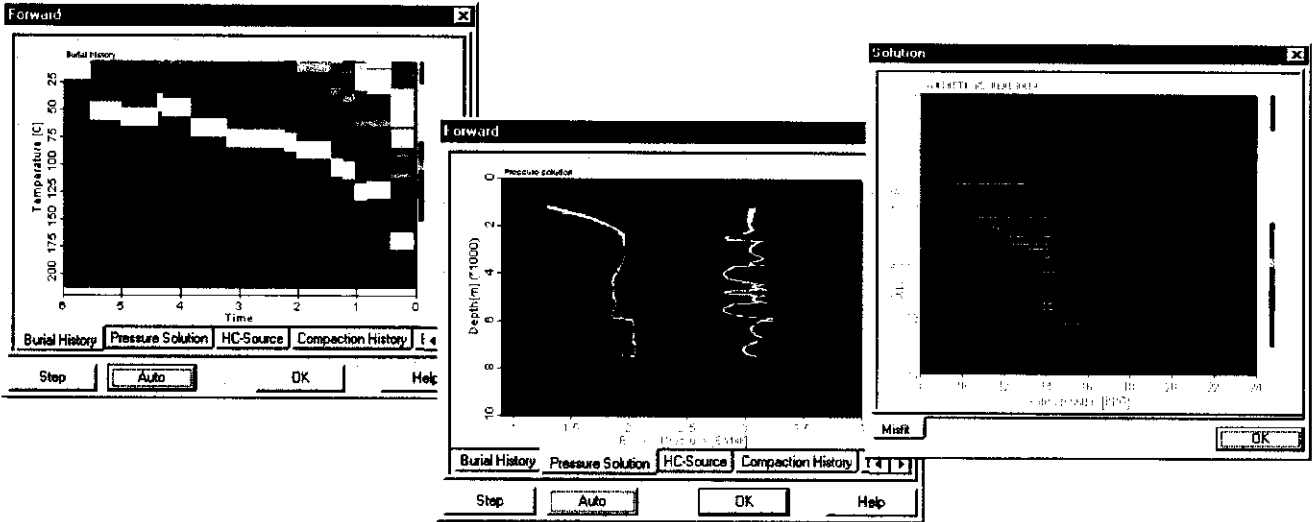


Figure 5-8 Forward Model Windows shown left and center; Misfit Window on Right

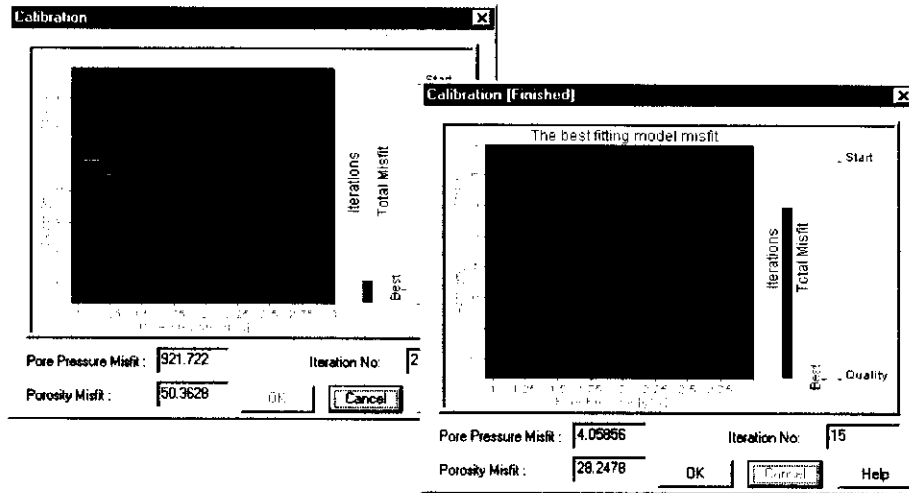


Figure 5-9 The inversion process between the synthetic and actual data minimizes the misfit

5.4 3-D Framework

After the control wells are calibrated, the five formation parameters that have been determined from inversion are distributed from the calibration wells to the surrounding areas. Generating contour maps for each horizon shows the anomalous values for the interpolated formation parameters. These contour display maps exhibit areas where the model can be improved by adjusting the formation factors to reduce the anomalous zones. Among the five parameters, the compaction constant was the most effective adjustment to fine-tune the model.

5.4.1 Adding Boundary and Infill Wells

In the Auger Basin study, most of the available key wells were located at the axial part of the basin. Several pseudo-wells were chosen as infill wells (Figure 5-10). These boundary wells (PW₁, PW₂, ect.) helped to distribute the formation parameters to the basin periphery.

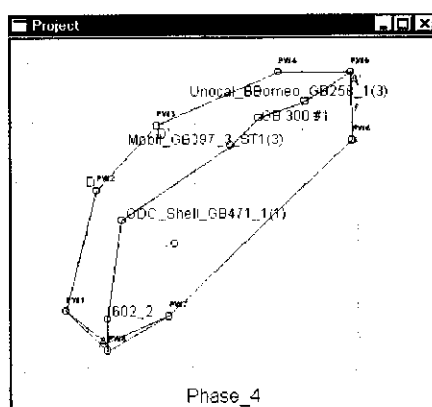


Figure 5-10 Boundary and Infill Wells

5.4.2 Using Parameters Transfer

The next step is to choose the well with the best fit between the synthetic and actual or definitive pore pressure and porosity throughout the entire basin. The geopressure modeling software facilitates a uniform transfer of parameters from this well to others in the basin.

5.4.3 Using Pore Pressure/porosity Misfit Maps

Mapping of the pore pressure and porosity misfit distribution in the entire basin is an important step to ensure the correct calibration. Areas where the misfit is maximum are shown on the Contour map in the center window of Figure 5-11. Interpolation can be used to minimize these misfit anomalies.

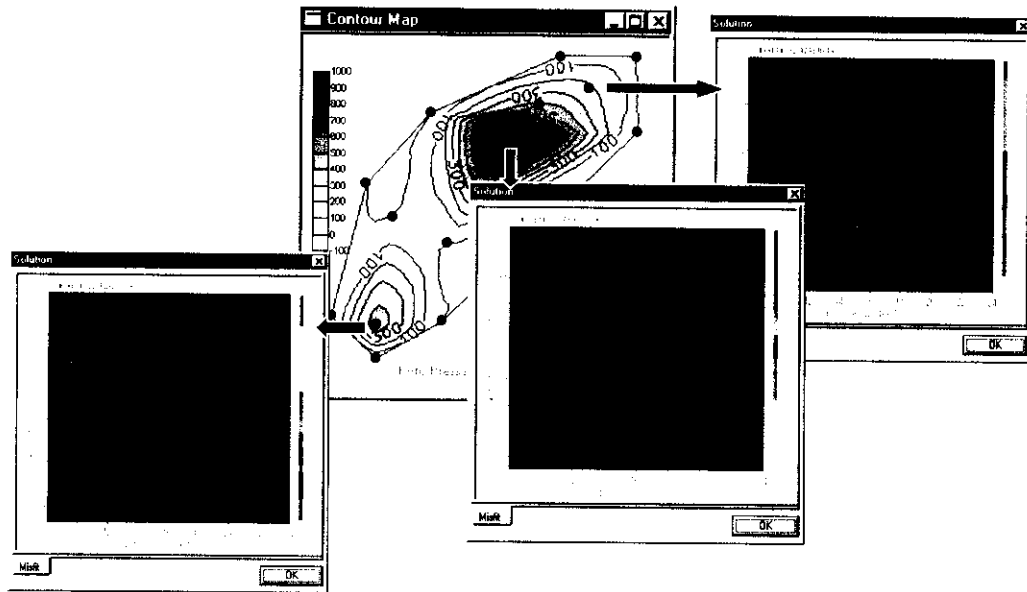


Figure 5-11 Reducing the Misfit by using an interpolation process

5.4.4 Fine-tuning the 3-D Framework

This important step in the calibration process can be gained by practice and experience. The essential steps include:

- Adjustment of the compaction constant.
- Investigate the misfit of the formation parameters at each individual horizon, especially at the shale-sand interface where the centroid effect can take place.
- Make a fine adjustment of the compaction constant in the less dominant horizons. In the Auger Basin for the R₆ and R₇ layers the synthetic pore pressure and porosity show relatively high mismatch in the GB 602 well #2 (Figure 5-12). Figure 5-13 shows the poor 3-D distribution of the formation parameters due to the fact that these two horizons are represented in this well only.

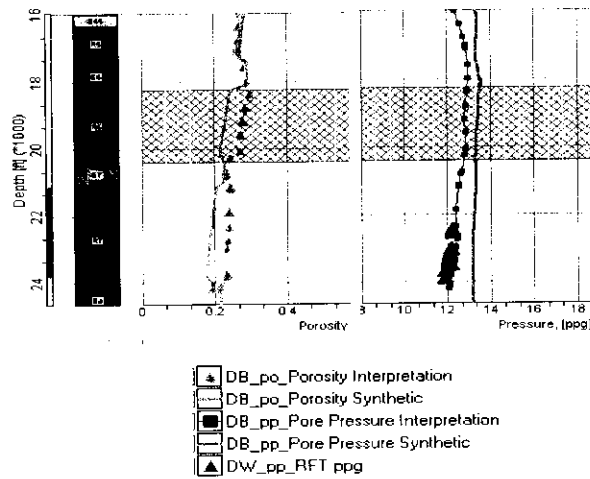


Figure 5-12 Individual horizon's fine-tuning

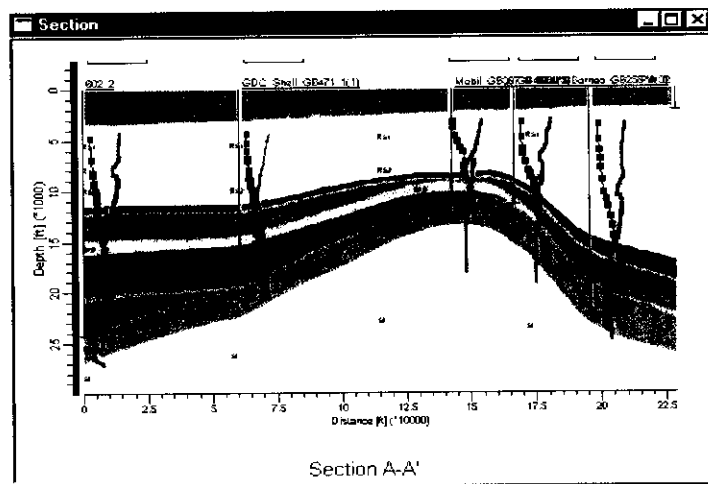


Figure 5-13 Geopressure cross section in the Auger Basin. GB 602 #2 penetrates the oldest section.

5.5 Specifying the Main Geological Framework

In the Auger Basin, salt wall (boundaries) and faults were the main features to model. In both cases, the fault display tool was used to create the surrounding boundary and the

main faults. The salt walls and faults were traced based on published geological documents and maps for this area. Because we are dealing with pressure compartmentalization rather than structural issues, boundaries and faults appear as vertical boundaries (Figure 5-14).

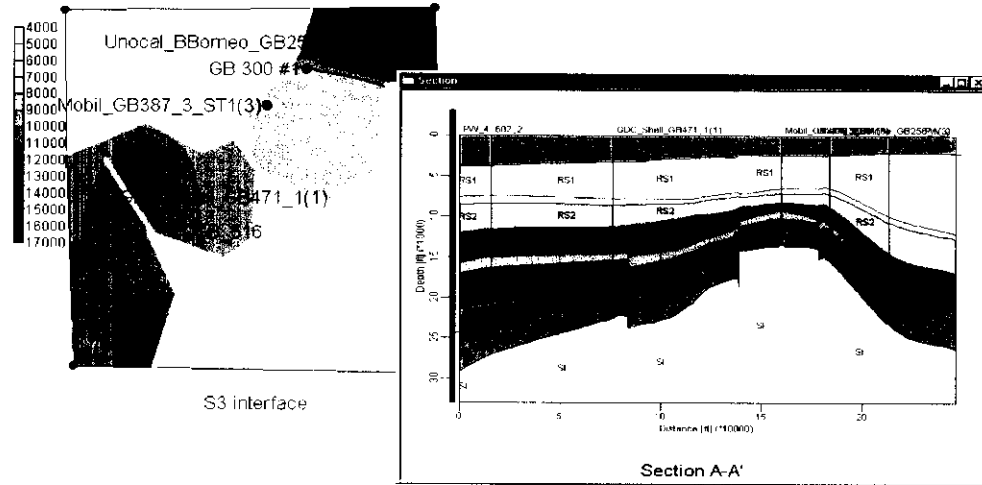


Figure 5-14 Auger Basin salt wall boundaries and fault on left, Geopressure compartments created by faults shown in Section on right.

5.6 Viewing Results in 3-D

It is helpful to be able to view the model and geopressure results in various three dimensional views. The figure below illustrates a fence-type cross section that can be rotated for viewing at any angle (Figure 5-15).

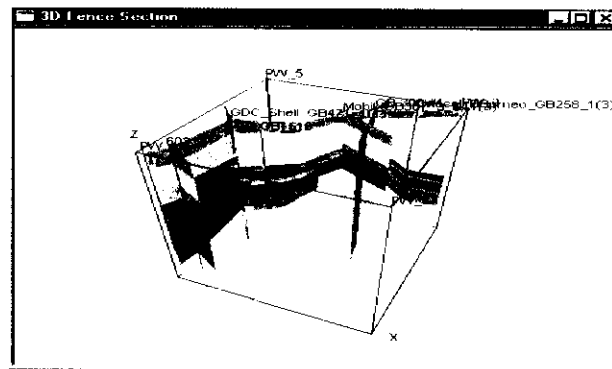


Figure 5-15 Fence-type cross-section through key Auger Basin wells

5.7 Testing the Predictive Effectiveness of the Model

The Auger Basin model was tested using the GB-471-1 well. This well was not used in model calibration. To generate a geopressure prediction, the user simply specifies the location of a proposed well either interactively using a mouse or by specifying geographic coordinates such as latitude and longitude. Figure 5-16 illustrates the location of the test well, GB-471-1 in the basin. The system will very quickly conduct a 3-D interpolation of all the formation factors at that point and generate a pore pressure and porosity profile for the proposed location. If seismic data is available that identifies the depth of key formations, the stratigraphic formation tops at the proposed well location can be depth-adjusted in the model to improve the results. Figure 5-17 shows the results of the test by comparing the pore pressure and porosity generated by the model with the definitive values.

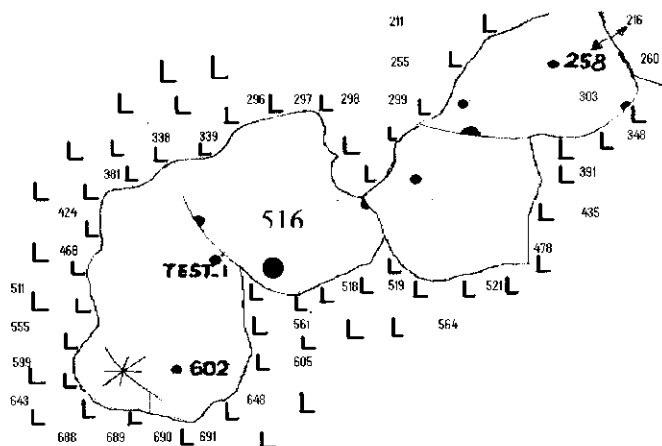


Figure 5-16 Location of Test Well in Auger Basin

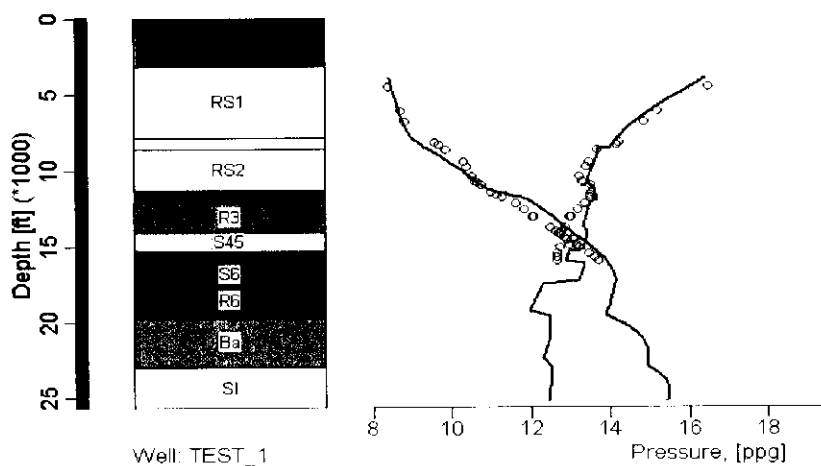


Figure 5-17 Blind test on GB 471. Solid lines are synthetic data generated by the model and circles are the definitive or actual values.

5.8 Pore Pressure Monitoring in Real-Time

After testing the competency of the model, pore pressure prediction results can be beneficial for real-time drilling. There is the possibility of surprises using 1-D pore pressure predictions “ahead of the bit”. With 3-D basin modeling, the deeper un-drilled pore pressure section can be calculated with more confidence for the drilling engineer. The model interpolates the adjusted synthetic pore pressure profile for the deeper formations in the surrounding area and projects to the active well. Misfit adjustments need to be updated routinely between the interpolated synthetic prediction and the actual well site data during drilling (Figure 5-18).

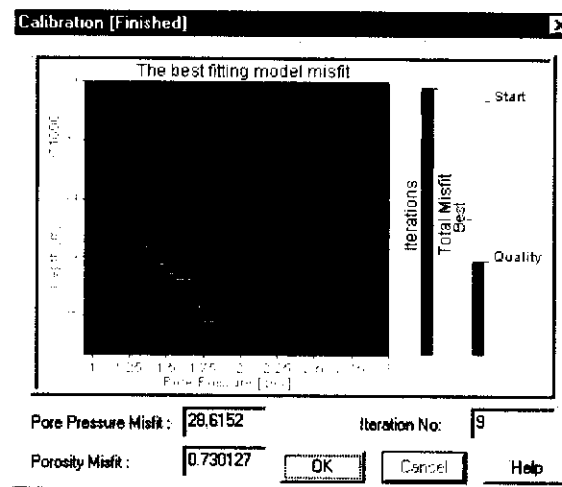


Figure 5-18 Real-Time Pressure Monitoring

5.9 Integration of Geophysical Data in the Geopressure Basin Model

Introducing geophysical data to the geological-based geopressure model improves the prediction efficiency. The geophysical data enhances the knowledge of the basin morphology, makes it possible to add more pseudo-wells and provides more details about the internal compartmentalization. Several ways that integration of geophysical data improves the geopressure basin model are described in the following:

5.9.1 Use of Seismic Velocity to Make Pseudo-wells

The average interval velocity gather at specific locations is a reconnaissance method to predict the sub-surface pressure profile. The addition of several pore pressure prediction

stations to the basin model can be used as pseudo-wells to provide more definition. Given seismic velocities prepared in accordance with the guidelines in this manual, the new velocity/pore pressure transforms in Chapter 4 can be used to generate a pore pressure and porosity profile at selected gather locations to make pseudo wells. This will increase the number of possible calibration points in the basin, especially in frontier areas where wells are scarce.

5.9.2 Sequence Boundaries

Mapping the sequence boundaries helps to detail the sub-surface structure. A great deal of basin history and the interaction between sediment input and salt withdrawal can be predicted. Moreover, sequence boundaries help visualize the main compartmentalization units in the basin.

The condensed high stand sections marking a sequence boundary usually represent the main seals in the geopressure systems. In GC 248 #1 (deep water GOM) the major sequence boundaries are marked by increases in the mud weight (Figure 5-19). The convergence of successive sequence boundaries at GC 473 #1 was responsible for changes in the pore pressure (Figure 5-20). The addition of geophysical data to the basin model greatly enhances the ability to identify these important elements and specify them to the basin geopressure model.

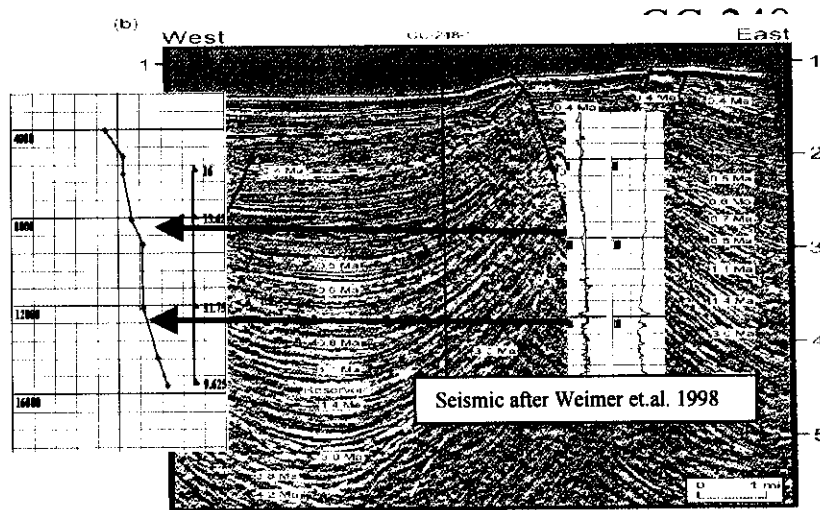


Figure 5-19 Shows how the change in major sequence boundary affects the pore pressure profile. An increase in the mud weight at 0.5 and 0.7 Ma boundaries is shown.



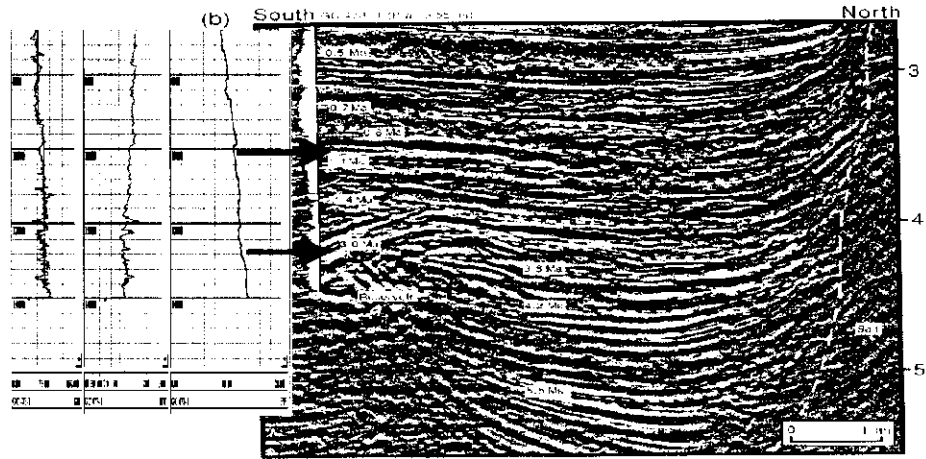


Figure 5-20 Shows the pore pressure changes drilling through different sequence boundaries and system tracks. Seismic after Weimer et al, 1998

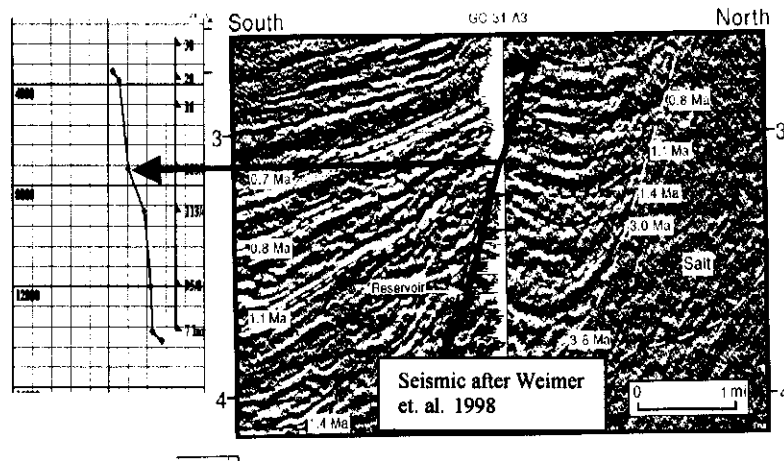


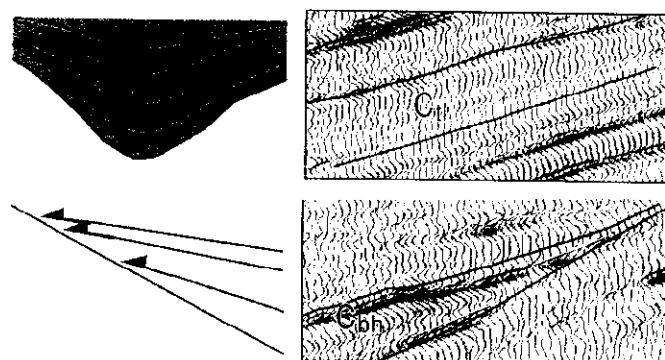
Figure 5-21 Shows how the fault juxtaposes two different systems. Drilling through the fault resulted in 2 ppg increase in mud weight.

5.9.3 Fault Juxtaposition

With the geophysical data added to the basin geopressure model, fault juxtaposition can be observed and modeled. Drilling through a fault plane sometimes is a challenging task because sequence boundaries are displaced across the fault plane. In tensional fault systems, the older sequence on the upthrown side juxtaposes a younger sequence on the downthrown side. This creates a difference in the compaction disequilibrium parameter across the fault. In GC 31 #3A, the well was drilled through a fault and the bore hole sequence boundaries changed from 1.1 my to 1.4 my (my is a million years of geologic time). This difference was responsible for a mud weight increase of 2 ppg (Figure 5-21).

5.9.4 Seismic Facies

By adding geophysical data to the geopressure basin model, seismic facies studies can be used to shed light on the lithology internal changes within the major sequence boundaries. Communication between different reservoirs and sealing efficiencies can be predicted by recognizing the characteristics of these seismic facies. Figure 5-22 is a generic case, showing how a free pressure communication can take place in the top section. Conversely where onlaps are shown in the lower section, pressure compartmentalization can exist.



After Prather 1998

Figure 5-22 External and internal geometry of seismic facies help predict pore pressure compartmentalization

5.9.5 Using Seismic Data to Enhance the Accuracy of the Geopressure Basin Model

With geophysical data incorporated in the geopressure basin model, the accuracy of the geological model can be enhanced.

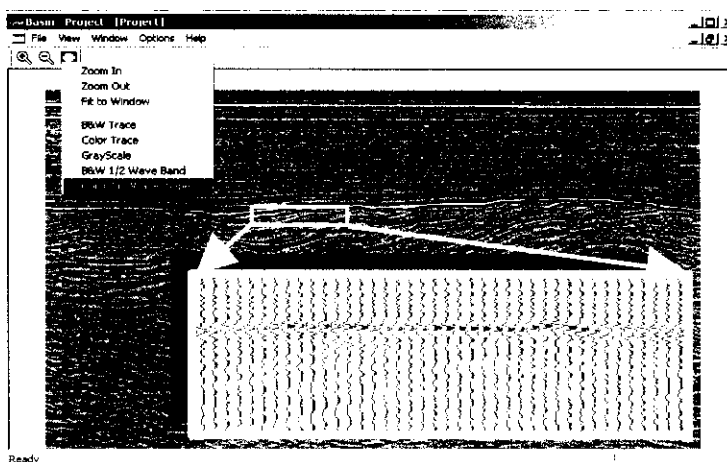


Figure 5-23 Use of seismic displays to adjust elevation of formation tops

5.10 Modeling Salt Tectonics

As discussed earlier, the presence of massive salt bodies associated with salt tectonics is a complicating factor for GOM drilling in general and geopressure prediction in particular. Due to the upward intrusion of the salt in the geological section gradually over geologic time, the compaction constant changed with time accordingly. Figure 5-24 illustrates the case where the compaction constant increases in the younger sediments (RS_1 , RS_2 and S_3) relative to the older section below R_3 . The combination of the vertical overburden gradient and the incremental upward stress due to the salt movement is the possible cause of this phenomenon in the Auger basin. Understanding this phenomenon might help indicate when in terms of geologic time the salt movement was active.

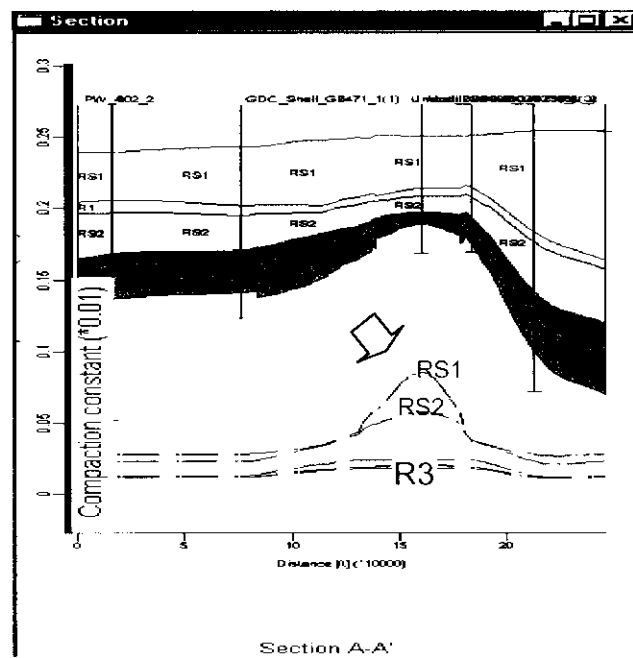


Figure 5-24 Shows the change in the compaction constant relative to the salt movement

6 Integrating Uncertainty in Prediction

6.1 Introduction

This chapter introduces the concepts related to quantifying uncertainty in geopressure prediction. As in previous chapters, the concepts will be illustrated with examples. As discussed in some detail in other parts of this manual, there are uncertainties in several components of the process involved in predicting geopressures. Chapter 2 describes the possible errors and uncertainties that are involved in the various geophysical and petrophysical measurements used to quantify a geopressure prediction. Guidelines are provided to help quantify the confidence that the analyst can have in this data. There are also uncertainties in the models that are used to predict, for example, pore pressure from velocity data.

It is possible to utilize the technology developed in the fields of statistics and probability to integrate uncertainty into the prediction results. In the course of the DEA 119 project, uncertainty analysis was determined to be an important aspect of the geopressure prediction process. The materials in this chapter document project activities in uncertainty analysis and point the way for more extensive future work in this area.

The kind of results illustrated in this chapter should be immediately recognized and appreciated by the drilling engineers. “Maximum” and “minimum” pore pressures are displayed along with the “mean” predicted pore pressure. The maximum and minimum bounds will have a certain “probability” associated with them. Armed with this data, the drilling engineer can consider the uncertainty in geopressure prediction and consequently its implication on well planning. In addition, the results can be used to justify the additional costs that are required to obtain more certain prediction results. For example, the cost of reprocessing seismic data, or of obtaining a high resolution seismic hazard survey might be justified if a more certain geopressure prediction might make it possible to eliminate a casing string.

A special Monte Carlo simulator was developed to provide a means of assessing the effects of uncertainties in input variables on predicting pore pressures as an integral part of the model developments in the DEA 119 Project. The simulator was developed as a Microsoft EXCEL macro that will be distributed to project participants. We plan to integrate this capability into Drillworks/PREDICT at a later date. This chapter addresses the use and results of the Monte Carlo simulator developed for this project.

6.2 Overview of Monte Carlo Simulation

Monte Carlo simulation is a statistical technique by which a quantity is calculated repeatedly, using randomly selected “what-if” scenarios for each calculation. Though the simulation process is internally complex, computer software performs the calculations as a single operation, presenting results in simple graphs and tables. These results approximate the full range of possible outcomes and the likelihood of each. When the Monte Carlo simulation is applied to uncertainty assessment, the range of possible results appears as a frequency distribution graph similar to the familiar bell-shaped curve, which non-statisticians can understand intuitively.

Monte Carlo simulation was named for Monte Carlo, Monaco, where the primary attractions are casinos containing games of chance. Games of chance such as roulette wheels, dice, and slot machines exhibit random behavior. The random behavior in games of chance is similar to how the Monte Carlo simulation selects variable values at random to simulate a model. When you roll a die, you know that a 1, 2, 3, 4, 5, or 6 will come up, but you don't know which will appear in any particular roll. It is the same with the variables that have a known range of values but an uncertain value for any particular time or event (e.g. interest rates, staffing needs, stock prices, inventories, phone calls per minute).

Monte Carlo simulation also has important limitations and these limitations are listed below:

- ❑ It does not distinguish between variability and uncertainty; uncertainty is treated as if it were variability, which may produce misleading results. The lack of knowledge of variable magnitudes is called "uncertainty".
- ❑ Ignoring correlations among exposure variables can bias Monte Carlo calculations. In the areas studied here, OBG and sonic interval velocities are treated as if they are not correlated.

For each uncertain variable (one that has a range of possible values), the possible values with a probability distribution are defined. Certainty is the percent chance that a particular forecast value would fall within a specified range. The type of distribution selected is based on the conditions surrounding that variable. Distribution types include:



The normal distribution is used in the simulator provided to participants. The simulator uses the top five models determined in the DEA 119 project to predict pore pressure and the uncertainty bounds in predicted pore pressure that is associated with the uncertainties in the input data.

6.3 Using Monte Carlo Simulation for Geopressure Prediction

The Monte Carlo simulator developed for the project assumes all variables are uncorrected and normally distributed. It has two optional modes of operation:

- ❑ Geopressure prediction from interval velocities using up to 18 shot points or CDP's in the general area of a proposed well.
- ❑ Geopressure prediction from acoustic data in the form of sonic travel time where there are varying uncertainties in the accuracy of the data with depth (maximum of 150 depth points).

When interval velocities are used as input, the simulator calculates a mean and a standard deviation from the data for each depth. When sonic log data are used as input, the user must enter a measure of the expected uncertainty in the travel time at each depth. The log reading is assumed to be the mean of a normal distribution, while the uncertainty estimate is used to estimate a standard deviation.

The user must also supply OBG data, which is used to calculate parameters describing an appropriate normal distribution. The expected value is assumed to be the mean, and the standard deviation is computed from a user specified margin (the 90% exceedance value) that when added to the mean will exceed 90% of the estimates of the OBG developed by the simulator.

Figure 6-1 illustrates the application of Monte Carlo Simulation in the pore pressure estimation process. The process is dependent on a random number generator for sampling the input variable values that are assumed to be normally distributed.

- At a given depth the variables (OBG and sonic) are sampled and pore pressure is computed by each of the five models. The sampling is repeated randomly a number of times to generate a distribution for the pore pressure.
- The process above is repeated for all other depths.
- The statistics reported for the predicted pore pressures for each model were calculated from the mean and standard deviation assuming those predictions are also normally distributed.

6.3.1 How to use the Simulator:

The simulator is built as an EXCEL spreadsheet.

General input Data:

- Well Name
- Air Gap (Kelly bushing elevation, ft)
- Water depth, ft

If seismic data analysis is required:

- 1 Input the velocity versus depth for up to 18 seismic lines.

NOTE: All the data shares a common vertical depth axis. If you have the velocity data with different depth points, interpolation has to be done to obtain velocity lines on one common depth. Since statistical uncertainties at each depth are determined from these data, a minimum of three shot points is required. Four or more should produce more reliable statistics.

- 2 Input "key" number 2 for cell G4.
- 3 Input the overburden gradient in ppg units with a certain error margin versus depth.

- 4 Run Macro.
- 5 Analyze the prediction on model-to-model bases or use the composite prediction.

If sonic data are available, then:

- 1 Input sonic data in micro sec/ft units in column T. Input the error margin in sonic measurements versus depth in column U (for example: 5 micro sec/ft for the shallow depths, and 3 micro sec/ft for deeper intervals).
- 2 Input “key” 1 in cell G4.
- 3 Run Macro.
- 4 View results.

Views:

Five models are programmed. The results of each model are presented in a separate view. The composite view shows the results of all models in one view.

Two examples are included to illustrate the results of Monte Carlo simulation.

6.3.2 Example 1: Uncertainty in Pore Pressure Analysis from Seismic Data

Example 1 demonstrates the processing of seismic lines velocity data to produce pore pressure prediction with the uncertainty bounds.

- Figure 6-2 shows the input seismic velocity data (labeled as site 1 to 10). The output of five models is presented in three different columns, namely: the mean, the upper and lower bounds which represents 90% of the predicted values are within these bounds.
- The example uses a constant uncertainty in the OBG data versus depth. The analyst may use a variable variation versus depth.
- Figure 6-3 shows sample prediction from two models.
- Figure 6-4 shows the summary of the combined results of five models.

6.3.3 Example 2: Processing of Wireline Sonic Data

- Filtered shale points sonic data was entered in Column T with 4 micro sec/ft possible error (90% confidence) and kept constant for all depths. Similarly, the OBG data. The OBG data were subjected to linearly decreasing error margin starting at 0.5 ppg at shallow depths (just below the mud line) to 0.2 ppg at total depth.
- Figure 6-5 shows prediction of two models and the combined results of all models are shown in Figure 6-6.



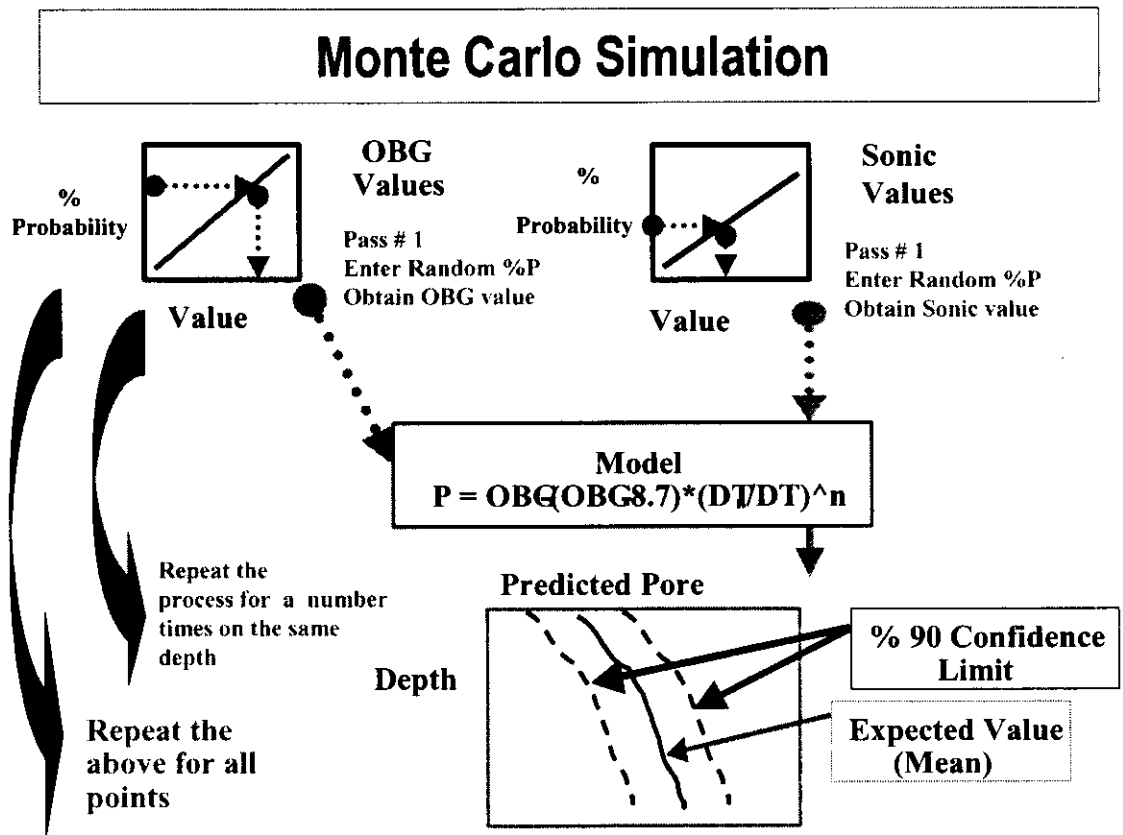


Figure 6-1 The Monte Carlo Simulator and the Pore Pressure Estimation Process

Location Information		Analysis Control				Notes: 1. Specify "1" in cell G 2. Specify "2" in cell G					
Air Gap	Water Depth	Number of Monte Carlo Trials		Log (1) / Seismic (2) Switch							
85	4598	1000		2							
Possible Interval Velocity Picks											
Depth(TVD KB)	Site 1	Site 2	Site 3	Site 4	Site 5	Site 6	Site 7	Site 8	Site 9	Site 10	Site 11
4890.924395	6425.506509	6425.507	6425.507	6425.507	6425.507	6334.391	6334.391	6334.391	6431.416	6425.507	
5078.848817	6494.297487	6494.687	6396.679	6396.679	6396.679	6394.605	6492.643	6394.605	6492.643	6396.547	6494.687
5267.28005	6460.349772	6459.654	6556.721	6556.721	6556.721	6556.144	6459.07	6556.144	6459.07	6459.07	6459.654
5457.564589	6621.71228	6621.188	6621.188	6621.188	6621.188	6519.518	6622.838	6519.518	6622.838	6622.838	6621.188
5651.203688	6690.97582	6690.315	6690.315	6690.315	6690.315	6790.381	6689.65	6790.381	6689.65	6689.65	6793.261
5848.342727	6862.333055	6756.985	6756.985	6756.985	6756.985	6756.174	6756.174	6756.174	6756.174	6756.174	6759.847
6047.473436	6827.903219	6933.27	6933.27	6933.27	6823.576	6822.832	6822.832	6822.832	6822.832	6822.832	6826.507
6247.031916	6891.742294	6893.768	6893.768	7002.362	6889.196	6889.196	6889.196	6889.196	6889.196	6889.196	6892.873
6450.196207	7075.802707	7075.06	7075.06	7075.06	7070.556	7070.556	7070.556	7070.556	7070.556	7070.556	6959.388
6658.76746	7263.470933	7260.518	7260.518	7260.518	7259.527	7259.527	7259.527	7262.852	7147.795	7263.54	
6871.193613	7340.827083	7341.581	7341.581	7223.834	7338.632	7338.632	7220.792	7218.638	7333.756	7220.327	
7087.612369	7537.962385	7420.354	7420.354	7416.534	7414.335	7293.954	7410.63	7294.189	7291.917	7289.523	
7306.417009	7504.856643	7496.94	7498.94	7495.232	7495.975	7492.145	7369.341	7486.396	7364.28	7365.112	
7520.231143	7194.865005	7195.179	7195.179	7321.06	7192.08	7318.061	7314.249	7311.893	7308.971	7309.604	
7728.497697	7123.46064	7120.382	7120.382	7120.382	7248.466	7113.937	7244.925	7249.083	7374.985	7375.78	
7934.471074	7037.208986	7170.4	7170.4	7170.4	7174.559	7307.972	7307.972	7305.246	7306.004	7441.77	
8141.945682	7226.670347	7227.351	7227.351	7227.351	7364.112	7364.112	7364.112	7365	7503.134	7370.223	
8352.904097	7276.720661	7277.001	7277.001	7422.469	7285.889	7427.598	7429.434	7564.038	7428.375	7568.07	
8569.611514	7621.914235	7760.884	7760.884	7621.877	7626.489	7630.028	7627.11	7485.884	7631.593	7633.238	
8794.353955	7829.128632	7691.392	7691.392	7691.392	7688.305	7547.914	7692.959	7693.552	7697.337	7558.154	
9021.005908	7753.193093	7753.193	7753.193	7753.193	7754.063	7754.063	7611.762	7759.241	7612.149	7760.751	

OBG Information		Model 1			Model 2			Model 3		
Expected	90% CI	Min (90%)	Mean	Max (90%)	Min (90%)	Mean	Max (90%)	Min (90%)	Mean	Max (90%)
8.71257	0.5	8.47208	8.618916	8.765752	8.679467	8.73143	8.783393	5.231448	5.551877	5.872306
8.96981	0.5	8.349582	8.540093	8.730604	8.693299	8.764896	8.836493	5.333872	5.751958	6.170044
9.2211	0.5	8.24365	8.454143	8.664635	8.724349	8.804515	8.884681	5.491565	5.966168	6.440771
9.46328	0.5	8.136364	8.365501	8.594639	8.750868	8.833693	8.916519	5.558558	6.091061	6.623563
9.70136	0.5	8.043332	8.259655	8.475979	8.78962	8.857236	8.924852	5.724295	6.225128	6.725961
9.92873	0.5	7.988826	8.195217	8.401608	8.830462	8.901125	8.971789	5.98849	6.498752	7.009015
10.15107	0.5	7.941514	8.140609	8.339704	8.858569	8.930655	9.002741	6.17276	6.688276	7.203792
10.3629	0.5	7.922399	8.107718	8.293037	8.900437	8.971751	9.043066	6.404299	6.917204	7.430109
10.56478	0.5	7.845989	8.031597	8.217205	8.890854	8.952851	9.014848	6.427986	6.945569	7.463153
10.76667	0.5	7.732987	7.924219	8.11545	8.863766	8.911088	8.958409	6.474974	6.980439	7.485903
10.96334	0.5	7.756236	7.941538	8.12684	8.890466	8.961153	9.03184	6.699668	7.225446	7.751224
11.15054	0.5	7.752704	7.932338	8.111973	8.886874	8.979433	9.071992	6.857172	7.392292	7.927412
11.33297	0.5	7.790166	7.951366	8.112566	8.932598	9.009575	9.086553	7.049315	7.562844	8.076372
11.49908	0.4	8.097156	8.198063	8.29897	9.169736	9.260386	9.351036	7.708022	8.119747	8.531473
11.65956	0.4	8.219835	8.344362	8.468889	9.274926	9.409756	9.544586	8.030171	8.461556	8.892941
11.80881	0.4	8.301212	8.432479	8.563745	9.33785	9.489919	9.641989	8.210857	8.646324	9.081791
11.9547	0.4	8.370614	8.476843	8.583071	9.383443	9.519594	9.655745	8.302565	8.73513	9.167696

Figure 6-2 Example No. 1



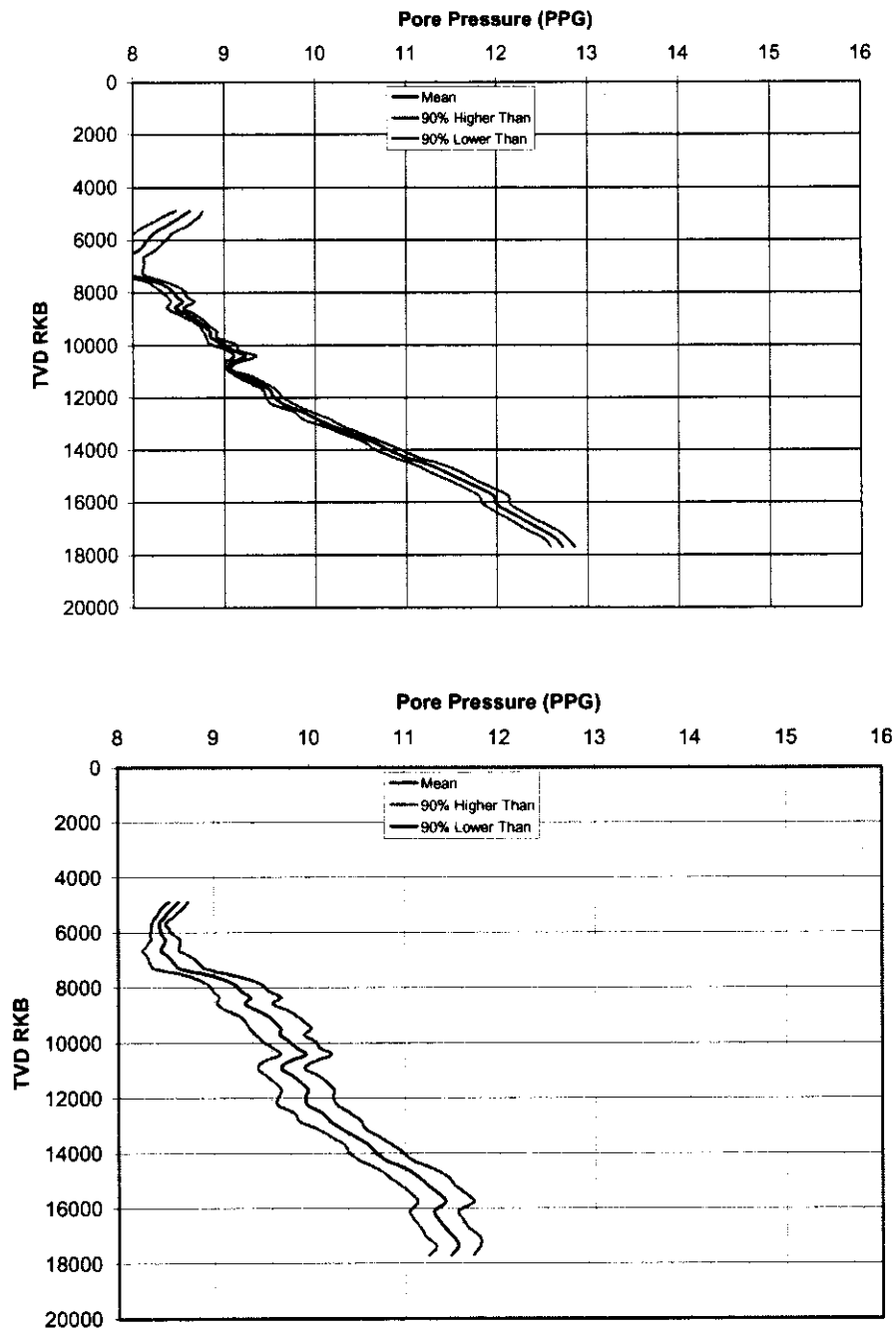


Figure 6-3 Example No. 1- Sample prediction from two models

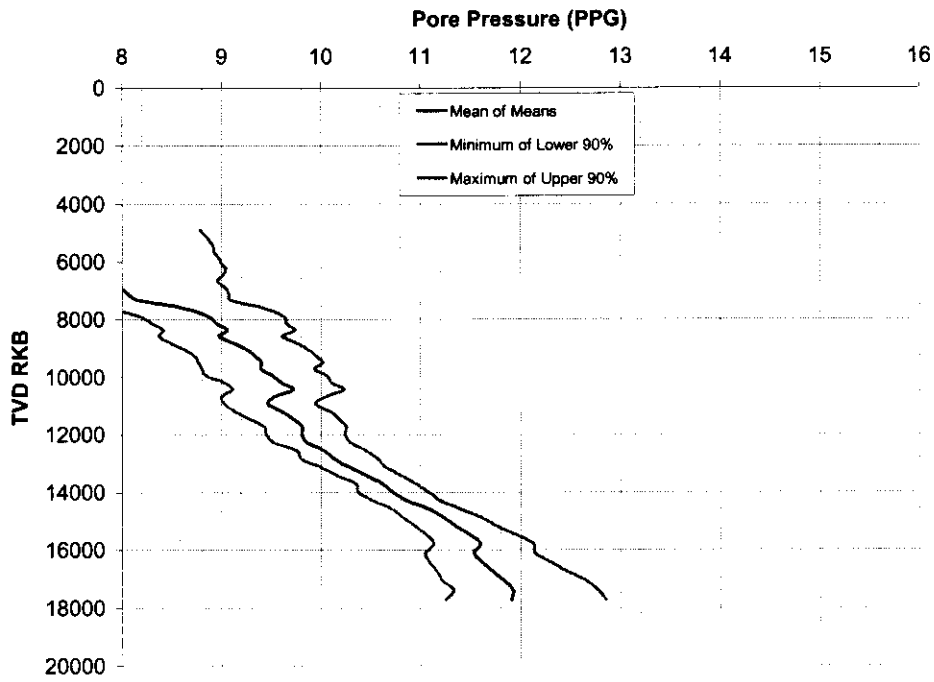


Figure 6-4 Example No. 1 - Composite Results of all 5 models



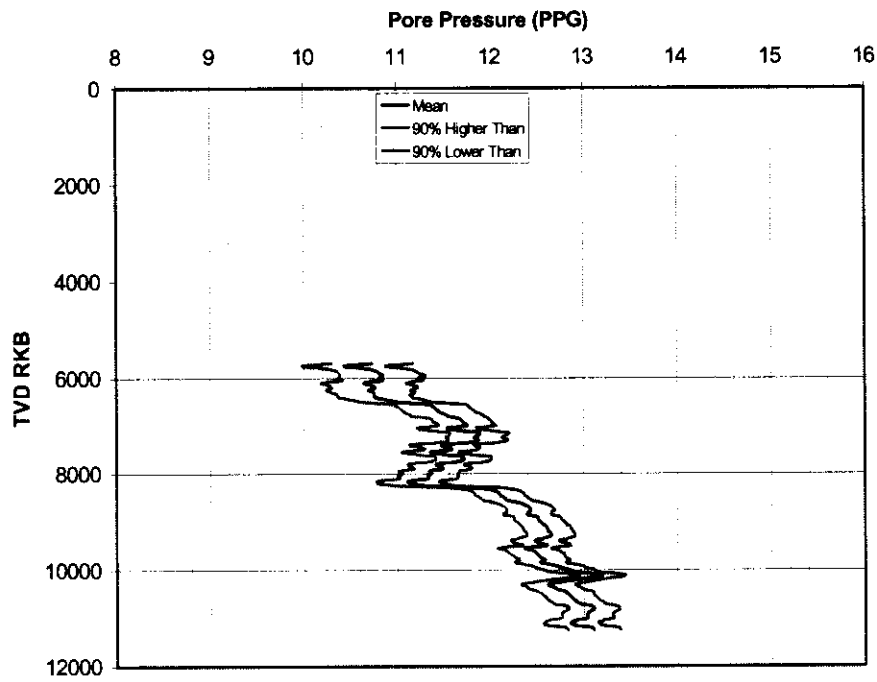


Figure 6-5 Example No. 2 – prediction of one model

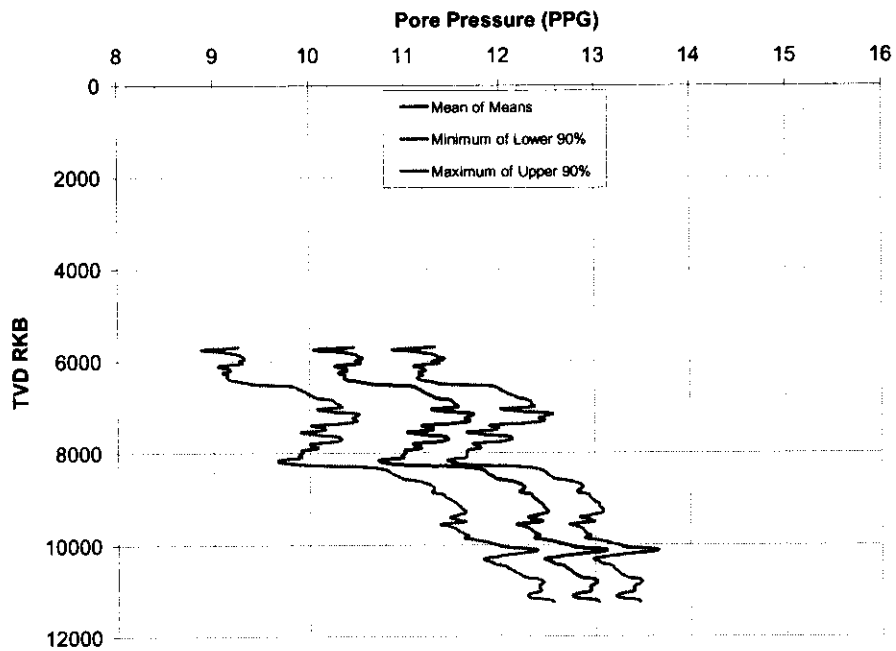


Figure 6-6 Example No. 2 - Composite Results of all 5 Models



7 Index

A		D	
Auger Basin.....	89, 91, 93	Data	
B		checklist	12
Basin model		density data	49
Auger Basin case study	93	drilling and logging	19
calibration.....	98	errors	26
correlation of data.....	96	geological and structural	18
data required.....	12, 96	management	18
seismic velocity	103	mud weight.....	38
software	90	quality rating	32
strategy	44	required, basin analysis.....	12
stratigraphy.....	91	required, single well analysis.....	12
testing	102	RFT points	34, 40
Bowers, Glenn.....	44, 61	seismic velocities	15
<i>See also</i> Appendix D		sonic log errors.....	27
<i>See also</i> Appendix B		text based	20
effective stress-velocity compaction trend ..	60	uncertainty of	23
fracture gradient estimation.....	5	weighting scheme.....	39
overpressures	43	wireline	19
pore pressure prediction	4	Database	
unloading.....	65	deep water	6
Virgin Curve.....	65, 66	Density logs	
C		adding missing data.....	50
Centroid		exponential equation	51
analysis procedure.....	72	power fitting equation	52
example	74	Dutta, Nader	
identify	72	<i>See also</i> Appendix C	
indications of.....	25, 27, 47, 75	seismic data processing.....	4
offset well data	49	E	
overpressures	44	Eaton equation	65
shale-sand interface	99	Error analysis	81
Compaction trend	60, 61, 69, 74, 80, 81	Example	
		basin analysis	89
		centroid	74
		effect of salt sections.....	55
		evaluation of fitting equations.....	53
		lithology effects	61
		need to filter density data.....	74

quasi-calibration 82, 83
 uncertainty analysis 112
 unloading 68
 Excess pore pressure 68

G

Gas show 34, 39, 41

H

Hobart, Steve 10
See also Appendix F
See also Appendix E
 overburden estimation 5
 velocity-effective stress relations 5

K

Kicks 26, 34, 39, 40, 66, 96

M

Monte Carlo 109
 interval velocities 110
 limitations 110
 sonic travel time 110

N

Neural network 7
 New models 7
See also Appendix A
 calibrated conventional 81
 empirical Quick-Look 81
 theoretical 81
 top five 85

O

Offset wells
 data for calibration 34
 quasi-calibration 82
 top of pressure transition 59
 Outlier 23, 31
 Overburden gradient
 interval velocities 54
 offset sonic data 55
 offset wells 49

P

Pseudo-wells 98
 seismic velocity 103

Q

Quasi-calibration 82
 Quick-Look evaluation 66, 81

R

RFT data quality 34
 clumping 35
 moment concept 36
 number of points 35
 pattern 37
 standard deviation method 37
 vertical coverage 34

S

Saleh, Saad
See also Appendix A
 Seismic interval velocities
 adjusting 56
 checklist 16
 quality of 16
 Single well analysis



compaction trend 60
offset calibration..... 48
overburden gradient..... 49
process..... 47
seismic data 57

excess pore pressure.....68
geologic and structure.....24
identifying65
overpressures.....47
predicting65
Virgin Curve68

T

Traugott 72

U

Uncertainty
 analysis 80, 109
 data 23
 in compaction trend..... 60
Unloading
 and centroid effect..... 74
 depth factors 67
 example 69

V

Virgin Curve65, 66, 67, 68, 69

W

Wellbore conditions
 drilling fluids and shale.....29
 log reponses23
 mud weight data38, 40
 RFT measurements34
 sonic data28, 30



8 Appendix

A. New Models for Pore Pressure Estimation in the Gulf of Mexico

By Dr. Saad Saleh, DEA 119 Report No. 6

B. State of the Art in Pore Pressure Estimation

By Dr. Glenn Bowers, originally published as DEA 119 Report No. 1

C. Best Practice for Processing Seismic Data for Geopressure Analysis

By Dr. Nader Dutta, originally published as DEA 119 Report No. 2

D. State of the Art in Fracture Gradient Estimation

By Dr. Glenn Bowers, originally published as DEA 119 Report No. 3

E. Pre-Drill Overburden Estimation

By Steve Hobart, originally published as DEA 119 Report No. 4

F. Velocity – Effective Stress Relations

By Steve Hobart, originally published as DEA 119 Report No. 5



KNOWLEDGE SYSTEMS, INC.

New Models for Pore Pressure Estimation in the Gulf of Mexico Deep Water

Saad Saleh

6/11/2001

CONFIDENTIAL

*This report is provided to DEA **Project 119** Project Participants under the terms of the
DEA Project 119 Participation Agreement and is thereby subject to restrictions of
confidentiality and non-disclosure to third parties.*

DEA Project 119

Report No. 6

Corporate Offices

Knowledge Systems, Inc.
P. O. Box 1279
Stafford, Texas 77497-1279
Phone: 281-879-1400
Fax: 281-879-1499
E-mail: sales@knowsys.com

European Office

Knowledge Systems, Inc.
P.O. Box 274 Paradis
5856 BERGEN
Norway
Phone: +47 55 92 45 62
Fax: +47 55 92 45 62
E-mail: sales @knowsys.com

Please visit the Knowledge Systems' website at <http://www.knowsys.com>

Information in this document is subject to change without notice, and does not represent a commitment on the part of Knowledge Systems. The software described in this document is furnished under a license agreement or non-disclosure agreement. It is against the law to copy the software on any medium except as specifically allowed in the license or non-disclosure agreement.

© Copyright Knowledge Systems, 1989-2001. All rights reserved. *DrillWorks* is a registered trademark of Knowledge Systems, Inc. *PostScript* is a registered trademark of Adobe Systems, Inc. *Windows* is a trademark of Microsoft Corporation

Document Information

Title: New Models for Pore Pressure Estimation in the Gulf of Mexico Deep Water	
Description:	
Author(s): Saad Saleh, James Bridges (lkellner-editor)	
Reviewer(s): Terry Miller	
Creation Date: 5/31/2001 11:31 AM	Last Date Modified: 6/4/2001 8:39 AM
Approved By:	Approval Date:
Will be sent to:	
Sources Used: (can be other documents used as sources)	
Project Number:	Document Number: 2001-000016

Table of Contents

1	Summary	1
2	Introduction	3
3	Model Development.....	6
3.1	Exponent Models	7
3.1.1	“Linear” Compaction Trends.....	8
3.1.2	Bowers’ Compaction Trend.....	8
3.2	Theoretical Models	9
3.3	Empirical Models.....	11
3.3.1	Multiple Regression Models (requires no OBG)	11
3.3.2	“Quick-Look” Models (require no OBG)	12
3.4	Calibration Philosophy.....	13
4	Error Analysis and Models Ranking.....	13
4.1	Introduction.....	13
4.2	Error Analysis and Discussion of Results	14
4.3	Regional Ranking of all Models	15
4.4	Uncertainty Analysis Based on Error Database	17
4.5	Five Best Performing Models	23
5	Conclusions	25
6	References	26
7	Appendix A: List of New Models	27
8	Appendix B: Error Analysis Results – Ranking of Models.....	35
8.1	Error Evaluation Equations	35
8.2	Confidence Grading in Definitive Pore Pressure	36

1 Summary

This report presents the results of work to develop new or modify existing models for estimating pore pressure in an exploration prospect in the deep water Gulf of Mexico (GOM). The new or modified models relied on the DEA 119 database to calibrate various parameters required for pore pressure prediction. The models use input data available for an exploration prospect well. All models require seismic interval velocity and overburden stress; and some also require water depth and true vertical depth. Most are modifications of standard industry approaches, and others are empirical relationships.

The primary objectives of this work:

- ❑ To develop new models that do not depend on trend line approaches.
- ❑ To calibrate industry-standard conventional models against the DEA 119 project's GOM database.

The new (theoretical and empirical) and modified existing models are optimized to meet the requirements and objectives set forth above.

This work produced the following results:

- ❑ Once calibrated to a limited data set, several models consistently predicted pore pressures for any given site with average errors of 0.5 to 0.6 ppg (4.5 to 5.5% relative errors). These models do not depend on a site-specific trend line.
- ❑ Calibrated theoretical models such as Bowers' effective stress-velocity equation and the Amoco-Baldwin-Butler effective stress-porosity relationship were among the top five ranked models. Other theoretical models showed similar results. Only a fraction of 1% in relative error separates the top ranked models from the average performance of all models.
- ❑ The regression analysis of the empirical models often predicted pore pressure more accurately than many of the optimized industry standard models. This should not be too surprising considering that many of these empirical models also had more free parameters available in the optimization process. Regardless of their good performance, these models should be applied with caution, as is the case with all locally calibrated empirical models.
- ❑ Neural networks and dimensional analysis approaches have been attempted with some promising results. However, the efforts required to develop working models using these techniques was beyond the scope of this project.
- ❑ The development of new models is further integrated with the advancement of uncertainty analysis. A risk-weighted pore pressure prediction based on uncertainty in input data is developed. This is discussed in detail in Chapter 6 of the DEA 119 Best Practice Procedures for Predicting Pre-Drill Geopressures in the Deep Water Gulf of Mexico.
- ❑ Database development was the cornerstone in this project. This unique database is unequalled for the GOM and the full utilization is yet to be realized.

Over 40 models were developed and tested on over 80 wells in the DEA 119 GOM database. The results of error analysis enabled the selection of the best five models listed below along with their optimized parameters:

Rank	Model No.	Description
First	TH-1 Theoretical	Baldwin-Butler porosity effective-stress formulation: $P(\text{psi}) = \text{OBG psi} - 5635 * (1 - \text{phiamoco})^{1.094}$ Where: OBG psi is the overburden stress in psi Phiamoco = porosity derived from Amoco empirical equation given as follows: $\text{Phiamoco} = 1.425 * (1 - (V/15000))$ V is velocity in ft/sec
Second	TH-13 Theoretical	Modified version of Bowers' velocity effective-stress relationship: $P(\text{psi}) = \text{OBG psi} - ((V - 5000) / 1.046)^{(1/1.069)}$
Third	BTL-B Improved Conventional	Exponent model with Bowers' curved trend: $P(\text{ppg}) = \text{OBG} - (\text{OBG} - 8.7) * (\text{DT}_{\text{BTL-B}} / \text{DT})^{2.227}$ Modified Bowers' trend Type B: $\text{DT}_{\text{BTL-B}} = 10^6 / (5000 + 14.22 * (0.052 * \text{TVD} * (\text{OBG} - 8.7))^{0.7415})$
Fourth	20-A Empirical	Multiple Regression Model: $P(\text{in ppg}) = -14.02 + 0.1982 * \text{DT} + 0.02251 * \text{OBG} - 0.0008785 * \text{Delta}^2 + 0.00005647 * \text{WD} + 0.0004002 * \text{ML} - 0.0004483 * \text{DT} * \text{DT} + 0.0005492 * \text{Delta}^2 * \text{Delta}^2 + 0.000002685 * \text{ML} * \text{DT} - 0.000009746 * \text{ML} * \text{Delta}^2 + 0.00003297 * \text{ML} * \text{OBG}$
Fifth	20-G Modified Conventional	Modified Exponent model with water depth term: $P(\text{in ppg}) = \text{OBG} - 0.8509 * ((\text{OBG} - 8.7)^{1.037}) * (\text{WD}^{-0.07403}) * ((200 * \text{EXP}(-0.00006 * \text{ML})) / \text{DT})^{2.571}$

Figure 1-1 Five Best Models

Because all parameters listed for the models (empirical or theoretical) were optimized from data in the DEA 119 deep water GOM database, they should be applied with caution in other geologic settings.

Three notes of caution are in order:

- ❑ Although these models predict pore pressures well at depths corresponding to the range of depth below mudline (mostly >4000 ft) where calibration data was available, their predictions can disagree significantly at shallow below mudline depths.
- ❑ Because all parameters listed for the models (empirical or theoretical) were optimized from data in the DEA 119 deep water GOM database, they should be applied with caution in other geologic settings.
- ❑ The new models were calibrated with sonic data (and not seismic data). The limited availability of seismic data compelled the use of the sonic data. Consequently, the calibration is affected by the vertical coverage of the calibration data. Shallow depths (0 to 3000 ft below mudline) are not typically covered by sonic data.

The recommended approach to applying the new models is as follows:

- ❑ Apply all the top five models to selected offset wells which are comparable to the prospect geologic and hydrodynamic condition.
- ❑ Compare the predictions made by the new models to definitive pore pressures. Select the best model(s) based on this comparison.

2 Introduction

This report documents the efforts (within DEA 119 project) to develop new and/or modify existing pore pressure prediction models for improved pore pressure prediction in the GOM deep water. The report documents how the study was conducted, the various models considered, and the calibration and model validation process.

A variety of tools and approaches were used during the course of the DEA 119 project:

- ❑ Conventional analysis using current industry models to establish benchmark data
- ❑ Advanced regression methods
- ❑ Basin analysis
- ❑ Advanced data clustering methods
- ❑ Neural networks
- ❑ Dimensional analyses

Significant time and effort was devoted to each of the above techniques. Unfortunately, the complexity of problem and the vast volume of data involved prohibited advancing the latter three approaches to total fruition. Considerable work remains for future studies. This project attempted and invested effort in new techniques that appear to be beyond any published information for pore pressure estimation to date.

All wells in the DEA 119 GOM database (over 100 wells) were analyzed with conventional industry models using the DrillWorks/PREDICT software. The results of this analysis provided the foundation for the development of new methods. As a by-product of the conventional analysis, the basic data required for exploring regression methods was available:

- Filtered sonic data
- Overburden stress
- Definitive pore pressure

Most of the results documented in this report are from the regression approach, which provided quick and tangible results. Using the GOM database (built as part of this project), a set of calibration data was developed to address universal and regional attributes. The calibration datasets used to “train” models were designed for application in the GOM database or for a limited regional scale. This report is primarily to address the results of the regression approach.

The development work in this project underwent several systematic interrelated phases:

Phase 1: Data preparation and conventional analysis using Drillworks/PREDICT software.

The data was retrieved from different sources as supplied by the participant companies. Included were logs, directional surveys, RFT data, and text information such as drilling records and well reports. The data was then processed with Drillworks/PREDICT Software for conventional analysis to produce the following:

- Basic plots of log data and views of all available data on a particular well
- Filtered and validated data
- Converted data values from measured depths to true vertical measurements
- Corrected data (temperature correction for resistivity, wellbore effect, etc.)
- Complete conventional analysis with all available methods

Phase 2: Established Definitive Pore Pressure for all wells

- Each well was assigned a definitive pore pressure based on the best prediction made from the conventional analysis.
- The selection of the definitive pore pressure was guided by the correlation with the known pore pressure measurements and indicators.
- The degree of confidence in the definitive pore pressure was determined based on the quantity and quality of pore pressure calibration data available for each well.

Phase 3: Preparation of Calibration Data

- The confidence grade was used to select well data for calibration.
- Data was exported with Drillworks/PREDICT at 200 ft sampling rate (sonic and OBG data).
- The apparent normal compaction trend from sonic data was documented for all wells in the GOM database.

Phase 4: Model Calibration

- Performed regression analysis
- Optimized model regression results
- Evaluated regression results for stability
- Checked results with different statistical software to ensure convergence and repeatability

Phase 5: Pore Pressure Prediction with Calibrated Models

- Predicted pore pressure on wells
- Adjusted definitive pore pressure if necessary

Phase 6: Error Analysis

- Performed error analysis on predicted pore pressure
- Plotted error probability curves, histograms and cumulative frequencies for each model

Phase 7: Identification and Evaluation of “Outliers”

An “outlier” is a well that averages more than 10% relative error. At this phase, the error analysis was benchmarked with geologic data to find possible correlations.

- Investigated geologic setting and structure
- Identified Unloading possibility
- Checked input data quality
- Ensured that the OBG was computed correctly

Phase 8: Regional Classifications of Wells

The objective of this phase was to study the effect of the geological setting (mini-basins), lithological attributes, and water depth to correlate these parameters with mud weight and temperature distribution in the GOM.

- Mini-basin Classification:** An evaluation was made of the geological setting of each well in the database. The ultimate objective was to define the basic geological signature from well logs and geographic location of the wells. The effort was focused on sub-salt wells with lithology determination based on published correlations, and defining pressure gradient above and below the salt. Eight wells that penetrated salt bodies were identified in the GOM database.
- Mapping of Mud Weight and Temperature Data:** The mud weight data for all current DEA 119 database wells was contoured to visualize regional trends. In addition, temperature data from all wells was organized and contoured at several depths (5,000 ft, 10,000 ft and 15,000 ft TVD below mudline). The effect of water depth and regional variation can be viewed and identified with the aid of the map.

3 Model Development

This study considered three different model types:

- 1 Generalizations of Eaton's sonic based pore-pressure prediction model, which are termed here as exponential models
- 2 Effective stress (or equivalent depth) theoretical models.
- 3 Purely empirical models.

Because these models are designed to predict pore pressure in an exploration context, seismic velocity and overburden are their basic input. Some of the empirical models also require water and below mudline depth as an input. Theoretical models attempt to calculate pore pressure based on a physical principle. Hence the parameters that characterize the model can be thought of as material properties, e.g., the A and B parameters in Bowers' (1994) velocity versus effective-stress relationship. Empirical models are essentially developed ad hoc and may or may not have an underlying physical basis. Often these models have some elements of a theoretical basis but also contain elements without one, e.g. Eaton's velocity model (the former) and his "linear" normal compaction trend lines (the latter), Bowers (1994). Regression models will only have theoretically based elements if they are included in the formulation. Because of this, it is difficult to develop any physical insight from results of regression-based models, in spite of the fact that they often can produce better fits to the data from which the regression parameters are determined

In essence, all of the models presented here can be characterized as regressions. The physical properties in the Amoco and Bowers' models are fit to produce the best predictions of pore pressures from sonic velocities and overburden. The exponential, or generalized Eaton, models are based implicitly on normal compaction trend lines with parameters that are regressed in association with the exponent to give the best predictions.

As a consequence, the material properties in the theoretical models and the exponents, together with the implicit normal trend lines, must be used with caution when applied to locations that do not share all the geological characteristics of the deep water GOM.

The following discusses the essential details of how the various models were developed. In general, each of the models assumed some general mathematical form with one or more free parameters. The free parameters were then varied systematically such that each model produced the minimum average error in its predicted pore pressure for all of the wells in a defined calibration dataset.

All wells in the GOM database were analyzed by conventional models and benchmarked. Several tools and approaches were used to further the development of new models and measure the effectiveness in predicting pore pressures.

The steps below highlight the data analysis process used in model development:

- Geostatistical Mapping
- Modeling: All models were based on two key inputs: seismic velocity (or sonic interval time) and overburden pressure. The data was reduced or simplified by:

- Sorting or grouping data
- Investigating the dependence among variables
- Predicting relationships between variables
- Constructing and testing hypotheses

3.1 Exponent Models

The general form of the exponent model is:

$$P = OBG - \sigma_{nc} [DT_{nc}/DT]^n \quad \dots\dots\dots \quad \text{EQN (3.1)}$$

Where:	P	Predicted pore pressure, psi
	OBG	Overburden pressure, psi
	σ_{nc}	OBG – Pn
	Pn	Normal pore pressure (in the GOM \cong 8.7 ppg)
	DTnc	Sonic measurement in normally compacted sediment
	DT	Observed sonic measurement
	n	An exponent (= 3 in published literature)

In typical application of the exponent model above, one must select the normal compaction trend. This process is highly subjective based on the available data. This approach is difficult to apply due to the following:

- ❑ The seismic data does not typically lend itself to a clear compaction trend at shallow depths.
- ❑ In some cases, undercompaction may start immediately below the mudline.

Therefore, this approach is not appropriate for our intended applications in which data to develop a normal compaction line is not available. We have investigated the effect of assuming different types of normal compaction lines as integral parts of the models and then optimizing the entire results as one basic equation. The different types of compaction trends studied are:

- ❑ Linear trend (on semi-log plot)
 - “Fixed” compaction trend (water depth independent)
 - “Automated” (water depth dependent)
- ❑ Bowers’ type (effective stress dependent)
- ❑ Empirical (depth dependent)

3.1.1 “Linear” Compaction Trends

Linear trends are so named because they are linear on a log DT versus depth plot. The various approaches that were taken to specify the normal compaction trend (DT_n versus depth) are discussed below. The specific parameter values given in each section were developed to best fit our data for the given form of the trend line equation.

UTL (Universal Linear Trend line)

The trend line study of over 50 wells in GOM database revealed that a universal trend of the following attributes could be used as an average trend:

$$DT_n = 200 * e^{(-0.0001 * ML)} \dots\dots\dots EQN (3.2)$$

Where:	DT _n	Normal sonic compaction trend
	ML	depth below mudline, ft
	Mudline intercept	200 micro sec/ft
	Slope	10 ⁻⁴ micro sec/ft ²

e is the base of natural logarithm.

ATL (Automated Trend line Model)

The “automated” universal trend is based on observations that there is possible correlation of the actual normal compaction sonic trend and water depth. This relationship is mathematically “automated” as follows:

$$DT_n = 200 * e^{(-Slope * ML)} \dots\dots\dots EQN (3.3)$$

Where:	Slope	[Ln(50/200)]/(WD-19000)
	WD	water depth in feet

Table 7-2 in Appendix A shows the modified Exponent models with the different types of linear trends.

3.1.2 Bowers’ Compaction Trend

The Bowers’ normal compaction trend line is based on a velocity versus effective stress relationship (Bowers, 1994).

$$V_n = V_{mudline} + A * \sigma^B \dots\dots\dots EQN (3.4)$$

Where:	V _n	Resultant Δt in a normally-pressured regime in microsec/ft
--------	----------------	--

V_{mudline}	Seismic interval velocity at the mudline ft/sec, (≈ 5000 ft/sec)
σ	Effective stress in normally compacted sediments. This can written as: OBG - P_n
OBG	Overburden Gradient , ppg
P_n	Normal pore pressure in PPG (usually 8.7 ppg)
A	Coefficient
B	Exponent

Rearranging the equation above in terms of sonic Δt 's:

$$\Delta t_n = 10^6 / [10^6 / \Delta t_{\text{mudline}} + A * (\text{OBG} - P_n)^B] \dots\dots\dots \text{EQN (3.5)}$$

Where:	Δt_n Sonic interval travel time (Δt) in a normally-pressured sediments in $\mu\text{sec}/\text{ft}$
$\Delta t_{\text{mudline}}$	Sonic Δt at the mudline in $\mu\text{sec}/\text{ft}$, (185-212 $\mu\text{sec}/\text{ft}$)
OBG	verburden Gradient Dataset, ppg
P_n	Normal PP in PPG (usually 8.7-9.0 ppg)

The required inputs are Δt at the mud line (usually 200 μsec), normal pore pressure gradient, overburden gradient, depth, and the coefficients A and B. The coefficients A and B can be varied as necessary to best fit a given geological/lithological setting. Pore pressure is calculated by substituting the Bowers value for DT_n into the exponent equation.

NOTE: Other normal compaction trends were studied but did not improve predictions over those discussed above. These are outlined in Appendix A, Table 7-3 along with an empirically determined curved compaction trend.

3.2 Theoretical Models

This section presents the basic theoretical models that ended highest in the rankings in more detail. We term them theoretical because they are based on finding the effective stress. Effective stress is related to sediment porosity (which is determined from velocity) or directly to velocity. Several models were discovered in the literature. In addition, about eight velocity-porosity transforms were combined with five porosity-effective stress transforms, to yield an additional 40 models. Each of these models contains a number of empirical parameters, such as matrix velocity, that can be adjusted to provide a better fit of the model to the data. These models are listed in Table 7-5 in Appendix A.

A brief discussion is given below of the better theoretical models. See DEA 119 Report No. 5 by Steve Hobart for a thorough review of all the theoretical models considered in this study.

TH-1

This model combines the Baldwin-Butler formulation of effective stress as a function of solidity with an empirical sonic-porosity transform patterned after the one given by Martin Traugott (then with Amoco) in the World Oil "Deepwater Technology" supplement of August 1997.

$$\text{Baldwin-Butler : } \sigma = \sigma_{\max} (1 - \phi)^\alpha$$

Where:	σ	effective stress
	σ_{\max}	effective stress where rock porosity is extrapolated to become zero
	ϕ	porosity
	α	lithology dependent exponent

Regressed values:

σ_{\max}	5635.47 psi
α	.09439
α	

$$\text{Amoco porosity equation: } \phi = (C / \Delta t_m) (1 - \Delta t_m / \Delta t)$$

Where:	C	empirical constant, published value was 43
	Δt_m	transit time of matrix, micro seconds/ft
	Δt	transit time of formation, micro seconds/ft

Regressed values:

C	95.04
Δt_m	66.67 micro seconds/foot

TH-13

This model is a regression on the form of the Bowers' velocity versus effective-stress relation ship (1993).

$$\sigma = ((10^6 / \Delta t - 5000) / A)^{1/B}$$

Where:	σ	effective stress, psi
	Δt	formation transit time, microseconds per foot
	A	empirical coefficient
	B	empirical exponent
Regressed values:		
	A	1.04628
	B	1.0689

3.3 Empirical Models

We consider two empirical models that either did or did not require OBG data. Three kinds of the latter were considered:

- Polynomial (second and third degrees)
- Exponential
- Logarithmic

The Empirical models were developed for the purpose of “Quick-Look” analysis. The analyst may elect to do a “quick-look” analysis using the models that require no OBG data.

NOTE: The lack of physical or theoretical basis for the empirical models (multiple regression, polynomial, etc.) may be argued against their general use. We should recognize that, these models are developed to best fit the data in the GOM. The theoretical models were calibrated in similar manner. The empirical models in some cases are rated better than the theoretical models in the error analysis. All models developed using the GOM database to “tune” the coefficients as described in this report should not be used in other areas.

3.3.1 Multiple Regression Models (require no OBG)

Multiple regression is an extension of simple linear regression. In multiple regression, we consider more than one independent variable and assess the combined ability of the independent predictors to account for changes in the dependent variable (pore pressure). This makes a good deal of sense, since rarely is the case that a single factor will account for all (or even a large portion) of the variability in our dependent variable (pore pressure). For example, we might expect factors other than sonic velocity to be predictive of pore pressure (e.g., OBG, temperature, and so on). A multiple regression analysis will allow us to look at the predictive power of each of these factors. The typical outcome of a

multiple regression analysis is an equation or "model" that represents the best set of independent variables for a particular dependent variable.

In attempting to fit a model or a regression equation to a set of data, we may proceed in either of two basic ways:

- Start with a model that contains all available candidates as predictors, then simplify the model by discarding candidates that do not contribute to explaining the variability in the dependent variable; or
- Start with a simple model and elaborate on it by adding additional candidates.

In either case we will wish (at any stage in the analysis) to compare a "full model" to a "reduced model".

The general form of the models considered here, which consider linear and second order terms, is as follow:

$$P = M + A*DT + B*OBG + C*WD + D * \Delta + E *DT*DT + F * DT*OBG + G*OBG*OBG + \text{etc..} \quad \text{..... EQN (3.6)}$$

Where:	P	Pore pressure
	A to G	Constants
	M	Intercept
	DT	Sonic interval time
	OBG	Overburden gradient
	WD	Water depth
	Delta	Difference between observed and normal compaction sonic interval time

Detailed considerations of the multiple regression models are presented in Appendix A, Table 7-7. Again, they do not rely on a trend line to be imposed by the analyst.

3.3.2 "Quick-Look" Models (require no OBG)

Table 7-8 in Appendix A lists the different models. Note that because of the many free parameters used in these models, they produced good results and they are highly ranked in the error analysis. Tips for using the Quick-Look models are listed below:

- Ensure that the sonic or seismic data is smoothed. The models are extremely sensitive to spiky acoustic data. If sonic log data is used, make sure to filter the sonic data with a 199 or 299-point boxcar filter.
- In some cases, these models are unstable. It is difficult to identify failure conditions. However, apply all of them on the same data and if they all are showing the same signature (instability), then it is prudent to disregard the models. The problem may

not be in the data; the nature of the mathematical function used is susceptible for instability.

- The polynomial models are less prone to instability.
- These models can be used only as a quick-look approach. They do not negate the need to perform a full analysis.

3.4 Calibration Philosophy

The wells in the database were grouped into three regions (West, East, and Middle region). A training dataset was selected from each region to calibrate the regression models specific to each region. These models are called “Regional Models” in order to distinguish them from the Universal Models (see discussion in Chapter 4 of Best Practice Procedures for Predicting Pre-Drill Geopressures in the Deep Water Gulf of Mexico), which are based on calibration of the best quality data from the entire GOM database.

The overall conclusion from this study is that the prediction from regional models did not improve on the performance of the universal models. The reason for this unexpected result is that the clustering of the wells into smaller groups limited the amount of quality calibration data. This, in turn, adversely affected the calibration of regressed models. In essence, the clustering scheme is important to capture the attributes of each individual area in the Gulf of Mexico. However, we may not have the necessary quality well data that can be used for calibration. The objectives of the regional model calibration process are:

- Explore the performance of models tailored for smaller areas and compare against results obtained from the universal models
- Define the compaction trend/exponents for conventional models for different mini-basins or areas.

The GOM wells were grouped into three geographical locations:

- East region: Wells with names starting with AT, MC, VK (Atwater valley, Mississippi Canyon, Visco Knoll)
- Middle region: Wells starting with EW, GC (Ewing Bank, Green Canyon)
- West region: Wells starting with EB (East Break)

Because the regional studies did not produce better results, the regional models are not included in this report.

4 Error Analysis and Models Ranking

4.1 Introduction

The predictive performance of all models has been established and rated by application of various error analysis techniques. The ranking procedure used 80 wells in the GOM database as the statistical sample.

The key elements of the ranking process are:

- Determine a “Definitive Pore Pressure” (DPP) for each well
- Define a degree of confidence in the proposed DPP

It is now possible to draw conclusions as to the % relative error or the absolute error (in ppg) expected from the application of the various regression models. A confidence grade related to the definitive pore pressure was included to refine the error estimates.

Coincidentally, the confidence rating also presented a way to classify and select wells on the basis of “certainty” in the definitive pore pressure. According to this study, the wells with a high confidence grade in the definitive pore pressure showed an absolute error average of 0.5 to 0.6 ppg. The lowest possible error reported was 0.52 ppg (for the Exponent model that utilizes Bowers’ curved trend line).

Figure 4-1 illustrates the process.

4.2 Error Analysis and Discussion of Results

The following results are presented:

- Error analysis results with no consideration to confidence grade or “outliers”
- Effect of confidence grade
- Effect of “outliers”
- Regional ranking

The top chart in Figure 4-2 shows the % relative error of selected models (20-A through 20-N). These models are combinations of empirical and modified conventional models. Models 20-J through 20-N are empirical models. Notice that the range of the % relative errors is between 5.5 and 6.5%. By including the confidence grade as a weighing factor, the weighted % relative error is shown on the same Figure at the bottom for comparison. It is concluded that the overall % relative error has decreased approximately 0.5 % by this adjustment. This suggests that the lack of calibration data available on some wells affected the results. Consequently, biased or erroneous definitive pore pressure may be responsible for some of the error generated from these models.

The bottom chart on Figure 4-2 shows the effect of the confidence grade in a different perspective. The average confidence grade for 80 wells is about 40%. There are 36 wells with confidence grade above 40%. If we consider only the wells with high confidence grade in the assigned pore pressure, the error analysis shows a decrease in the % relative error for ALL models. In this case, appreciable and significant reduction is approximately 0.4% relative error (or 0.03 to 0.04 ppg). Again, this suggests that biased definitive pore pressure is responsible for a portion of the model errors.

If we select the wells with confidence grade over 50%, only 22 wells meet this criteria. For those wells, the % relative error unexpectedly increased slightly for almost all models. The possible explanation is that averaging over only 22 wells adversely affected the statistical significance of the sampled wells.

The chart on Figure 4-3 shows the effect of “outlier” wells on error statistics. The outliers are the wells which have more than 10% average relative errors. These wells were subjected to screening and evaluation of data quality. There are apparent data quality problems or errors. In addition, there is a possibility that the definitive pore pressure is erroneous. If we discard the error values of 12 outlier wells, then we get significant reduction (approximately 1% relative error which corresponds to 0.07 to 0.1 ppg) in the overall average error for all models.

Accordingly, the following conclusions can be made:

- The quality of the calibration data needed to establish a definitive a pore pressure for a well affects the error statistics significantly. The weighted % relative error is lower from the % unweighted relative error by a total of approximately 0.5% (which represents \approx 10% reduction in the errors).
- Considering only the high quality well data, further error reductions are realized for all models. This is demonstrated when well selection is limited to only those wells with a confidence grade $>40\%$. The average CG for all wells is approximately 40%.
- As the data quality threshold is increased further (from 40% CG to 50% CG for example), fewer wells meet the criteria and the error measurement starts to increase as the smaller number of wells become a statistical factor in the error analysis.
- Outlier wells with suspected poor data quality affect the error statistics significantly. Discarding the outlier wells from the sample data realizes a further reduction in the overall average error of about 1%.

4.3 Regional Ranking of all Models

Table 8-1 in Appendix B lists the error statistics for all models based on predictions made on 80 wells. If we consider the performance of the universal models on three regional settings (East, West, and Middle region), the ranking of the models is different from one area to the next as shown in Table 8-2.

- Models 20-H, A-U-6, and 20-B are top performers for the East wells. The Modified Bowers’ curved trend (model BTL-D) is the top performer in the Middle region. The modified curved trend (NCTL-0.9) is the highest ranked in the West region.

Note that the East wells are predicted with the best consistency. The West region has the lowest prediction consistency and the highest error

- It is recognized the West region is geologically different from the east wells and all models performed relatively poor in the western region (approximately 1% relative error higher than others).

Regionally trained models did not fare well in comparison with the universal models. In fact, they did not perform very well in the same region. The regional model’s prediction for wells in the same region as well as outside their region is shown in Table 8-3. For example, the models trained with a dataset from the East region performed with an average relative error of 5.5% (0.64 ppg). However, if we use the Eastern trained models to predict wells in the West, the average error is about 8.2% (0.99 ppg). This is expected as the models were used in areas beyond their ‘training’.

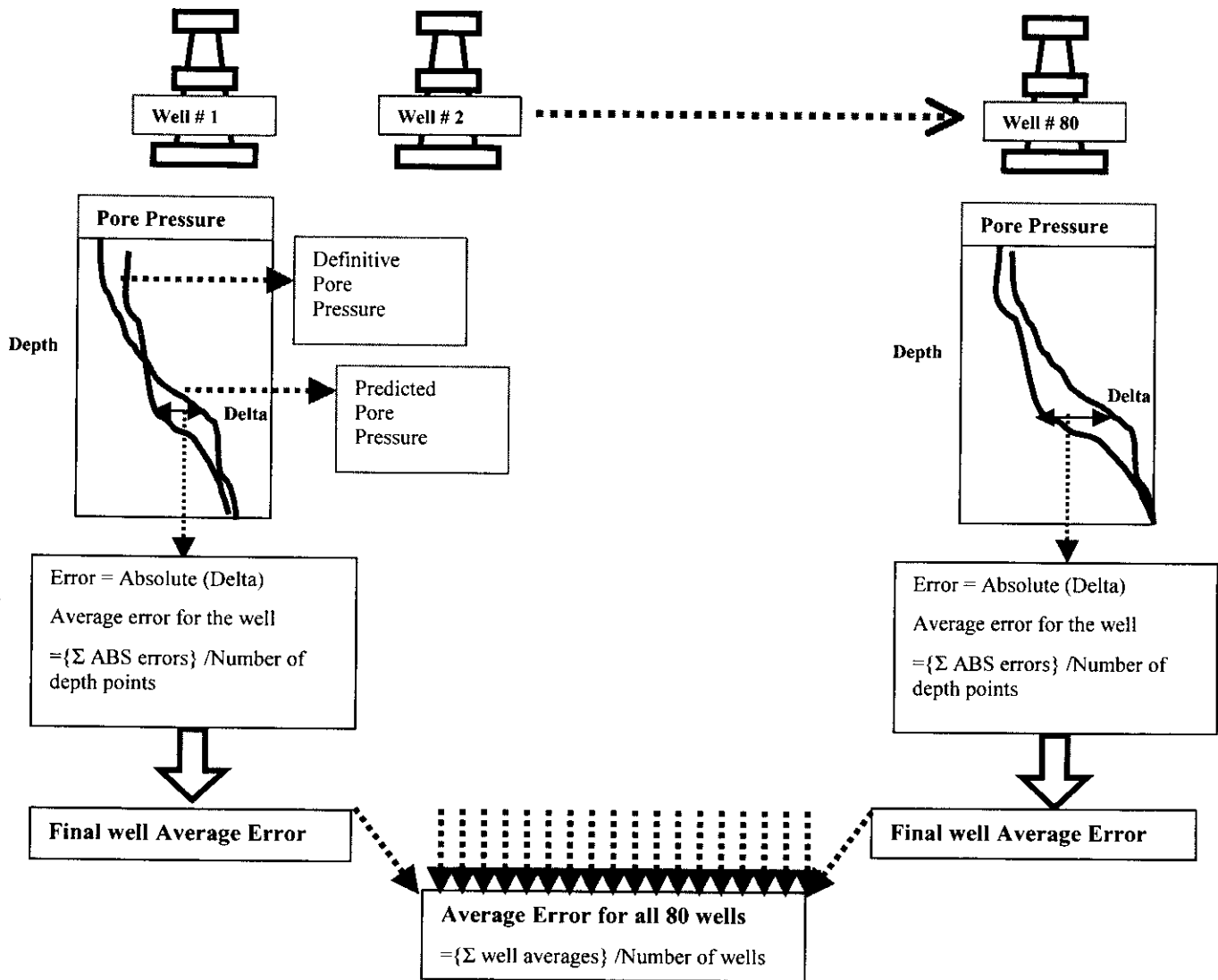


Figure 4-1 A Schematic Illustration of the Error Analysis Process

4.4 Uncertainty Analysis Based on Error Database

Each model has been used to predict pore pressure for 80 wells in the DEA-119 database. Each well has a certain “uncertainty” in the Definitive Pore Pressure, DPP. This uncertainty has been “quantified” by a “Confidence Grade”, CG. The detailed discussion on the Confidence Grade has been presented in Chapter 2 of the Best Practice Procedures for Predicting Pre-Drill Geopressures in the Gulf of Mexico. Accordingly, the Confidence Grade affects the error estimates made on a particular well.

- 1 Use a model to predict pore pressure versus depth for a well. The well data contains two variables (Sonic and OBG) and a known pore pressure. All three have some uncertainty in their values.
- 2 Compare the predicted pore pressure versus the “definitive” pore pressure. Compute the error statistics for the model.
- 3 Repeat Steps 1 to 2 for all wells in the database. Approximately 80 wells were predicted.
- 4 Tabulate the Error data for wells and for the model.
- 5 Generate the Error Probability Plot for the model.

Repeat the process (Steps 1-5) for all the models.

Figure 4-2 depicts that a tabulated average error values for 80 wells generated by a particular model (the results of performing steps 1 to 5). The error data is converted into a cumulative frequency curve (termed here as an error probability curve). The straight line in the error probability plot represents a trend of normally distributed values. The data points that deviate from the straight line are not following a normal distribution. These data points represent “outlier wells” which are typically subject to further evaluation to re-evaluate the Definitive Pore Pressure, or simple re-checking the data quality input into the model.

Further details are presented in the Error Probability Plots for the top two Theoretical models in Figure 4-5 and for both the Modified Compaction trend model and the Exponent model in Figure 4-6.

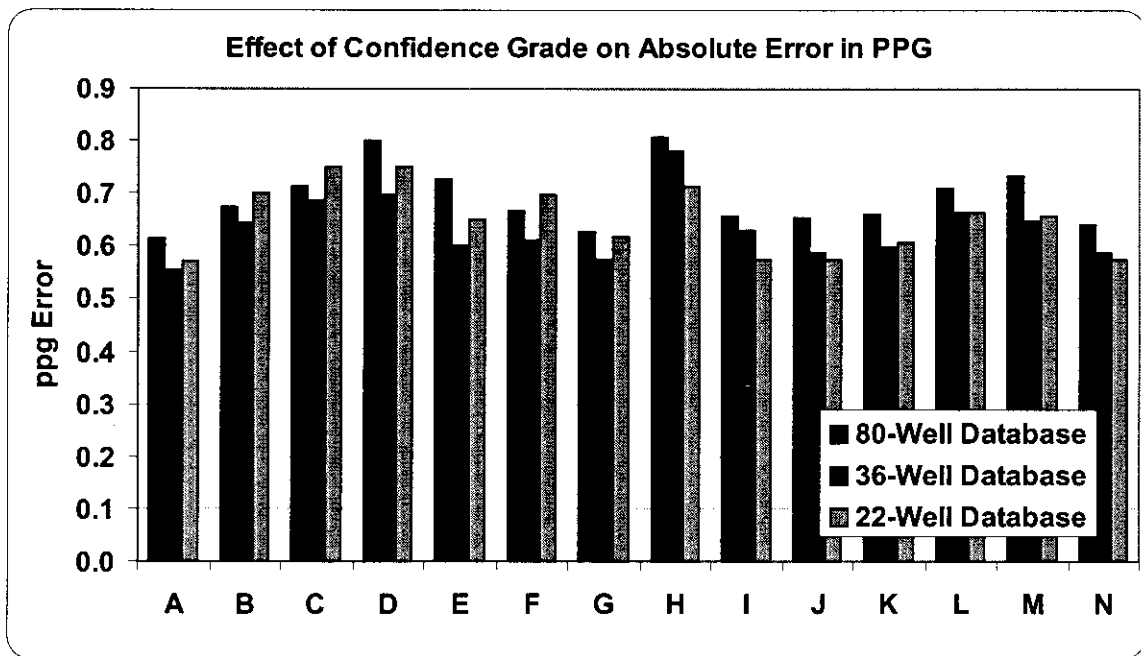
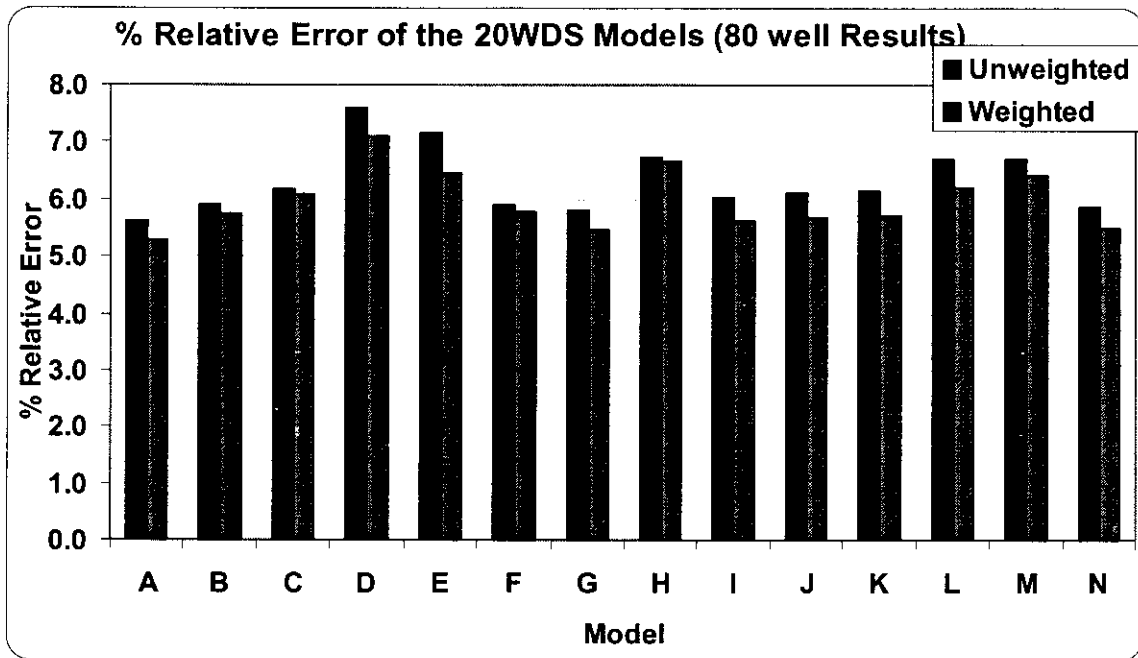


Figure 4-2 Relative Error of Universal Models and Confidence Grades

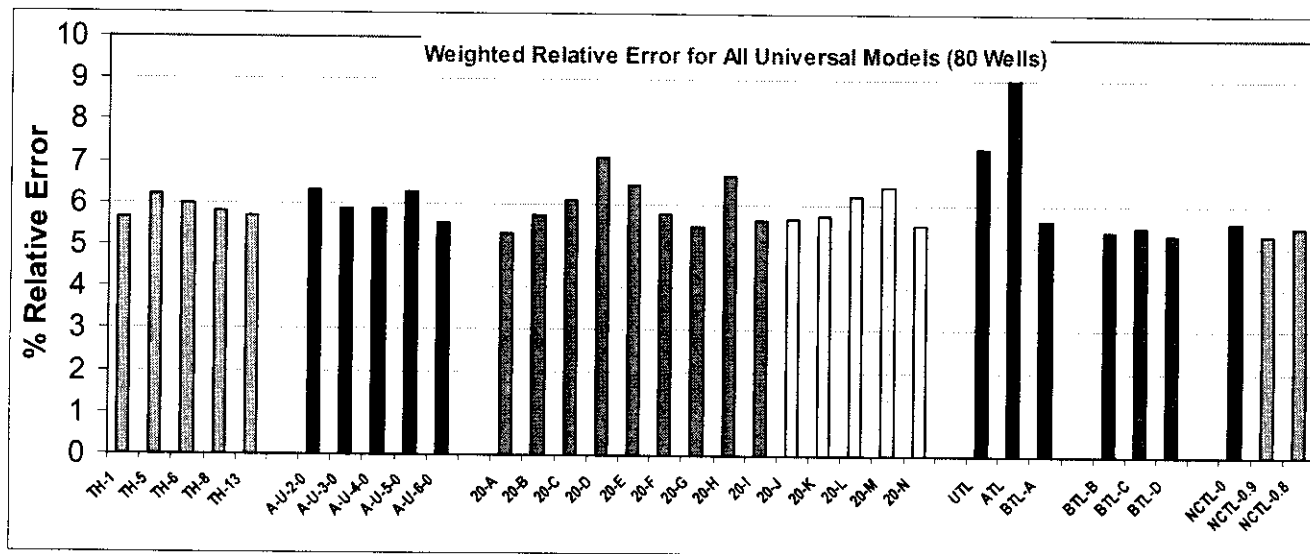
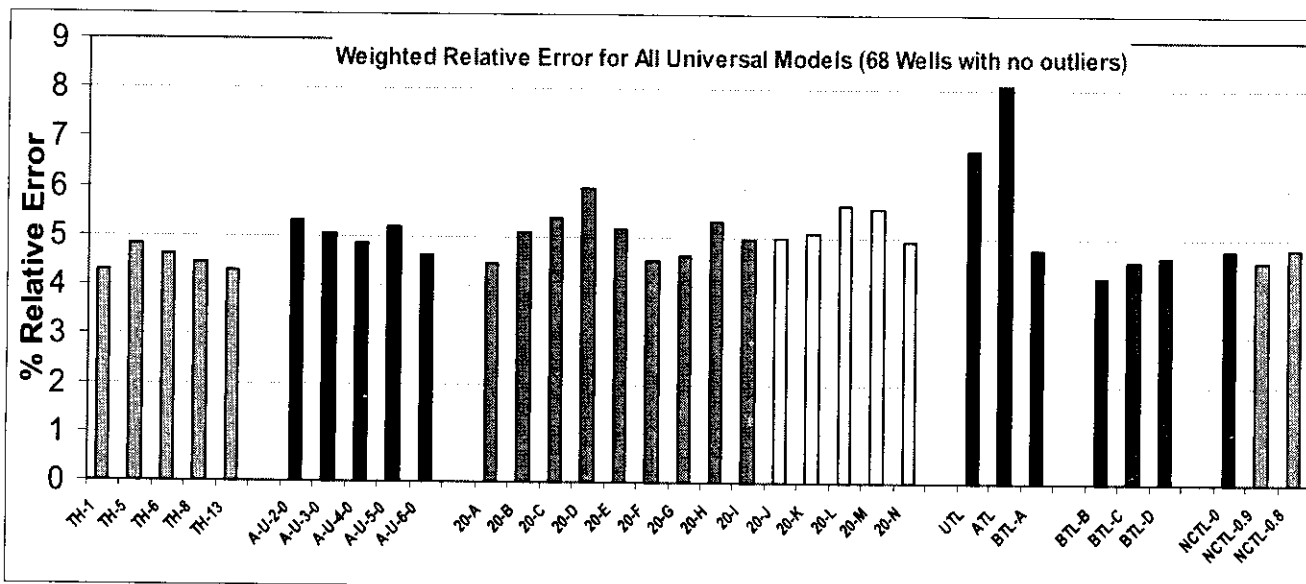


Figure 4-3 Effect of Outlier Wells on Error Statistics

Error Probability Plot

Model Error Statistics presented as a probability plot

Well	%RE
1	5%
2	7%
3	3.6%
4	5.8%
.	.
.	.
.	.
.	.



Normal Probability Plot

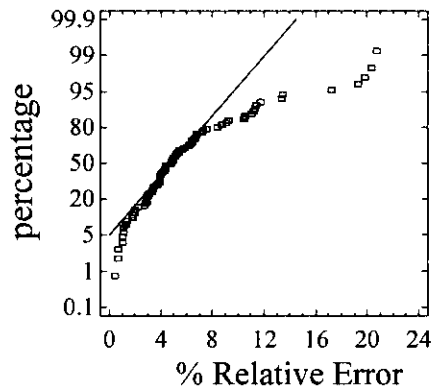
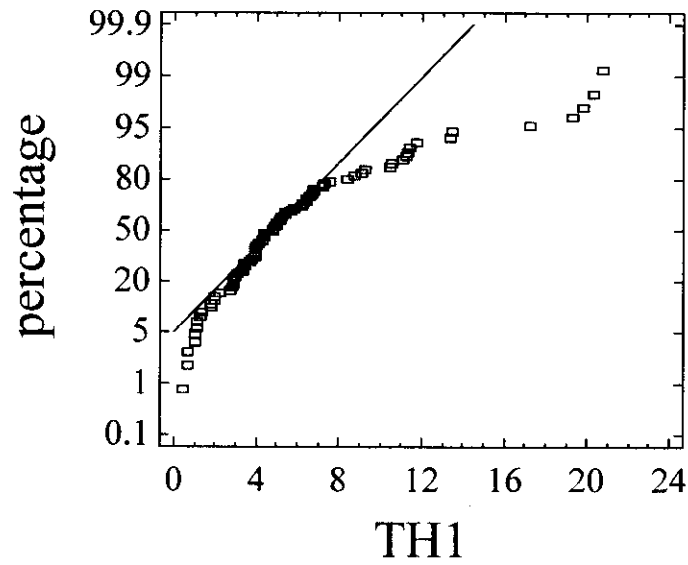


Figure 4-4 Example of Error Probability Plot

Normal Probability Plot



Normal Probability Plot

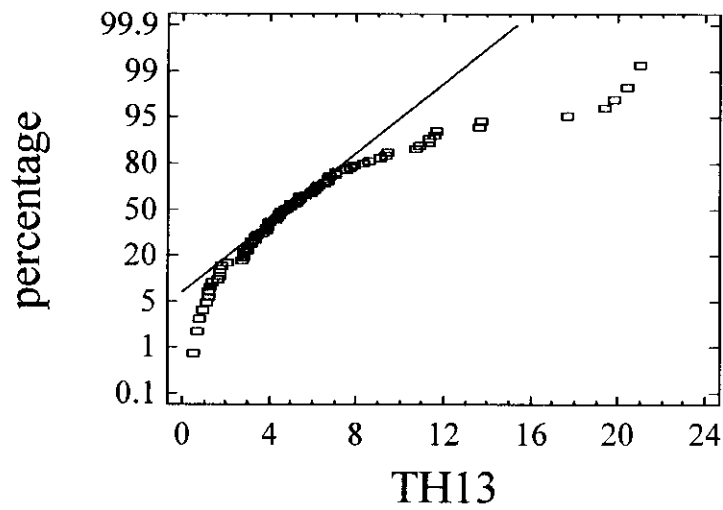
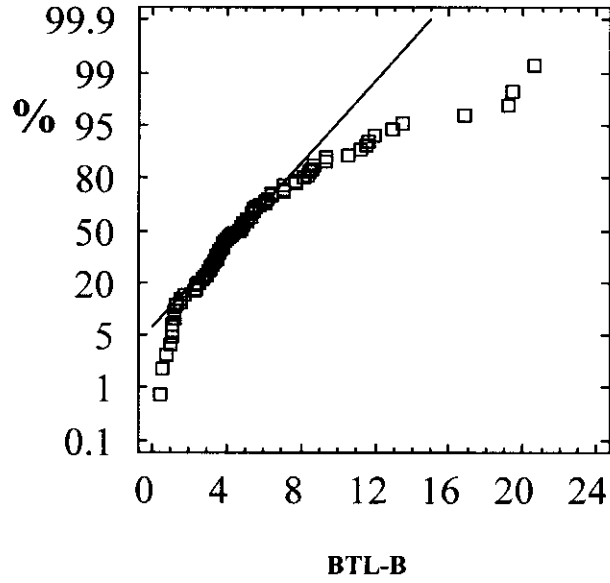


Figure 4-5 Probability Plots for Top Two Theoretical Models

Normal Probability Plot



Normal Probability Plot

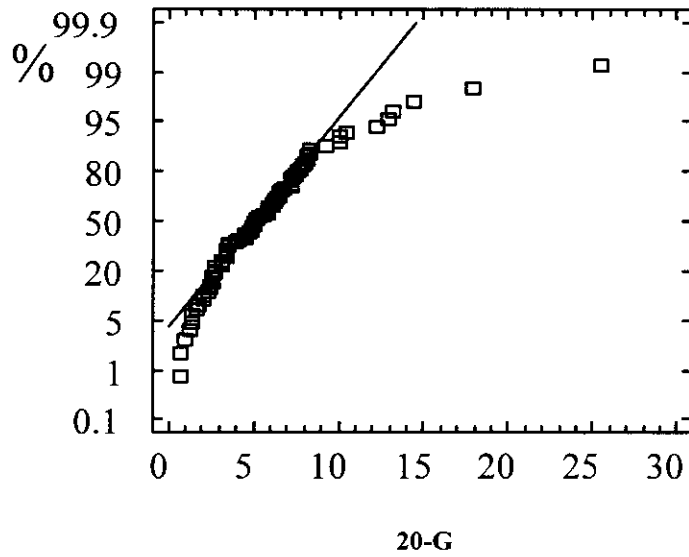


Figure 4-6 Probability Plots for Bowers' Modified Compaction Trend and a Modified Exponent Model

4.5 Five Best Performing Models

Table 4-1 lists the five models that performed the best on all the test wells. These models were selected based on the following:

- Error ranking or ability to accurately predict pore pressure of test wells
- Stability or lack of tendency to not predict pore pressure on some wells

This latter criteria was applied subjectively based on the experience gained during the error analysis.

At this point it is important to set forth the following considerations:

- The application of the top five models to seismic data is limited (due to limited seismic data available in the current DEA 119 database).
- As a result of the above, the training data is selected from sonic data. The sonic data in general has limited coverage to shallow depths. Typically sonic data start at about 3000 to 4000 ft below the mud line.

Therefore, there are some unavoidable limitations to the new models stemming from the utilization of sonic data (instead of seismic) and their limited vertical coverage of shallow formations. The suggested approach to select one or more of the top five models is as follows:

- Apply all the models to offset wells.
- Compare the performance of each model against the definitive pore pressures assigned to the offset wells.
- Check the performance of the models at shallow depth
- Select one that best match the definitive pore pressure at all depths (shallow and deep).

We must also recognize that the difference between the top 5 and the top 20 models is less than 1% relative error (or 0.07 ppg). Appendix A, Table 7-1 lists variables definitions.

Rank	Model No.	Description
First	TH-1 Theoretical	Baldwin-Butler porosity effective-stress formulation: $P(\text{psi}) = \text{OBG psi} - 5635 * (1 - \text{phiamoco})^{1.094}$ <p>Where: OBG psi is the overburden stress in psi Phiamoco = porosity derived from Amoco empirical equation given as follows: $\text{Phiamoco} = 1.425 * (1 - (V/15000))$ V is velocity in ft/sec</p>
Second	TH-13 Theoretical	Modified version of Bowers' velocity effective-stress relationship: $P(\text{psi}) = \text{OBG psi} - ((V - 5000)/1.046)^{(1/1.069)}$
Third	BTL-B Improved Conventional	Exponent model with Bowers' curved trend: $P(\text{ppg}) = \text{OBG} - (\text{OBG} - 8.7) * (\text{DT}_{\text{BTL-B}} / \text{DT})^{2.227}$ <p>Modified Bowers' trend Type B: $\text{DT}_{\text{BTL-B}} = 10^6 / (5000 + 14.22 * (0.052 * \text{TVD} * (\text{OBG} - 8.7))^{0.7415})$ </p>
Fourth	20-A Empirical	Multiple Regression Model: $P(\text{in ppg}) = -14.02 + 0.1982 * \text{DT} + 0.02251 * \text{OBG} - 0.0008785 * \text{Delta}^2 + 0.00005647 * \text{WD} + 0.0004002 * \text{ML} - 0.0004483 * \text{DT} * \text{DT} + 0.0005492 * \text{Delta}^2 * \text{Delta}^2 + 0.000002685 * \text{ML} * \text{DT} - 0.000009746 * \text{ML} * \text{Delta}^2 + 0.00003297 * \text{ML} * \text{OBG}$
Fifth	20-G Modified Conventional	Modified Exponent model with water depth term: $P(\text{in ppg}) = \text{OBG} - 0.8509 * ((\text{OBG} - 8.7)^{1.037}) * (\text{WD}^{-0.07403}) * ((200 * \text{EXP}(-0.00006 * \text{ML})) / \text{DT})^{2.571}$

Table 4-1 List of Best Ranked Models

5 Conclusions

A systematic data analysis process is critical to the success of model development. By utilizing the extensive DEA 119 database for the GOM, it was possible to test a variety of analytical approaches in working towards the development of new models.

- Improvements were made on the conventional analysis models that reduced the bias in the selection of a trend line. The Eaton equation was modified to eliminate dependence on a site-specific trend line, instead universal compaction trends were established based on studies made on the entire GOM database sonic data. In conjunction with a universal trend, regressed universal exponents were derived for several regions in the GOM. Improvements were introduced to Bowers' curved trend.
 - The modified Eaton equation and Bowers' curved trend performed extremely well (averaging 5.3% relative error, 0.62 ppg over 80 wells studied).
 - The introduction of empirically derived and simplified curved compaction trends improved on the Bowers' curved trend (approximately 0.3% relative error or 0.25 ppg).
- Simplified empirical models competed very well with the theoretical models. The rating of pure empirical models with no theoretical or physical significance scored just as well as those that have a theoretical foundation. For example, Model 20-A scored 5.279% relative error, which competed very well with the top two theoretical models that stand at 5.675% and 5.688% respectively.
- The effect of uncertainties in the assigned definitive pore pressure as well as suspected data quality can be easily identified. This caused the error statistics for the top models increase at least 0.3 ppg.
- If we consider the uncertainty in the definitive pore pressure assigned to each well, the models developed in this project scored an average error of about 4% or about 0.5 ppg. The 0.5 ppg error margin is considered attainable with the current models.
- Regression techniques must be enhanced and optimized to attain stable and reproducible results. Many other new techniques explored in this project are very promising. The clustering methods are particularly intriguing. Further work is necessary to develop robust pore pressure prediction based on these new approaches.
- The best way to utilize the new models is to apply all of them on offset wells. The best performing model is then used for the prospect well.
- It is very important that the analyst use these new models with caution. It is advisable to use the new models in conjunction with the standard methods. However, this cautionary note does not reduce the confidence in the new models.

6 References

Bowers, G. L., 1994, "Pore Pressure Estimation from Velocity Data: Accounting for Overpressure Other Than Undercompaction", SPE 27488 presented at the SPE IADC Conference, 15-18 February 1994.

Bowers, G. L., 2001, "Determining an Appropriate Pore-Pressure Estimation Strategy", presented at the Offshore Technology Conference, Houston, TX, April 30, 2001.

GAML software Dr. Eric Eslinger, Eric Geoscience, Inc. 10 Sussex Road, Glenmont, NY 12077, 518-439-8447 (tel), 518-439-8582 (fax).

Vignaux, G A, and Scott, J L, 2001, "Simplifying Regression Models Using Dimensional Analysis", Institute of Statistics and Operations Research, Victoria University of Wellington, Wellington, New Zealand (Internet Web Site).

7 Appendix A: List of New Models

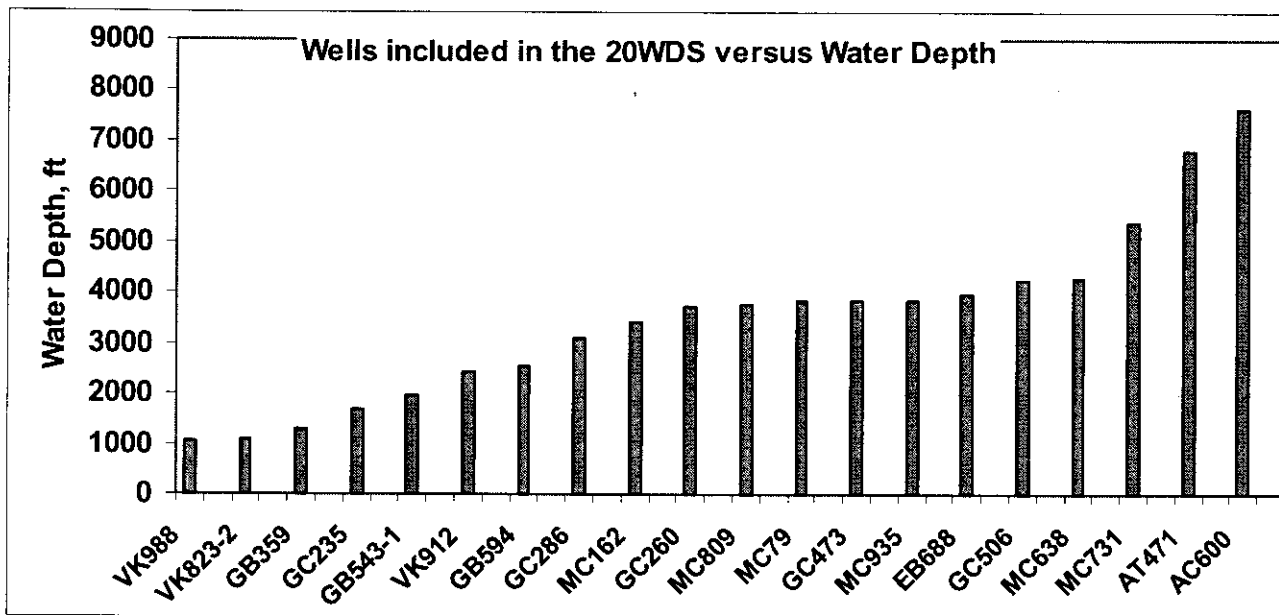


Figure 7-1 List of Wells used in the Universal Calibration Data versus Water Depth

Variable	Description
AG	Air gap, ft
DT	Sonic travel time in micro sec /ft
Tn2	Normal compaction trend for sonic slowness (Universal Trend Line) $Tn^2 = 200 * EXP(- 10 * 10^{-5} * ML)$ ML = total vertical depth below mud line 200 is sonic interval velocity at mud line (water) EXP = Exponential (base e)
Delta2	= Observed DT – Tn2 $Delta2 = (DT - 200 * EXP(-10 * 10^{-5} * ML))$ Where ML is vertical depth below mud line
ML	Vertical Depth below mud line, ft
OBG	Overburden gradient, ppg
OBGpsi	Overburden stress, psi
TVD	Vertical depth below Kelly bushing
WD	Water depth, ft

Table 7-1 List of Variables

Model Name	Model
<p>UTL</p>	<p>Universal Trend Line Method</p> <p>Pore Pressure in PPG = $OBG - (OBG - 8.7) * (Tn2/DT)^{1.8333}$</p> <p>Where</p> <p>OBG = Overburden in ppg DT = Sonic log value in micro sec per ft Tn2 = Sonic delta T from normal trend</p> <p>Universal Trend line Equation</p> <p>$Tn2 = 200 * EXP(-10 * 10^{-5} * ML)$</p> <p>ML = Depth below mud line $10 * 10^{-5}$ is the slope of the line 200 is the sonic value (micro sec/ft) at mud line depth</p>
<p>ATL</p>	<p>Automated Trend Line Method</p> <p>Pore Pressure in PPG = $OBG - (OBG - 8.7) * (ATLDT/DT)^3$</p> <p>Where</p> <p>ATLDT = "Apparent" or Automated Trend sonic time in micro sec/ft OBG is in ppg</p> <p>Equation of the Apparent Trend Method</p> <p>$ATLDT = 200 * EXP(- Slope * DBML)$ Slope = $[Ln (50/200)] / (WD - 19000)$ WD = Water depth in feet</p>

Table 7-2 Conventional Exponent with Universal Linear Trends

Model Name	Normal Curved Trend Models
BTL-A Bowers' Standard Trend	Pore Pressure in ppg = $OBG - (OBG - 8.7) * (DT_{BTL-A} / DT)^3$ Where DT_{BTL-A} is the standard Bowers' curved trend given by: $DT_{BTL-A} = (10^6 / ((10^6 / 200) + 14.22 * (0.052 * TVD * (OBG_{Amoco} - 8.7))^0.725))$ Where OBG_{Amoco} = Overburden gradient in ppg derived from Amoco Empirical equation OBG_{Amoco} in ppg = $[8.5 * WD + (16.3 + \{TVD - WD - AG\} / 3125)^0.6] * (TVD - WD - AG) / TVD$ AG = Air gap in feet TVD = TVD from KB in feet
BTL-B Modified Bowers' Trend	$P \text{ (ppg)} = OBG - (OBG - 8.7) * (DT_{BTL-B} / DT)^{2.22713}$ Modified Bowers' Trend Type B is shown below: $DT_{BTL-B} = (10^6 / ((10^6 / 200) + 14.22 * (0.052 * TVD * (OBG - 8.7))^0.741536))$
BTL-C Modified Bower Trend	$P \text{ (ppg)} = (OBG - (OBG - 8.7) * (DT_{BTL-C} / DT)^{1.66073}) / (5.82484 * 10^{-14} * ML^3 - 1.75013 * 10^{-9} * ML^2 + 1.47731 * 10^{-6} * ML + 1.00206)$ $DT_{BTL-C} = (10^6 / ((10^6 / 200) + 112.182 * (0.052 * TVD * (OBG - 8.7))^0.478881))$
BTL-D Modified Bower Trend	$P \text{ (ppg)} = ((OBG - (OBG - 8.7) * (DT_{BTL-A} / DT)^{2.11807}) / (2.91242 * 10^{-14} * ML^3 - 8.75063 * 10^{-10} * ML^2 + 7.38655 * 10^{-7} * ML + 1.00103))$ Where DT_{BTL-A} is the standard Bowers' curved trend defined above

Table 7-3 Conventional Exponent Model With Curved Trends

Trend line Name	Exponent Model with Normal Sonic Curved Trend
NCT-A	$P \text{ (ppg)} = \text{OBG} - (\text{OBG} - 8.7) * (\text{DT}_{\text{NCT-A}} / \text{DT})^{3.03915}$ <p>Where the new curved trend of sonic travel time $\text{DT}_{\text{NCT-A}}$ is given by :</p> $\text{DT}_{\text{NCT-A}} = 200 - 133 * (1 - \text{EXP}(-0.000196248 * \text{ML}))$
NCT-B	$P \text{ (ppg)} = (\text{OBG} - (\text{OBG} - 8.7) * (\text{DT}_{\text{NCT-B}} / \text{DT})^{2.02989}) / (2.91242 * 10^{-14} * \text{ML}^3 - 8.75063 * 10^{-10} * \text{ML}^2 + 7.38655 * 10^{-7} * \text{ML} + 1.00103)$ <p>Where $\text{DT}_{\text{NCT-B}}$ is given by:</p> $\text{DT}_{\text{NCT-B}} = 200 - 133 * (1 - \text{EXP}(-0.00021314 * \text{ML}))$
NCT-C	$P \text{ (ppg)} = (\text{OBG} - (\text{OBG} - 8.7) * (\text{DT}_{\text{NCT-C}} / \text{DT})^{1.16451}) / (5.82484 * 10^{-14} * \text{ML}^3 - 1.75013 * 10^{-9} * \text{ML}^2 + 1.47731 * 10^{-6} * \text{ML} + 1.002)$ <p>Where $\text{DT}_{\text{NCT-C}}$ is given by:</p> $\text{DT}_{\text{NCT-C}} = 200 - 133 * (1 - \text{EXP}(-0.000271597 * \text{ML}))$

Table 7-4 List of New Empirical Curved Trends (above)

Model Name	Model
TH-1	$P \text{ (psi)} = \text{OBGpsi} - 5635.47 * (1 - \text{phiamoco})^{1.09439}$ <p>Where: OBGpsi is the overburden stress in psi Phiamoco = porosity derived from Amoco empirical equation given as follows: $\text{Phiamoco} = 10^{-6} * 95.04 * 15000 * (1 - (V/15000))$ V is velocity in ft/sec</p>
TH-5	$P \text{ (psi)} = \text{OBGpsi} - \text{EXP}((\text{phiamoco} / (1 - \text{phiamoco}) - 22) / -2.67428)$ <p>Phiamoco defined above.</p>
TH-6	$P \text{ (psi)} = \text{OBGpsi} - (V/340.759)^{(1/0.425396)}$ <p>Where V is the sonic velocity in ft/sec Modified Baker Hughs Equation</p>
TH-8	$P \text{ (psi)} = \text{OBGpsi} - ((3162.89 * (V - 3162.89)) / (14616 - 1.0319 * (V - 3162.89)))$ <p>V as defined above in ft/sec</p>
TH-13	$P \text{ (psi)} = \text{OBGpsi} - ((V - 5000) / 1.04628)^{(1/1.0689)}$ <p>Modified version of Bowers' velocity effective stress relationship equation</p>

Table 7-5 List of Theoretical Models

Model #	Models for Pore Pressure in ppg
20-B	$OBG-(OBG-9.5)*((200*\exp(-10*10^{-5}*ML))/DT)^{1.55738}$
20-C	$OBG-(OBG-9)*((200*EXP(-10*10^{-5}*ML))/DT)^{0.930674} /EXP(0.0000368258*ML)$
20-D	$OBG-0.000812854*ML*(Tn2/DT)^{2.10441}$
20-E	$OBG-2.00528*((200*EXP(-3.5*10^{-5}*ML))/DT)^{2.09359}$
20-F	$OBG-2.21827*(WD/ML)^{-0.352213}*((200*EXP(-6*10^{-5}*ML))/DT)^{2.51771}$
20-G	$OBG-0.850935*(OBG-8.7)^{1.03723} *WD^{-0.0740325} * ((200*EXP(-6*10^{-5}*ML))/DT)^{2.57094}$
20-H	$OBG-6.40575*(TVD/ML)^{-1.25829}*(Tn2/DT)^{2.37027}/(1 - 0.86*ML /18000)$
20-I	$OBG-0.318811*(OBG-8.7)^{1.3205}*(TVD/ML)^{0.135429}*((200*EXP(-9*10^{-5}*ML))/DT)^{2.67979}/(1-0.8*ML/18000)$

Table 7-6 List of Modified Conventional Models

Notes:

- Model 20-B is the familiar Exponent model. Notice that the following parameters were modified as a result of regression: The exponent is 1.5 instead of the commonly used value of 3. The normal pressure term (9.5 ppg) is NOT reflecting the actual normal pore pressure. However, it is pure regression modification. Also, notice that the Universal Trend Line for normal compaction trend is already embedded in the equation.
- Model 20-C is similar to 20-B, but a smoothing function has been utilized to “despike” predicted pore pressure and make the model less sensitive to spiky sonic data.
- Models 20-D, E, and F are not recommended due to the following reasons:
 - Unstable functions
 - Extremely smooth predicted pressure profile make less responsive to possible pressure variations.

Model #	Pore Pressure in psi	Notes
20-A	$P \text{ (in ppg)} = -14.0211 + 0.198153*DT + 0.0225094*OBG - 0.000878519*\Delta^2 + 0.0000564718*WD + 0.000400204*ML - 0.000448282*DT*DT + 0.000549243*\Delta^2*\Delta^2 + 0.00000268461*ML*DT - 0.00000974607*ML*\Delta^2 + 0.0000329711*ML*OBG$	This Model pore pressure in ppg
A-U-2	$P = 18484.1 - 108.22*DT - 1.17161*OBGpsi + 0.00790683*DT*OBGpsi + 0.0000447737*OBGpsi*OBGpsi + 0.215409*DT*DT - 0.00227194*WD*DT + 0.716822*WD*Tn2/DT - 2703.29*Tn2/DT*Tn2/DT - 3450.45*Tn2/DT$	MAE= 312 psi C= 97.9 %
A-U-3	$P = 60066.3 - 452.657*DT - 1.64744*OBGpsi + 0.0195693*DT*OBGpsi + 0.0000900978*OBGpsi*OBGpsi + 0.999372*DT*DT - 0.00764004*WD*DT + 1.62879*WD*Tn2/DT - 9370.81*Tn2/DT*Tn2/DT - 1.7667*Tn2/DT*OBGpsi - 0.00618473*ML*DT - 0.0000646034*ML*OBGpsi$	MAE= 303.6 psi C = 98%
A-U-4	$P = 1168.01 - 22.841*DT + 0.0306561*OBGpsi + 0.00177506*DT*OBGpsi + 0.0000199375*OBGpsi*OBGpsi + 0.0611955*DT*DT + 0.00210672*WD*DT + 0.00316411*ML*DT$	MAE= 323 psi C=97.7 %
A-U-5	$P = -30932.6 + 242.69*DT - 0.611496*DT*DT + 1.2897*OBGpsi - 0.00000353943*OBGpsi*OBGpsi - 0.00190378*WD*DT + 0.00087067*ML*DT - 399.904*Tn2/DT + 0.0000149128*(Tn2/DT)*ML*WD + 7377.35*DTBDTratio + 0.165357*DTBDTratio*WD$	MAE = 303 psi C = 97.8%
A-U-6	$P = -17273.5 + 299.726*DT - 0.716238*DT*DT + 0.407705*OBGpsi + 0.0000231315*OBGpsi*OBGpsi + 0.00144786*WD*DT - 46.3236*\Delta^2 - 0.089399*\Delta^2*\Delta^2 - 12275.2*DTBDTratio + 10608.8*DTBDTratio^2 - 19718.9*Tn2/Dt + 7195.02*Tn2/DT*Tn2/DT + 1.39526*ML*Tn2/DT - 0.092107*ML*DTBDTratio$	MAE= 291 psi C = 98.1 %

Table 7-7 List of Multiple Regression Models

Notes:

$DTBDTratio = (\text{Bowers' normal trend sonic, } DT_{BTL-A} / \text{Observed sonic measurement})$

Where DT_{BTL-A} is the standard Bowers' curved trend given by:

$$DT_{BTL-A} = (10^6 / ((10^6/200) + 14.22 * \{0.052 * TVD * (OBG_{Amoco} - 8.7)\}^{0.725}))$$

Where OBG_{Amoco} = Overburden gradient in ppg derived from Amoco Empirical equation

$$OBG_{Amoco} \text{ in ppg} = [8.5 * WD + (16.3 + \{TVD - WD - AG\} / 3125)^{0.6} * (TVD - WD - AG)] / TVD$$

AG = Air gap in feet

TVD = TVD from KB in feet

MAE = Mean Absolute Error in psi

C = Coefficient of correlation

Model #	Models for Pore Pressure in ppg	Type
20-J	$\text{Exp}(2.27028+0.00628184*\text{Delta}2)$	Exponential
20-K	$1/(0.102592 - 0.000546436 * (\text{DT}-200*\text{EXP}(-10*10^{-5}*ML)))$	Logistic
20-L	$8.7+ 1.45906* \text{EXP}(0.0227996*\text{delta}2)$	Exponential
20-M	$8.7 + 0.101479 * \text{Delta}2 - 0.000156528 * \text{Delta}2^2$	Polynomial
20-N	$9.28534+0.0328181*(\text{DT}-(200*\text{exp}(-11.583*10^{-5}*ML)))+0.000831152*(\text{DT}-(200*\text{exp}(-11.583*10^{-5}*ML)))^2-0.00000447506*(\text{DT}-(200*\text{exp}(-11.583*10^{-5}*ML)))^3$	Polynomial

Table 7-8 List of Universally Trained Quick-Look Empirical Models (Require No OBG)

Notes:

A universal trend line (mudline intercept at 200 microsecond/ft, slope of $-10*10^{-5}$) is constant for all models.

All these models share one common theme: all these models can predict pore pressure from knowing three inputs: water depth, sonic, and overburden gradient. Below is definitions of input variables:

□ DT is sonic interval velocity, micro sec/ft.

□ Delta2 is given by

$$\text{Delta}2 = (\text{DT}-200*\text{EXP}(-10*10^{-5}*ML))$$

Where ML is vertical depth below mud line

8 Appendix B: Error Analysis Results – Ranking of Models

After the Definitive Pore Pressure (DPP) for each well in the database is established, the error for predicted pore pressures is evaluated by the following criteria:

- Average absolute error in ppg
- Average relative error (RE)

The following is a brief discussion of the fundamental equations used along with the development of uncertainty bounds for any given model.

8.1 Error Evaluation Equations

The average **absolute** error is the averaged error value of a particular well, which is defined as follows:

$$AE = \Sigma \text{Absolute } (DPP_i - P_i) / N \quad \dots\dots\dots \text{(EQN B.1)}$$

Where	AE	Average Absolute error over a depth interval in <u>a well</u>
	P _i	Predicted pore pressure at depth i
	DPP _i	Definitive pore pressure at depth i
	N	Number of depth increments

The average absolute error of all wells (AAE) is calculated as follows:

$$AAE \text{ (all wells)} = \Sigma AE / n \quad \dots\dots\dots \text{(EQN B.2)}$$

Where **n** is the number of wells used in the prediction.

The Average **Relative** Error (ARE) is computed as follows:

$$\% \text{ ARE (one well)} = 100 * [\Sigma \text{Absolute } (DPP_i - P_i) / DPP_i] / N \quad \dots\dots\dots \text{(EQN B.3)}$$

The average relative error for all wells is then computed as follows:

$$\% \text{ ARE for all wells} = \Sigma ARE / n \quad \dots\dots\dots \text{(EQN B.4)}$$

Where:	n	is the number of wells (used in the prediction).
	N	is the number of the depth increment

8.2 Confidence Grading in Definitive Pore Pressure

Determination of a DPP was guided entirely by the availability of calibration data, such as but not limited to RFT's, Mud Weights, kicks, well flow, and gas shows. The quality of the calibration data for a given well is also a measure of the degree of confidence determined for the selected DPP. The quality of the calibration data for each well should be determined to gauge confidence in the DPP. This process establishes the yard stick by which we determine performance for each of the predictive models. Error values for the predictive models are then ranked and weighted according to the degree of confidence determined for the DPP.

A set of rules and guidelines have been established and programmed to evaluate the Confidence Grade (CG). The confidence grade in estimated pore pressure for a well is used as a weighting factor in the error analysis as follows:

$$\text{Weighted Average Relative Error} = \frac{\sum CG_J * RE_J}{\sum CG_J} \dots\dots\dots(\text{EQN B.5})$$

Where: RE_J is the relative error for Well No. J

The same equation can be written for the weighted average absolute error.

Model	Weighted %RE (80 Wells)			Weighted Absolute Error, ppg		
	Average	Minimum	Maximum	Average	Minimum	Maximum
TH-1	5.675	0.181	8.704	0.645	0.017	0.939
TH-5	6.208	0.147	9.384	0.704	0.015	0.998
TH-6	5.983	0.171	8.105	0.674	0.020	0.922
TH-8	5.808	0.268	9.344	0.654	0.026	0.953
TH-13	5.688	0.166	8.836	0.648	0.016	0.951
Above: Theoretical Models, Below: Multiple Regression Models						
A-U-2-0	6.340	0.311	9.463	0.708	0.032	1.047
A-U-3-0	5.879	0.251	8.910	0.662	0.030	0.990
A-U-4-0	5.895	0.233	8.918	0.666	0.027	1.050
A-U-5-0	6.285	0.326	9.687	0.721	0.037	1.153
A-U-6-0	5.557	0.206	8.471	0.646	0.018	1.111
Below: List of Models Empirical and Modified Conventional Models						
20-A	5.279	0.000	8.066	0.613	0.000	1.065
20-B	5.747	0.000	11.055	0.675	0.000	1.229
20-C	6.091	0.257	11.119	0.716	0.026	1.232
20-D	7.115	0.290	10.777	0.800	0.029	1.123
20-E	6.469	0.413	12.656	0.729	0.046	1.262
20-F	5.766	0.152	10.287	0.667	0.017	1.143
20-G	5.479	0.142	9.782	0.629	0.014	1.089
20-H	6.682	0.222	21.363	0.807	0.022	3.362
20-I	5.620	0.000	12.065	0.659	0.000	1.963
20-J	5.672	0.235	7.764	0.655	0.025	1.077
20-K	5.719	0.210	8.087	0.662	0.022	1.130
20-L	6.217	0.332	8.292	0.712	0.034	1.160
20-M	6.422	0.240	13.857	0.735	0.026	1.380
20-N	5.498	0.169	7.591	0.641	0.018	1.060
Below: The Linear and Curved Trend Models						
UTL	7.361	0.168	11.595	0.854	0.020	1.293
ATL	9.295	0.206	13.778	1.064	0.022	1.532
BTL-A	5.637	0.176	8.583	0.635	0.016	0.947
BTL-B	5.361	0.179	8.697	0.616	0.016	0.967
BTL-C	5.465	0.210	8.151	0.622	0.022	1.057
BTL-D	5.305	0.171	9.236	0.611	0.017	1.025
NCTL-0	5.585	0.171	7.715	0.643	0.016	0.880
NCTL-0.9	5.293	0.103	7.943	0.612	0.010	0.941
NCTL-0.8	5.472	0.257	8.284	0.634	0.026	1.067

Table 8-1 List of Universal with the Error Analysis Results

Universal Models Rating Per Region						
Rating	Predicting East Region		Predicting Middle Region		Predicting West Region	
	Model	% Unweighted RE	Model	% Unweighted RE	Model	% Unweighted RE
1	20-H	5.165	BTL-D	4.784	NCTL-0.9	6.297
2	A-U-6-0	5.257	BTL-A	5.103	BTL-B	6.303
3	20-B	5.276	NCTL-0.9	5.134	20-N	6.372
4	20-F	5.298	20-E	5.296	20-A	6.402
5	20-G	5.391	NCTL-0	5.303	BTL-C	6.413
6	20-A	5.419	20-A	5.382	NCTL-0.8	6.447
7	20-I	5.472	NCTL-0.8	5.420	BTL-D	6.478
8	20-C	5.481	BTL-B	5.472	A-U-6-0	6.608
9	NCTL-0.8	5.502	BTL-C	5.474	20-I	6.688
10	BTL-B	5.600	20-G	5.478	NCTL-0	6.732
11	BTL-C	5.633	TH-1-0.9	5.537	20-K	6.868
12	TH-13	5.663	TH-13	5.688	20-J	6.898
13	NCTL-0.9	5.663	20-F	5.690	20-G	6.937
14	TH-1	5.665	20-B	5.717	BTL-A	6.942
15	A-U-4-0	5.702	TH-1	5.735	A-U-4-0	6.997
16	20-N	5.750	A-U-6-0	5.743	TH-8	7.024
17	TH-6	5.768	20-N	5.772	20-L	7.164
18	BTL-D	5.791	20-K	5.786	20-B	7.247
19	A-U-5-0	5.822	20-J	5.798	TH-1	7.257
20	20-M	5.825	TH-5	5.847	TH-13	7.297
21	20-J	5.976	20-D	5.904	A-U-3-0	7.331
22	TH-1-0.9	5.994	20-M	5.937	20-F	7.350
23	A-U-3-0	6.015	TH-8	6.005	A-U-2-0	7.512
24	TH-6-0.9	6.037	20-C	6.077	20-C	7.543
25	20-K	6.066	A-U-4-0	6.131	TH-6	7.603
26	TH-8	6.084	TH-6-0.9	6.152	A-U-5-0	7.706
27	TH-5	6.142	TH-5-0.9	6.162	20-E	7.835
28	A-U-2-0	6.152	A-U-3-0	6.201	TH-1-0.9	7.920
29	NCTL-0	6.233	TH-6	6.268	TH-5	8.195
30	UTL	6.420	20-I	6.411	20-D	8.216
31	BTL-A	6.469	A-U-5-0	6.419	TH-6-0.9	8.303
32	20-L	6.690	20-L	6.474	20-H	8.500
33	TH-5-0.9	7.023	UTL	6.562	20-M	9.055
34	ATL	7.125	A-U-2-0	7.000	TH-5-0.9	9.524
35	20-E	7.875	20-H	7.817	UTL	9.568
36	20-D	8.253	ATL	8.814	TH-8-0.9	11.693
37	TH-8-0.9	9.874	TH-8-0.9	9.736	ATL	12.956

Table 8-2 Universal Models Ranked based on Regional Performance

	West Wells			Middle Wells			East Wells		
	Number of wells 21			Number of Wells 21			Number of Wells 37		
	West Predicting West	Middle Predicting West	East Predicting West	West Predicting Middle	Middle Predicting Middle	East Predicting Middle	West Predicting East	Middle Predicting East	East Predicting East
Weighted Errors									
Average % RE	8.48	8.54	8.21	8.77	6.49	6.47	8.32	7.40	5.50
Lowest % RE	6.99	6.52	6.73	6.62	5.79	5.63	5.92	6.50	4.54
Average Error in ppg	0.97	0.94	0.93	1.11	0.76	0.79	0.97	0.85	0.64
Lowest Error in ppg	0.80	0.74	0.77	0.79	0.67	0.69	0.69	0.73	0.52
Best Models									
First Place	W-K	M-K	E-I	W-J	M-J	E-J	W-C	M-J	E-I
Second Place	W-J	M-J	E-K	W-K	M-K	E-G	W-K	M-N	E-H
Third Place	W-L		E-J	W-L	M-G	E-A		M-M	E-J
Fourth Place			E-J	W-C	M-C	M-K		M-K	E-L

RE= Relative Error in %
 Averaged Values for Models A to N

Table 8-3 Regional Models Predictions Performance based on Geographical Areas



KNOWLEDGE SYSTEMS, INC.

State of the Art in Pore Pressure Estimation

Glenn Bowers

5/25/1999

CONFIDENTIAL

This report is provided to DEA Project 119 Project Participants under the terms of the DEA Project 119 Participation Agreement and is thereby subject to restrictions of confidentiality and non-disclosure to third parties.

DEA Project 119

Report No. 1

Corporate Offices

Knowledge Systems, Inc.
P. O. Box 1279
Stafford, Texas 77497-1279
Phone: 281-879-1400
Fax: 281-879-1499
E-mail: sales@knowsys.com

European Office

Knowledge Systems, Inc.
P.O. Box 274 Paradis
5856 BERGEN
Norway
Phone: +47 55 92 45 62
Fax: +47 55 92 45 62
E-mail: sales @knowsys.com

Please visit the Knowledge Systems' website at <http://www.knowsys.com>

Information in this document is subject to change without notice, and does not represent a commitment on the part of Knowledge Systems. The software described in this document is furnished under a license agreement or non-disclosure agreement. It is against the law to copy the software on any medium except as specifically allowed in the license or non-disclosure agreement.

© Copyright Knowledge Systems, 1989-2000. All rights reserved. *DrillWorks* is a registered trademark of Knowledge Systems, Inc. *PostScript* is a registered trademark of Adobe Systems, Inc. *Windows* is a trademark of Microsoft Corporation

Document Information

Title: State of the Art in Pore Pressure Estimation	
Description: DEA 119, Report No. 1	
Author(s): Glenn Bowers	
Reviewer(s): Myleen Sjodin	
Creation Date: 10/5/2000 9:43 AM	Last Date Modified: 10/5/2000 9:54 AM
Approved By: Jim Bridges	Approval Date: 5/25/1999
Will be sent to:	
Sources Used: (can be other documents used as sources)	
Project Number:	Document Number: 2000-000005

Table of Contents

1	Introduction.....	1
2	Direct Methods.....	4
2.1	Resistivity/Sonic	4
2.1.1	Hottman & Johnson	4
2.1.2	Pennebaker/McClure	5
3	Vertical Effective Stress Methods.....	7
3.1	Sonic/Resistivity	8
3.1.1	Equivalent Depth	8
3.1.2	Mean Stress Equivalent Depth	9
3.2	Sonic.....	10
3.2.1	Bellotti & Giacca	10
3.2.2	Hart, Flemings, & Deshpande	10
3.3	Resistivity	11
3.3.1	Bryant	12
3.3.2	Alixant & Desbrandes.....	12
4	Horizontal Effective Stress Methods	14
4.1	Sonic/Resistivity	14
4.1.1	Eaton.....	14
4.1.2	Compaction Trends.....	15
4.2	Sonic.....	21
4.2.1	Weakley	21
4.3	Resistivity	22
4.3.1	Rasmus & Gray Stephens.....	22
5	Other Effective Stress Methods	23
5.1	Sonic.....	23
5.1.1	Bowers	23
5.1.2	Wilhelm	24
5.2	Resistivity	25
5.2.1	Holbrook	25
6	References.....	30

1 Introduction

The literature on pore pressure estimation has grown extensively since Hottman and Johnson (1965) started it all with their classic paper. All pore pressure estimation methods are based on the premise that pore pressure influences compaction-dependent shale properties such as porosity, density, sonic velocity, and resistivity. Any wireline or geophysical measurement that is sensitive to pore pressure will be referred to as a *pore pressure indicator*.

There are two general approaches for converting pore pressure indicator measurements into pore pressure estimates:

Direct Methods

Effective Stress Methods

Direct methods directly relate the amount a pore pressure indicator diverges from its normal trend line to the pore pressure gradient at the depth. There are basically two direct methods: crossplots, pioneered by Hottman and Johnson (1965), and overlays, first proposed by Pennebaker (1968).

Effective stress methods are based upon Terzaghi's effective stress principal (Terzaghi, 1943), which states that compaction of geologic materials is controlled by the difference between the total confining pressure and the pore fluid pressure. This difference, termed the *effective stress*, represents the portion of the total stress carried by the rock or sediment grains.

Most effective stress methods consist of three steps:

The vertical effective stress (σ) is estimated from a pore pressure indicator measurement.

The overburden stress (OB) is determined from measured or estimated bulk density data.

The pore fluid pressure (P) is obtained from the difference

$$P = OB - \sigma \quad (1)$$

All new pore pressure methods published since the late 60's have been effective stress approaches. They differ only in the way that they determine effective stresses. These techniques can be subdivided into three categories

Vertical Methods

Horizontal Methods

Other

Vertical methods, such as Foster and Whalen's Equivalent Depth method (1966), compute the effective stress from normal trend data at the same *pore pressure indicator value* as the depth of interest (see Fig. 1). Horizontal methods, such as Eaton's Method (Eaton, 1975), compute the effective stress from normal trend data at the same *depth* as the depth of interest. "Other" methods do something else. Lane and Macpherson (1976) were the first to suggest categorizing pressure techniques as horizontal or vertical methods. At the time their paper was written, there were no published methods in the

“Other” category. Table 1 categorizes various pore pressure estimation methods that have been published for sonic velocity/transit time and resistivity.

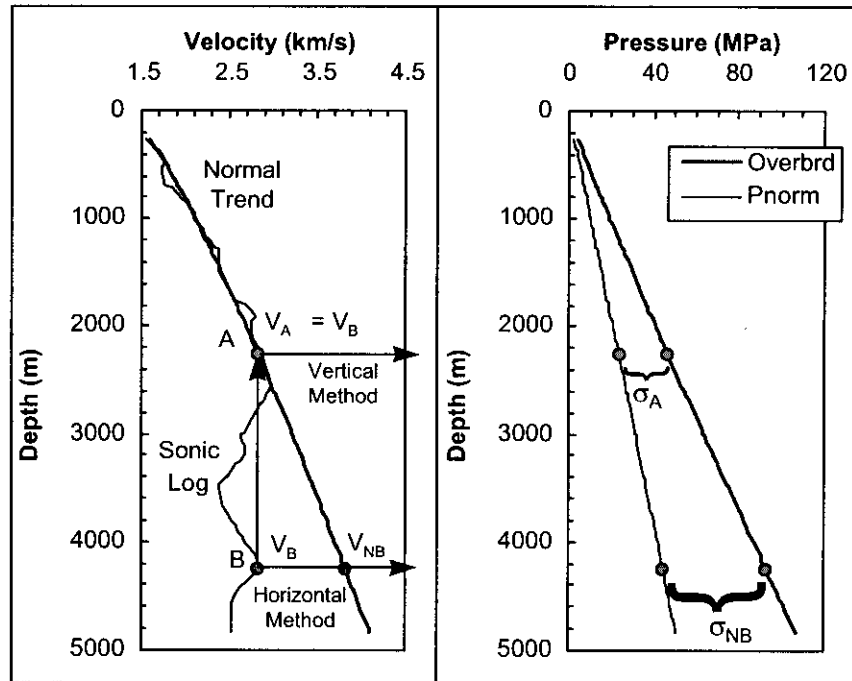


Fig. 1 - Vertical vs horizontal pore pressure estimation methods. Vertical methods use normal trend data at the same pore pressure indicator value as the depth of interest (Point A). Horizontal methods would use normal trend data at the same depth (Point B).

Direct	Effective Stress		
	Vertical	Horizontal	Other
Sonic/Resistivity • Hottman & Johnson • Pennebaker/McClure	Sonic/Resistivity • Equivalent Depth • Mean Stress Equivalent Depth Sonic • Bellotti & Giacca • Hart & Flemings Resistivity • Bryant • Alixant & Desbrandes	Sonic/Resistivity • Eaton Sonic • Weakley Resistivity • Rasmus & Gray Stephens	Sonic • Bowers • Wilhelm Resistivity • Holbrook

Table 1 - Classification of published pore pressure estimation methods.

The next four sections will provide overviews of the solution methods listed in Table 1. Eaton's method will be looked at in some detail, since it is one of the most widely used approaches in the industry (Yoshida, et al, 1996). Particular attention will be paid to the sensitivity of Eaton's method to the normal trend curve that is assumed for velocity or interval transit time. In deepwater areas, a semi-log normal trend, which has become more or less the industry standard, can lead to erroneous results.

2 Direct Methods

2.1 Resistivity/Sonic

2.1.1 Hottman & Johnson

Hottman & Johnson's method (1965) uses a crossplot to relate departures from the normal trend line of a pore pressure indicator to the pore pressure gradient at that depth. Regional well log data and pore pressure measurements are used to plot and fit sets of X vs Y data, where X is a measure of normal trend departure, and Y is the pore pressure gradient. Hottman & Johnson (H&J) developed crossplots for both resistivity, and sonic transit time, where X and Y were defined as follows:

Resistivity

$$X = \frac{R_n}{R}, \quad Y = \text{Pore Pressure Gradient (psi/ft)} \quad (2)$$

Sonic Transit Time

$$X = \Delta t - \Delta t_n, \quad Y = \text{Pore Pressure Gradient (psi/ft)} \quad (3)$$

The subscript "n" denotes the normal trend value.

Crossplots reflect the geologic conditions of the area in which they were developed. As was noted by Mathews & Kelly (1967): "Charts developed for a given area cannot be used in other geologic areas; new charts must be developed". Figures 2 and 3 show some of the resistivity and sonic transit time crossplots that have been published.

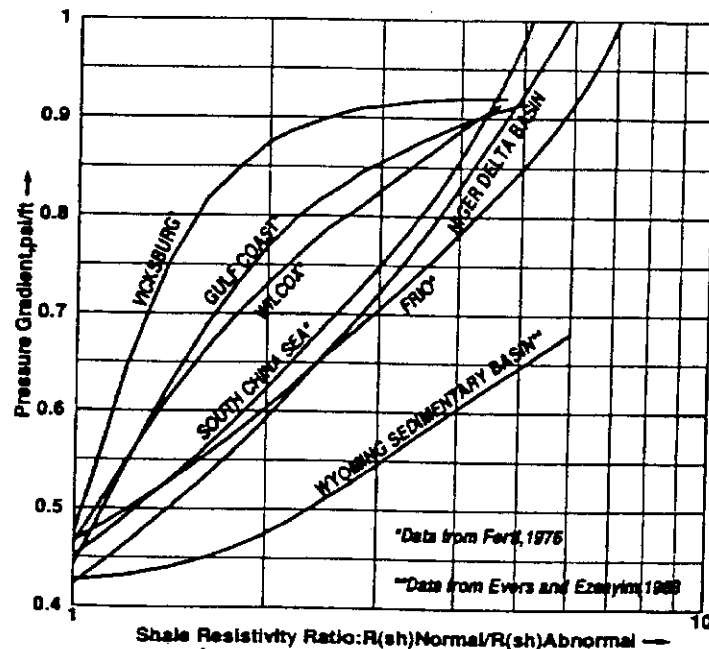


Fig. 2 Published pore pressure crossplots for resistivity (from Owolabi, et. al, 1990).

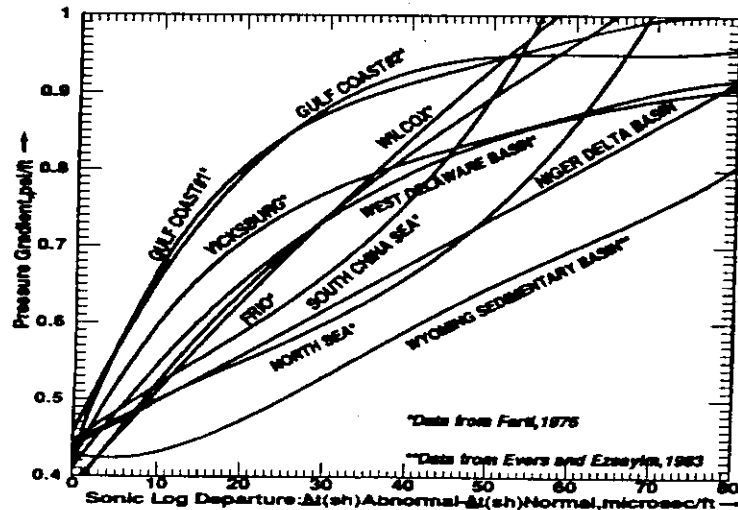


Fig. 3 Published pore pressure crossplots for sonic transit time (from Owolabi, et. al, 1990).

This author has found that H&J's original Gulf Coast sonic transit time crossplot generally provides an upper bound for pore pressures in most Tertiary basins, and *will overestimate pore pressure in the deepwater Gulf of Mexico.*

Eaton (1972) and Lane & Macpherson (1976) both proposed that the accuracy of H&J crossplots could be improved by including the effect of changes in overburden stress. Although they did not say so, what they were basically suggesting was a three-dimensional crossplot, where the third axis would be overburden gradient. The approach they actually followed was to: 1) compute the overburden gradient at the depth of each X-Y pair, 2) divide the X-Y data into different ranges of overburden gradients, and then 3) fit an X-Y curve for each overburden gradient range.

It appears that this refined H&J method never really caught on, which is not surprising. If the overburden stress must be calculated, then it is simpler to just use an effective stress approach. Nevertheless, it is important to keep in mind that changes in overburden stress can influence H&J crossplots. This is particularly relevant in areas like the deepwater Gulf of Mexico, where water depths and salt thicknesses sometimes vary significantly over relatively short distances.

2.1.2 Pennebaker/McClure

Pennebaker's original paper (1968) focused on pore pressure prediction from seismic interval transit times. Similar to Hottman & Johnson (1965), he also presented an X-Y crossplot for computing pore pressures, but with:

$$X = \frac{\Delta t}{\Delta t_n}, \quad Y = \text{Pore Pressure Gradient (psi/ft)} \quad (4)$$

His crossplot can be approximated with the following equation:

$$Y = 1.017 - 0.531 X^{-5.486} \quad (5)$$

Pennebaker recognized that for any given normal trend, Eq. 5 could be used to construct Δt vs depth curves for a series of different pore pressure gradients. He printed these curves on a transparent overlay so that pore pressure gradients could be directly read from an interval transit time-depth plot.

Like Hottman & Johnson's original crossplot (1965), Pennebaker's relation was based primarily upon well data from the Texas and Louisiana Gulf Coast. However, he attempted to generalize his method to include different geologic ages and even different lithologies. He assumed that the interval transit time normal trend for all rocks followed the same slope when plotted versus depth on a log-log plot. A change in geologic age and/or lithology would simply cause the normal trend to undergo a lateral shift parallel to the interval transit time axis. Therefore, he proposed that one overlay could be applied world-wide by simply shifting it to account for lithology/age changes.

Overlays for conductivity, and bulk density were also eventually developed by Pennebaker and his co-workers. When Pennebaker left Humble Oil in the early 70's, the overlay "torch" was passed to Leo McClure. Since then, McClure has been instrumental in getting this technology transferred to the rest of the industry. In fact, except within Exxon, the overlay method is probably more widely associated with McClure's name than Pennebaker's.

Over the years, it has become apparent that one world-wide pore pressure overlay is generally not sufficient for any given pore pressure indicator. Practitioners of the Pennebaker method typically have libraries of local overlays. However, the "Pennebaker shift" still remains a part of the method, as demonstrated in Figure 4, which is from a paper by Gill (1986).

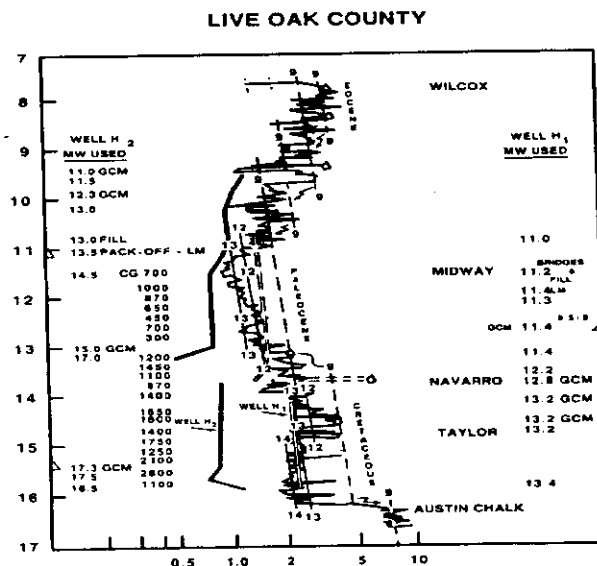


Fig. 4 Example of overlay shifting (from Gill, 1986).

3 Vertical Effective Stress Methods

Vertical methods assume that normally pressured and overpressured formations follow the same, unique relation for compaction as a function of effective stress. In other words, overpressured and normally pressured formations with identical velocities are assumed to have identical effective stresses (see Fig. 5). The Equivalent Depth method uses this concept to graphically solve for effective stresses, while other vertical methods do so analytically. Fig. 6 illustrates how a velocity-effective stress relation could be constructed from normal trend data.

Normally pressured and overpressured formations do not always follow the same effective stress relation. In those situations, vertical effective stress methods can significantly underestimate the pore pressure, as illustrated in Fig. 7.

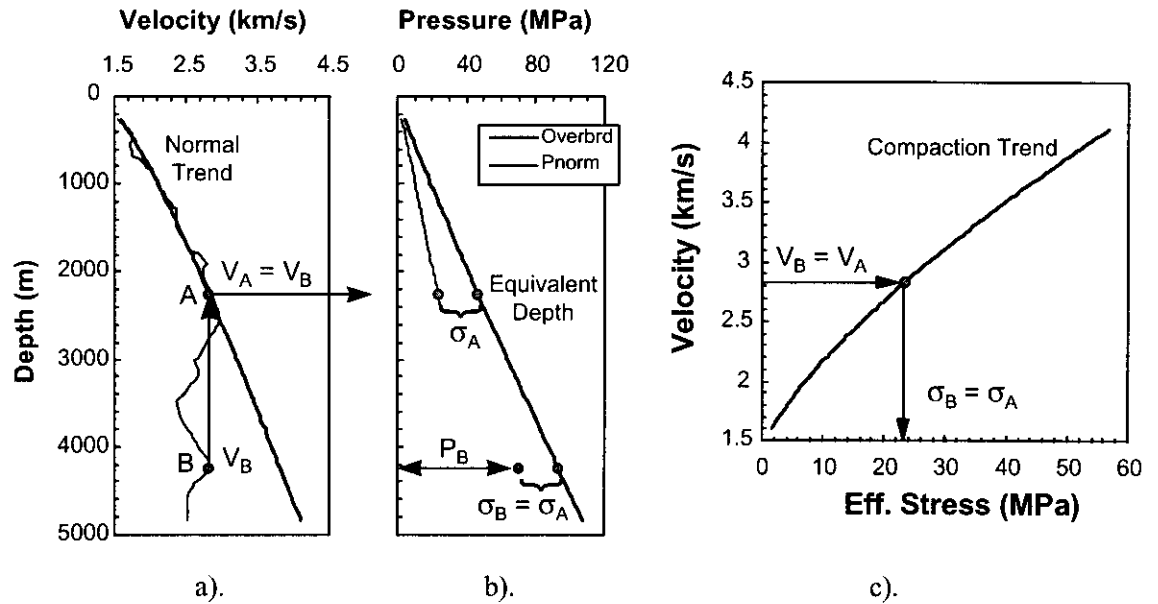


Fig. 5 - Vertical effective stress methods.

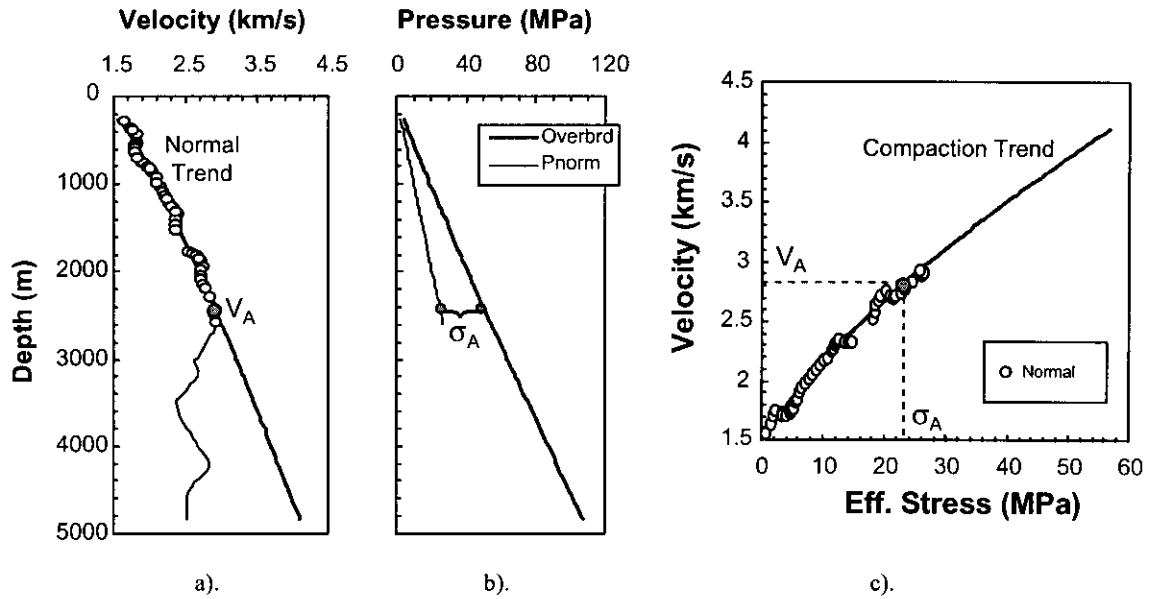


Fig. 6 - Calibration of a vertical effective stress method from normal trend data.

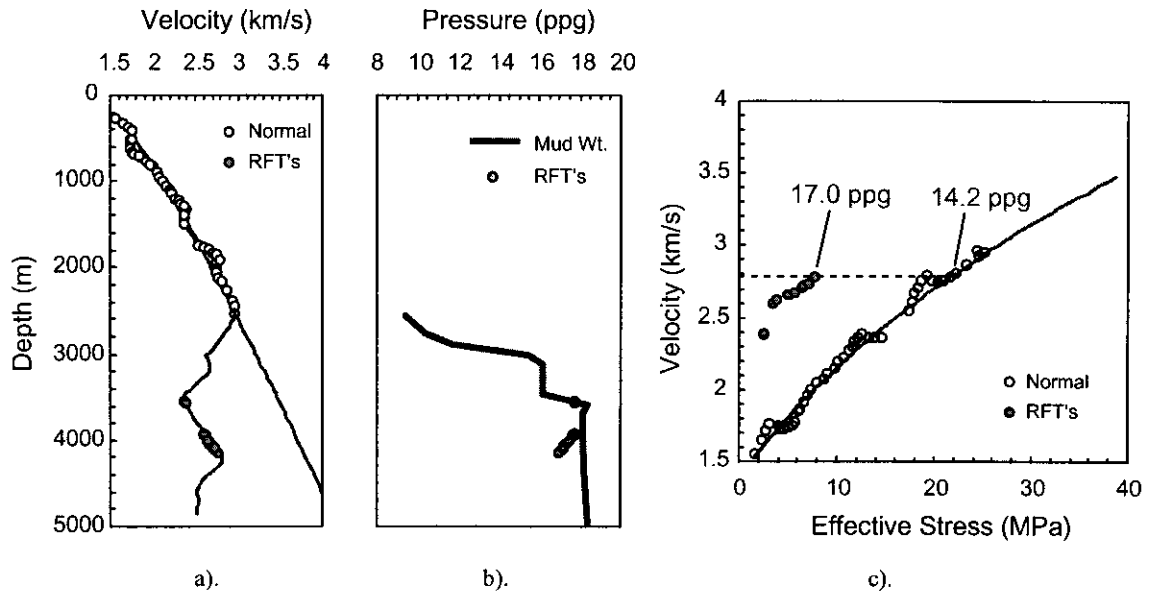


Fig. 7 - Case where vertical effective stress methods fail.

3.1 Sonic/Resistivity

3.1.1 Equivalent Depth

The Equivalent Depth method graphically solves for the effective stress. For the sonic log data in Fig. 5a, the effective stress at B would be equated to the effective stress

computed from the overburden stress and normal pore pressure at A (Fig. 5b). In other words,

$$\begin{aligned} P_B &= OB_B - \sigma_A \\ &= OB_B - (OB_A - P_{NA}) \end{aligned} \quad (6)$$

where P_{NA} is the normal (hydrostatic) pore pressure at point A. The point where the vertical projection of a pore pressure indicator intersects the normal trend line (Point A in Fig. 5) is termed the *equivalent depth*. It is from the equivalent depth concept that vertical methods get their name.

The Equivalent Depth method is one of the most frequently mentioned pore pressure estimation techniques in the literature, and yet, its originators are rarely cited. The first use of the Equivalent Depth method appears to have been in a paper by Foster and Whalen (1966), who focused on pore pressure estimation from formation factor. A subsequent paper by Ham (1966) discussed the application of the Equivalent Depth method to sonic, density, and resistivity data.

3.1.2 Mean Stress Equivalent Depth

Traugott (1997) proposed a modified version of the Equivalent Depth method, defined in terms of the *mean* effective stress σ_M :

$$\sigma_M = \frac{(\sigma + \sigma_h + \sigma_H)}{3} \quad (7)$$

where σ is the vertical effective stress, and σ_h and σ_H are the minimum and maximum horizontal *effective* stresses.

This approach would be difficult to implement in areas in which $\sigma_h \neq \sigma_H$, since there is no generally accepted method for determining σ_H . However, in tectonically relaxed areas, where the horizontal stresses are the same in all directions, the horizontal effective stresses can be defined in terms of the vertical effective stress as follows:

$$\sigma_h = \sigma_H = K\sigma \quad (8)$$

where K is the *effective stress ratio*. Equation 7 can then be written as:

$$\sigma_M = \left(\frac{1+2K}{3}\right)\sigma = \left(\frac{1+2K}{3}\right)(OB-P) \quad (9)$$

For the example in Fig. 5, Traugott's modified Equivalent Depth method requires:

$$\sigma_{MB} = \left(\frac{1+2K_B}{3}\right)(OB_B - P_B) = \sigma_{MA} = \left(\frac{1+2K_A}{3}\right)(OB_A - P_{AN}) \quad (10)$$

and therefore,

$$P_B = OB_B - \left(\frac{1+2K_A}{1+2K_B}\right)(OB_A - P_{NA}) \quad (11)$$

If the effective stress ratio does not change with depth, then the modified and original Equivalent Depth methods will give the same results. If the effective stress ratio

increases with depth, the modified version will yield higher pore pressures than the original method, and vice-versa.

All other effective stress methods discussed in this report compute pore pressures from the vertical effective stress, not the mean effective stress.

3.2 Sonic

Fertl (1976) considered wireline sonic logs to be the best data source for pore pressure estimation due to the log's relatively low sensitivity to hole size, formation temperature, and pore water salinity. Two sonic-based vertical methods are presented here. Bellotti & Giacca (1978) directly tie velocity to effective stress, while Hart, et. al., (1995) relate effective stress to a porosity parameter calculated from sonic transit time.

3.2.1 Bellotti & Giacca

Effective Stress Calculation

Bellotti and Giacca (1978a) introduced the following velocity-effective stress relation:

$$V = V_{\min} + \frac{V_{\max} \sigma}{A \sigma + B} \quad (12)$$

where V_{\min} is the minimum soil velocity, V_{\max} is the sonic velocity of the rock matrix, σ is the vertical effective stress, and A and B are additional calibration parameters. The corresponding equation for effective stress is:

$$\sigma = \frac{(V - V_{\min}) B}{V_{\max} - A(V - V_{\min})} \quad (13)$$

Density-Velocity Relation

In a companion article to (1978a), Bellotti & Giacca (1978b) also proposed the following equation for estimating density from velocity/interval transit time data:

$$\rho = \rho_{\max} - 1.228 (\rho_{\max} - \rho_f) \frac{(\Delta t - \Delta t_{\max})}{(\Delta t + \Delta t_f)} \quad (14)$$

where $\Delta t = 1 \times 10^6 / V$ = interval transit time, ρ_{\max} , ρ_f are the densities of the rock matrix and pore fluid, and Δt_{\max} , Δt_f are the interval transit times for the rock matrix and pore fluid. For the Po Valley, they assumed the following values for these parameters

$$\begin{aligned} \rho_f &= 1.03 \text{ g/cc}, & \Delta t_f &= 200 \text{ } \mu\text{s/ft} \\ \rho_{\max} &= 2.75 \text{ g/cc}, & \Delta t_{\max} &= 53 \text{ } \mu\text{s/ft} \end{aligned}$$

3.2.2 Hart, Flemings, & Deshpande

Hart, Flemings, & Deshpande (1995) used a two-step process to calculate effective stress. First they applied a porosity-interval transit time relation proposed by Issler (1992) to convert velocity to porosity. The resulting porosities were then substituted into Athy's (1930) exponential porosity-effective stress relation.

Porosity Calculation

Issler's (1992) porosity-velocity relation is:

$$\phi = 1 - \left(\frac{V}{V_{\text{mx}}} \right)^{1/X} \quad (15)$$

where ϕ is porosity, V is sonic velocity, V_{mx} is the sonic velocity of the rock matrix, and X is a fitting parameter. Hart, et. al. (1995) used the parameters suggested by Issler (1992), which are:

$$V_{\text{mx}} = 14,925 \text{ ft/s}, \quad X = 2.19$$

Effective Stress Calculation

Athy's (1930) porosity-effective stress relation has the following form:

$$\phi = \phi_0 e^{-\eta\sigma} \quad (16)$$

where ϕ_0 and η are fitting parameters, and is σ the vertical effective stress. Eqs. 15 and 16 can be combined into the following velocity-effective stress relations:

$$V = V_{\text{mx}} (1 - \phi_0 e^{-\eta\sigma})^X \quad (17)$$

$$\sigma = \frac{1}{\eta} \ln \left(\frac{\phi_0}{1 - \left(\frac{V}{V_{\text{max}}} \right)^{1/X}} \right) \quad (18)$$

Porosities calculated from Eq. 15 may not agree with porosities calculated from other data, such as bulk density. Whether or not they do is really immaterial, as long as they are only used to calculate effective stresses. The accuracy of the sonic-derived porosities does become an issue if they are used to calculate overburden stresses.

3.3 Resistivity

With the advent of LWD resistivity, a number of resistivity-based pore pressure estimation methods were published in the late 1980's, early 1990's. They all consist of three basic steps

- Convert resistivity to "porosity".
- Convert "porosity" to vertical effective stress.
- Subtract the vertical effective stress from the overburden stress to obtain pore pressure.

There is no generally accepted porosity-resistivity relation for shales, and each of the LWD-inspired pore pressure estimation methods uses a different approach. The resulting porosities should probably be regarded more as dimensionless, temperature-normalized resistivities, rather than "true" porosities.

Four resistivity-based effective stress methods are discussed in this report. Two are vertical methods (Bryant, 1989, and Alixant & Desbrandes, 1989), one is a horizontal

method (Rasmus, et. al., 1991), while the fourth (Holbrook & Hauch, 1987) falls into the "Other" category.

3.3.1 Bryant

Porosity Calculation

Bryant (1989) chose the following form of Archie's equation:

$$\phi = \sqrt{\frac{R_w}{R}} \quad (19)$$

where R is the measured resistivity, R_w is pore water resistivity, and ϕ is porosity. R_w is assumed to linearly decrease from the seafloor down to a plateau that begins where the temperature equals 180 °F, and ends where the temperature reaches 400 °F. Seawater resistivity is assumed at the seafloor. The value along the plateau is calibrated locally.

Effective Stress Calculation

Bryant adopted the porosity-effective stress relation proposed by Baldwin & Butler (1985),

$$\sigma = \sigma_{\max} (1-\phi)^\alpha \quad (20)$$

where σ is the vertical effective stress, σ_{\max} and α are parameters, and $1-\phi$ was referred to by Baldwin & Butler (1985) as *solidity*. Bryant used Baldwin & Butler's (1985) value of 7.35 for α , but left σ_{\max} as a free parameter for local calibration. More generally, σ_{\max} and α may both have to be adjusted to fit local data.

Generic Overburden Stress Relation

Bryant's paper also includes the following "generic" overburden stress relation for Tertiary basins, derived from data from the Texas Gulf Coast:

$$\begin{aligned} \text{OB} = & 0.444 * \text{WD} \\ & + D \{ E + 2.64 \times 10^{-5} D - 1.97 \times 10^{-9} D^2 \\ & \quad + 6.60 \times 10^{-14} D^3 - 5.97 \times 10^{-19} D^4 \} \end{aligned} \quad (21)$$

where OB is the overburden stress (psi), WD is water depth (ft.), D is true vertical depth below mudline (ft.), and E is the overburden gradient (psi/ft) at the mudline. E can be adjusted to local conditions. Bryant's default value for E was 0.850 psi/ft.

3.3.2 Alixant & Desbrandes

Porosity Calculation

Alixant & Desbrandes (1991) use a modified version of a relation proposed by Perez-Rosales (1975):

$$\frac{R}{R_{wb}} = 1 + G \frac{(1-\phi)}{(\phi-\phi_r)} \quad (22)$$

or

$$\phi = \frac{G+(R/R_{wb}-1)\phi_r}{G+(R/R_{wb}-1)} \quad (23)$$

where R is the measured resistivity, R_{wb} is the resistivity of the shale's *bound water*, ϕ is porosity, and G and ϕ_r are parameters used for calibration. Alixant & Desbrandes (1991) assumed $G = 1.85$, $\phi_r = 0.1$, which are the values Perez-Rosales obtained for sand.

R_{wb} is analytically calculated from a regional temperature profile using the following equation:

$$R_{wb} = 297.6 T^{(-1.76)} \quad (24)$$

where T is temperature in degrees F. The assumption is that shales have no free water, only bound water, and that the salinity of bound water remains constant with depth.

Effective Stress Calculation

The following porosity-effective stress relation is borrowed from soil mechanics:

$$\varepsilon = \phi/(1-\phi) = r_1 - I_c \log(\sigma) \quad (25)$$

which can be inverted to:

$$\sigma = 10^{(r_1 - \varepsilon)/I_c} \quad (26)$$

The quantity $\varepsilon = \phi/(1-\phi)$ is known as the *void ratio*. Values for r_1 and I_c are calibrated with local data. In their paper, Alixant & Desbrandes (1991) assumed $r_1 = 3.84$, $I_c = 1.1$.

4 Horizontal Effective Stress Methods

Horizontal methods compute the effective stress from normal trend parameters and the normal pressure effective stress *at the depth of interest*. For point B in Fig. 8, this would be velocity V_{NB} , and the effective stress σ_{NB} .

4.1 Sonic/Resistivity

4.1.1 Eaton

Eaton's original method (1975) consists of the following five equations:

Sonic Velocity V:

$$\sigma = \sigma_N \left(\frac{V}{V_N} \right)^3 \quad (27)$$

Interval Transit Time Δt :

$$\sigma = \sigma_N \left(\frac{\Delta t_N}{\Delta t} \right)^3 \quad (28)$$

Resistivity R:

$$\sigma = \sigma_N \left(\frac{R}{R_N} \right)^{1.2} \quad (29)$$

Conductivity C:

$$\sigma = \sigma_N \left(\frac{C_N}{C} \right)^{1.2} \quad (30)$$

d_{XC} -exponent:

$$\sigma = \sigma_N \left(\frac{d_{XC}}{d_{XC_N}} \right)^{1.2} \quad (31)$$

where, as before, the subscript "n" denotes the normal trend line value at the depth of interest.

Fig. 8b illustrates what Eaton's method is actually doing. The velocity V_{NB} and effective stress σ_{NB} are used to fix one point on the true compaction trend. The remainder of the curve between (V_{NB}, σ_{NB}) and (V_B, σ_B) is then approximated with Eq. 27.

It can be seen in Fig. 8b that if the normal compaction trend has a shape similar to Eaton's equation, *effective stresses* calculated in overpressure with Eaton's method will lie close to the true compaction trend. This means that Eaton's method and vertical effective stress methods will produce similar results. As the shape of the normal trend

curve diverges from Eaton's equation, so will the amount of agreement between Eaton's method and vertical methods.

4.1.2 Compaction Trends

Sonic Velocity Compaction Trends

Hottman & Johnson (1965) assumed that the normal trend for interval transit time could be represented by a semi-log straight line. This assumption continues to be standard practice throughout much of the industry.

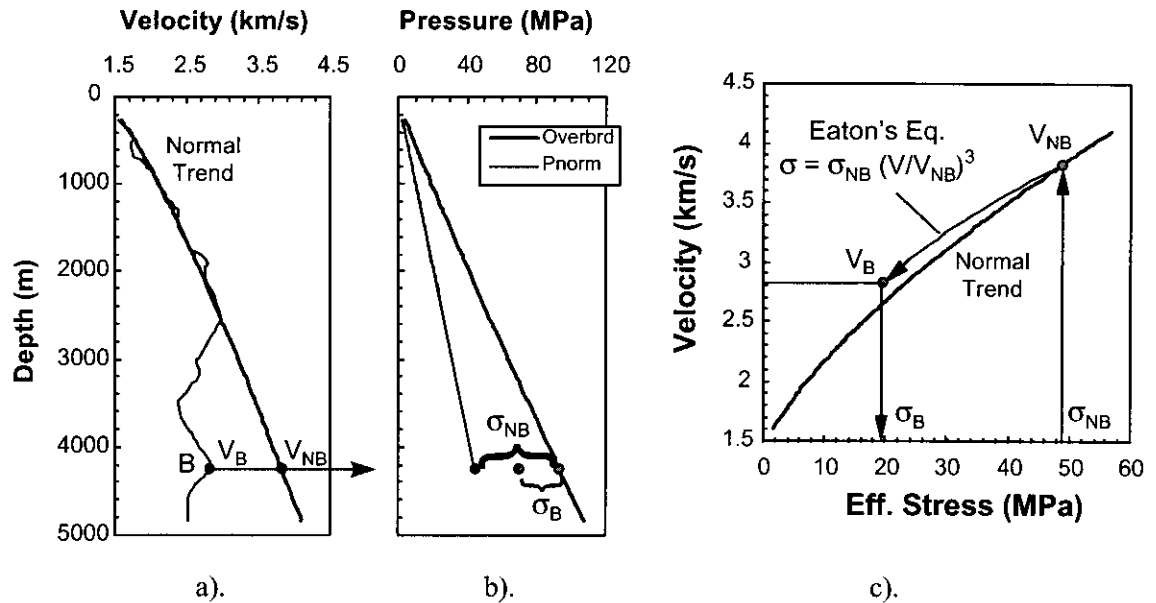


Fig. 8 - Horizontal effective stress methods - Eaton's method.

A semi-log straight line implies sonic travel time satisfies an equation of the form:

$$\log(\Delta t) = A - B \cdot \text{Depth}; \quad \Delta t = 10^A 10^{-B \cdot \text{Depth}} \quad (32)$$

The corresponding effective stress relations are:

$$\log(\Delta t) = A - B \cdot \sigma; \quad \Delta t = a 10^{-B \cdot \sigma} \quad (33a)$$

$$\log(V) = A + B \cdot \sigma; \quad V = a 10^{B \cdot \sigma} \quad (33b)$$

Other velocity-effective stress equations discussed in this report, and one additional relation suggested by Hamouz and Mueller (1984), are listed below:

Bellotti & Giacca (1978):

$$V = V_{\min} + \frac{V_{\max} \sigma}{A \sigma + B} \quad (34-a)$$

Hart, Flemings, & Dishpande (1995):

$$V = V_{\max} (1 - \phi_0 e^{-n \sigma})^X \quad (34-b)$$

Bowers (1995):

$$V = V_0 + A \sigma^B \quad (34c)$$

Hamouz & Mueller (1984):

$$\log(\Delta t - \Delta t_{mx}) = A - B\sigma, \quad \Delta t - \Delta t_{mx} = a 10^{-B*\sigma} \quad (34d)$$

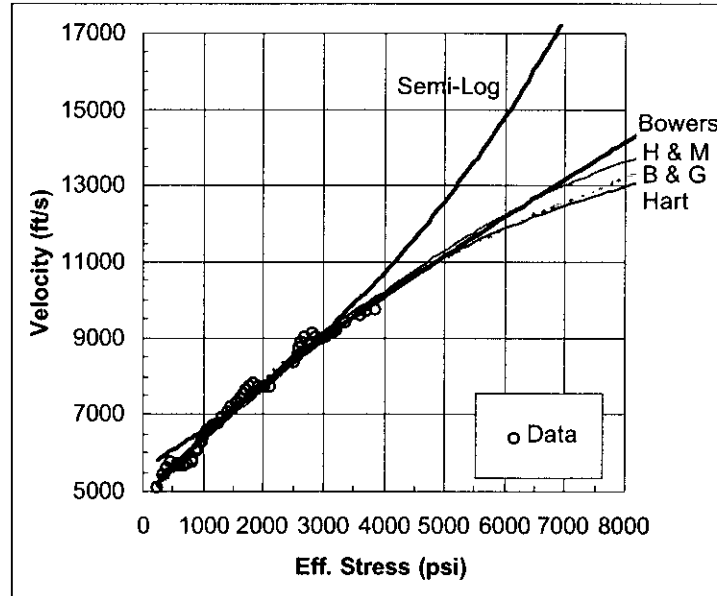


Fig. 9 - Comparison of various compaction trend equations.

Table 2 - Curve fits of the velocity effective stress data in Fig. 9. Velocities are in ft/s, interval

Method	Equation	Parameter Values
Semi-Log	$\log(\Delta t) = A - B*\sigma$	$A = 2.252$; $B = 7.04 \times 10^{-5}$
Bellotti & Giacca	$V = V_{min} + \frac{V_{max} \sigma}{A \sigma + B}$	$V_{min} = 4600$; $V_{max} = 14,925$ $A = 0.7911$; $B = 7539$
Hart, et. al.	$V = V_{max} (1 - \phi_0 e^{-\eta \sigma})^X$	$\phi_0 = 0.409$; $\eta = 2.36 \times 10^{-4}$ $V_{max} = 14,925$
Bowers	$V = V_0 + A \sigma^B$	$V_0 = 4600$; $A = 7.20$; $B = 0.80$
Hamouz & Mueller	$\log(\Delta t - \Delta t_{mx}) = A - B*\sigma$	$A = 2.120$; $B = 1.50 \times 10^{-4}$ $\Delta t_{mx} = 65$

transit time is in $\mu s/ft$, and stress is in psi.

For comparison purposes, Equations 33 and 34 were fit to the normal trend data shown in Fig. 6. The results are plotted in Fig. 9. Table 2 lists the parameters chosen for each relation. At effective stresses below 5000 psi, all relations except the semi-log curve track similar trends. Agreement between the semi-log curve and the other relations is

limited to the interval between 1000 psi and 3000 psi. Outside this range, the semi-log trend predicts lower effective stresses.

Fig. 10 shows how effective stresses computed with the Equivalent Depth method would change if a semi-log compaction trend were used instead of a power law relation such as Bowers' (1995). The change will generally be small. This is because the Equivalent Depth method uses normal trend data from *above* the top of overpressure, where both compaction trends are in relatively good agreement. Differences may not be small at very shallow depths, but with semi-log normal trends, shallow data are often ignored ("unconsolidated sediments").

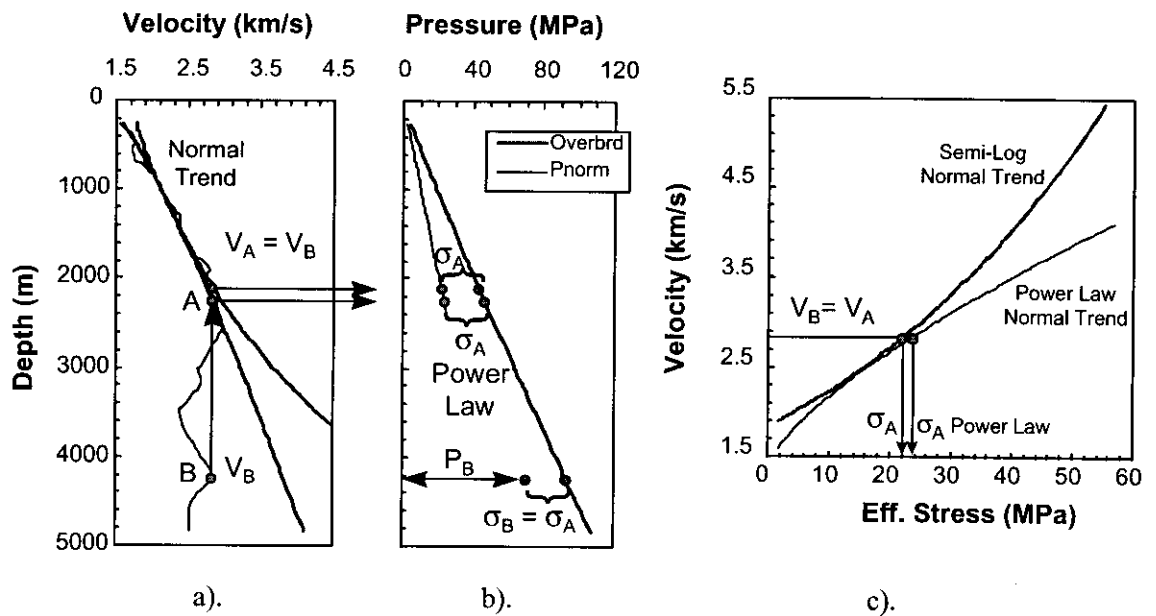


Fig. 10 - Effect of semi-log straight line vs power law sonic normal trends on the Equivalent Depth method.

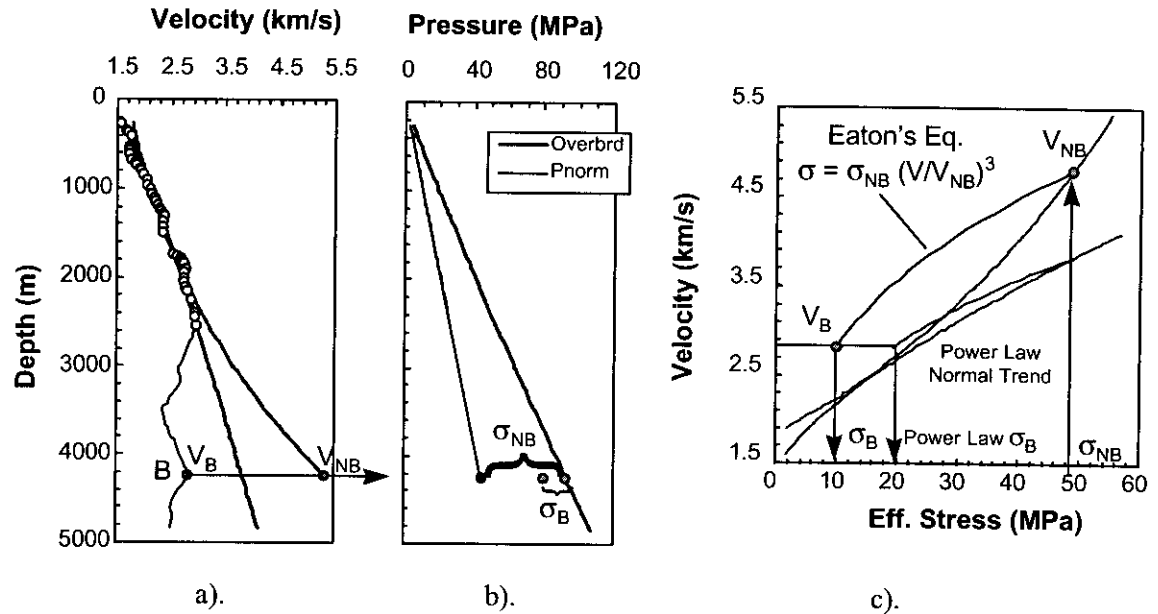


Fig. 11 - Effect of semi-log straight line vs power law sonic normal trends on Eaton's Method.

It is with horizontal methods like Eaton's that the shape of the semi-log trend starts to become important. For the effective stress at Point B in Fig. 11, the Eaton solution for a semi-log trend is half the value computed with a power law curve. This relates back to what was said earlier; the farther a compaction trend diverges from the shape of Eaton's relation, the farther the effective stress will diverge from the "true" compaction trend.

People have been successfully applying Eaton's method with semi-log normal trends since the method was first published almost 25 years ago. Consequently, there must be cases where the effective stresses in overpressured zones really do diverge from the main compaction trend. In fact, the well in Fig. 7 is an example of this.

Reversal zones are an indication of potentially high overpressures, and when such overpressures occur, the reversal data will usually diverge from the main compaction trend on the effective stress plot (Bowers, 1995). However, not all reversal zones have ultra-high pore pressure. Reversal data sometimes track the same effective stress trend as lower pressured and normally pressured intervals. All of the pore pressure estimation methods classified as "Other" attempt to account for cases where high pressure and lower pressure data track different trends.

As has been discussed, semi-log normal trends force effective stresses computed in overpressure to *always* diverge from the main compaction trend, whether you want them to or not. And the amount of divergence will increase with distance below the top of overpressure. In areas like the deepwater Gulf of Mexico, where the top of overpressure can begin near the mudline, semi-log normal trends can cause deep pore pressures to be significantly overestimated. One way to compensate for this is to use multiple semi-log trend lines, with the slope of each segment adjusted to keep the pore pressures reasonable. The other alternative is to use a curved trend line like one of those listed in Eqs. 34.

The drawback with a curve trend line is that they will typically underestimate pore pressures in high pressure reversal zones. This can be compensated for by increasing the Eaton exponent. Fig. 12 shows the effect of using an exponent of 5.5 with a power law normal trend. The effective stress at Point B is nearly identical to that calculated in Fig. 11 with a semi-log trend line.

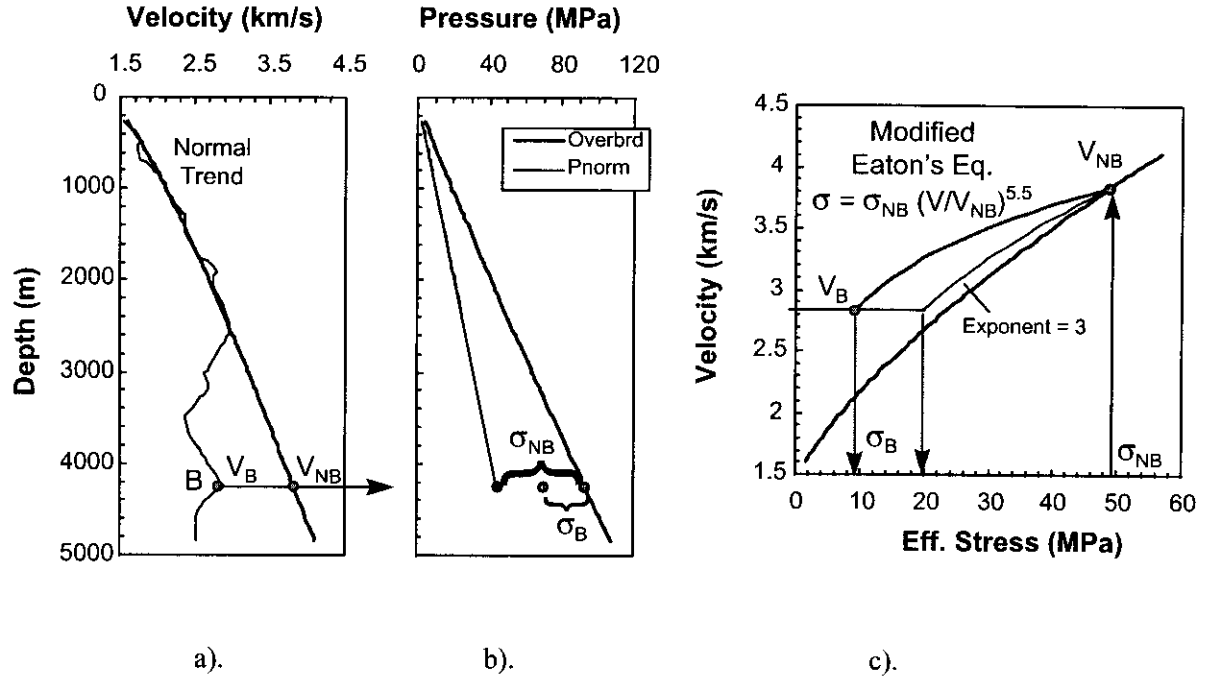


Fig. 12 - "Modified" Eaton method.

Resistivity Compaction Trends

The normal trend for resistivity is also typically assumed to be a semi-log straight line of the form:

$$\log(R) = A + B \cdot \text{Depth}; \quad R = a 10^{B \cdot \text{Depth}} \quad (35)$$

or in terms of effective stress,

$$\log(R) = A + B \cdot \sigma; \quad R = a 10^{B \cdot \sigma} \quad (36)$$

Foster & Whalen (1966) discussed how Athy's porosity-effective stress relation (Eq. 16) and Archies' formation factor equation $F = R/R_w = a \phi^{-m}$, could be combined to derive a semi-log relation of the form:

$$\log(F) = A + B \cdot \sigma; \quad F = a 10^{B \cdot \sigma} \quad (37)$$

Eq. 37 corresponds to the following resistivity-effective stress relation:

$$\log(R) = \log(R_w) + A + B \cdot \sigma; \quad R = R_w a 10^{B \cdot \sigma} \quad (38)$$

Eq. 38 indicates that the normal trend line for resistivity will only satisfy a semi-log relation if R_w remains constant. Curvature in the $\log(R_w)$ -depth profile will introduce curvature in the $\log(R_N)$ trend line.

In wells where the top of overpressure comes in deep, Eaton's method may only have to be applied over a relatively short distance. Temperature and salinity changes between the top of overpressure and the TD of the well may be small. Consequently, a semi-log normal trend drawn through the last few hundred feet of normally pressured data may be sufficient. However, when the top of overpressure comes in shallow, changes in the R_w profile may make it difficult to find a suitable normal trend.

Ideally, both salinity and temperature changes should be accounted for. At the very least, if bottomhole temperature data are available, one of the following equations can be used to compensate for temperature changes (Traugott, 1997):

$$\text{Arps Relation: } R_{\text{ref}} = R \frac{(T+6.77)}{(T_{\text{ref}}+6.77)} \quad (39)$$

$$\text{Exxon Relation: } R_{\text{ref}} = R \frac{(T-6)}{(T_{\text{ref}}-6)} \quad (40)$$

where R and T are the actual resistivity and temperature measurements, and R_{ref} is what the resistivity would be at the reference temperature T_{ref} . Fig. 13 compares raw and temperature-compensated resistivity data calculated from Eqs. 39 and 40. It can be seen that it does not really matter whether Eq. 39 or 40 is used for temperature compensation. Both make it much easier to identify a normal trend line.

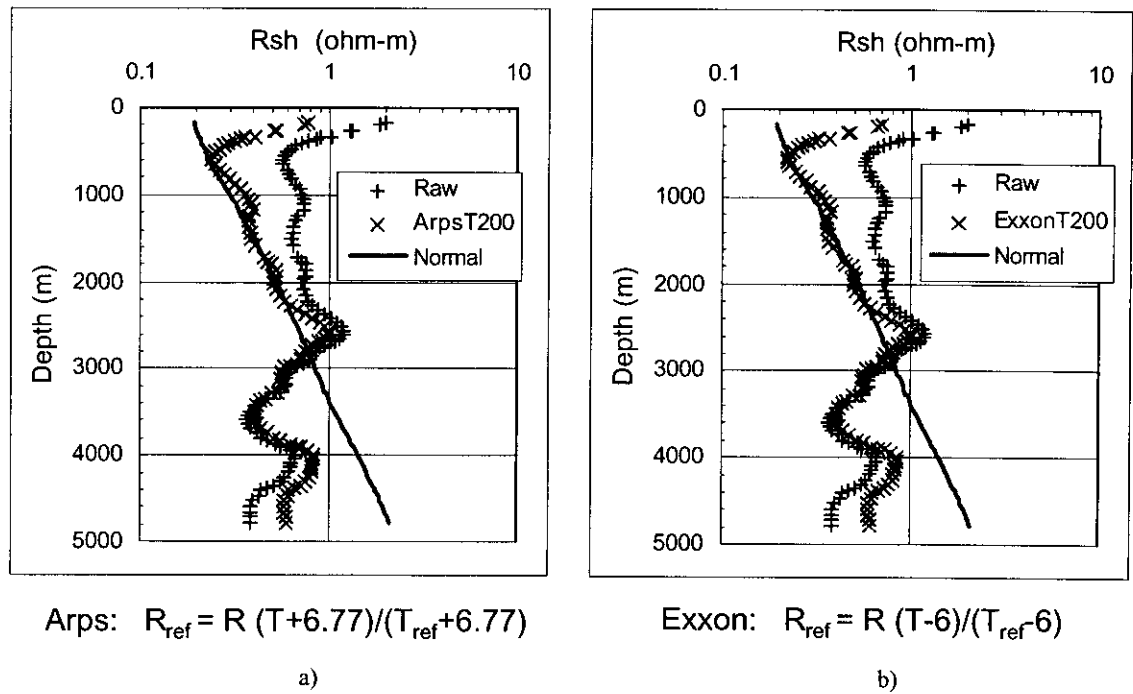


Fig. 13 - Temperature-compensated resistivity.

4.2 Sonic

4.2.1 Weakley

Weakley (1989, 1991) discussed strategies for calibrating Eaton's velocity/interval transit time equation to known pore pressures. In his 1989 paper, Weakley did so by rotating and shifting a semi-log normal trend line below the top of overpressure. From Eq. 27, it can be seen that increasing the normal trend velocity will decrease the effective stress, and therefore increase the pore pressure estimate. Decreasing the normal trend velocity will have the opposite effect. Continuity between the "normal trends" above and below the top of overpressure was not a requirement. As a result, this approach could lead to some pretty bizarre-looking normal trends.

Weakley presented a revised procedure in 1991, comprised of the following steps:

The interval transit time-depth plot is divided into lithological sections, and a representative line segment is drawn for the velocity trend within each section.

When a velocity jump occurs at the interface between adjacent line segments, the deeper segment is shifted until the jump is eliminated. The net result is a continuous velocity profile.

A semi-log normal trend line is drawn through intervals estimated to be in normal pressure.

The Eaton exponent is adjusted to match known pore pressures below the top of overpressure.

As discussed previously, increasing the Eaton exponent above 3 will increase the resulting pore pressure estimates, and vice-versa. Weakley (1991) provided the following formula for calculating the Eaton exponent necessary to match a particular pore pressure:

$$N = \frac{\log\left(\frac{OB-P}{OB-P_n}\right)}{\log\left(\frac{V}{V_n}\right)} \quad (41)$$

where N is the Eaton exponent, OB is the overburden stress, P is the known pore pressure, V is the velocity at the depth where P is specified, and P_N and V_N are the normal trend values for pore pressure and velocity at the depth where P is specified. OB, P, and P_N can be expressed in any units, including pressure gradient and equivalent mud weight.

4.3 Resistivity

4.3.1 Rasmus & Gray Stephens

Rasmus & Gray Stephens (1991) incorporate all porosity-related MWD/LWD measurements to develop progressively refined estimates of porosity, clay/matrix volumes, and effective stress. These quantities are related to the MWD/LWD measurements through a series of response equations. As each MWD/LWD sensor passes the point of interest, the new data and its response equation are factored into the solutions. An optimization procedure searches for the best fit of the currently active response equations.

Rasmus & Gray Stephens (1991) present response equations for torque, penetration rate, resistivity, gamma ray, bulk density, neutron porosity, and sonic velocity. Their method divides porosity into two parts: the porosity for normal pressure, and the excess porosity due to overpressure. Porosity in normal pressure is assumed to only be a function of clay volume, not effective stress (Rasmus, 1993). Consequently, if clay volume remains constant, their normal trend curves for porosity and resistivity are vertical lines (depth plotted vertically).

Full application of this approach would be difficult without specially designed software (Rasmus & Gray Stephens use Schlumberger's GLOBAL™ technique). Consequently, this discussion will only consider pore pressure estimation from resistivity.

Porosity Calculation

A modified version of the Simandoux equation (Serra, 1986) for shaly sands is used:

$$\phi - \phi_N = \left(\frac{1}{R} - \frac{V_{cl}}{R_{cl}} \right)^{1/m} \quad (42)$$

where ϕ is porosity, ϕ_N is the normal trend porosity at the depth of interest, R is the measured resistivity, V_{cl} is clay volume, and R_{cl} is clay resistivity. The difference $\phi - \phi_N$ is termed the *overpressure porosity*. For normal pressure, $\phi = \phi_N$, and $R = R_{cl}/V_{cl}$, which, as previously discussed, implies the porosity and resistivity normal trends depend only upon clay content.

Porosity Calculation

The effective stress is calculated from the following equation:

$$\sigma = \sigma_N 10^{-b(\phi - \phi_n)} \quad (43)$$

where σ_N is the effective stress for normal pressure at the depth of interest: It is because σ_N appears in the effective stress relation that this approach is classified as a horizontal method.

5 Other Effective Stress Methods

“Other” effective stress methods allow for cases like Fig. 7, where normally pressured and overpressured formations do not follow the same, unique relation for compaction as a function of effective stress.

5.1 Sonic

5.1.1 Bowers

It is probably easiest to explain Bowers’ method (1995) by applying it graphically. It can be viewed as a “modified” Equivalent Depth method. Effective stresses are calculated at *two* points along the normal trend curve: 1) the standard equivalent depth, which would be Point A in Fig. 14, and 2) the point where the velocity curve reaches its peak value V_{max} . The effective stress at Point B is then calculated from the following equation:

$$\sigma_B = \sigma_{MAX} \left(\frac{\sigma_A}{\sigma_{MAX}} \right)^U \quad (44)$$

where σ_A is the effective stress at the equivalent depth A, σ_{MAX} is the effective stress corresponding to V_{max} , and U is a parameter calibrated with local data. For the Gulf Coast and the Gulf of Mexico, $U = 3.13$ (Bowers, 1995).

Eq. 44 would be used to calculate effective stresses wherever velocities below the top of overpressure are less than V_{max} . As can be seen in Fig. 14c, Eq. 44 places the reversal data onto a faster compaction curve, similar to what was accomplished in Fig. 12 by raising the Eaton exponent.

To avoid having to graphically solve for σ_A and σ_{MAX} , Bowers (1995) introduced an analytical relation of the form:

$$V = V_0 + A \sigma^B \quad (45)$$

where V is velocity, σ is the vertical effective stress, and V_0 , A and B are calibration parameters.

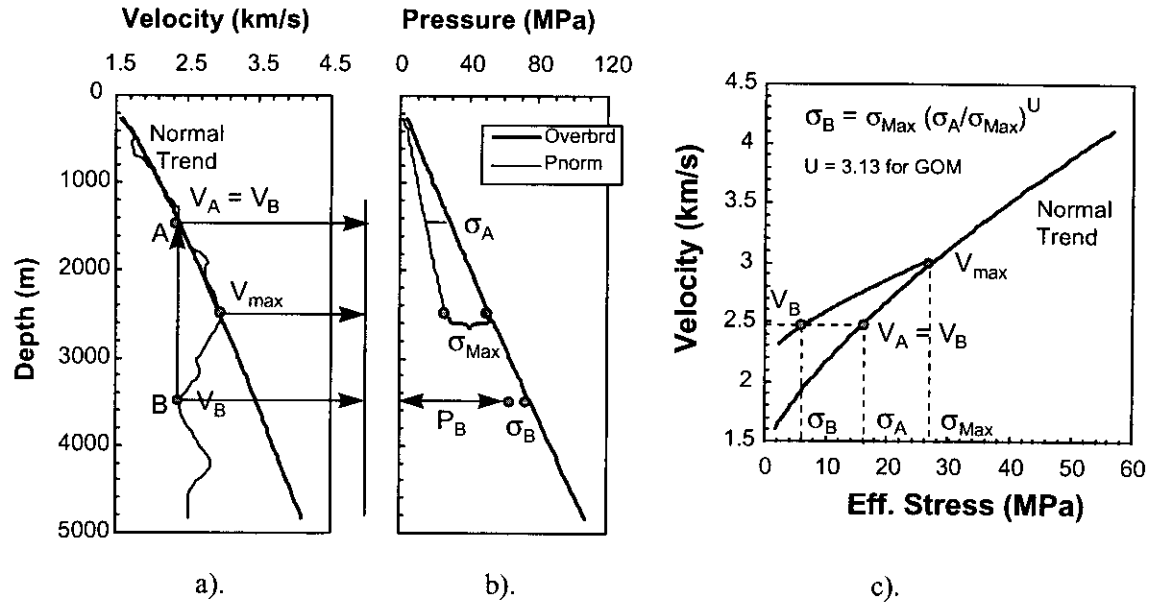


Fig. 14 - Bowers' (1995) pore pressure estimation method.

5.1.2 Wilhelm

Wilhelm's method (1998) is based upon the idea that diagenetic changes are an important part of the compaction process. As a formation is buried, it is assumed that compaction does not progress along any single trend line. Rather, compaction continually crosses from one trend line to the next as diagenesis evolves. Cases like Fig. 7, in which velocity reversal data diverge from the main compaction trend, are attributed to diagenetic differences. To account for these effects, Wilhelm makes use of a velocity-porosity-effective stress-temperature-CEC (cation exchange capacity) relation.

Calibration of the model requires temperature and CEC data. Temperature is obtained from available well data. The CEC profile is not based upon measured data. Rather it is chosen to align predicted pore pressures with known pressure data. No details of the model have ever been published. The general "flavor" of the model is summarized in Fig. 15, which was downloaded from Wilhelm's website.

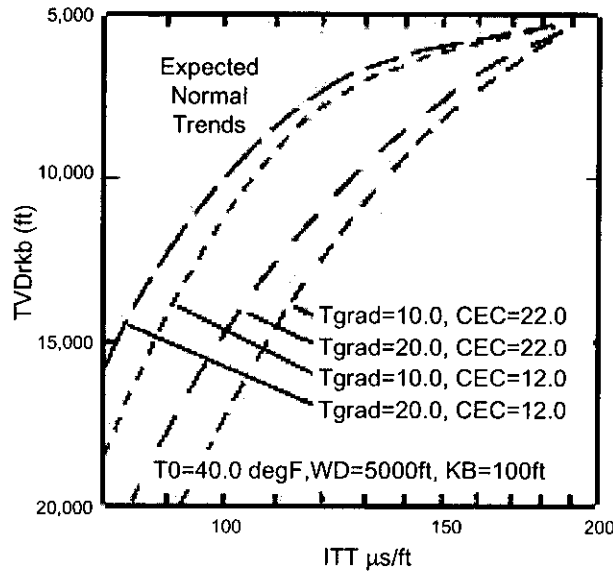


Fig. 15 - Wilhelm's (1998) pore pressure estimation method.

5.2 Resistivity

5.2.1 Holbrook

Holbrook's approach (1987, 1995) estimates pore pressures in sand, shale, limestone, and any combination of the two. Porosity is computed from resistivity by using shale volume to interpolate between end member Archie-type relations for clean sands, shales, and limestones. Effective stresses are obtained by using shale volume to interpolate between porosity-effective relations for different minerals. The parameters in these relations are fixed, and assumed to apply world-wide, in all geologic ages. The model is calibrated by adjusting the water resistivity profile to match known pore pressures.

Porosity Calculation

Three end-member porosity-formation factor relations are used (Fig. 16a). All converge at the point $\phi=0.44$, $F = 3.62$. The clean sand curve is the Humble equation:

$$\phi_{sd} = \left(\frac{.62}{F} \right)^{1/2.15} \quad (46)$$

The starting point for limestones is the Borai equation:

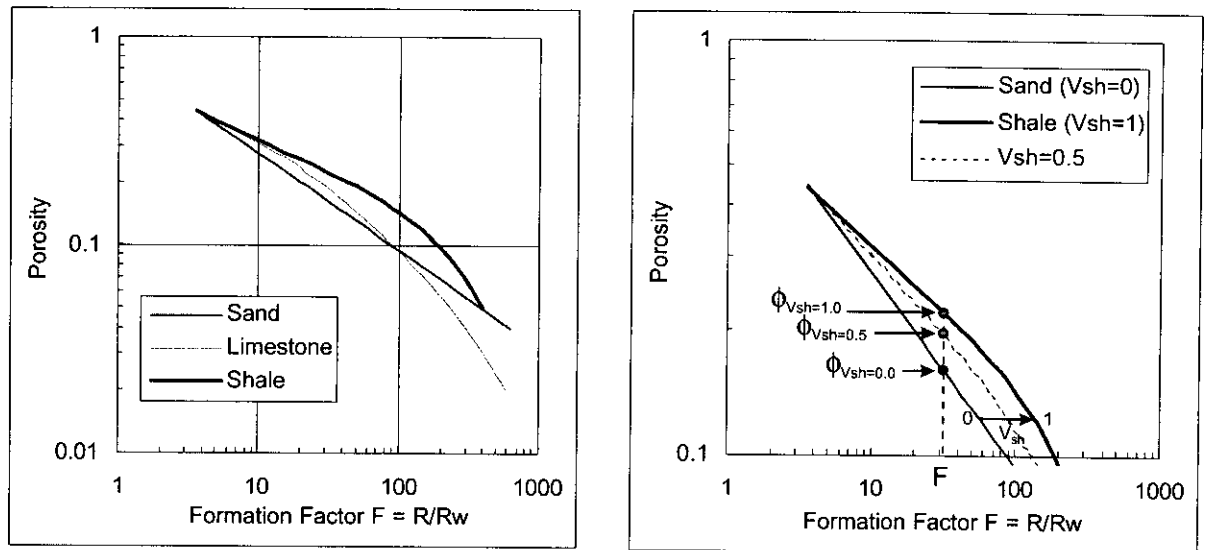
$$\phi_{ls} = \left(\frac{1}{F} \right)^{1/m} \quad (47)$$

where

$$m = 2.2 - 0.035/(\phi + .042) \quad (48)$$

This relation is used for formation factors greater than approximately 22. At lower values, a different, unspecified relation is used. No details are provided for the clean shale curve. This may mean that there is no analytical relation for shale. The points may just be stored in a look-up table.

Porosity is computed from formation factor by linearly interpolating between end member curves. Relative distance between end members is measured parallel to the formation factor axis. Fig. 16b shows shale/sand porosities corresponding to a given formation factor measurement at V_{sh} values of 0.0, 0.5, and 1.0.



a).

b).

Fig. 16 - Holbrook's (1995) porosity-formation factor relations. Fig. a- end members for "clean" shale, sand, and limestone. Fig. b- porosity calculation in a sand/shale mix with 50% shale volume.

Shale Volume Determination

The fractional volume of solids that is shale " V_{sh} " is computed from the gamma ray reading " Γ " as follows:

$$V_{sh} = [\Gamma - \Gamma_{sd}] / [\Gamma_{sh} - \Gamma_{sd}] \quad (49)$$

where Γ_{sd} and Γ_{sh} are the baseline values for "clean" sand and "pure" shale, respectively. The clean sand and pure shale baselines are statistically derived from the gamma ray measurements. Shale volume is equated to the relative distance of the gamma ray readings between the clean sand and pure shale baselines. Fig. 17 illustrates this process.

As the gamma ray data are recorded, they are sorted into sand and shale populations. Measurements less than a certain cut-off value are classified as sand, while those above another cut-off value are considered shale. Each population's mean and standard deviation are computed incrementally along the well. The clean sand baseline for each

depth interval is set two standard deviations below the mean for the sand population; the pure shale baseline is located two standard deviations above the shale population's mean.

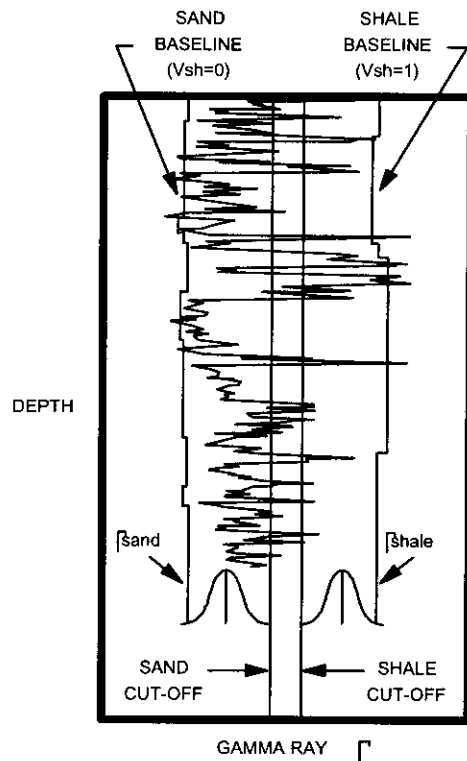


Fig. 17 - Determining "clean" sand and "pure" shale gamma ray baselines.

Porosity Calculation

End member porosity-effective stress relations are specified for five basic mineral types: 1) pure shale, 2) quartz sand, 3) limestone, 4) anhydrite, and 5) halite sands. Each have the general form:

$$\sigma = A(1 - \phi)^B \quad (50)$$

where σ is the vertical effective stress, ϕ is the porosity, and $(1-\phi)$ is referred to as *solidity*. This is the same type of equation used by Bryant (1989). Table 3 lists the A and B values for the various end members:

Mineral	A (MPa)	B
Quartz Sand	896.318	13.219
Average Shale	127.215	8.728
Limestone	82.737	13.000
Anhydrite	10.928	20.000
Halite Sand	0.586	31.909

Table 3: End-member parameters in the porosity-effective stress relation.

To compute effective stress from porosity in a sand/shale mixture, shale volume is used to linearly interpolate between the sand and shale compaction curves (see Fig. 18a). This corresponds to the following analytical relation:

$$\log(\sigma) = \log(\sigma_{sd}) - V_{sh} [\log(\sigma_{sd}) - \log(\sigma_{sh})]$$

or

$$\sigma = \sigma_{sd} (\sigma_{sh} / \sigma_{sd})^{V_{sh}} \tag{51}$$

where σ_{sd} and σ_{sh} are the effective stresses at which the solidity ($1-\phi$) intersects the clean sand, and pure shale compaction curves, respectively.

The compaction trend followed by normally pressured and moderately overpressured formations is referred to by Holbrook (1998) as the *loading limb*. For cases in which high pressure data diverge from the main compaction trend, he introduces an additional curve called the *unloading limb*, which departs from the loading limb at the estimated past maximum effective stress σ_{MAX} (Fig. 18b). This is similar to the approach developed by Bowers (1995) for velocity.

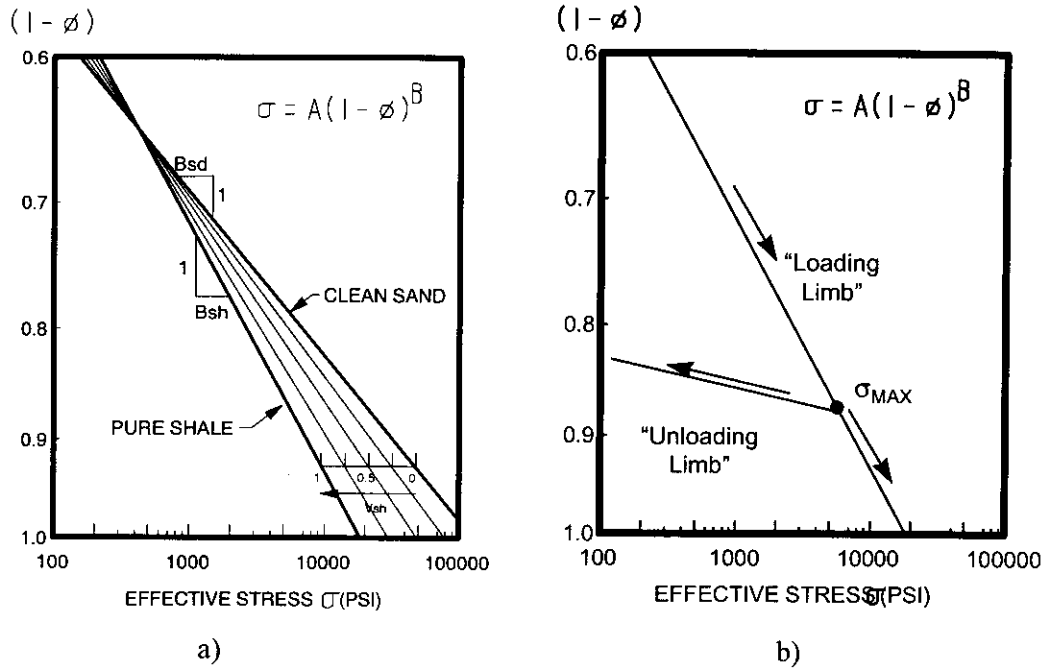


Fig. 18 - Porosity-effective stress for sand/shale mixtures.

6 References

- Alixant, J. L., and Desbrandes, R., "Explicit Pore-Pressure Evaluation: Concept and Application", *SPE Drilling Engineering*, Sept., 1991.
- Baldwin, B., and Butler, C. O., "Compaction Curves", *AAPG Bull.*, V. 69, No. 4 (April, 1985), 622-626.
- Bellotti, P., and Giacca, D., "Seismic data can detect overpressures in deep drilling", *Oil and Gas Journal*, Aug. 21, 1978.
- Bellotti, P., and Giacca, D., "Pressure evaluation improves drilling performance", *Oil and Gas Journal*, Sept. 11, 1978.
- Bowers, G. L., "Pore Pressure Estimation from Velocity Data; Accounting for Overpressure Mechanisms Besides Undercompaction", *SPE Drilling & Completions*, June, 1995.
- Bowers, G. L., "A Procedure for Determining an Appropriate Pore Pressure Estimation Strategy", AADE Industry Forum on Pressure Regimes in Sedimentary Basins and Their Prediction, September 2-4, Lake Conroe, TX, 1998.
- Bryant, T. M., "A Dual Pore Pressure Detection Technique", SPE 18714, 1989.
- Clavier, C., Coates, G., and Dumanoir, J., "Theoretical and Experimental Bases for the Dual-Water Model for Interpretation of Shaly Sands", *SPE Journal*, April, 1984.
- Eaton, B. A., "The Effect of Overburden Stress on Geopressure Prediction from Well Logs", *Journal of Petroleum Technology*, August, 1972.
- Eaton, B. A., "The Equation for Geopressure Prediction from Well Logs", SPE 5544, 1975.
- Fertl, W. H., *Abnormal Formation Pressures*, Elsevier Scientific Publishing Co., New York, 1976, pp. 210.
- Foster, J. B., and Whalen, J. E., "Estimation of formation pressures from electrical surveys-Offshore Louisiana", *Journal of Petroleum Technology*, Feb., 1966.
- Gill, J. A., "Charged Shales: Self-Induced Pore Pressures", IADC/SPE 14788, 1986.
- Ham, H. H., "A method of estimating formation pressures from Gulf Coast well logs", *Trans.-Gulf Coast Assn. Of Geol. Soc.*, 16, 185-197, 1966.
- Hamouz, M. A., and Mueller, S. L., "Some New Ideas for Well Log Pore-Pressure Prediction", SPE 13204, 1984.
- Hart, B. S., Flemings, P. B., and Deshpande, A., "Porosity and pressure: Role of compaction disequilibrium in the development of geopressures in a Gulf Coast Pleistocene Basin", *Geology*, v. 23, 1995.
- Holbrook, P. W., and Hauck, M. L., "A Petrophysical-Mechanical Math Model for Real-Time Wellsite Pore Pressure/Fracture Gradient Prediction", SPE 16666, 1987.
- Holbrook, P.W., Maggiori, D.A., and Hensley, R., "Real-Time Pore Pressure and Fracture-Pressure Determination in All Sedimentary Lithologies", *SPE Formation Evaluation*, December, 1995.

- Holbrook, P., "Method for determining regional force balanced loading and unloading pore pressure regimes and applying them in well planning and real-time drilling", AADE Industry Forum on Pressure Regimes in Sedimentary Basins and Their Prediction, September 2-4, Lake Conroe, TX, 1998.
- Hottman, C. E., and Johnson, R. K., "Estimation of Formation Pressures from Log-Derived Shale Properties", *Journal of Petroleum Technology*, August, 1965.
- Issler, D. R., "A New Approach to Shale Compaction and Stratigraphic Restoration, Beaufort-Mackenzie Basin and Mackenzie Corridor, Northern Canada", *AAPG Bulletin*, V. 76, No.8, Aug. 1992.
- Lane, R. A., and Macpherson, L. A., "A Review of Geopressure Evaluation From Well Logs - Louisiana Gulf Coast", *Journal of Petroleum Technology*, September, 1976.
- Matthews, W. R., and Kelly, J., "How to predict formation pressure and fracture gradient", *The Oil and Gas Journal*, Feb., 1967.
- Owolabi, O. O., Okpobiri, G. A., and Obomanu, I. A., "Prediction of Abnormal Pressures In The Niger Delta Basin Using Well Logs", Paper No. CIM/SPE 90-75, 1990.
- Pennebaker, E. S., "An Engineering Interpretation of Seismic Data", SPE 2165, 1968.
- Perez-Rosales, C., "Generalization of Maxwell Equation for Formation Factor", SPE 5502, 1975.
- Rasmus, J. C., and Gray Stephens, D. M. R., "Real-Time Pore-Pressure Evaluation From MWD/LWD Measurements and Drilling-Derived Formation Strength", *SPE Drilling Engineering*, December, 1991.
- Rasmus, J. C., personal communication, January, 1993.
- Scott, D., and Thomsen, L. A., "A Global Algorithm for Pore Pressure Prediction", SPE 25674, 1993.
- Serra, O., *Fundamentals of Well-Log Interpretation, 2. The Interpretation of Logging Data*, Developments in Petroleum Science, 15B, Elsevier Science Publishers, New York, 1986.
- Terzaghi, K., *Theoretical Soil Mechanics*, John Wiley & Sons, Inc., New York (1943).
- Traugott, M. "Pore/fracture pressure determinations in deep water", *Deepwater Technology*, Supplement to August, 1997 *World Oil*.
- Weakley, R. R., "Use of Surface Seismic Data to Predict Formation Pore Pressure (Sand Shale Depositional Environments)", SPE 18713, 1989.
- Weakley, R. R., "Use of Surface Seismic Data to Predict Formation Pore Pressure Worldwide", SPE 21752, 1991.
- Wilhelm, R., Franceware, L. B., and Guzman, C. E., "Seismic pressure-prediction method solves problem common in deepwater Gulf of Mexico", *Oil & Gas Journal*, Sept., 1998.
- Yoshida, C., Ikeda, S., and Eaton, B. A., "An Investigative Study of Recent Technologies for Prediction, Detection, and Evaluation of Abnormal Formation Pressure and Fracture Pressure in North and South America", IADC/SPE 36381, 1996.



KNOWLEDGE SYSTEMS, INC.

**Seismic Prediction of
Geopressure: Some Basic
Principles and the Best-Practice
Methodology**

Nader Dutta

6/28/1999

CONFIDENTIAL

*This report is provided to **DEA Project 119** Project Participants under the terms of the
DEA Project 119 Participation Agreement and is thereby subject to restrictions of
confidentiality and non-disclosure to third parties.*

DEA Project 119

Report No. 2

Corporate Offices

Knowledge Systems, Inc.
P. O. Box 1279
Stafford, Texas 77497-1279
Phone: 281-879-1400
Fax: 281-879-1499
E-mail: sales@knowsys.com

European Office

Knowledge Systems, Inc.
P.O. Box 274 Paradis
5856 BERGEN
Norway
Phone: +47 55 92 45 62
Fax: +47 55 92 45 62
E-mail: sales@knowsys.com

Please visit the Knowledge Systems' website at <http://www.knowsys.com>

Information in this document is subject to change without notice, and does not represent a commitment on the part of Knowledge Systems. The software described in this document is furnished under a license agreement or non-disclosure agreement. It is against the law to copy the software on any medium except as specifically allowed in the license or non-disclosure agreement.

© Copyright Knowledge Systems, 1989-2000. All rights reserved. *DrillWorks* is a registered trademark of Knowledge Systems, Inc. *PostScript* is a registered trademark of Adobe Systems, Inc. *Windows* is a trademark of Microsoft Corporation

Document Information

Title: Seismic Prediction of Geopressure: Some Basic Principles and the Best-Practice	
Description:	
Author(s): Nader Dutta	
Reviewer(s):	
Creation Date: 10/5/2000 9:44 AM	Last Date Modified: 10/5/2000 9:44 AM
Approved By:	Approval Date:
Will be sent to:	
Sources Used: (can be other documents used as sources)	
Project Number:	Document Number: 2000-000004

Table of Contents

1	Introduction.....	1
2	Basic Velocity Concepts	2
2.1	What is Velocity?	2
2.2	What is rock velocity?	4
2.3	What is seismic velocity?.....	7
3	Brief Review of Seismic Velocity Analysis.....	8
3.1	CMP Geometry	8
3.2	NMO.....	8
3.3	NMO in a Horizontally Stratified Earth.....	11
3.4	NMO for a Dipping Layer	12
3.5	NMO for n-Layers with Arbitrary Dips.....	13
4	Velocity Analysis	15
4.1	Procedure.....	15
4.2	Velocity Smoothing, Calibration, Resolution and Interpretation.....	20
5	Guide to Velocity Analysis for Geopressure Work.....	25
6	Examples of Applications of Seismic Velocity for Pressure Prediction.....	27
6.1	3-D Applications	28
6.2	1-D/2-D Applications	31
7	References.....	39

1 Introduction

An accurate prediction of pore pressure is critical to successful exploration and production of hydrocarbon. In deepwater, high rig rates dictate the strategy employed in any drilling campaign – again, accurate pressure prediction helps with proper casing and mud program and helps avoid down time in rig operation, most often associated with stuck-pipes and lost circulation. Before a well is drilled, estimates of pore pressures are required to plan the well. At that stage, seismic data, being the only data available, are used extensively for pressure prediction. Seismic techniques exploit the fact that a geopressured formation exhibits several of the following properties when compared with a normally pressured section at the same depth: (1) Higher porosities, (2) Lower bulk densities, (3) Lower effective stresses, (4) Higher temperatures, and (5) Lower interval velocities.

The seismic methods detect changes of interval velocities with depth, from velocity analysis of Common Depth Point (CDP) seismic data. Pennebaker (1968) was one of the first authors to describe in detail the seismic techniques to indicate depth and magnitude of abnormal pressures. Pennebaker's paper stimulated much interest throughout the industry and is still used with considerable success.

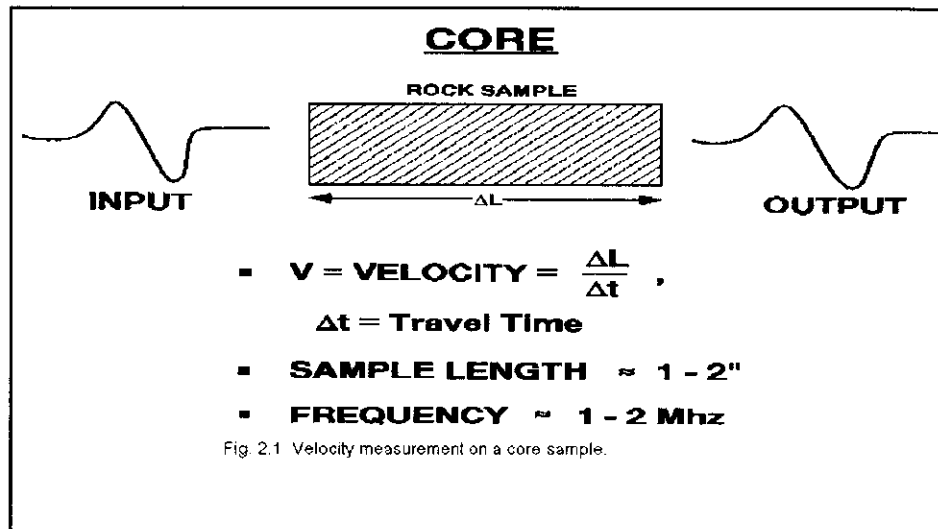
Since Pennebaker's pioneering work, many authors described how seismic velocities could be used for Geopressure analysis: Reynolds (1970), Reynolds et al (1971), Reynolds (1973), Bilgeri and Ademenio (1982), Dutta (1997). Unfortunately, the velocities have quite often been misused for pressure work, despite the caution of geophysicists that not every velocity data obtained from seismic velocity analysis could be used for this purpose. Most often the seismic velocities are obtained to produce a 'nice looking stacked section' to highlight the structural aspects of the geology. Geopressure on the other hand deals mostly with stratigraphic changes (shaly intervals, for examples, developed due to depositional changes). A routine use of stacking velocities for pressure prediction, without proper understanding of how the seismic velocities are acquired, processed, and interpreted, and their limitations, could, and has resulted in disastrous consequences.

In this report, we focus on the basics of seismic velocity analysis. This is followed by the 'best practice' methodology that has evolved over many years of this author's experience in using velocities for pressure prediction in deepwater sedimentary environment. This report is not intended for 'experienced geophysicists'- rather, those who need to use seismic velocities for pressure prediction, but are not geophysicists by training. Experienced geophysicists who have used velocities for pressure prediction, may skip over the basics and focus on the 'best practice scenario' and the examples given at the end of the report.

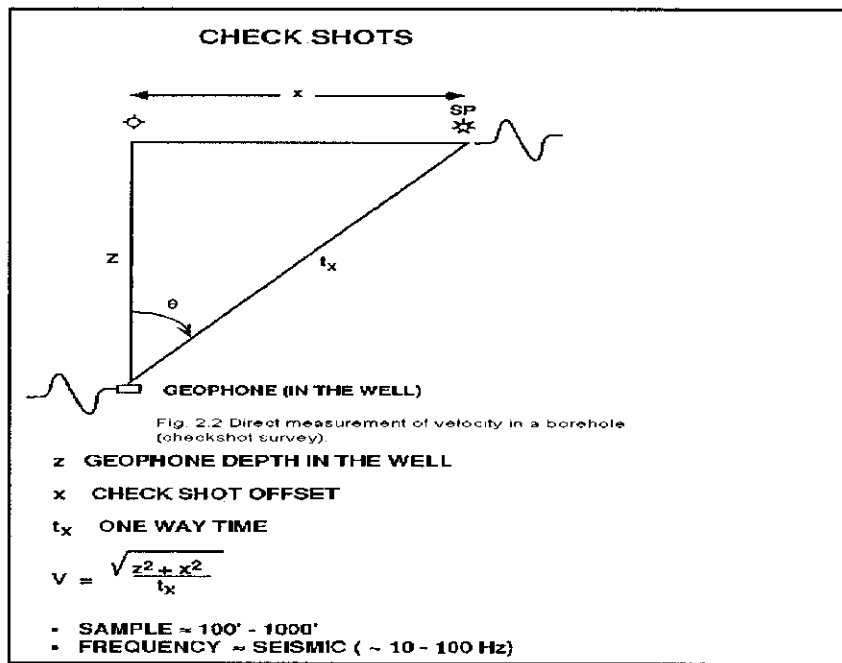
2 Basic Velocity Concepts

2.1 What is Velocity?

Velocity is a quantity that positions the drill bit on the seismic; it lets us display the traditional seismic section, usually referred in two-way time, in depth. It is also the most abused and misused quantity in geophysics. With proper care, seismic data can provide indirect estimates of true 'rock' or 'propagation' velocity (Al Chalabi, 1973). The latter is the wave propagation velocity in rocks and is related to factors such as the rock type and texture, pore shape and pore pressure, pore fluid type and composition, confining pressure and temperature. The direct way of measuring rock velocity is to carry out a non-destructive measurement using pulse propagation technique under simulated geologic conditions in laboratory, such as the one shown schematically in Fig.2.1.



Alternately, in situ measurements of rock velocity can be carried out using checkshot (Fig.2.2), or sonic log measurement (Fig.2.3).



In contrast, seismic velocities are *indirect* measurements and are usually determined with objectives other than estimating rock velocities. While the former is created to make a seismic section yield the best stack, the latter is a physical quantity related to rock and fluid properties. Thus, unless proper care is exercised in acquiring, processing.

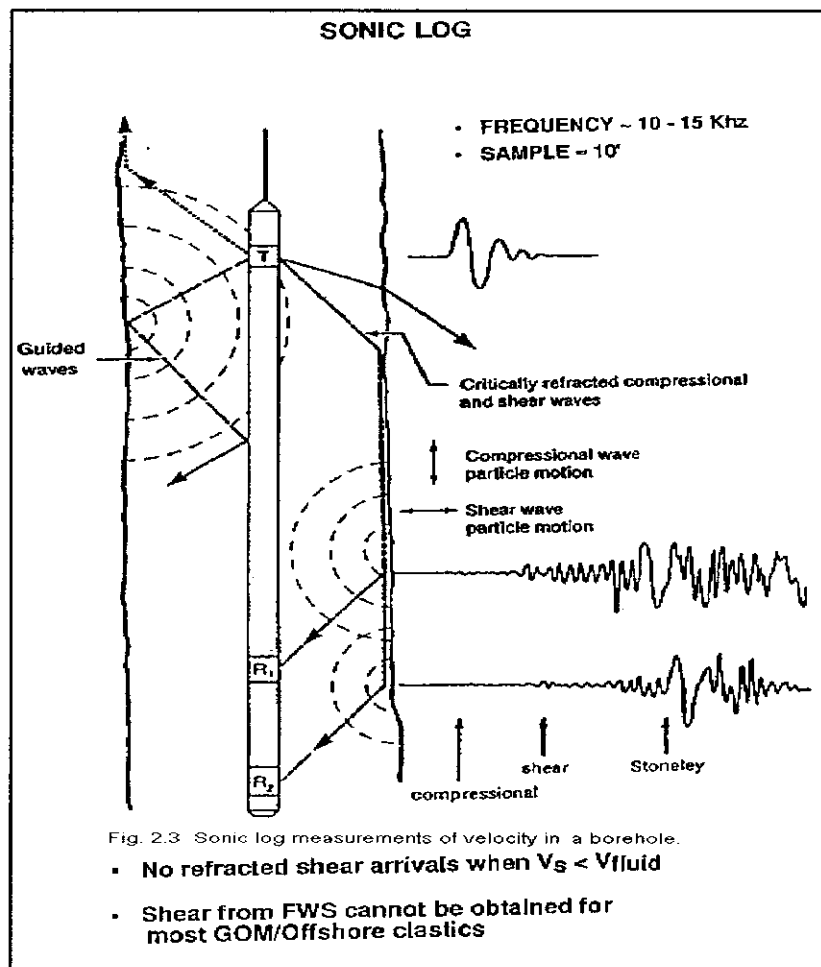


Fig. 2.3 Sonic log measurements of velocity in a borehole.

- No refracted shear arrivals when $V_s < V_{fluid}$
- Shear from FWS cannot be obtained for most GOM/Offshore clastics

Calibrating and analyzing the seismic velocity data, it may not have any relationship with rock velocity – a quantity of interest that can yield information about pore pressure. *Therefore, relating seismic velocity to rock velocity is the most critical component in the estimation of pore pressure from seismic.*

2.2 What is rock velocity?

Velocity of wave propagation in a piece of rock is called 'rock velocity'. It is not to be confused with seismic wave propagation velocity. This section is not intended to give a full description of what controls rock velocity- a quantity needed for pressure prediction. Rather, it is a reminder that rock velocity (P- and S- wave) is a complex quantity. It depends on many parameters: porosity, fluid saturation, state of stress, pore fluid type, pore and confining stress, temperature, pore fluid property, lithology, clay content and frequency of the propagating waves. Furthermore, these parameters are not independent of each other. A full description of these dependencies can be obtained from controlled laboratory measurements. In Nur and Wang (1989), the readers can find a collection of some pertinent papers that deal with this complex system. Below, we point out a few

significant features relevant to our discussions on pore pressure prediction using seismic velocities. Gross lithologies exhibit large P-wave velocity distributions (Fig.2.4).

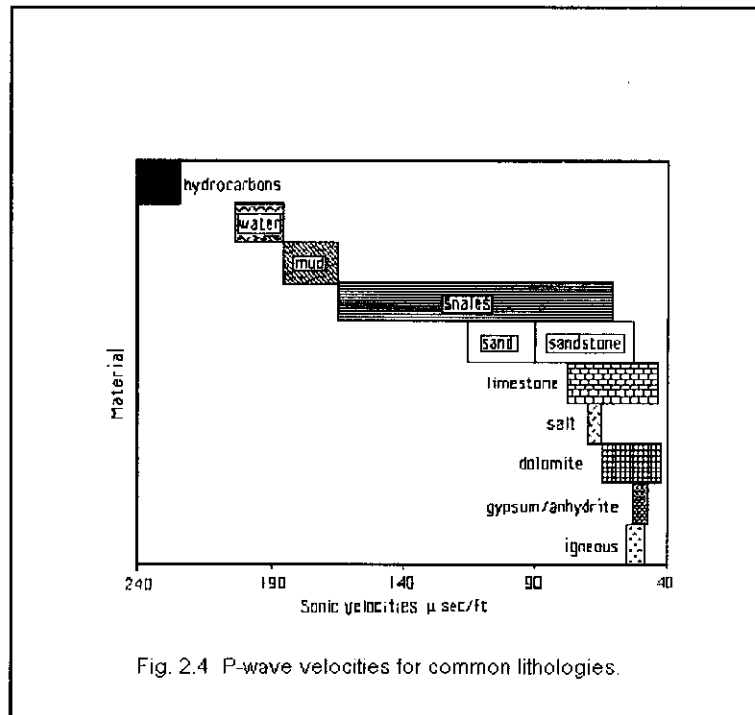


Fig. 2.4 P-wave velocities for common lithologies.

We note that:

The distributions of sandstone and shale velocities overlap considerably. In deepwater setting, for normally compacted sediments, often sand and shale velocities overlap completely. Shale densities are typically slightly higher than the corresponding sand densities.

Velocities in overpressured zones are lower than those found at hydrostatic pressures. Low velocities caused by highly pressured zones are often related to thick shale zones that have low sand occurrence (less than 10 %). This is most common in poorly consolidated, relatively young sediments (Gulf of Mexico, Tertiary).

In shallow water sediments, often sands and shales have locally identifiable velocity versus depth trends. Such trends are very useful for pressure analysis. However, in deepwater sediments, such trends are usually absent. Pressures higher than normal often happens in sediments just below the mudline. In deepwater settings, these pressured sands are known to be hazardous, and drilling through them has cost the industry an enormous sum of money. This is known as the 'shallow water sand flow problem' (SWF) and the readers are referred to a recent conference on this issue (MMS/ERCH Conference on SWF, Woodland, 1998).

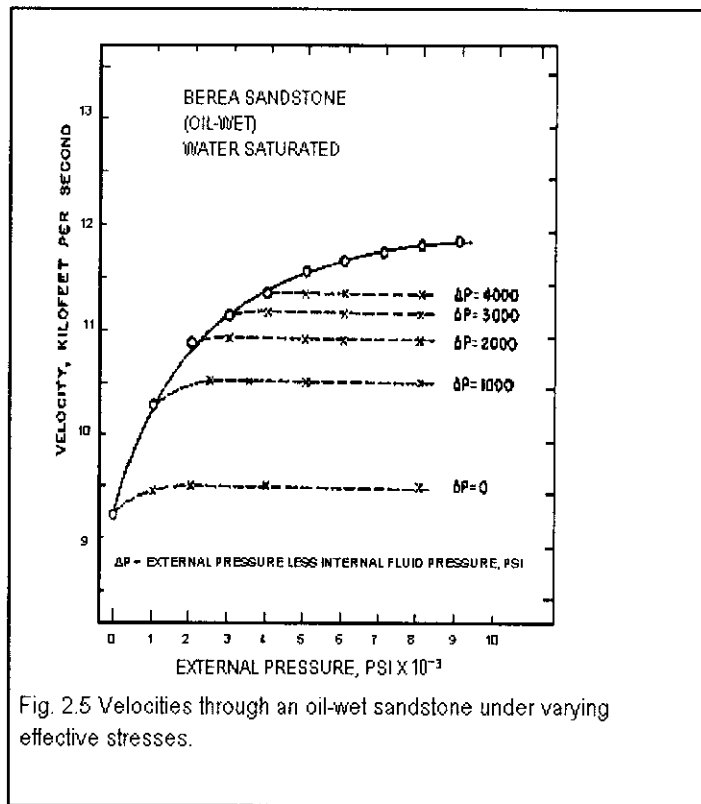


Fig. 2.5 Velocities through an oil-wet sandstone under varying effective stresses.

A typical example of the effect of the external pressure and effective pressure (defined as the difference between the external or confining pressure and pore fluid pressure) on the velocity of a Berea sandstone is shown in Fig. 2.5, taken from Wyllie et al (1957). It suggests that:

The velocity increases with increasing effective stress. The increase is at first rapid but decreases with increasing effective stress until an approximate constant terminal velocity is attained.

For zero effective stress the velocity at first increases rapidly and then slowly, and almost linearly.

For small effective pressures the behavior is very similar to that at zero effective stress. At higher differentials, the initial velocity rise is not observed.

Different samples of equal porosity from the same rock, or the same sample used repeatedly, may show a variation in measured velocity for a fixed low external pressure. However, the terminal velocity in all these cases is the same.

All of these observations, made in 1957 by Wyllie et al, are also observed in deepwater settings and are pertinent for developing a transform to relate effective stress and pore pressure to rock velocity. For applications to deepwater sediments, it should be noted that the non-linear portions of these curves for low effective stresses are the most relevant ones to higher pore pressures at deeper depths.

Although laboratory measurements have added much to our understanding of rock properties, such measurements of velocities on core samples are fraught with one

problem- that of restricted sampling! Seismic wave velocity quite often differs from those measured on small core samples. This is referred as the “up-scaling problem”- a discussion of which is beyond the scope of the present work. There is another issue with this type of measurement - frequency. How can one reconcile data from ultrasonic measurements with those from seismic frequency bandwidth (10-100 Hz)? Thus, proper scaling and calibration of velocities are critical to its success for pressure prediction.

In Fig. 2.2 we showed the schematic of checkshot survey- a way to obtain velocity data from direct measurements in a borehole. In this type of measurement, both the sampling and the frequency problems are solved - the measured intervals are of the order of 100-1000 ft and conventional seismic sources employ frequency bandwidths of 10-100 Hz. Another type of rock velocity data is obtained from borehole measurements- sonic logs. They operate at 5-10 KHz frequency range. The measurements are carried out using refraction principle as shown in Fig. 2.3. Here the sampling intervals are of the order of several feet. Velocity information obtained from sonic logs are most frequently used for pressure analysis, especially because these measurements are the only one that can yield a wealth of data on shales under in situ conditions.

2.3 What is seismic velocity?

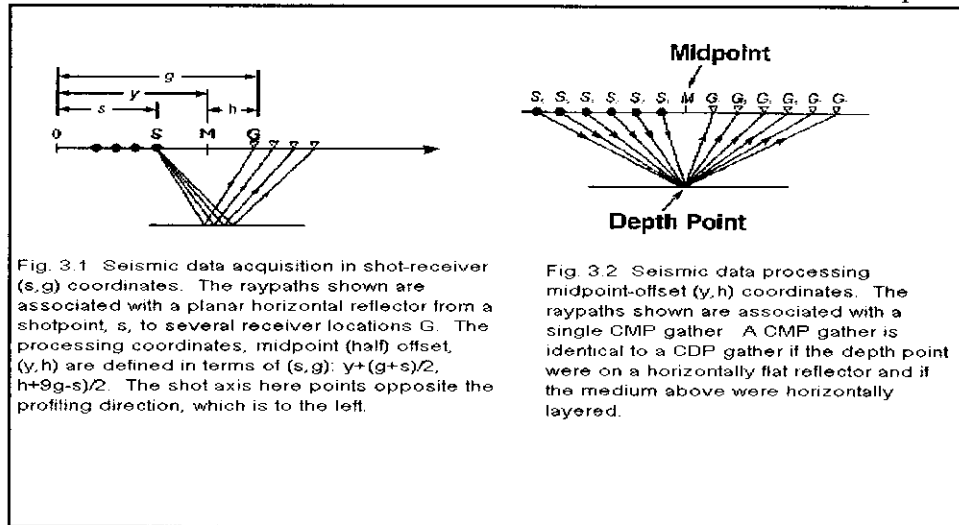
The nomenclature for velocity used by seismologists are confusing at best. These include *interval and apparent velocity, average and root-mean-squared (RMS) velocities, instantaneous, phase and group velocity, normal-moveout (NMO) velocity, stacking and migration velocity!* As stated earlier, the velocity that can be obtained from the seismic data is the stacking velocity. For flat-layered earth model, the stacking velocity is related to the NMO velocity, which in turn is related to RMS, average and interval velocity. For rock property and pore pressure analysis, we need interval velocity, which is the average velocity between two seismic intervals (could be reflectors). These relationships are explained below (based largely on Yilmaz, 1987; Al-Chalabi, 1973; Taner and Koehler, 1969; Hubral and Krey, 1980).

3 Brief Review of Seismic Velocity Analysis

3.1 CMP Geometry

The Common Mid Point (CMP) technique of recording and processing of seismic data was patented in the 1950's. The technique uses redundant recording to improve the S/N ratio of seismic data – the so-called stacking process.

In Fig. 3.1, we show the coordinates in which the seismic data are acquired: shot -

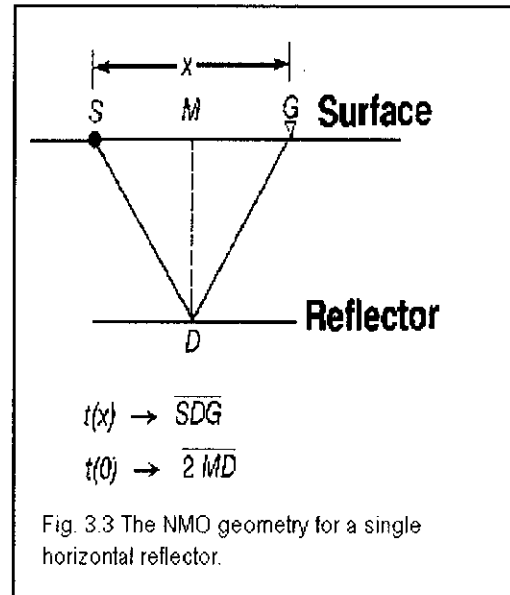


receiver (s, g)

co-ordinates. The raypaths shown are appropriate for recording in a flat-layered earth, from a shotpoint S to several receiver locations denoted by G. In Fig 3.2, we show the CMP geometry. Seismic data processing is done in midpoint-offset co-ordinates (y,h). The raypaths shown are associated with a single CMP gather. This is identical to a Common Depth Point (CDP) gather, if the layers are horizontal and flat. Velocity estimation requires the data recorded at nonzero off sets provided by CMP recording. With estimated velocities, corrections for non-zero offsets are made and data compressed, in midpoint-offset co-ordinates, to a stacked section. Quite frequently, two more processing steps are followed: Deconvolution and Migration. Simply put, the Deconvolution process acts on the seismic data along the time axis and it sharpens the temporal resolution of the data. On the other hand, the Migration process moves dipping events to their true subsurface positions and collapses diffraction, thereby increasing lateral resolution.

3.2 NMO

Fig. 3.3 shows a simple geometry of reflection from a single flat layer. Let x be the distance between the source, S and receiver, G (offset), v the velocity of the medium,



assumed constant, above the first reflecting surface, $t(0)$ twice the traveltime along the vertical path MD and $t(x)$ the traveltime for the ray along the path SDG. Then, it can be shown easily using the Pythagorean theorem that,

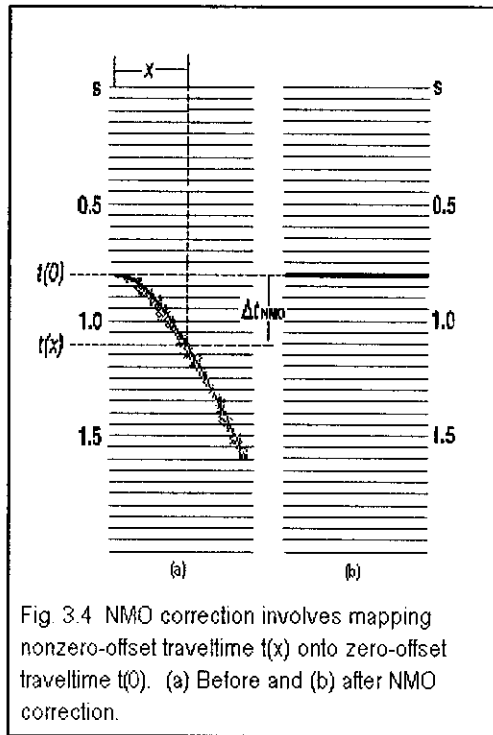
$$t^2(x) = t^2(0) + x^2/v^2 \quad (1)$$

Equation (1) for the traveltime describes a hyperbola in the plane of two-way time versus offset – a very fundamental relationship. We note that for the geometry depicted in Fig.3.3 the CMP and CDP are identical, since the layers are flat and horizontal.

From Eq. (1), the NMO correction is given by the difference between the two traveltimes, $t(x)$ and $t(0)$:

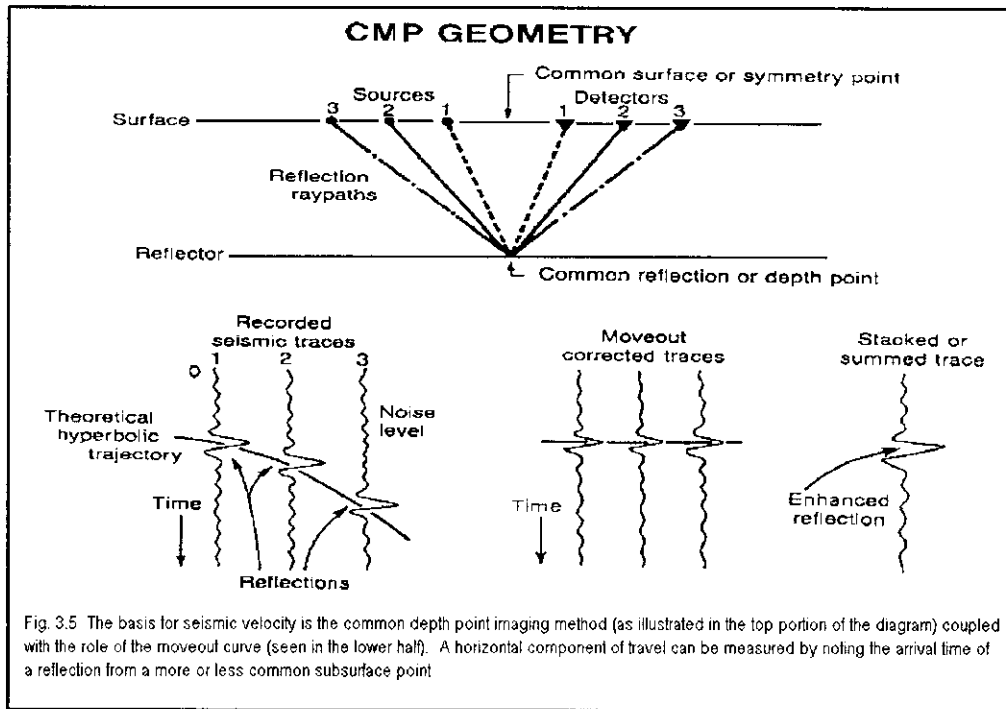
$$\begin{aligned}
 t_{\text{NMO}} &= t(x) - t(0) \quad (2) \\
 &= t(0) \{ [1 + (x/v_{\text{NMO}} t(0))^2]^{1/2} - 1 \} .
 \end{aligned}$$

Once the NMO velocity is estimated, the traveltimes can be corrected by using above equation, as shown in Fig. 3.4.



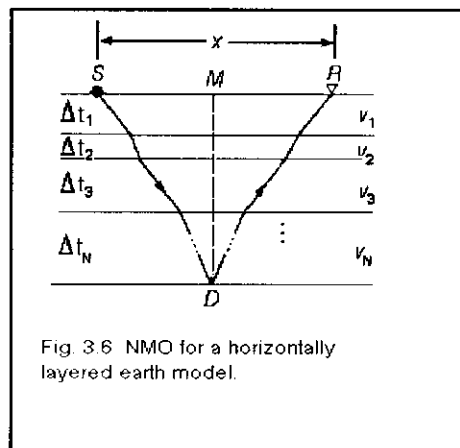
Traces in the NMO-corrected gather then are summed to obtain a stack trace at the particular CMP location. This is shown in graphical form in Fig. 3.5 for three offsets.

The objective of the stacking is to improve the S/N ratio of seismic data. Seismic data must have NMO correction applied before stacking is done. This correction results in enhancement of signal and cancellation of noise by the stacking process. This process is repeated for all the CMP gathers and traveltimes to produce a stacked seismic section. We note that the resulting velocity function - the NMO or the stacking velocity function - is "that velocity which maximizes signal in the CMP or-CDP stacking process". This has some severe consequences, and imposes limitations on the velocity analysis, and if not recognized and reconciled, can limit its use for pressure analysis. Some of these are discussed below.



3.3 NMO in a Horizontally Stratified Earth

The NMO equation for the single flat layer becomes considerably complex for n-horizontally-stratified layers. Tanner and Koehler (1969) derived the following travelttime equation for this system (Fig. 3.6):



$$t^2(x) = c_0 + c_1x^2 + c_2x^4 + \dots \quad (3)$$

where

$$c_0 = t^2(0), \quad (4)$$

and

$$c_1 = 1/V_{RMS}^2, \quad (5)$$

and c_2, c_3 , etc. are complicated functions that depend on layer thickness and interval velocities, as described in Fig. 3.6. The rms velocity V_{RMS} down to the point D is defined as

$$V_{RMS}^2 = t(0)^{-1} \sum_{i=1}^N v_i^2 t_i(0), \quad (6)$$

where t_i is the vertical two-way time through the i -th layer and

$$t(0) = \sum_{i=1}^N t_i. \quad (7)$$

A further approximation to the travelttime equation given in Eq.(3) can be realized by assuming that the offset is small compared to depth ("small-spread approximation"). In this case, the series in Eq.(3) can be truncated as follows:

$$t^2(x) = t^2(0) + x^2/V_{RMS}^2. \quad (8)$$

When we compare Eq.(1) with Eq.(8), we realize that the velocity required for NMO correction for a horizontally stratified medium is equal to the rms velocity, provided the small-spread approximation is made.

3.4 NMO for a Dipping Layer

In reality, horizontal layers are rarely encountered. The situation is much more complex when layers are not horizontal. Figure 3.7 shows the CMP and CDP geometry of a single dipping layer. They are not the same in this case. M is the midpoint of the source to receiver distance, SG . The common depth point, D , is not below M , but it is D' . The zero-offset time is the two-way time along the raypath from M to D' (and not D). The travelttime, $t(x)$, along the path SDG can be written as:

$$t^2(x) = t^2(0) + x^2 \cos^2 \theta / v^2, \quad (9)$$

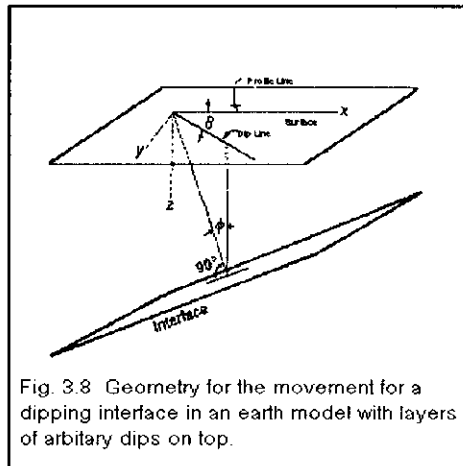
which is, again, the equation of a hyperbola. However, the NMO velocity is now given by the medium velocity divided by the cosine of the dip angle:

$$V_{NMO} = v/\cos \theta \quad (10)$$

Proper stacking of a dipping event requires a velocity that is greater than the velocity of the medium above the reflector, since $\cos \theta$ is less than or equal to 1. This clearly suggests that a horizontal layer with a high velocity can yield the same moveout as a dipping layer with a low velocity, and hence the same stacks, in small-spread

approximation. This ambiguity can result in a different stacking velocity function, for seemingly similar looking stacks!

3.5 NMO for n-Layers with Arbitrary Dips

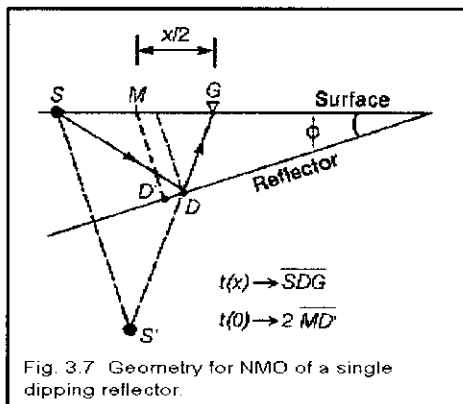


The NMO correction for a stack of layers, all with different dips, is fairly complex. We refer to the work by Hubral and Krey (1980). The basic geometry is given in Fig. 3.8. The objective is to compute the travelttime equation for a raypath along S, the source point, to a depth point, D, and then back up to the receiver location, G, as shown by the arrows (see Fig. 3.7). The midpoint of the path is M. However, the CMP ray from M hits the dipping interface at normal incidence at D'. The relevant travelttime equation is:

$$t^2(x) = t^2(0) + x^2/v_{NMO}^2 + \text{higher order terms}, \tag{11}$$

where the NMO velocity is

$$v_{NMO}^2 = [1/t(0)\cos^2\beta_0] \sum_{i=1}^N v_i^2 \Delta t_i(0) \prod_{k=1}^{i-1} [\cos^2\alpha_k / \cos^2\beta_k] . \tag{12}$$



It should be noted that for a single dipping layer, Eq.(12) reduces to Eq.(10). Moreover, for a horizontally layered earth, Eq.(12) reduces to Eq.(6) as it must. As long as dips are gentle and the spread is small, the traveltime equation is approximately represented by a hyperbola, Eq.(8), and the velocity required for NMO correction is approximately the rms velocity function of Eq. (6).

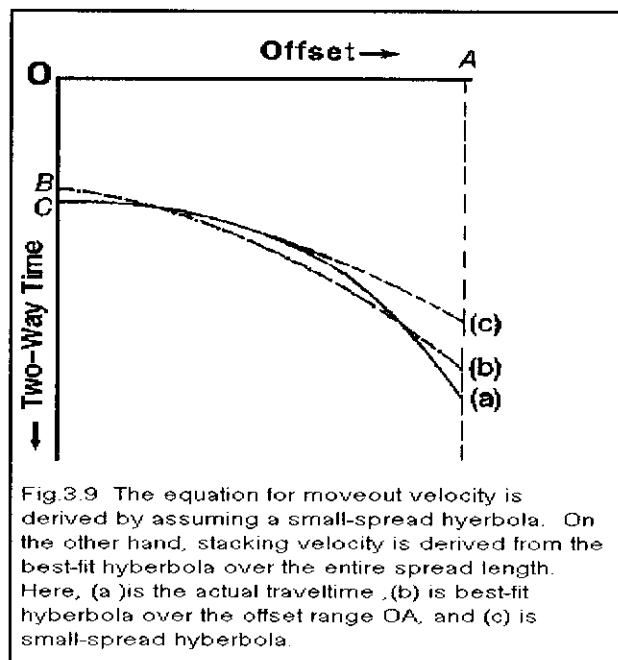
After making the small-spread and small dip approximation, the NMO is hyperbolic and is given by

$$t^2(x) = t^2(0) + x^2/v_{NMO}^2 \quad (13)$$

The hyperbolic moveout velocity should be distinguished from the stacking velocity that optimally allows stacking of traces in a CMP gather. The hyperbolic form is used to define the best stacking path:

$$t_{st}^2(x) = t_{st}^2(0) + x^2/v_{st}^2, \quad (14)$$

where v_{st} is the velocity that allows the best fit of the traveltime curve on a CMP gather to a hyperbola within the spread length. This hyperbola is not necessarily the small-spread hyperbola implied by Eq.(13). The differences can be significant, especially for a large spread commonly used these days. These differences are shown in Fig.3.9. The difference between the stacking velocity, v_{st} and NMO velocity, v_{NMO} , is called “spread-length bias” and should be accounted in the velocity analysis.



4 Velocity Analysis

4.1 Procedure

Equation (14) contains the basis for velocity analysis for a CMP gather. This equation describes a line on the t^2 versus x^2 plane. The slope of the line is $1/v_{st}^2$ and the intercept value at $x=0$ is $t(0)$. In practice a least-square method is used to do the curve fitting. A real data example is shown in Fig. 4.1.

Velocities estimated from the $t^2 - x^2$ analysis are shown by triangles on the velocity spectrum. The actual velocity picks are also shown on the velocity spectrum, and the

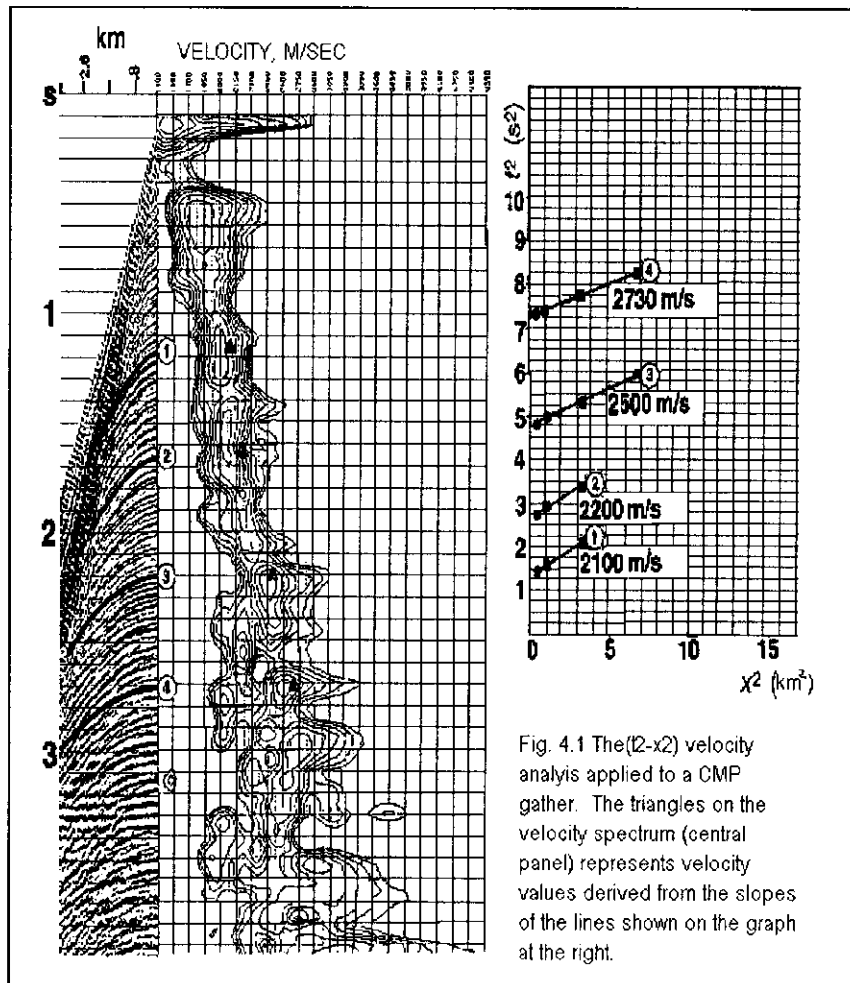
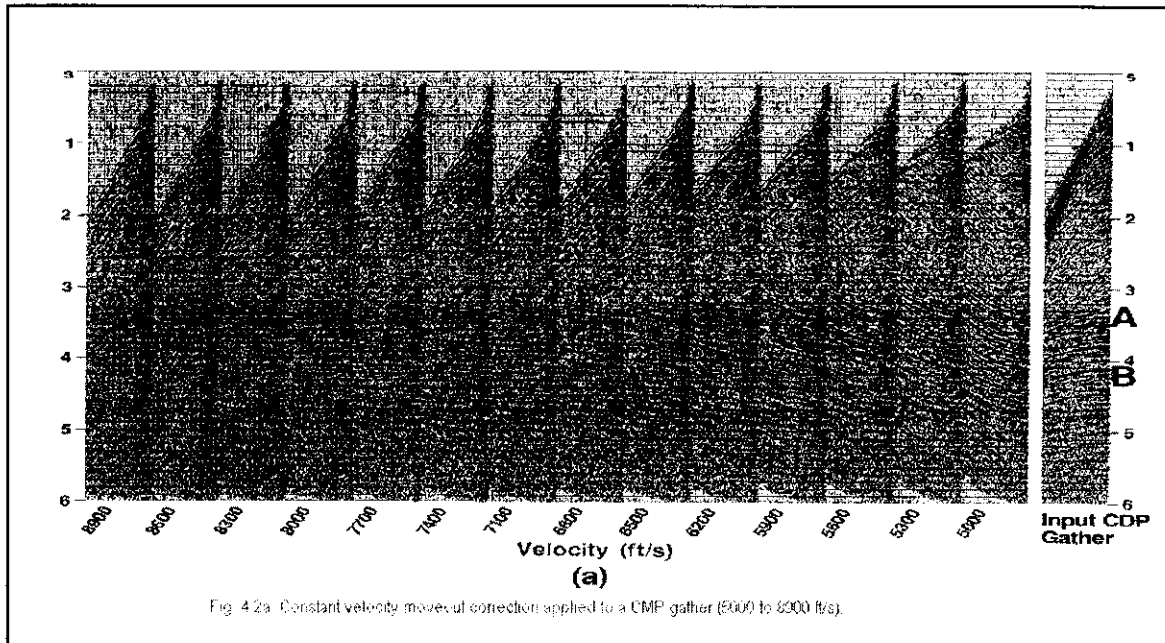
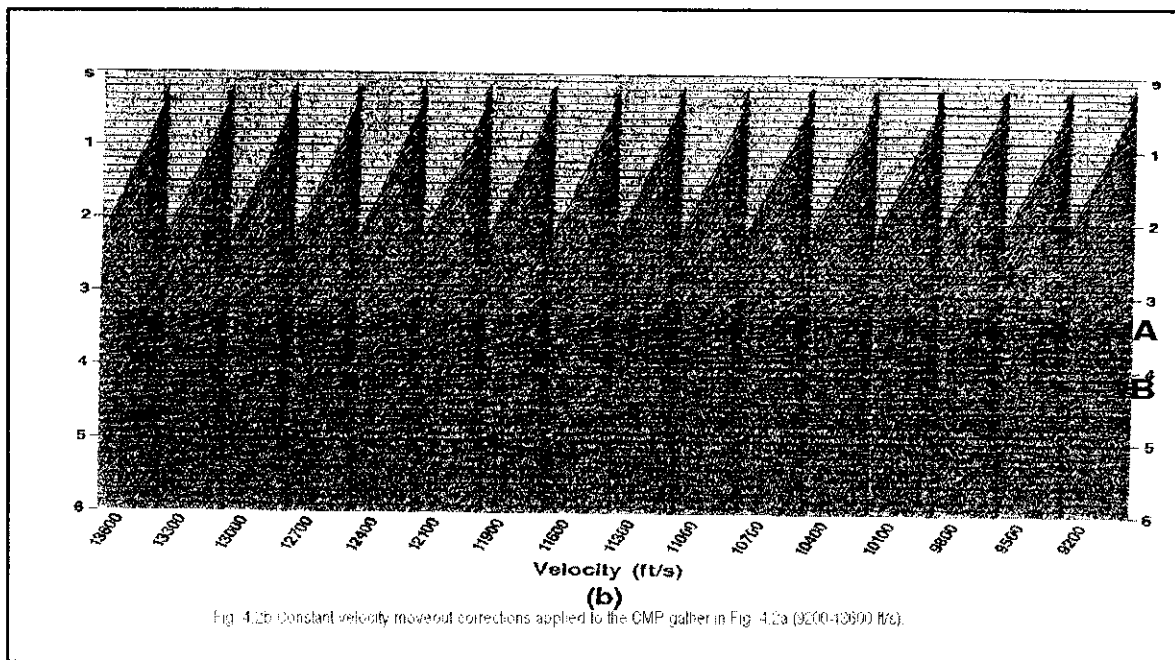


Fig. 4.1 The (t^2-x^2) velocity analysis applied to a CMP gather. The triangles on the velocity spectrum (central panel) represents velocity values derived from the slopes of the lines shown on the graph at the right.

agreement between the two is good. An alternative method to carry out velocity analysis is shown in Fig. 4.2a.



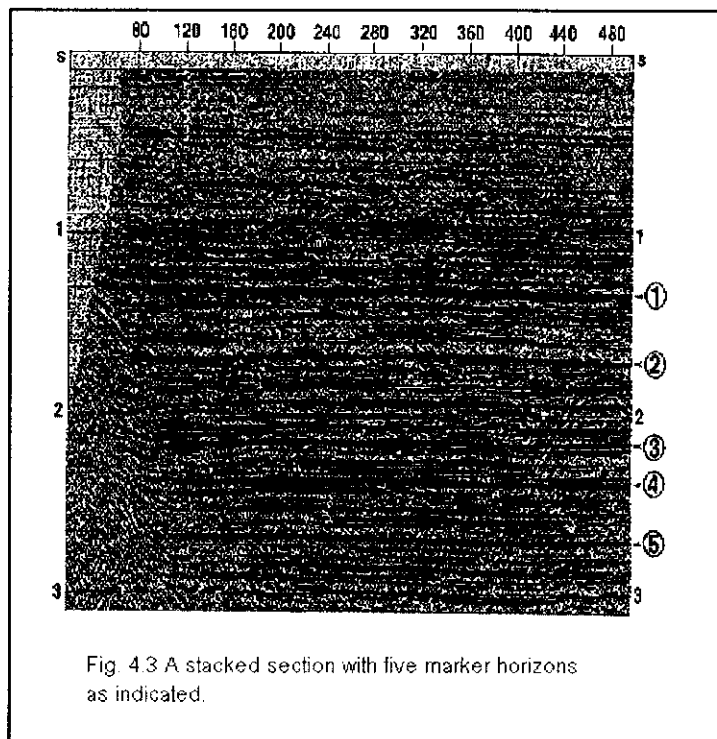
It is called constant velocity scan (CVS) method. The data in Fig. 4.2b is repeatedly NMO corrected using a range of constant velocity values between 5000 and 13,600 ft/sec with the aid of a high speed computer.



The NMO corrected gathers are displayed beside each other in the form of a panel. Events marked as A and B suggest how the procedure works. For a certain velocity

value, these events would be flat; otherwise they would be curved, if velocities are either over-corrected or under-corrected. Thus, event A appears to be flat (or stacks well) with a velocity of 8300 ft/sec. Similarly, the event B appears to stack well with a velocity of 8900 ft/sec. By proceeding this way, one can build a velocity function that is appropriate for the NMO correction of this gather. The process is repeated as often as necessary for the remaining gathers of a seismic line.

For pore pressure prediction or other stratigraphic work, one commonly uses Horizon Velocity Analysis (HVA). This is an efficient and accurate way to get velocity information at every CMP location along selected key horizons, as opposed to the conventional velocity analysis that provides velocity information at every time gate at selected CMP locations. It is tedious and expensive, but highly recommended for structural or stratigraphic work. Figures 4.3 and 4.4 show examples of HVA analysis: Figure 4.3 shows a stacked section with several marked horizons and the one in Fig. 4.4 shows the stacking velocity functions over the same horizons. The vertical and



horizontal axes in each panel are stacking velocity and CMP axis, respectively.

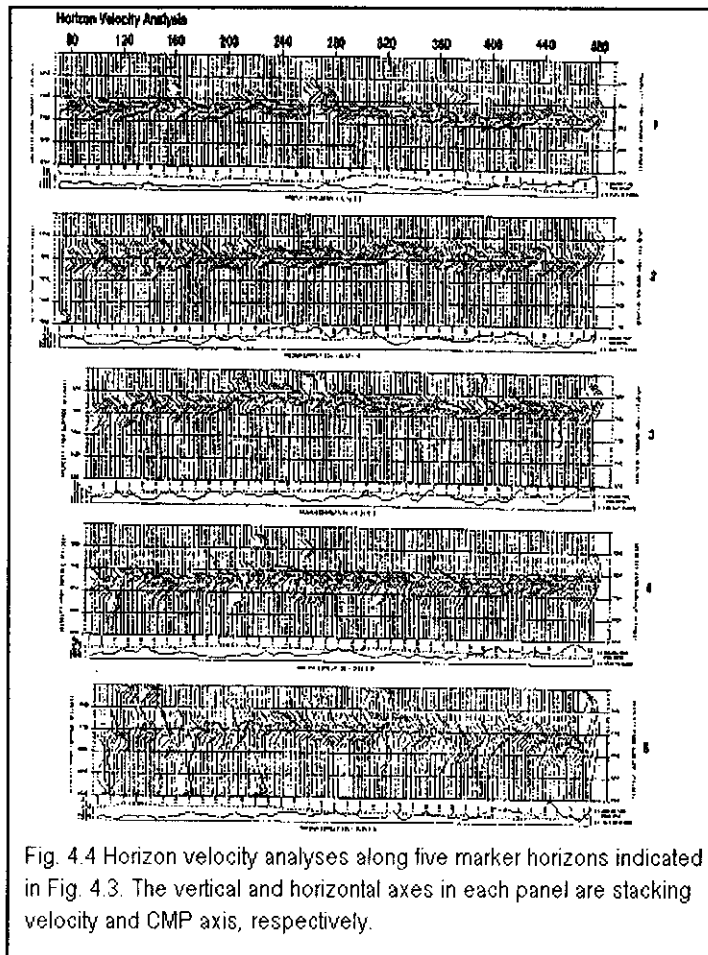


Fig. 4.4 Horizon velocity analyses along five marker horizons indicated in Fig. 4.3. The vertical and horizontal axes in each panel are stacking velocity and CMP axis, respectively.

No matter which method is used, we must realize that the quality of the velocity function is dictated by the quality of the stack- that function which flattens a certain event in a gather. This means using a quantitative measure to obtain a velocity function based on the amplitude and continuity of stacked event(s) - not rock velocity! This has a significant consequence- not all velocity functions that yields the best stack can be considered a true rock velocity. Below we give reasons why velocity estimation from seismic stacking velocity analysis is limited:

- S/N ratio of the gathers
- Muting
- Spread length used for data acquisition
- Stacking fold
- Choice of coherency measure
- True departure from hyperbolic moveout (e.g. anisotropy)
- Time gate length
- Bandwidth of data

In general, as events on a velocity analysis are picked deeper and deeper (in time), the quality of the velocity function degrades. This is because one encounters a range of velocity functions, which flattens an event, thus posing ambiguity and lack of accuracy in the picked velocity function.

For pore pressure calculation, one uses interval velocities derived from stacking velocities, as discussed earlier. For the sake of completeness, we summarize below the limitations to calculations of interval velocities (using Dix's model) from stacking velocities:

Layered geometry assumptions for Dix-velocity calculation

Assumption of homogeneous and isotropic layer properties

Lack of precision in data analysis (picking of reflection times, etc.)

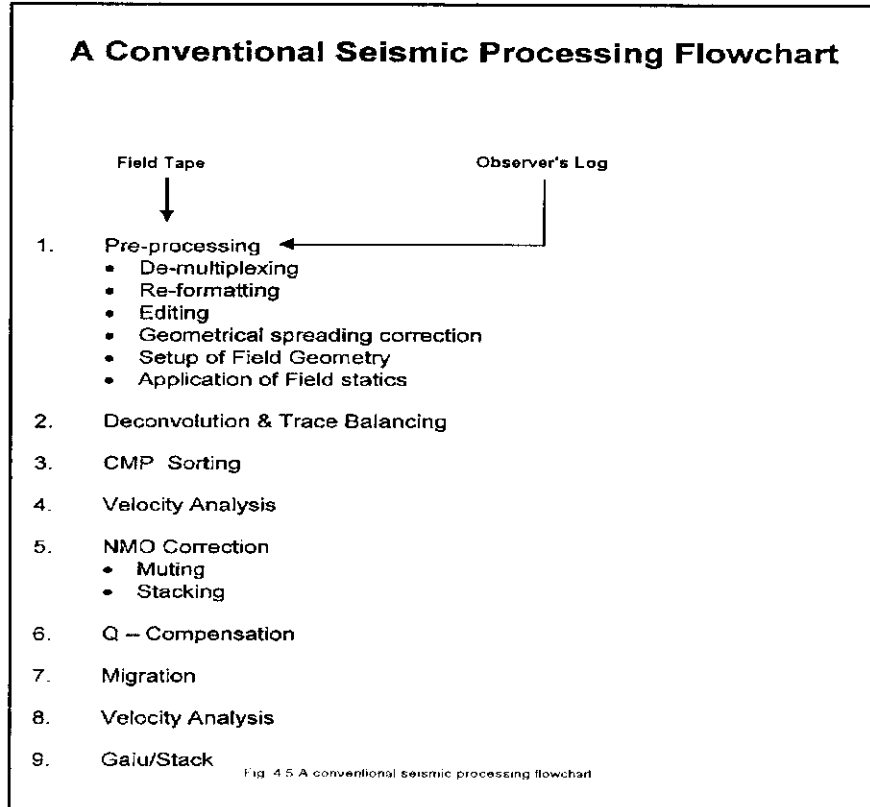
Improper use of the Dix calculation (interval velocities calculated in a narrow interval)

Poor resolution

Ray path bending through complex geology

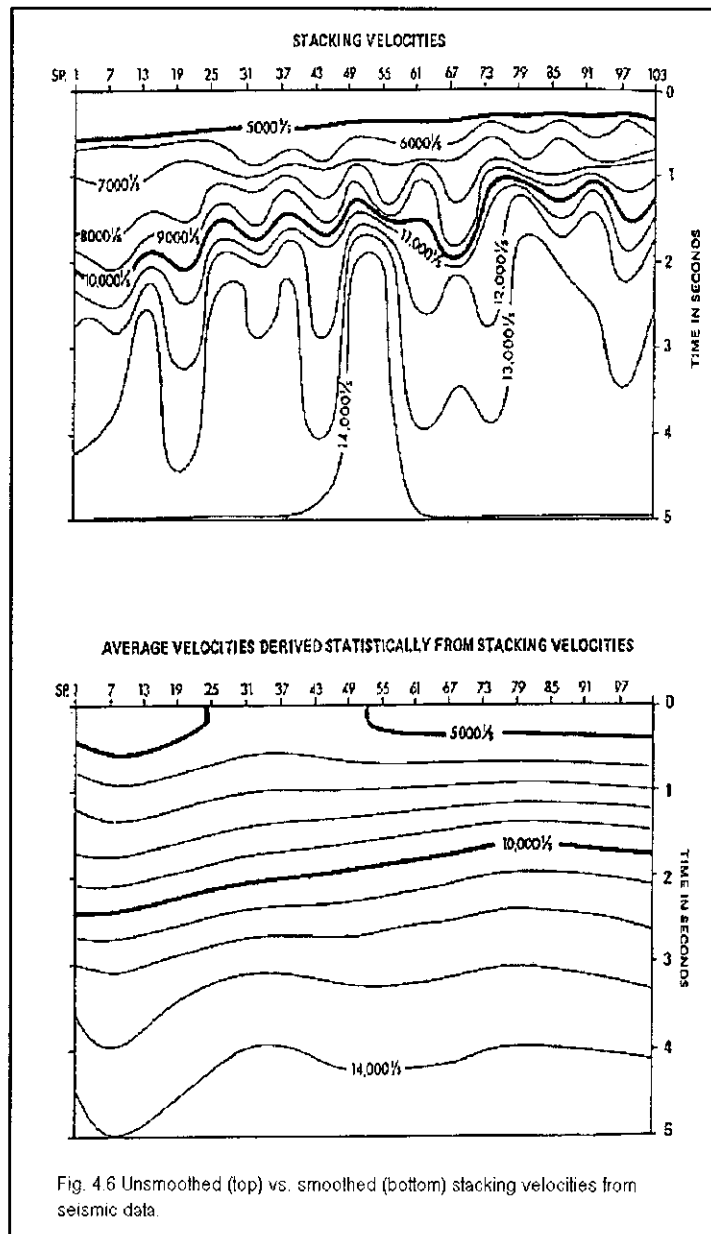
Spatial sampling

A conventional seismic processing flowchart for velocity analysis is given in Fig. 4.5.



4.2 Velocity Smoothing, Calibration, Resolution and Interpretation

Velocity smoothing is an essential step in conditioning velocities for pore pressure prediction work. Smoothing (and interpolation) is done both in time and space. An example is given in Fig. 4.6.



The top figure shows unsmoothed stacking velocities, whereas the bottom figure shows smoothed velocities. Obviously, interval velocities from respective sections in this figure would be associated with different interval velocities! Which model is valid? One does not know this *a priori*. For this reason velocity calibration is an essential step in conditioning seismic velocities for pressure prediction. This step is discussed below.

Velocity calibration is usually done with checkshot data from well surveys. Due to ray path bending, seismic interval velocities are higher than the vertical velocities measured during the well surveys. Sometime this is referred as apparent anisotropy, as opposed to true anisotropic rock propagation velocities! There are two methods to account for the discrepancy between the seismic and the checkshot velocities. The first method involves comparing time-depth relationships from checkshot surveys to those derived from the seismic data. The second, a preferred method, involves comparing interval velocities from the checkshots to those derived from the seismic stacking velocity analysis using Dix' s method. The procedure involves obtaining a correction function versus two way time at the well location (or analogue well location) which is then

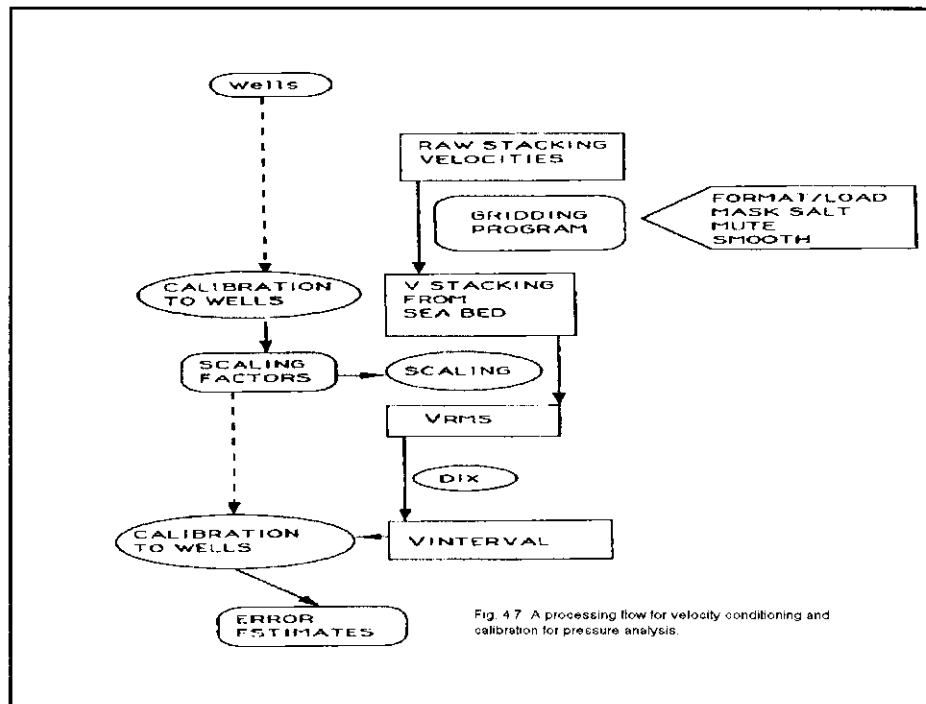


Fig. 4.7 A processing flow for velocity conditioning and calibration for pressure analysis.

applied to the entire velocity field. Typically, several velocity functions around a well are used to construct this calibration function. This allows an error analysis, which must follow such a calibration scheme. The entire procedure is shown schematically in Fig. 4.7. It is recommended that the procedure be tested on crossing seismic lines for accuracy and consistency. *Pressure prediction should never be done based on a single velocity function at a CMP location!*

Any application of seismic velocity for pressure prediction must include an understanding of the velocity resolution attendant in the velocity analysis process. The

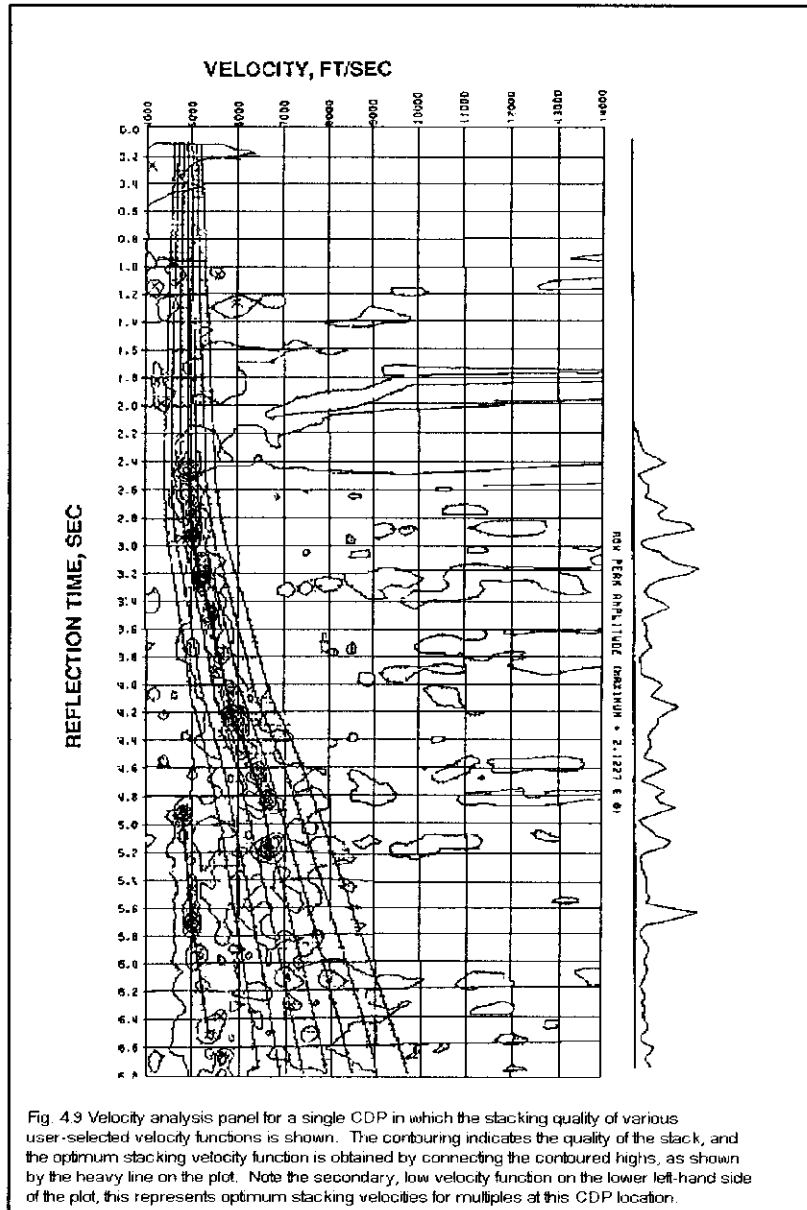
table in Figure 4.8 shows vertical (temporal) and lateral resolution of conventional velocities: temporally the interval velocities from the conventional stacking velocity analysis do not have frequencies higher than 2-4 Hz.

VELOCITY RESOLUTION			
	Vertical	Lateral	Comment
Low resolution Spec data and standard	0-2 Hz (400-500 ms)	~1 mile	Constant pressures in 500-800 foot interval; smeared geology
Reprocessed lines, Closer picks and QC	0-4 Hz (200-400 ms)	~1000 feet	250-400 foot interval; improved geological resolution
High resolution Seismic amplitudes (AI) at Every seismic trace	(8,10)-(50-60) Hz (10-20 ms)	~100 feet	100-200 foot interval; improved geologic resolution
'Frequency gap'	4,(8-10)Hz		Need a prior model based on well data and integration with other geologic data (facies,...)

Fig 4.8 Velocity resolution from seismic data.

This leads to pressure analysis in layers no thinner than perhaps 400 ft for typical Gulf Coast sediments. Seismic inversion of either stacked data (post-stack AI inversion) or pre-stack data (using full wave- form analysis and inversion of gathers at various CDP's) can add higher resolution.

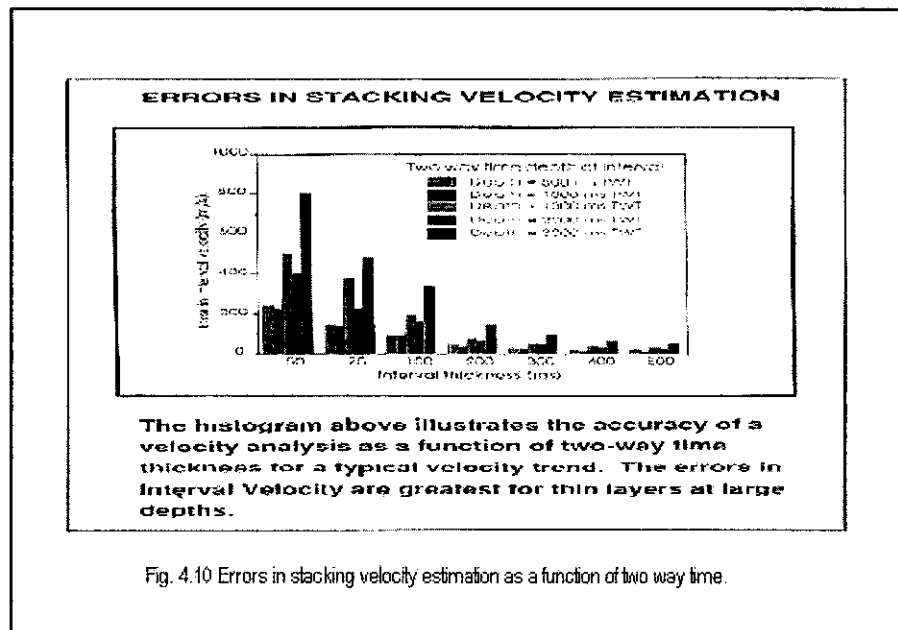
Velocity interpretation is also an essential step in converting stacking velocities to rock velocity. There are many pitfalls in the procedure, some of which have already been pointed out. A major pitfall, not discussed so far, needs mentioning. Figure 4.9 shows velocity analysis for a single CDP in which the stacking quality of various user-selected velocity functions is shown.



The contouring indicates the quality of the stack, and the optimum stacking velocity function is obtained by connecting the contoured highs, as shown by the heavy line on the plot. Note the secondary, low velocity function on the lower left-hand side of the plot;

this represents optimum stacking velocities for multiples for this CDP at this location. However, *a priori* one does not know whether this lowering of velocity is due to higher than normal pore pressure in that interval as opposed to multiples. It could also be due to lithology changes (from carbonates to clastics, for example). Ambiguities of these types are very common in the velocity analysis steps and must be reconciled by using other data and knowledge to interpret the seismic velocity field. Even the very simple step of velocity smoothing as described above can lead to either destroying the local geology or creating a new geology, either of which could lead to unphysical pressure model, and must be avoided.

Error analysis must accompany every velocity analysis employed for pressure prediction. In Fig. 4.10 we show the errors in stacking velocity estimation.



The figure depicts a histogram of errors in velocity analysis as a function of two-way time thickness. A typical velocity trend is used for the sake of calculation. Interval thickness is shown in milliseconds and errors in velocity are shown in m/s. This figure clearly shows that errors in interval velocity are greatest for thin layers at large depths. This inherently will pose a limit on the accuracy of predicted pressures using seismic interval velocity.

5 Guide to Velocity Analysis for Geopressure Work

Quite often velocities are misused for pressure prediction; stacking velocities need a lot of care before being used for this purpose. Before the work begins, a clear understanding of the purpose of the work must be defined: Are the velocities needed for 'regional' understanding of pressure (typically a grid of 100x100 mile)? Detailed image of subsurface pressure at the prospect scale (3x3 mile)? At reservoir scale (100-200 ft bed)? At well bore scale (30-40" by 20,000 ft)? The care and details employed at each of this scale vary and require integration of a host of data, other than the seismic, such as well velocity, logs and geology. Velocity analysis is a tedious process and is usually carried out repetitively; at each step additional data and interpretation are used to add resolution and accuracy. The steps below are intended to provide a guide to the process.

A general understanding of the geology should precede any velocity analysis. Locating stacked and interpreted seismic sections does this best. All available wells must be posted at appropriate locations along with key geologic horizons.

Conventionally processed stacking velocities are usually unsuitable for pressure prediction work, because they are created for best looking stack and may have very little to do with the rock velocity.

The seismic gathers must be available for quality control.

The processing flow must be clearly identified on the seismic section. Velocities must be processed for de-multiple, DMO and pre-stack migration. For areas with salt, such as in the deepwater Gulf of Mexico, one must apply appropriate salt mask and mute.

The stacking velocity, RMS velocity or the interval velocities given at the top of a stacked seismic section should not be used for pressure prediction work, without looking at the gathers and semblance or velocity spectrum plots for quality assurance.

Detailed velocity analysis is best done on a workstation, such as ProMAX or similar tools. Essential steps include closely spaced velocity analysis, lateral consistency in the velocity field, smoothing, calibration and interpretation.

Usual criterion for picking velocity (such as semblance maximum on velocity spectra) may not be suitable for pressure prediction work. Picking that velocity which flattens an event from near to far offsets may work better. If an event can not be flattened across its full offset range, then every effort must be made to optimize flattening it across as far an offset range as possible (say from near to middle range).

Velocity calibration is an essential step in conditioning velocities for pressure prediction. Comparing seismic RMS and interval velocities with those from checkshot surveys best does this. However, if checkshot data are not available, a notion of rock velocity must be used to constrain the velocity field, if possible, from analogue studies.

Never make prediction based on a single velocity function, say at the well location. The velocity field must be checked for lateral and vertical consistency, so that any wild fluctuation or spikes are not present. It is recommended that any velocity analysis for pressure prediction work must proceed with examination of at least a dozen gathers around the well.

Velocity picking should be done in several steps of successively increasing detail. Most detailed picking should be event oriented to ensure that no bias is introduced by Dix-calculations for intervals of varying thickness.

Quality control displays such as NMO-corrected gathers should be used to check accuracy of velocity picks

As the histogram in Fig. 4.10 indicates, never pick velocities in layers with thickness less than 50 ms, especially at relatively large depths (say, at 3 sec. two-way time or beyond).

For regional scale velocity analysis for pressure prediction work, velocities should be picked at least in a 1x1-km grid or less. Special care must be exercised while interpolating the velocity field. This is because any 'velocity spikes', due to anomalous 'picks', can be exaggerated by the interpolation process.

Velocities must be smoothed by a simple mathematical function, such as a low order polynomial. Fancy smoothing algorithms, such as spline, may not be worth the trouble it may pose. These functions tend to follow the undulations in the velocity field too literally and sometime create 'geology' when none is present.

Velocity structures observed within a spread-length must be investigated carefully. These may not be due to geologic variations.

16. Every effort must be made to relate the seismic interval velocities to the rock velocity. The velocity field must be constrained by the knowledge of the range of known rock velocities in that area. For example, velocities in excess of 10,000 ft/s in the deepwater Gulf of Mexico must be carefully examined. Any comparison with well log sonic velocities must be done only after the sonic log has been checkshot corrected.

Conventional analysts are trained to pick velocities 'faster' as depths increase. This may not be a good practice when picking velocities for quantitative pressure analysis. In fact as pore pressure builds up due to undercompaction, velocities do not increase with depth as rapidly with burial as it would have without any pressure effect.

Special care must be exercised with the layer where velocity has been picked last (namely, at the end of the data set where reliable velocity 'picks' can be made). Quite often, the interval velocity is held constant in that layer and then extrapolated to greater depths-beyond where there is no data to pick velocity! This is a 'bad' practice and must be avoided.

All velocity analysis must accompany an error analysis. Every pick must include a quality assurance procedure (say, 1 for good, 2 for questionable and 3 for bad).

6 Examples of Applications of Seismic Velocity for Pressure Prediction

In a recent DEA-119 survey, it was clear that most people use seismic data for pressure prediction, either directly through velocity analysis as described earlier in this report, or indirectly, through basin analysis routines which utilize seismically picked horizons and compaction data as input. Here we shall present some examples of the former. These examples did follow the guidelines for best practice of velocity analysis as outlined in the preceding section.

We note that the velocity resolution of the seismic interval velocity is low; the frequency content is no more than 2- 4 Hz. Thus, the pressure estimate using conventional velocity analysis is fairly “gross” and it may not provide estimates within reservoir layers, where RFT measurements are made. For pressure estimates in the reservoir scale, one would require high frequency velocity information from other sources, such as acoustic impedance data. The current technique can be and has been extended to applications at

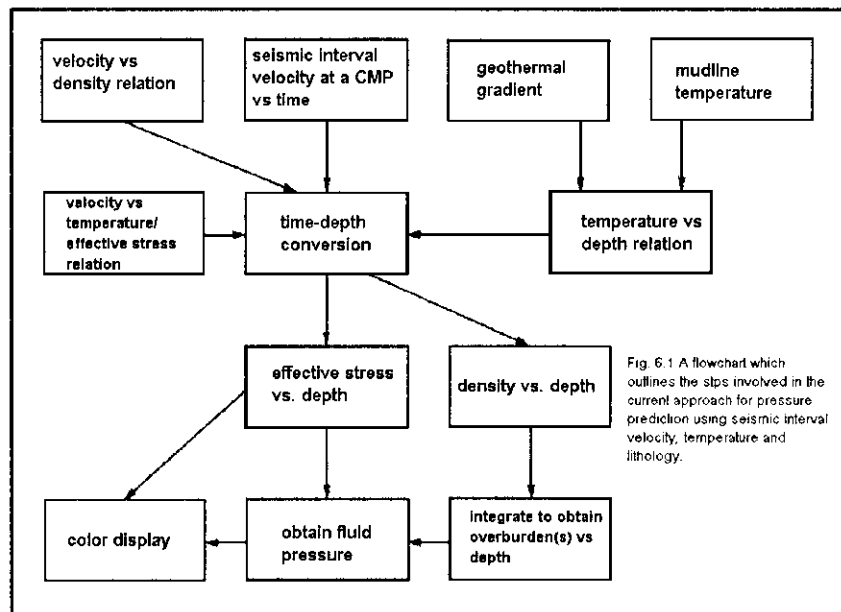


Fig. 6.1 A flowchart which outlines the steps involved in the current approach for pressure prediction using seismic interval velocity, temperature and lithology.

reservoir scale (Dutta and Ray, 1996) using velocities obtained from inversion of acoustic impedance of seismic data.

In Fig. 6.1 we show a flow chart for pressure prediction using seismic velocity (without well control). It is assumed that the velocities are conditioned following the procedure described so far. We note that seismic velocities are used twice: once for generating a pseudo-density which will eventually yield overburden and then for deriving effective stress at each velocity location (CMP location), through user-specified transform between velocity and effective stress. Alternatively, the same velocities can also be used in the traditional fashion, such as those based on Eaton (1968) or Hottmann and Johnson (1965) methods. These methods rely on Normal Compaction Trend (NCT) analysis of seismic velocity versus depth function(s) and then use the velocity deviation from the NCT as a

measure of pore pressure, through empirical calibration functions. Some of these techniques are described in Dutta (1987).

Once velocity analysis is completed, pressure prediction can be made in different dimensions, depending upon requirement: 1-D, 2-D, and 3-D. Below we present some examples, which show the power of the seismic velocity as a tool for pressure prediction.

6.1 3-D Applications

For 3-D applications (for regional pressure work) velocities come from either 3-D velocity survey or a grid of closely spaced 2-D seismic lines. Typically, such analyses proceed in several stages as shown in the following several figures. The First phase in Fig. 6.2 essentially consists of a calibration phase of interval velocities derived from the

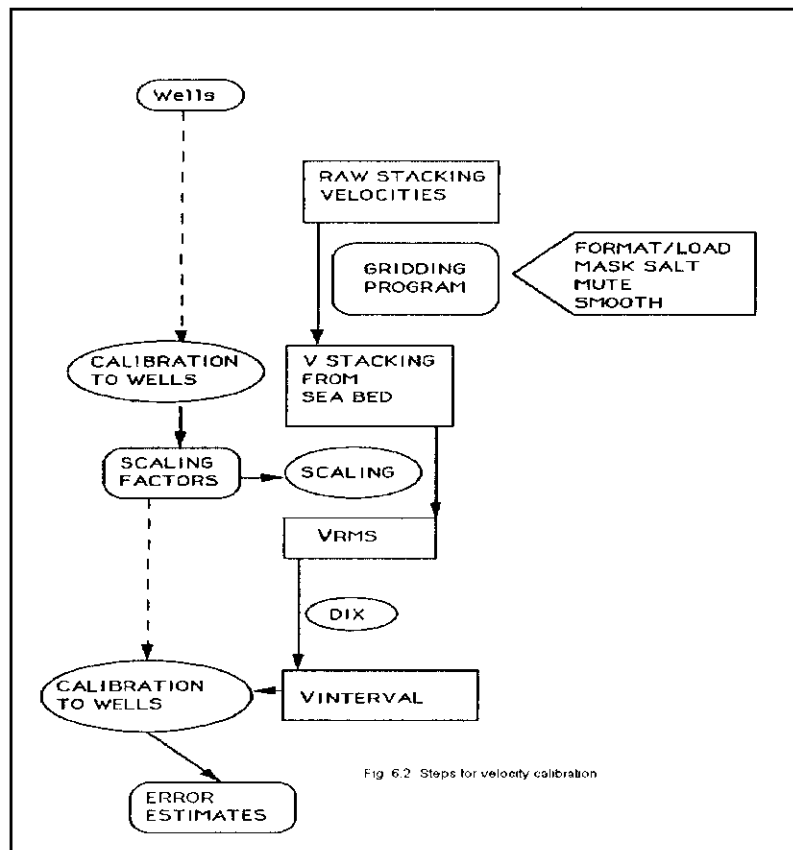


Fig. 6.2 Steps for velocity calibration

conventional stacking velocities using available well controls. The steps are self-explanatory. This step requires access to a 3-D gridding software where velocity conditioning, including lateral and temporal smoothing and interpolation is carried out. Salt masking and other quality control steps are also applied at this step. The output of this process is a velocity cube in 3-D, which is then loaded on a seismic workstation and visualized using any visualization software, such as EarthVision of Dynamic Graphics, Inc. The next phase of the process in Fig. 6.2, deals with transforming the 3-D velocity cube to a cube of 3-D effective stress or pressure. The subsequent phase consists of depth conversion using the velocity data, so that the pressure maps can be displayed in depth, and not two way time. The last phase of the process, Fig. 6.3, consists of taking slices of the pressure cube along major horizons and projecting them in map view. This allows us to get a better understanding of the relationship between pore pressure and the occurrence of major sand and shale units.

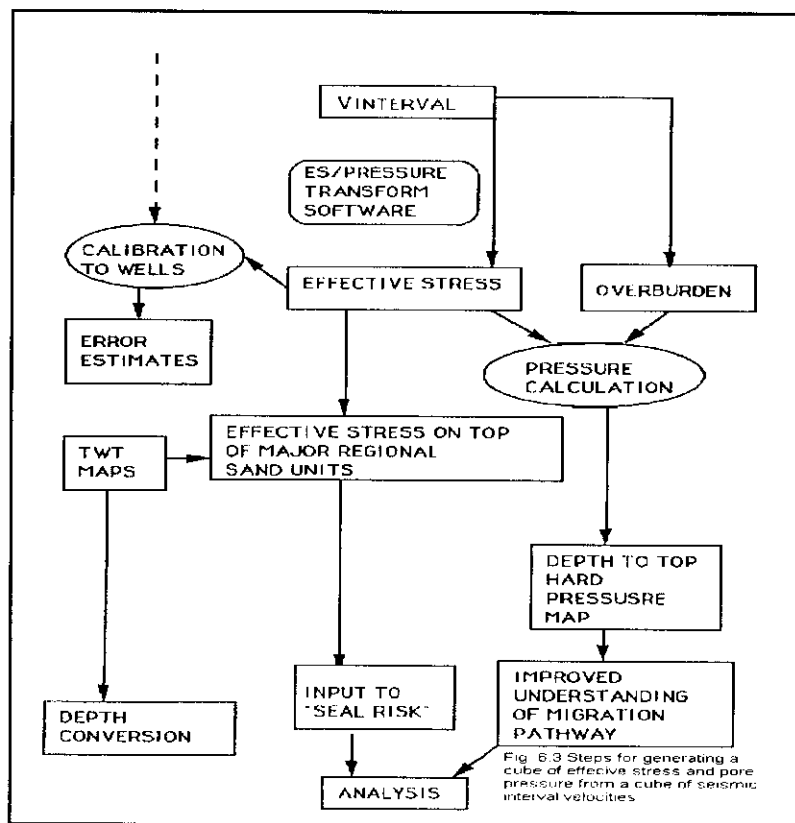


Fig. 6.3 Steps for velocity calibration following those in Fig. 6.2.

Figure 6.4 shows an application of this procedure, taken from Dutta (1997) from the deepwater, Gulf of Mexico. The area of study is shown in the inset. Here a 3-D model of effective stress has been developed over a prospective play fairway. The model covers an area of 140x102 km, with water depth greater than 330 m.

Figure 6.4 is a map of effective stress, in psi, and projected at a prospective horizon over many blocks. The color codes in this figure represent the risk associated with hydraulic seal failure. This sort of maps has helped the explorationists to high-grade areas of low top seal risk, and downgrade risky areas.

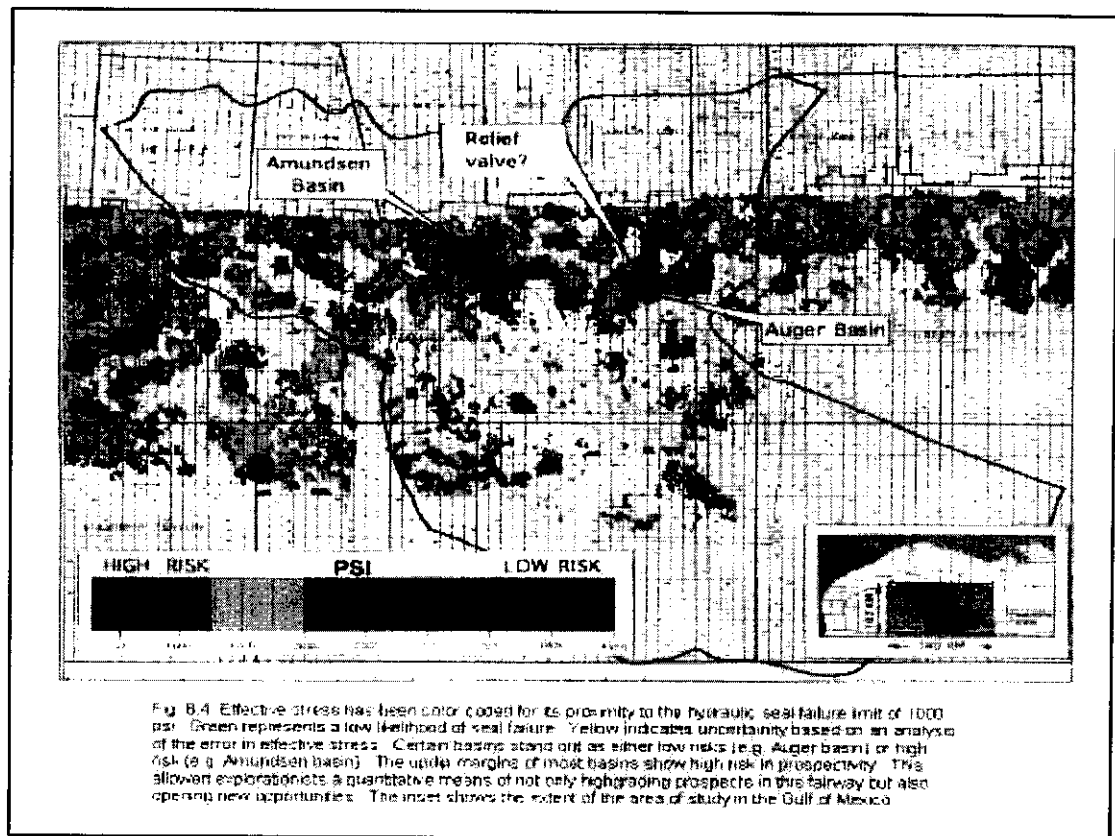
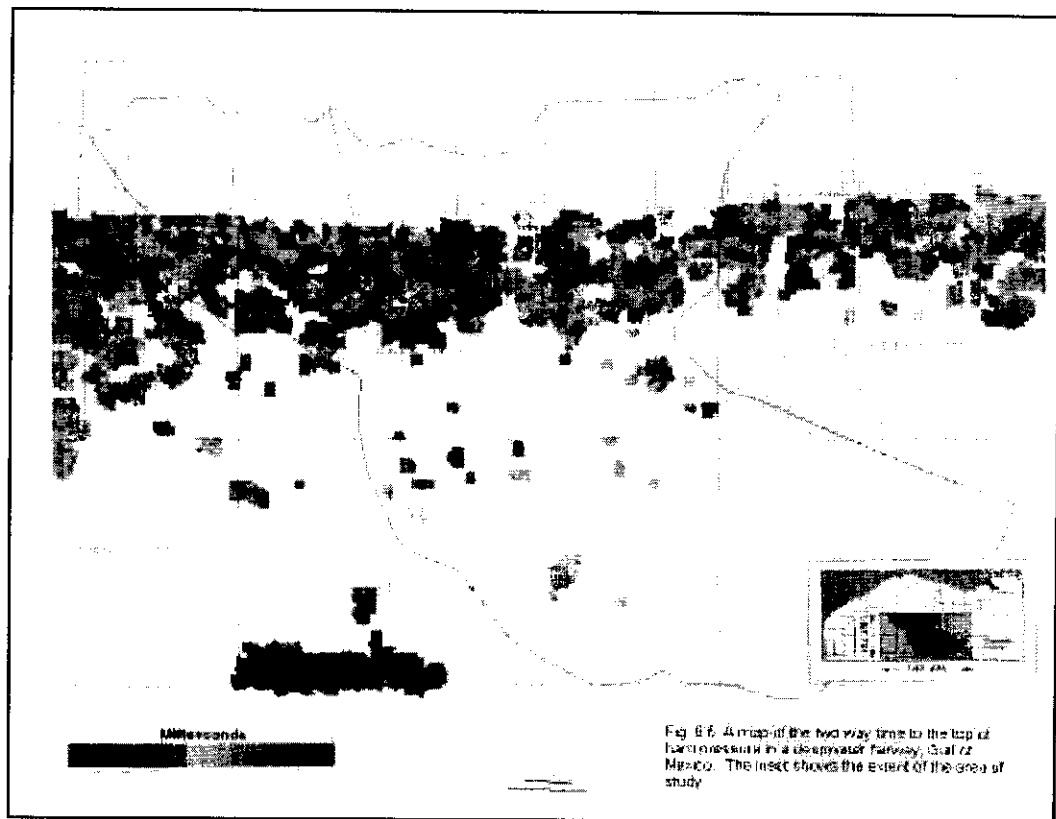
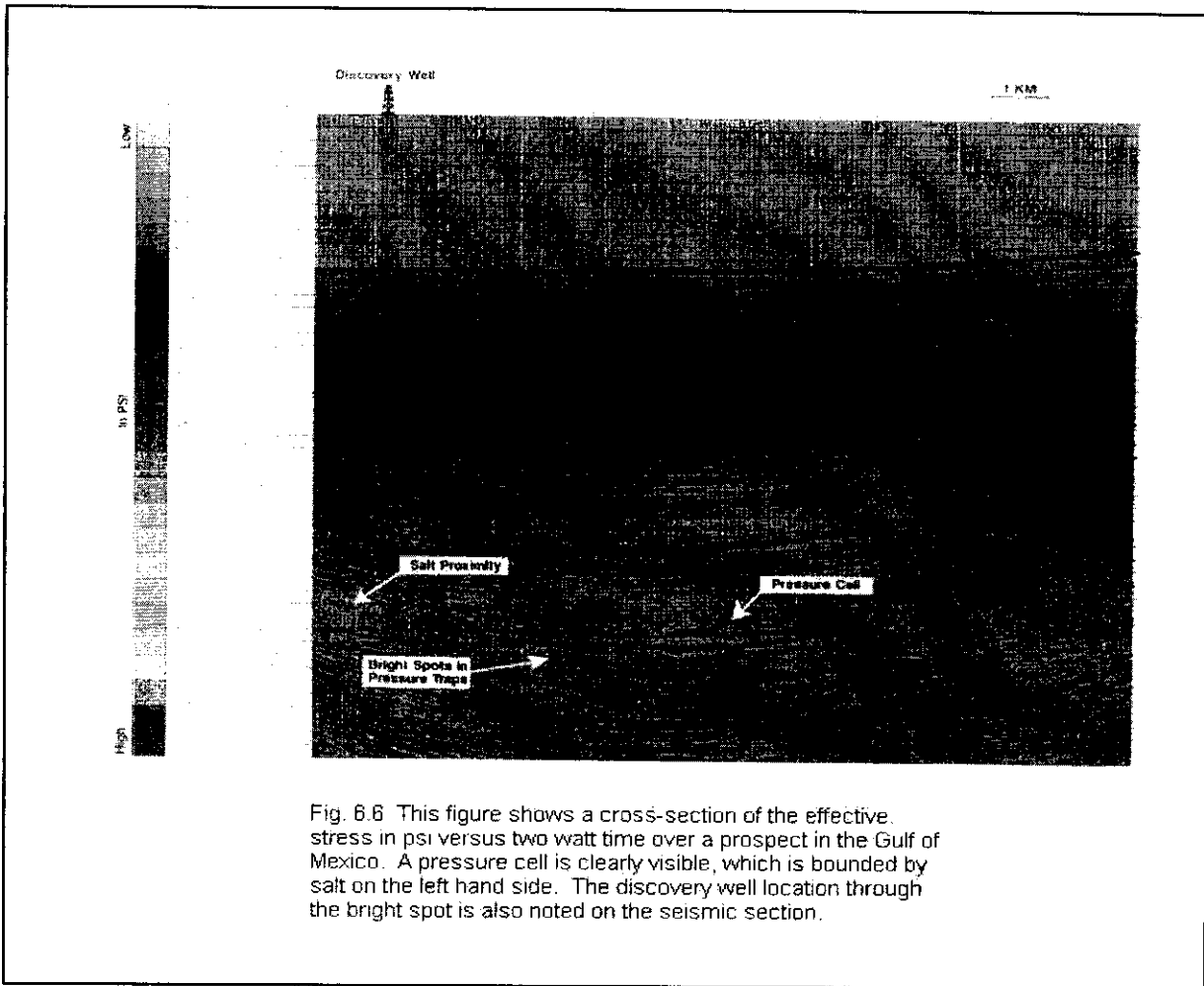


Figure 6.5 is a map of top of hard pressure in the same fairway as a function of two way time. Here the top of hard pressure has been defined as that depth (or time) where the effective stress reaches a threshold value of 1000 psi. Analysis such as the ones shown here in 3-D, should always use gridded velocities which are no more than 0.5 km apart. Otherwise, the interpolation process may create geology which are neither present nor realistic.

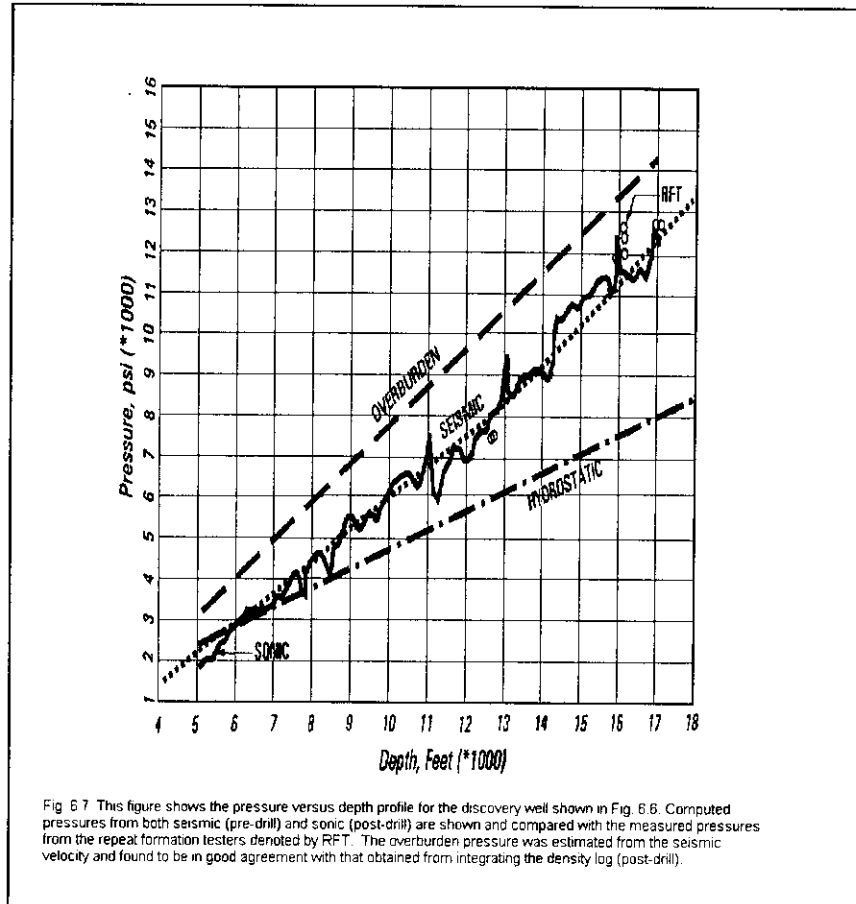


6.2 1-D/2-D Applications

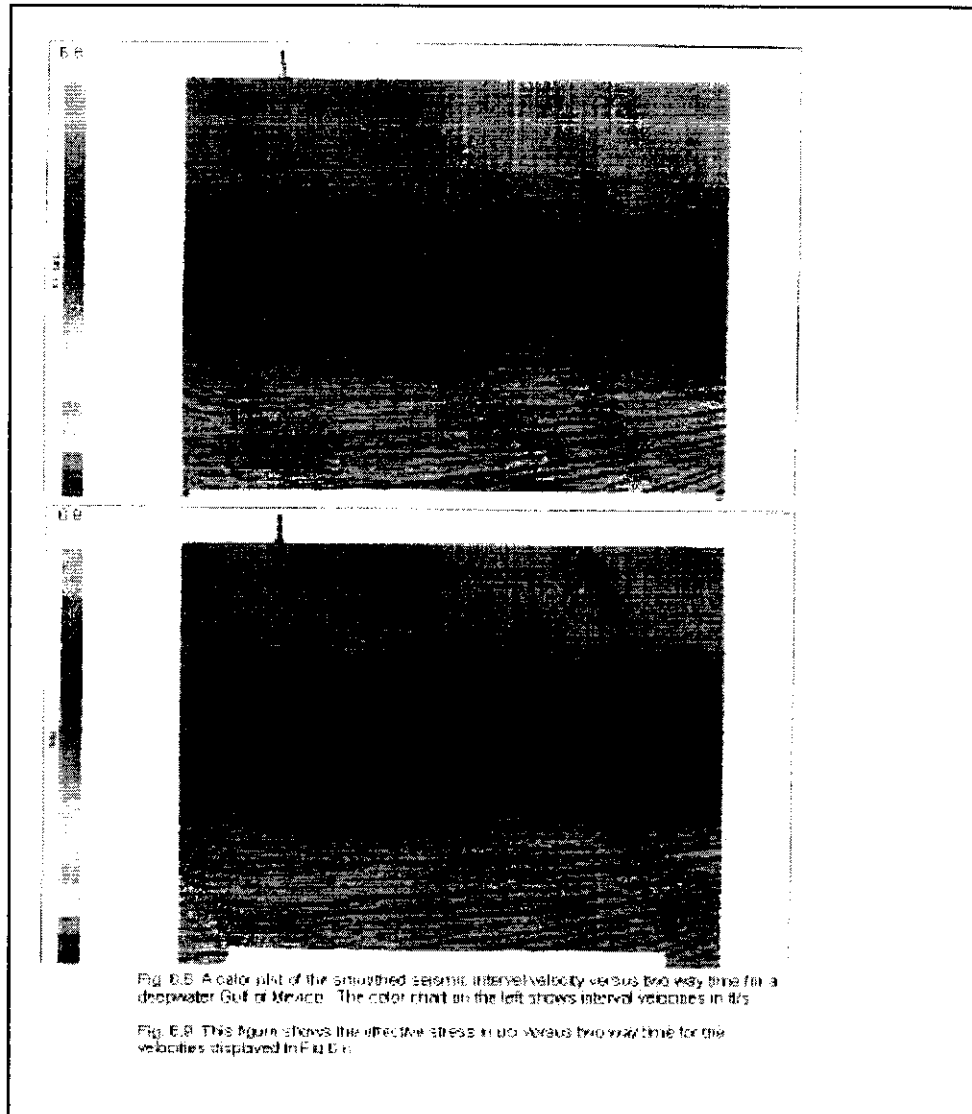
As we discussed earlier in this report, at the prospect scale, the resolution of the seismic velocity analysis can be greatly enhanced by picking velocities at every CMP. In this way, a very detailed subsurface image of pressure and effective stress can be obtained both at the prospect scale and the well-bore scale. An example of such an analysis from the deepwater, Gulf of Mexico is shown in Fig.6.6, on a 2-D seismic line, which has been subjected to the best practice procedure outlined in the paper earlier. This procedure has preserved a great deal of stratigraphic detail. Figure 6.6 shows the effective stress, in psi, as a function of two-way time and common depth point (CDP) locations. The figure shows the existence of a pressure cell associated with stratigraphic variations within the prospect. It also indicates pressure traps in the vertical direction, shown as reversals of effective stresses.



A comparison of the predicted pressures with the RFT data from the well is shown in Fig. 6.7. The comparison is good, and the predictions are within 400 psi of the formation pressure.



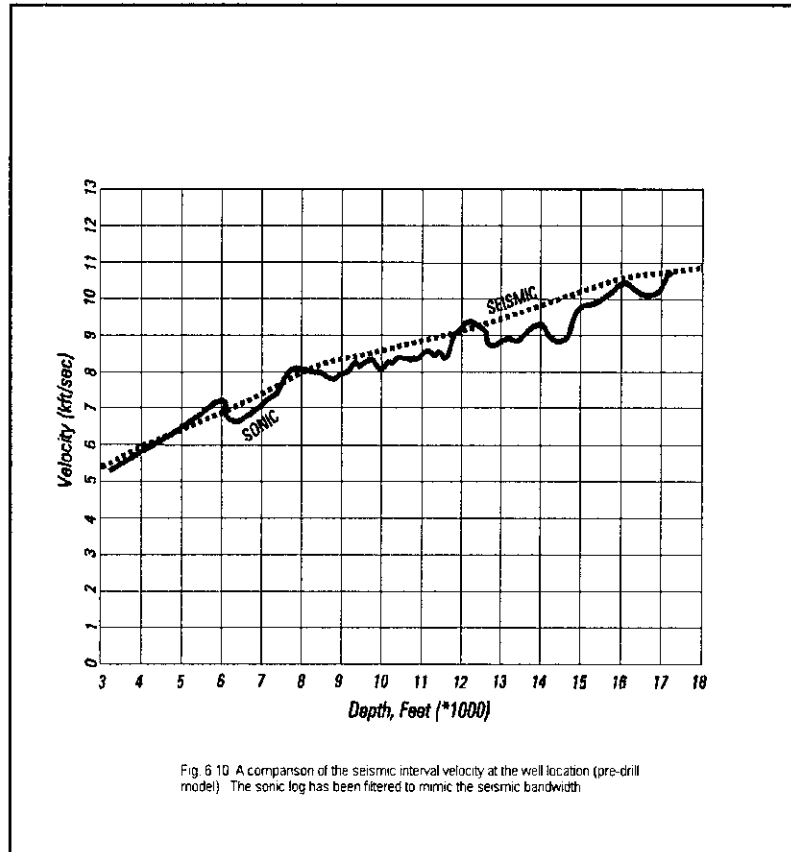
Another example from the deepwater Gulf of Mexico is shown in Figs. 6.8 – 6.12. The color plot of Fig. 6.8 shows the seismic interval velocities together with stacked traces. We note the general conformity of the structure with the derived velocity field from the stacking velocity data, using the best practice procedure outlined earlier. The color scale of velocity on the left side of Figs. 6.8 and 6.9 is expressed in ft/s.



The predicted 2-D cross-section of effective stress, in psi, is shown in Fig. 6.9 as a function of two-way time and CDP number. The color scale of this figure ranges from 470 to 4150 psi. A gradual increase of effective stress (meaning a decrease in fluid pressure) is apparent from left to right (away from the well). This suggests relatively more compaction (and consequent expulsion of water) as one moves away from well and moves updip to the right. Thus, an increase in effective stress up-dip and away from the well location suggests an active migration pathway of fluids.

Turning next to pressure estimation using sonic log, Fig. 6.10 shows a comparison of the band passed calibrated sonic log and seismic interval velocity at the well location: the two velocities are in good agreement showing a general goodness of the velocity analysis

of the reflection seismic data. Such comparison must be made, whenever possible, to assure that a high quality of velocity has been used for pressure prediction.



The predicted effective stresses from both seismic and sonic are shown in Fig. 6.11. The line marked "hydrostatic" shows the expected effective stress variation, had the fluid pressure been in hydrostatic equilibrium. The Geopressure in this well began at approximately 6 kft below the seismic datum where the predicted effective stresses depart from the hydrostatic line.

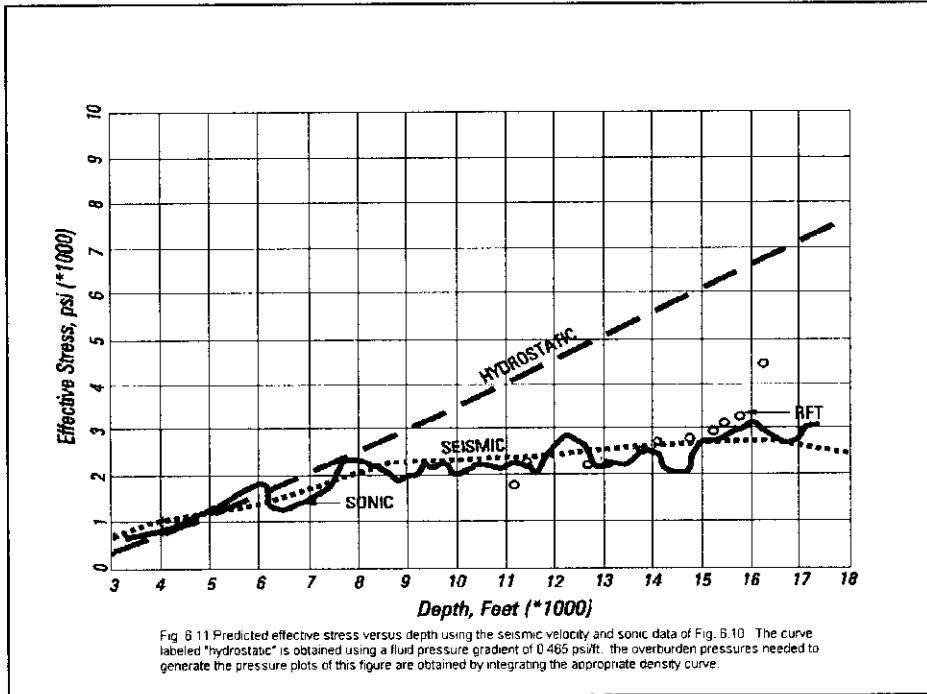
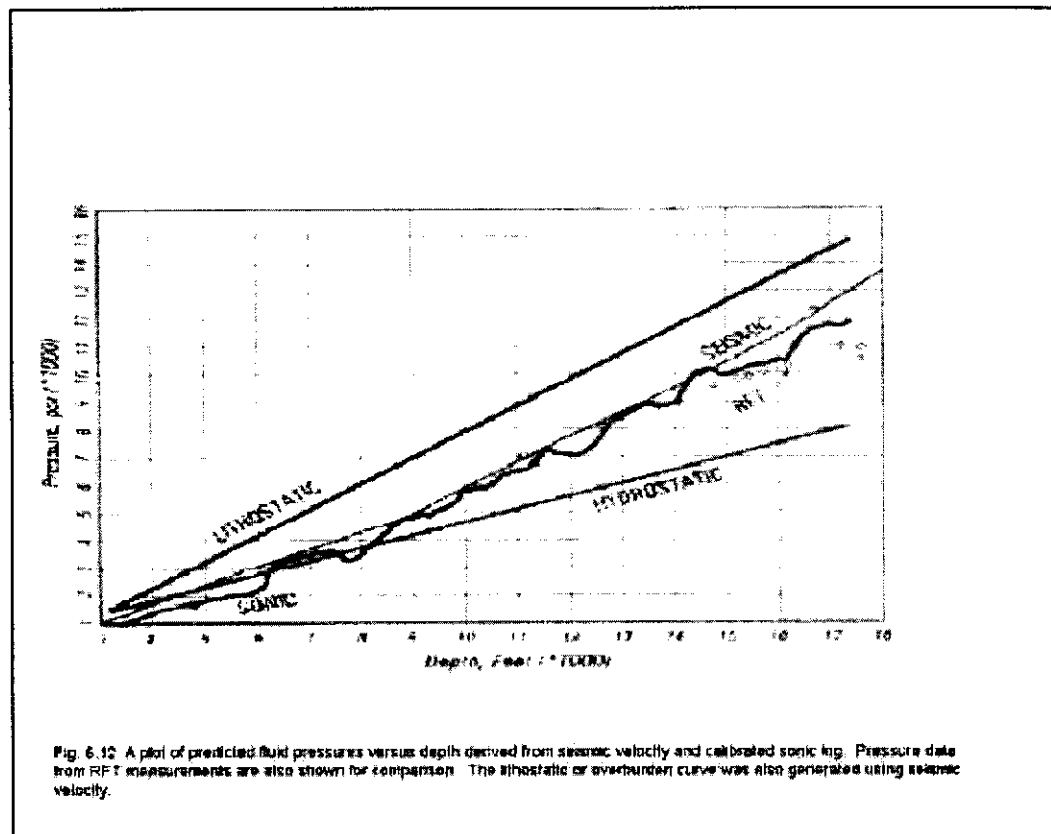


Fig. B.11 Predicted effective stress versus depth using the seismic velocity and sonic data of Fig. B.10. The curve labeled "hydrostatic" is obtained using a fluid pressure gradient of 0.465 psi/ft. The overburden pressures needed to generate the pressure plots of this figure are obtained by integrating the appropriate density curve.

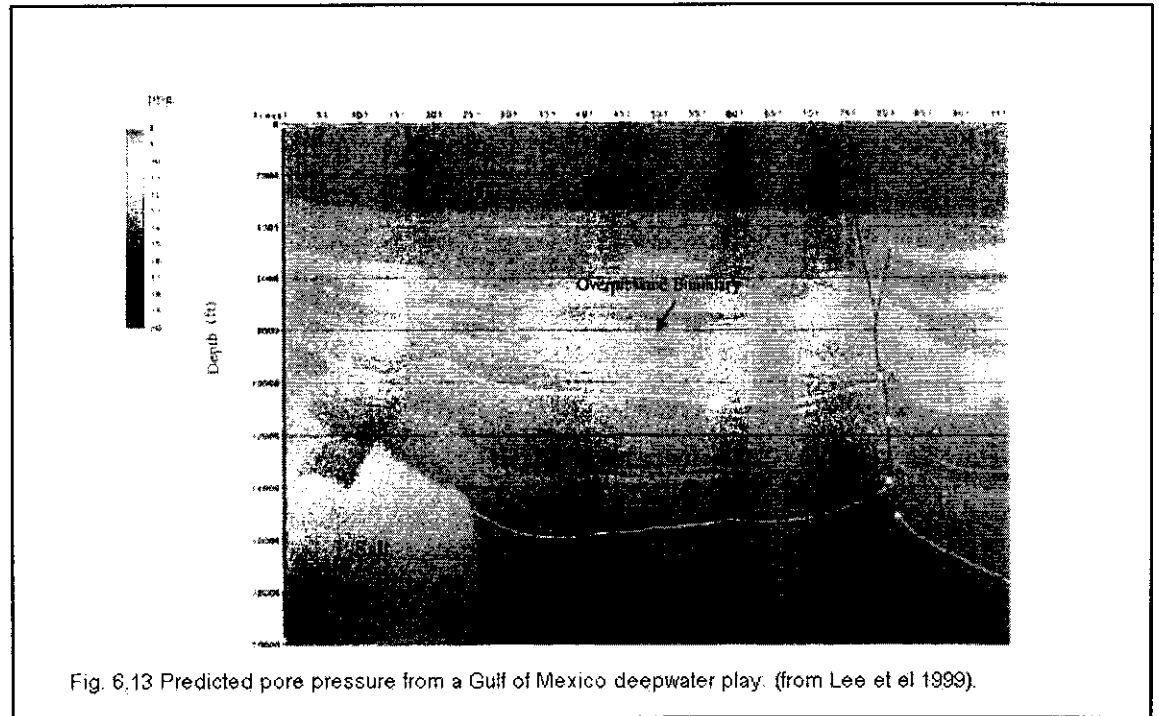
The predicted pore pressures from seismic are compared with those predicted from sonic log in Fig. 6.12. The predicted pressures from these two velocity sources at two different scales are in good agreement with each other and with those obtained by RFT measurements (shown by diamonds in Fig. 6.12)



These examples reveal that: (i) carefully processed seismic velocities can yield good estimates of pore pressure, without any well control, (ii) active migration pathway of fluids can be imaged by 2-D/3-D effective stress maps using seismic velocity data, and (iii) the predicted pore pressures at the well using both seismic and sonic data are in good agreement with each other and with an independent set of data: the RFT measurements.

In Fig. 6.13, we show predicted pore pressure from a deepwater Gulf of Mexico play, taken from Lee et al (1999). Green represents normal pressures and yellows a pore pressure of 10 ppg, which is defined as the overpressure threshold. Lateral pore pressure varies about 1-2 ppg between the footwall and the hanging wall of the normal faults. These results were obtained using seismic velocity analysis in conjunction with tomographic inversion of velocities to add high frequency to the data. The procedure is very complex; it uses all the pre-stack data and requires calibration. Thus, it can not be used in the regional sense. However, it is a powerful tool in the prospect scale, once a well has been drilled.

Drilling experience has indicated that when seismic velocities are processed and conditioned as outlined in this paper, it can yield pressures to within 0.50 ppg at target depths in deepwater, provided the low-frequency trends of seismic interval velocities are of good quality and are within 5-10% of well velocities.



7 References

- Al-Chalabi, M., 1973, Series approximations in velocity and travelttime computations: *Geophys. Prosp.*, 21, 783-795.
- Dix, C. H., 1955, Seismic velocities from surface measurements: *Geophysics*, 20, 68-66.
- Dutta, N. C. and Ray, A., 1996, Subsurface image of geopressed rocks using seismic velocity and acoustic impedance inversion: 58th Annual Meeting Eur. Assoc. Geosci. Eng., Amsterdam (extended abstract).
- Dutta, N. C., (Editor) 1987, *Geopressure*, Geophysics Reprint Series No. 7, Society of Exploration Geophysicists, Tulsa, OK.
- Dutta, N. C., 1997, Pressure prediction from seismic data: Implications for seal distribution and hydrocarbon exploration and exploitation in the deepwater Gulf of Mexico: in *Hydrocarbon Seals*, Norwegian Petroleum Society Special Publication No. 7, Eds. Moller-Pederson, P. and Koestler, A. G., Elsevier Press.
- Eaton, B. A., 1968, Fracture gradient-prediction and its application in oil field operations: *J. Pet. Tech.*, October: 1353.
- Hottmann, C. E., and Johnson, R. K., 1965, Estimation of formation pressures from log-derived shale properties; *J. Pet. Tech.*, June: 717-722.
- Hubral, P., and Krey, T., 1980, Interval velocities from seismic reflection time measurements: *Society of Exploration Geophysicists Monograph*.
- Lee, S., Shaw, J., Ho, R., and Steeb, D., 1999, Deepwater reservoir prediction using seismic and geomechanical methods: *Leading Edge*, June 1999.
- Nur, A. M. and Wang, Z., 1989, *Seismic and acoustic velocities in reservoir rocks, Vol. I, experimental studies*; SEG Reprint Series No. 10.
- Tanner, M. T., Koehler, F., 1969, Velocity spectra- digital computer derivation and applications of velocity functions: *Geophysics*, 39, 859-881.
- Wyllie, M. R. J., Gregory, A. R., and Gardner, G. H. F., 1957, An experimental investigation of factors affecting elastic wave velocities in porous media: *Geophysics*, 23, 459-493.
- Yilmaz, O., 1987, *Seismic data processing, Investigations in Geophysics No. 2*, Society of Exploration Geophysics,



KNOWLEDGE SYSTEMS, INC.

State of the Art in Fracture Gradient Estimation

Glenn Bowers

8/20/1999

CONFIDENTIAL

*This report is provided to DEA Project 119 Project Participants under the terms of the
DEA Project 119 Participation Agreement and is thereby subject to restrictions of
confidentiality and non-disclosure to third parties.*

DEA Project 119

Report No. 3

Corporate Offices

Knowledge Systems, Inc.
P. O. Box 1279
Stafford, Texas 77497-1279
Phone: 281-879-1400
Fax: 281-879-1499
E-mail: sales@knowsys.com

European Office

Knowledge Systems, Inc.
P.O. Box 274 Paradis
5856 BERGEN
Norway
Phone: +47 55 92 45 62
Fax: +47 55 92 45 62
E-mail: sales @knowsys.com

Please visit the Knowledge Systems' website at <http://www.knowsys.com>

Information in this document is subject to change without notice, and does not represent a commitment on the part of Knowledge Systems. The software described in this document is furnished under a license agreement or non-disclosure agreement. It is against the law to copy the software on any medium except as specifically allowed in the license or non-disclosure agreement.

© Copyright Knowledge Systems, 1989-2000. All rights reserved. *DrillWorks* is a registered trademark of Knowledge Systems, Inc. *PostScript* is a registered trademark of Adobe Systems, Inc. *Windows* is a trademark of Microsoft Corporation

Document Information

Title: State of the Art in Fracture Gradient Estimation	
Description: DEA 119, Report No. 3	
Author(s): Glenn Bowers	
Reviewer(s): Myleen Sjodin	
Creation Date: 10/5/2000 9:44 AM	Last Date Modified: 10/5/2000 9:44 AM
Approved By: Jim Bridges	Approval Date: 8/20/1999
Will be sent to:	
Sources Used: (can be other documents used as sources)	
Project Number:	Document Number: 2000-000006

Table of Contents

1	Introduction.....	1
2	Fracture Theories.....	2
2.1	Underlying Assumptions	2
2.2	Hoop Stress Approach	5
2.2.1	Case I - Impermeable Wellbore, Impermeable Closed Crack	6
2.2.2	Case II - Impermeable Wellbore, Permeable Closed Crack	7
2.2.3	Case III - Permeable Wellbore, Permeable Closed Crack	8
2.3	Minimum Stress Approach	10
2.4	Conclusions.....	13
3	Minimum Stress Methods.....	13
3.1.1	Hubbert & Willis.....	13
3.1.2	Matthews & Kelly	14
3.1.3	Pennebaker.....	15
3.1.4	Eaton.....	16
3.1.5	Christman.....	17
3.1.6	Pilkington.....	18
3.1.7	Daget & Parigot.....	19
3.1.8	Daines	19
3.1.9	Brennan & Annis.....	21
3.1.10	Zamora.....	22
3.1.11	Simmons & Rau	25
3.1.12	Singh & Emery.....	26
3.1.13	Holbrook, Maggiori, & Hensley.....	26
4	Hoop Stress Methods.....	27
4.1.1	Hubbert & Willis.....	27
4.1.2	Haimson & Fairhurst	28
4.1.3	Bellotti & Giacca.....	28
4.1.4	Anderson, Ingram, & Zanier	29
4.1.5	Aadnoy & Larsen	30
5	Direct Methods.....	31
5.1.1	Rocha & Bourgoyne	31
5.1.2	Barker & Wood	32
5.1.3	Breckels & van Eekelen.....	33
5.1.4	MacPherson & Berry	35
5.1.5	Salz.....	35
6	References.....	36

1 Introduction

Twenty-three different methods for estimating fracture gradients were found in the literature; an impressive, and somewhat overwhelming number of papers. After searching for similarities, these techniques were grouped into four categories, based upon their underlying solution approach:

- Minimum Stress Methods (long cracks)
- Hoop Stress Methods (short cracks)
- Fracture Mechanics Methods (all length cracks)
- Direct Methods

Table 1 shows how each of the methods reviewed in this study were classified:

Minimum Stress	Hoop Stress	Fracture Mechanics	Direct
<ul style="list-style-type: none"> • Hubbert & Willis • Matthews & Kelly • Pennebaker • Eaton; Eaton & Eaton • Christman • Pilkington • Daget & Parigot • Daines • Brennan & Annis • Simmons & Rau • Zamora • Holbrook, Maggiori, & Hensley • Singh & Emery 	<p>Impermeable Cracks</p> <ul style="list-style-type: none"> • Hubbert & Willis • Anderson, Ingram, & Zanier • Aadnoy & Larsen <p>Permeable Cracks</p> <ul style="list-style-type: none"> • Haimson & Fairhurst • Bellotti & Giacca 	<p>Fully Pressured Crack</p> <ul style="list-style-type: none"> • Abou-Sayed, Brechtel, & Clifton <p>Any Crack Pressure Profile</p> <ul style="list-style-type: none"> • Rummel 	<p>Depth</p> <ul style="list-style-type: none"> • Bellotti & Giacca • Rocha & Bourgoyne • Barker & Wood <p>Depth & Pore Pressure</p> <ul style="list-style-type: none"> • Breckels & van Eekelen <p>Pore Pressure</p> <ul style="list-style-type: none"> • Salz

Table 1 - Classification of published pore pressure estimation methods.

Minimum stress methods assume significant mud losses will occur when the wellbore pressure equals the minimum *in situ* stress. Hoop stress methods are based upon analytical solutions for stresses around a wellbore. They predict massive mud losses when the wellbore pressure causes the minimum *hoop stress* along the wellbore wall (the stress tangential to the wellbore) to equal the rock's tensile strength.

Usually, the wellbore is assumed to have pre-existing cracks, and the tensile strength term is dropped. This has two benefits. First, it eliminates having to guess at a tensile strength, and second, it makes for a more realistic fracture gradient model (according to fracture mechanics theory, the fracture gradient for a crack-free wellbore is infinity). Hoops stress methods can be further divided into two categories, based upon whether the cracks are considered to be permeable or impermeable when closed:

The theoretically soundest approach for predicting fracture gradients is fracture mechanics, which determines the conditions under which a fracture will begin and end propagating. It has been used for years to design hydraulic fracturing treatments. There are no exact closed-form fracture mechanics solutions for cracks propagating from a wellbore wall. However, Abou-Sayed, et. al. (1978) published a table of parameters developed by Paris & Sih that can be used to estimate crack length vs wellbore pressure for the case of a fully pressured crack. And Rummel (1987) has developed analytical relations for approximating the solution for cracks with any type of pressure distribution.

The main drawback with the fracture mechanics approach is that it requires information not generally known: fracture toughness, initial crack lengths, and fluid pressure distributions along cracks. Hydraulic fracturing simulators can numerically model the evolution of pressure along a propagating crack, but running a simulator to predict fracture gradients is obviously not feasible. Therefore, fracture mechanics is not a viable alternative for estimating fracture gradients for well planning purposes, and these methods will not be covered in detail in this report. However, some insights that fracture mechanics can provide on the wellbore fracturing process will be discussed in the next section.

The last group of fracture gradient prediction methods classified as “direct”, are not based upon any underlying theoretical model. They just directly correlate fracture gradient to some other parameter, such as depth, or pore pressure gradient.

There are some fundamental differences between hoop stress and minimum stress approaches that need to be understood. Each has its own realm of applicability; they should not be considered interchangeable. Therefore, the next section explains in some detail the underlying assumptions behind hoop stress and minimum stress methods, and the areas of applicability for each. The remainder of this report then provide overviews of the hoop stress, minimum stress, and direct methods listed in Table 1.

2 Fracture Theories

2.1 Underlying Assumptions

The underlying assumptions behind hoop stress and minimum stress methods can best be explained by considering leak-off test behavior. For future reference, Fig. 1 shows the terminology that will be used to describe key points along a leak-off test curve.

Leak-off tests typically come in one of two types, as illustrated in Fig. 2. For the test in Fig. 2-a, leak-off occurs without breakdown, while in Fig. 2-b, leak-off and breakdown occur simultaneously. In situ stress tests using packers to isolate a portion of the wellbore, and laboratory hydraulic fracturing data typically look the curve in Fig. 2-b. Fig. 2-a looks more like a typical casing shoe leak-off test.

Fig. 3 compares an actual casing shoe leak-off test (LOT) with in situ stress test data from Daneshy, et. al., (1984). It can be seen that Stress Tests 2 and 3 look very similar to the LOT. The large difference between the pressure build-up curve for Stress Test 1 and the build-up curves for the other two cycles can be attributed to differences in the lengths of the cracks that were present at the start of each cycle.

Cracks present at the start of Stress Test 1 apparently were too short to cause a noticeable change in wellbore volume prior to breakdown. However, these cracks evidently went through a significant growth spurt during breakdown, because during Stress Test 2, they had sufficient volume to cause a break in the pressure build-up curve when leak-off occurred. The similarity between the pressure build-up curves for the LOT and Stress Test 2 suggests that pre-existing cracks for the LOT were significantly longer than the cracks present at the start of Stress Test 1.

Leak-Off Pressure (LOP)

- Point where slope deviates from initial straight-line pumping trend
- Where a fracture opens, starts taking fluid

Minimum Stress (MS)

- Pressure at which fracture starts closing during shut-in
- Corresponds to the minimum in situ stress
- Slope decrease reflects reduced rate of fluid loss as crack closes

Breakdown Pressure

- Point at which pressure starts dropping significantly while pumping
- Indicates unstable crack growth

Initial Shut-In Pressure (ISIP)

- Pressure recorded immediately after pump is stopped, well is shut-in

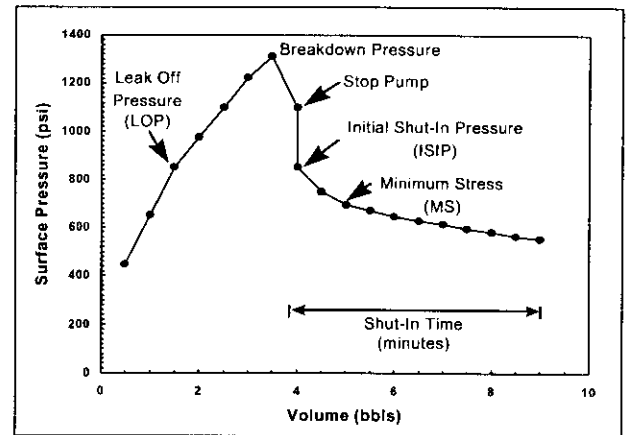


Fig. 1 - Leak-off test terminology.

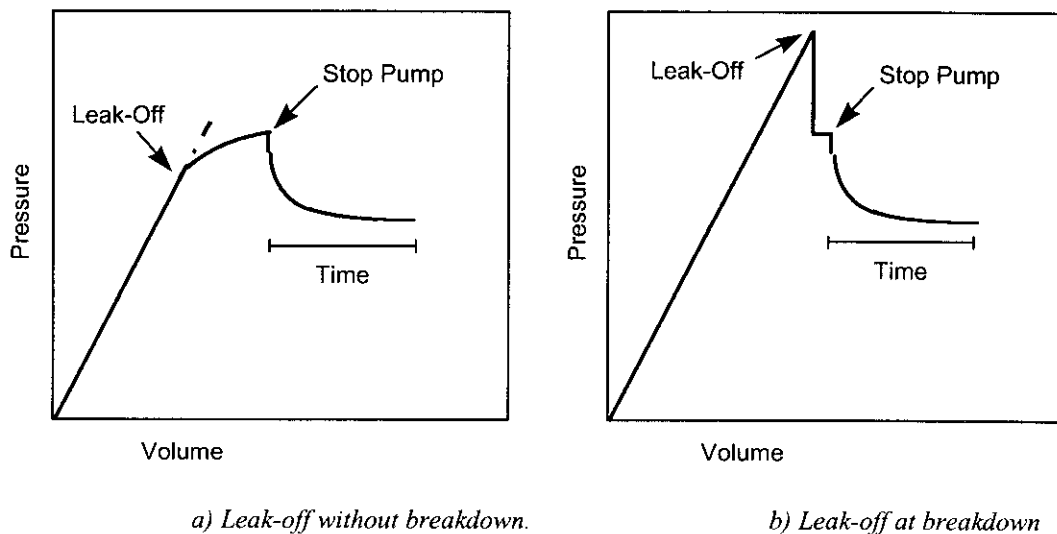


Fig. 2: Types of leak-off tests.

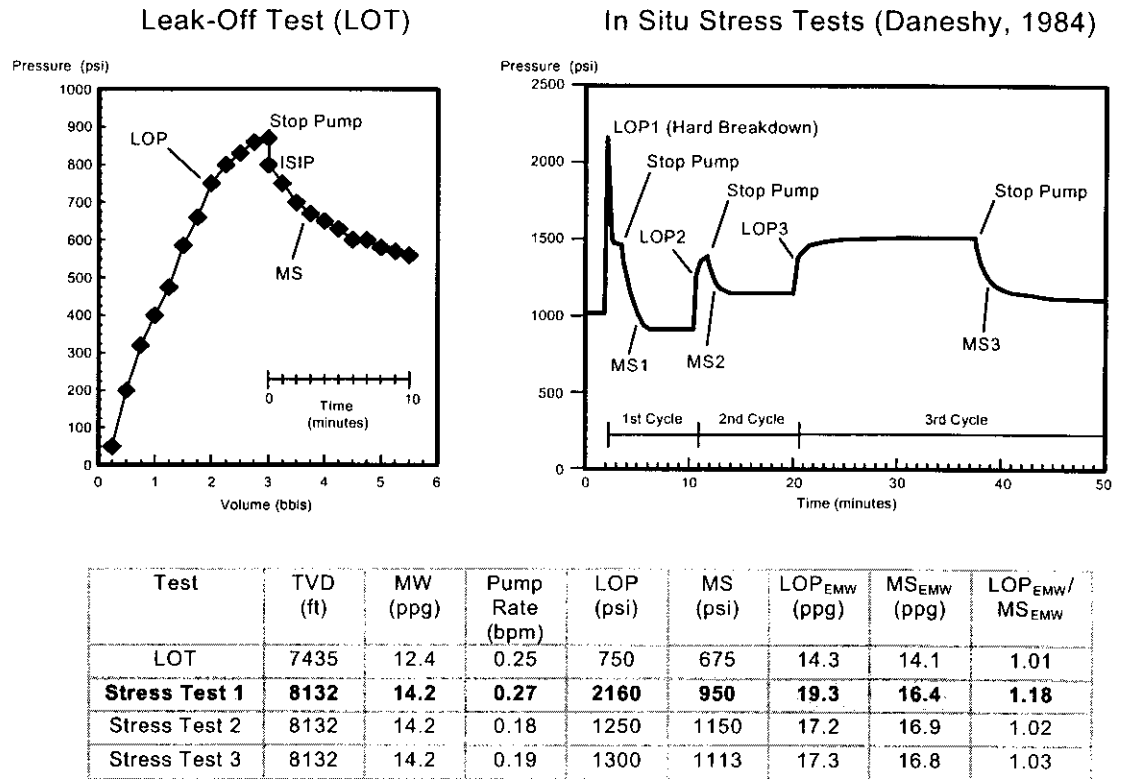


Fig. 3: Leak-off test vs in-situ stress test (Daneshy, et. al, 1994)

As will be discussed next, hoop stress methods assume that leak-off is highly sensitive to near wellbore-effects, which would be the case when pre-existing cracks are short. Minimum stress methods assume near wellbore effects are negligible, which is what would be expected with longer cracks. The last column of the table in Fig. 3 gives an indication of how much the leak-off pressures for the LOT and three stress tests were influenced by near-wellbore effects. Relative to the estimated in situ minimum stress, Stress Test 1 had a significantly higher leak-off pressure, which again suggests it had shorter pre-existing cracks.

To give some idea of the applicability of hoop stress and minimum stress methods, these approaches were used to estimate the fracture gradients for the LOT and stress tests in Fig. 3. The results are listed in Table 2. Here, PP, OB, MS, and FG are the pore pressure, overburden stress, minimum stress, and fracture gradients, respectively. The pore pressures were assumed to be 0.5 ppg less than the mud weights used. Overburden stresses were calculated from Eaton's (1972) Gulf Coast relation.

Minimum stress methods are normally calibrated to match leak-off pressures, but for this example, the fracture gradient was simply assumed to be the actual MS. The columns labeled "Case I", "Case II", and "Case III" were calculated from hoop stress solutions

that make different assumptions about the permeability of the wellbore and its pre-existing cracks (see next section):

- Case I: Impermeable wellbore wall, cracks impermeable when closed.
- Case II: Impermeable wellbore wall, cracks permeable when closed.
- Case III: Permeable wellbore, cracks permeable when closed.

In this particular instance, Case II yields the same fracture gradient predictions as the minimum stress method, but this will not always hold true. The measured fracture gradients are listed in bold, while the best fracture gradient predictions are highlighted in gray.

Test	TVD (ft)	PP (ppg)	OB (ppg)	MS (ppg)	FG (ppg)	Hoop Stress Fracture Gradient Estimates		
						Case I (ppg)	Case II (ppg)	Case III (ppg)
LOT	7435	11.9	18	14.1	14.3	16.3	14.1	15.2
Test 1	8132	13.7	18.1	16.4	19.3	19.1	16.4	17.75
Test 2	8132	13.7	18.1	16.9	17.2	20.1	16.9	18.5
Test 3	8132	13.7	18.1	16.9	17.3	20.1	16.9	18.5

Table 2 -Fracture gradient predictions for the LOT and in situ stress tests in Fig. 3.

The minimum stress approach does the best job of predicting fracture gradients for the three tests in which leak-off occurred without breakdown, but substantially underestimates the breakdown pressure for Test 1. At the other extreme, Case I provides an excellent estimate of the breakdown pressure for Test 1, but fails miserably at predicting the other leak-off pressures.

The bottom line is that none of these fracture gradient prediction methods were able to accurately predict all of the leak-off pressures in Table 2. At least two methods were needed. In general, hoop stress methods are best suited for predicting leak-off pressures for wellbores with short pre-existing cracks, where leak-off and break-down occur simultaneously (Fig. 2b). Minimum stress methods are more appropriate for wellbores with longer pre-existing cracks, where leak-off can occur without break-down (Fig. 2a).

2.2 Hoop Stress Approach

The starting point for all hoop stress methods is Kirsch's solution for the stresses in a plate with a circular hole (Volterra & Gaines, 1971). Kirsch solved this problem in 1898, and it was first applied in the field of hydraulic fracturing by Hubbert & Willis in 1957. As shown in Fig. 4, the act of replacing rock by drilling fluid disturbs the in situ stress field within a distance of about 3 wellbore radii of the wellbore.

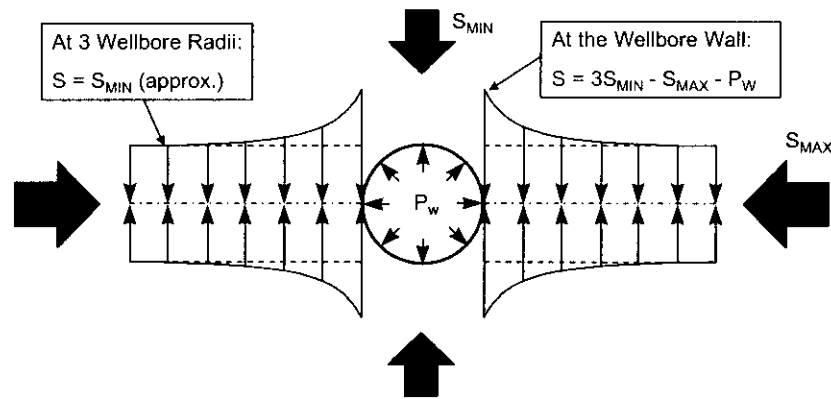


Fig. 4 - Kirsch's solution for stress concentration near a wellbore (Volterra & Gaines, 1971).

Whether or not fractures oriented parallel to the wellbore axis will open is governed by the stresses acting tangential to the wellbore wall, S_{θ} , termed *hoop stresses*. The minimum hoop stress S_{θ} (compression +) occurs where S_{θ} is parallel to the minimum in situ stress squeezing the wellbore (see Fig. 3), and equals

$$S_{\theta} = 3 S_{MIN} - S_{MAX} - P_w \quad (1)$$

where P_w is the wellbore pressure, and S_{MIN} and S_{MAX} are the minimum and maximum in situ stress acting perpendicular to the wellbore. In a tectonically relaxed environment, $S_{MIN} = S_{MAX} = S_h$ for a vertical well, while for a horizontal well, $S_{MIN} = S_h$, $S_{MAX} = S_v$, where S_h and S_v are the in situ horizontal and vertical stresses, respectively.

As can be seen from Eq. 1, increasing P_w decreases S_{θ} . Lost returns are predicted when the net hoop stress squeezing a crack along the wellbore wall reaches zero, which is why hoop stress methods are most appropriate for wellbores with short cracks. As a crack becomes longer, it becomes progressively less sensitive to the effects of the near wellbore region.

The wellbore pressure at which leak-off occurs depends upon both the permeability of the crack while closed, and the permeability of the wellbore wall. These effects can be bounded by three cases:

- Case I: Impermeable wellbore wall, cracks impermeable when closed.
- Case II: Impermeable wellbore wall, cracks permeable when closed.
- Case III: Permeable wellbore, cracks permeable when closed.

2.2.1 Case I - Impermeable Wellbore, Impermeable Closed Crack

Clamping of the crack faces by S_{θ} is opposed by the pressure of the fluid within the crack P_c . Therefore, the fracture will open when:

$$S_{\theta} - P_C = 3 S_{MIN} - S_{MAX} - P_W - P_C = 0 \quad (2)$$

In Case I, the fluid pressure within the crack is assumed equal to the in situ pore pressure, P_0 (see Fig. 5). This results in the following crack opening (fracture gradient) criteria:

$$P_W = 3 S_{MIN} - S_{MAX} - P_0 \quad (3)$$

This solution was first proposed by Hubbert & Willis (1957).

2.2.2 Case II - Impermeable Wellbore, Permeable Closed Crack

Case II assumes that the crack faces are rough, so that even when the crack is closed, it has sufficient permeability for its fluid pressure P_C to equalize with the wellbore pressure P_W (Fig. 6). Therefore, with $P_C = P_W$, Eq. 2 leads to the fracture criterion:

$$P_W = \frac{(3S_{MIN} - S_{MAX})}{2} \quad (4)$$

This equation can be obtained as an end-member of a more general solution derived by Haimson & Fairhurst for Case III.

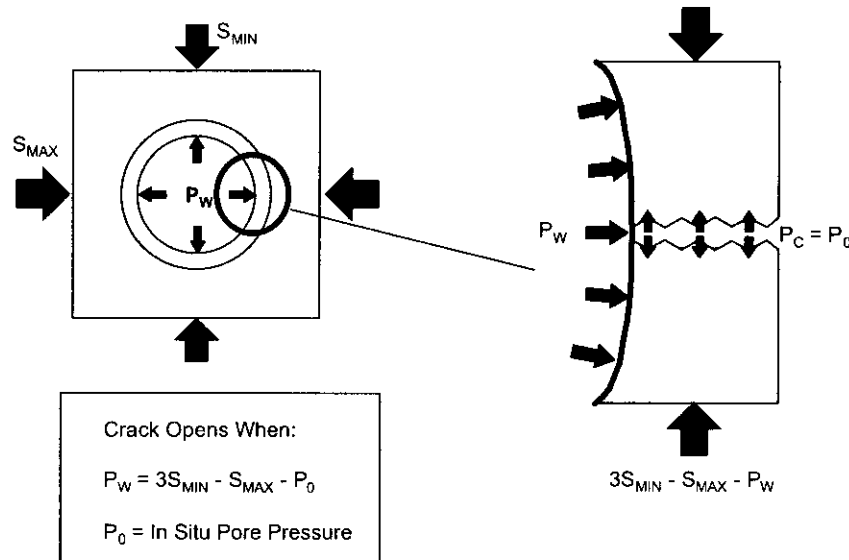


Fig. 5 - Fracture opening criteria for an impermeable wellbore, and impermeable closed crack (Hubbert & Willis, 1957).

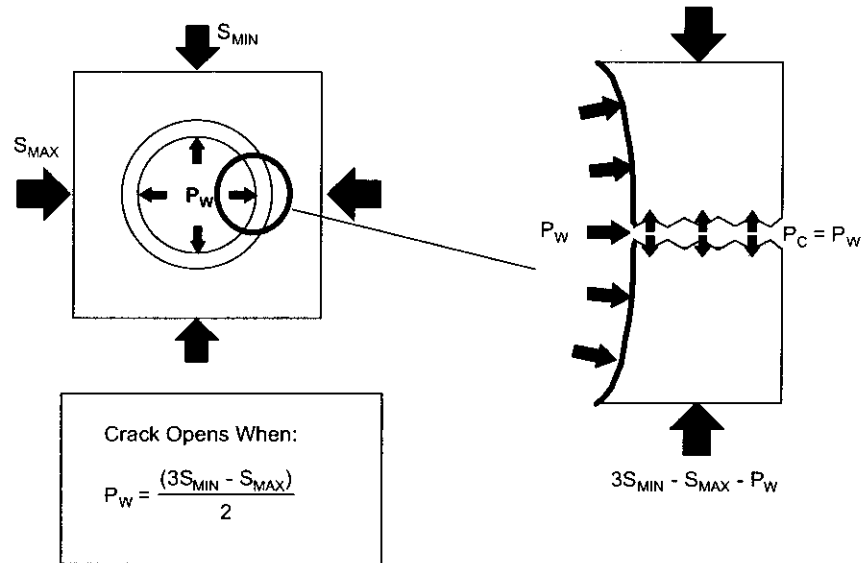


Fig. 6 - Fracture opening criteria for an impermeable wellbore, and permeable closed crack (Haimson & Fairhurst, 1970).

2.2.3 Case III - Permeable Wellbore, Permeable Closed Crack

Haimson & Fairhurst (1970) added a new twist to the Kirsch solution by incorporating the effects of drilling fluid invasion into the wellbore wall. Assuming the well was drilled somewhat overbalanced, invasion increases the pore fluid pressure just inside the wall (see Fig. 7). The increase in pore pressure from P_0 to P_W makes the rock along the wellbore try to expand, similar to what would happen if the wellbore were heated. Constraint by material ahead of the invasion front inhibits this expansion, which causes the hoop stress to increase. Again, this is similar to what would happen if the wellbore were heated.

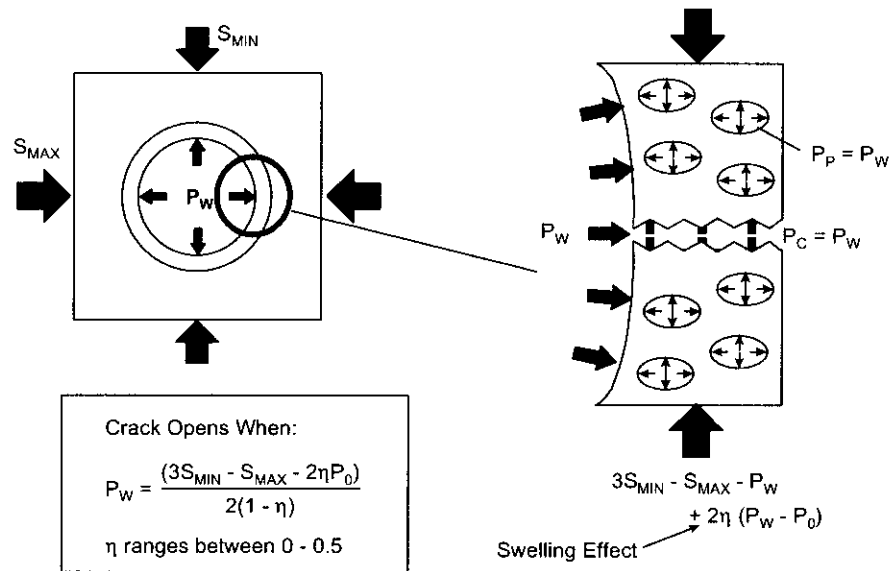


Fig. 7 - Fracture opening criteria for a permeable wellbore, and permeable closed crack (Haimson & Fairhurst, 1970).

This constrained swelling effect adds an additional compressive stress term to the Kirsch hoop stress relation (Eq. 2), with S_θ now equal to:

$$S_\theta = 3 S_{MIN} - S_{MAX} - P_W + 2\eta (P_W - P_0) \quad (5)$$

with

$$\eta = \frac{\alpha(1-2\nu)}{2(1-\nu)} \quad (6)$$

and where ν is Poisson's ratio, $\alpha = 1 - K/K_G$, K is the bulk modulus of the dry rock, and K_G is the bulk modulus of the rock grains. Since the pressure in the crack is also assumed to equal P_W , the Haimson & Fairhurst hydraulic fracturing criteria is:

$$P_W = \frac{(3S_{MIN} - S_{MAX} - 2\eta P_0)}{2(1-\eta)} \quad (7)$$

For impermeable rocks, $\eta = 0$, which reduces Eq. 7 to:

$$P_W = \frac{(3S_{MIN} - S_{MAX})}{2} \quad (8)$$

which is the same as the Case II fracture criterion. For highly compressible rocks, $\alpha = 1$, and Eq. 7 reduces to:

$$P_W = (1 - \nu) [2(S_{MIN} - P_0) - (S_{MAX} - S_{MIN})] + P_0 \quad (9)$$

2.3 Minimum Stress Approach

Hoop stress methods only predict when a fracture at the wellbore wall can open. However, they give no indication of what happens next. Will the crack suddenly take off, like Fig. 2b, or will it grow in a more controlled manner, like Fig. 2a? We can gain some insight on how the crack might grow by examining what the stress field looks like ahead of the crack at the moment it opens.

Fig. 3 compares fracture gradient predictions for hypothetical vertical and horizontal wells drilled in an area where the overburden stress S_v equals 1.3 times the horizontal stress S_h . The predicted fracture opening pressures for the case of a permeable fracture/impermeable wellbore wall, are:

Vertical well: $P_w = S_h$

Horizontal well: $P_w = 0.85 S_h$

We will postpone, for the moment, the question of what the stresses are at the crack tips, and focus on the stress fields the cracks will have to plow through if they are to grow.

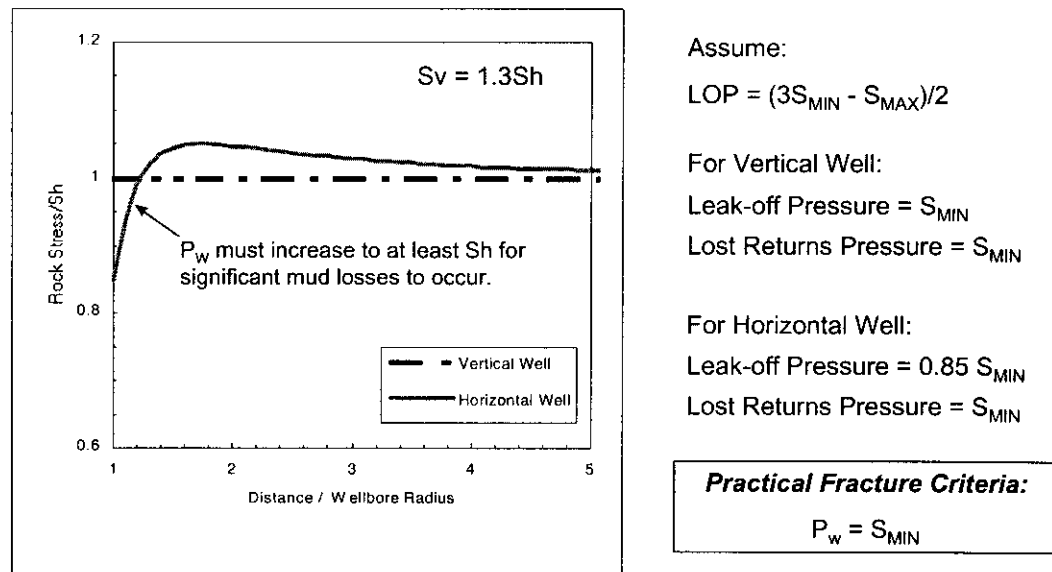


Fig. 8 - Stresses ahead of a crack at the moment $P_w =$ leak-off pressure.

For the vertical well, the pressure of the fluid in the crack just equals the horizontal stress S_h , so any slight increase in wellbore pressure should make the crack grow rapidly. With the horizontal well, however, the compressive stresses ahead of the crack increase significantly. Judging from the stress field, it seems reasonable that the wellbore pressure will have to increase to at least S_h , before rapid crack growth is possible. This same argument can be made anytime the predicted fracture gradient comes out less than the minimum in situ stress, which is the fundamental idea behind the minimum stress approach for estimating fracture gradients.

The above rationale is based upon elastic solutions for stresses near a wellbore, solutions that do not take into account the affect of the crack tip. The proper way to analyze this problem is with fracture mechanics. Fig. 9 presents the fracture mechanics solutions for crack length versus wellbore pressure for the two wells in Fig. 8. These results were calculated from the solution for a fully pressured crack given in the paper Abou-Sayed, et. al. (1978).

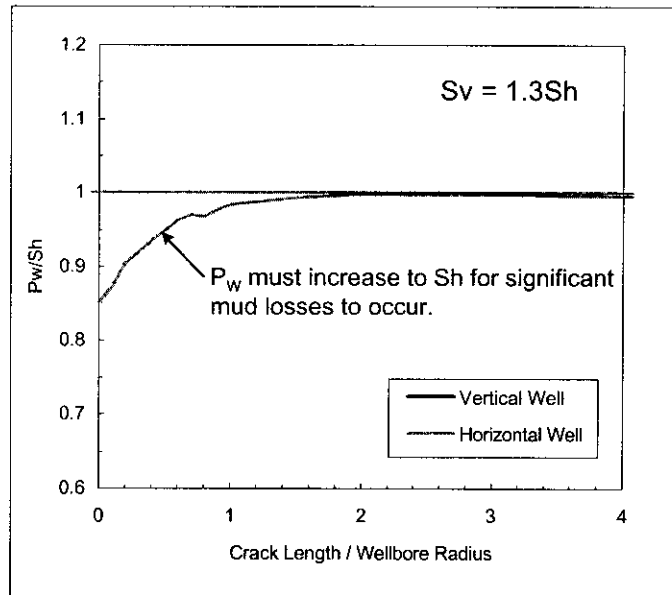


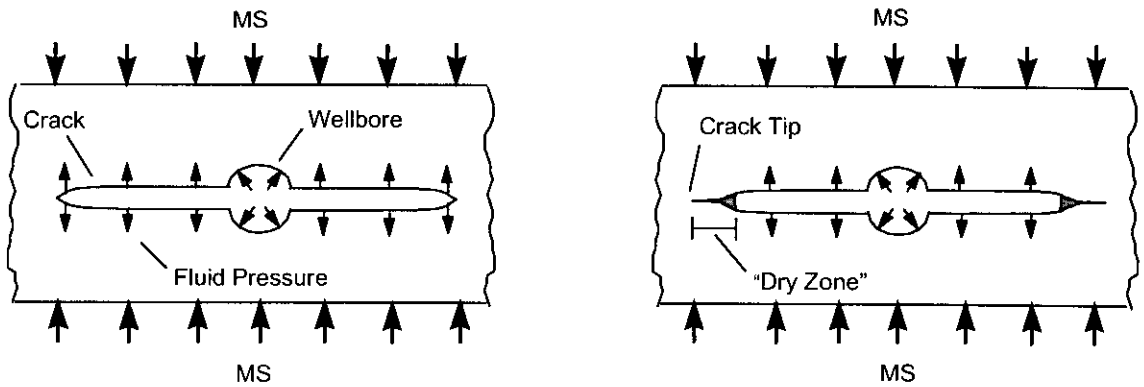
Fig. 9 - Crack length vs wellbore pressure for wells in Fig. 8.

It can be seen that fracture mechanics also predicts that the minimum in situ stress is a good, general lower bound for rapid crack growth/massive mud losses.

Fracture mechanics also explains why leak-off typically occurs at pressures greater than the minimum in situ stress. Theory predicts (Barenblatt, 1956), and laboratory observations confirm (Biot, 1981) that the tips of hydraulic fractures have the tapered "cusp" shape shown on the right side of Fig. 10. The width of the fracture becomes so narrow that it is impossible for fracturing fluid to reach the crack tip, leaving a so-called "dry zone". The existence of dry zones has been confirmed by Daneshy, et. al. (1984), who cored a hydraulically fractured wellbore.

Since the fluid pressure inside a crack with a dry zone acts over a smaller portion of the crack's surface than the minimum stress squeezing the crack closed (see Fig. 10), a wellbore pressure greater than the minimum stress is required to open the crack. Any additional effects that inhibit pressure communication along the crack (mud solids, clay swelling, etc.) will further boost the fracture extension pressure. To illustrate this point, the left side of Fig. 11 compares the pressure vs crack length relationships for the cases of a fully pressured crack, and a fully sealed crack (Rummel's approximate solution, 1987). In the first case, unlimited crack growth occurs when the wellbore pressure just equals the minimum stress. In the second, unstable crack growth does not occur.

The right side of Fig. 11 shows the effects of a more realistic dry zone that is 1% of the total crack length. This makes the fracture gradient about 2% higher than the minimum stress, similar to what observed in Fig. 3 for the LOT, and Stress Tests 2 and 3. This also brings out the point that pressure increases that occur after leak-off are entirely due to pressure losses along the crack.



Fully Pressured Crack

$LOP = MS$

- Assume crack fully conductive while closed.
- Wellbore pressure must still equal the minimum stress to open crack.

Partially Pressured Crack

$LOP > MS$

- Full communication inhibited by narrow, tapered crack shape, mud solids.
- Wellbore pressure must exceed the minimum stress to open crack.

Fig. 10 - Leak-off pressure (LOP) vs minimum in situ stress (MS).

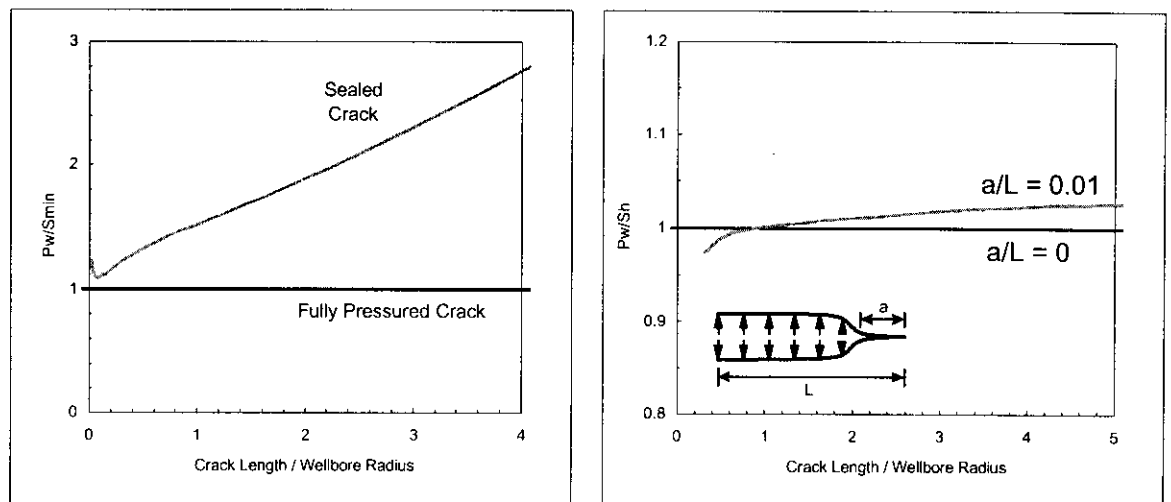


Fig. 11 -Effect of crack permeability on crack growth.

2.4 Conclusions

Hoop stress methods focus on when a small crack at the wellbore will open, but they give no indication of whether crack growth will be stable or unstable. In some instances, they may give excessively optimistic fracture gradient predictions, while in others they may be excessively low. Given the uncertainties in what crack lengths may be encountered while drilling a well, minimum stress methods are, in this author's opinion a better approach for predicting fracture gradients.

3 Minimum Stress Methods

All minimum stress methods considered in this report are based upon the following equation attributed to Hubbert & Willis (1957):

$$FG = K(OB-PPG) + PPG \quad (10)$$

where

- FG = the fracture gradient
- OBG = the overburden gradient
- PPG = pore pressure gradient
- K = the effective stress ratio, also termed the matrix stress coefficient

Differences among the methods are due to the way in which the effective stress ratio is determined. K can be locally calibrated with FG's measured in leak-off tests using the relation

$$K = \frac{(FG-PPG)}{(OBG-PPG)} \quad (11)$$

3.1.1 Hubbert & Willis

Hubbert & Willis (1957) used the following relation for K :

$$K = \frac{(1-\sin\theta)}{(1+\sin\theta)} \quad (12)$$

where θ is the internal friction angle of the rock. In their paper, they assumed $\theta = 30^\circ$, which results in a value of $K = 0.33$.

Their stress ratio relation represents the theoretical lower bound for K, known in soil mechanics as the *coefficient of active stress* " K_a " (Lambe & Whitman, 1969). It defines the lowest value the horizontal stress can be without normal faults developing in a flat-lying formation. In tectonically relaxed areas, K is typically much larger than K_a .

3.1.2 Matthews & Kelly

Matthews & Kelly (1967) assume K (what they called the “matrix stress coefficient”) to be a function of the vertical effective stress. This point is often overlooked, because their paper shows matrix stress coefficient plotted as a function of depth. However, Matthews & Kelly (M&K) intended these curves to be used as K “normal trend” lines. The effective stress corresponding to the K value at any given depth is calculated by assuming a 1 psi/ft overburden gradient, and a 0.465 psi/ft normal pressure gradient, which means

$$\sigma = S_v - P_N = 1 \times \text{TVD} - 0.465 \times \text{TVD} = 0.535 \times \text{TVD} \quad (13)$$

where σ and S_v are the effective, and total overburden stresses, respectively, and P_N is normal pore pressure at that depth.

M&K’s procedure for finding K at any depth at any pore pressure is as follows:

Compute the pore pressure at the depth of interest.

Use a 1 psi/ft overburden stress gradient to find the effective stress σ .

Use Eq. 13 to find the depth TVD_N where that effective stress would occur in normal pressure (the *equivalent depth*):

$$\text{TVD}_N = \frac{\sigma}{0.535} \quad (14)$$

Pick the stress ratio at that depth from the appropriate normal trend curve.

Fig. 12 shows graphically, how K is being determined.

Local overburden gradients can easily be taken into account by using the correct overburden stress to compute σ in Step 2. Eq. 14 would still be used to find TVD_N , because it is the link that ties σ to the K vs effective stress relation that is hidden behind M&K’s K vs equivalent depth curves. It should be pointed out, however, that M&K never intended their stress ratio curves to be used generically. They emphasized that: “Actual fracture data for an area are therefore needed before a depth-versus-K curve can be drawn there”.

When developing locally calibrated effective stress relations, it is recommended that the equivalent depth portion of the M&K method be by-passed. In other words, develop a stress ratio vs effective stress relation, instead of working through stress ratio vs depth normal trend curves.

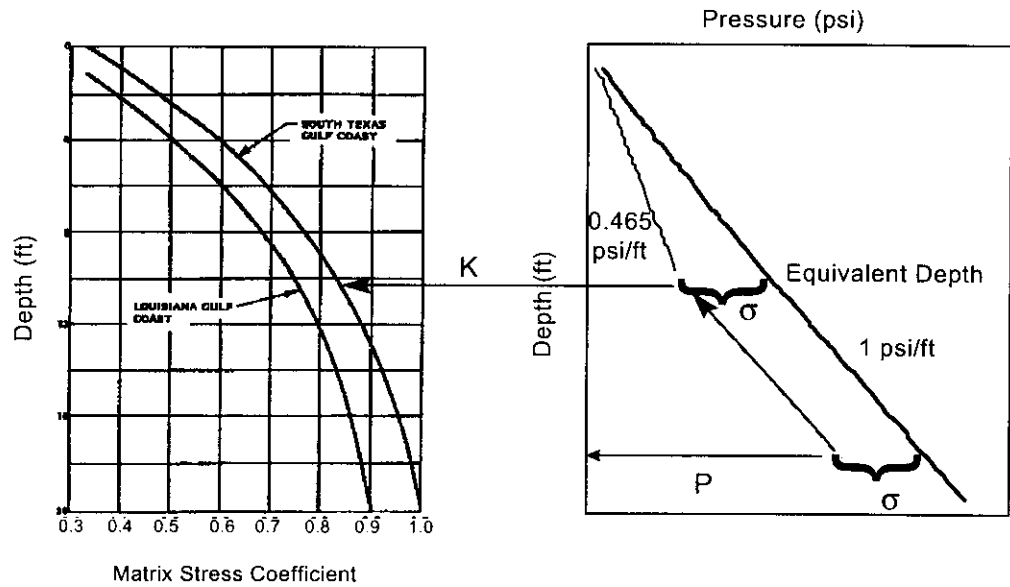


Fig. 12 - Matthews & Kelly method.

3.1.3 Pennebaker

Pennebaker (1968) presents one stress ratio vs depth curve that is assumed to apply everywhere (Fig. 13). Locally calibrated K vs depth relations are basically a generalized version of Pennebaker's method. As discussed previously, such curves are often mislabeled "Matthews & Kelly" curves.

In his paper, Pennebaker (1968) observes that K could depend upon depth, geologic age, and location, but "... it is believed that overburden gradient, which in itself influenced by geologic age, is the controlling factor". Given this belief, and the fact that he presents several overburden stress vs depth relations tied to geologic ages (see Fig. 13), it is somewhat surprising that he decided to use only one K vs depth curve.

Pennebaker's method is well suited for local calibration.

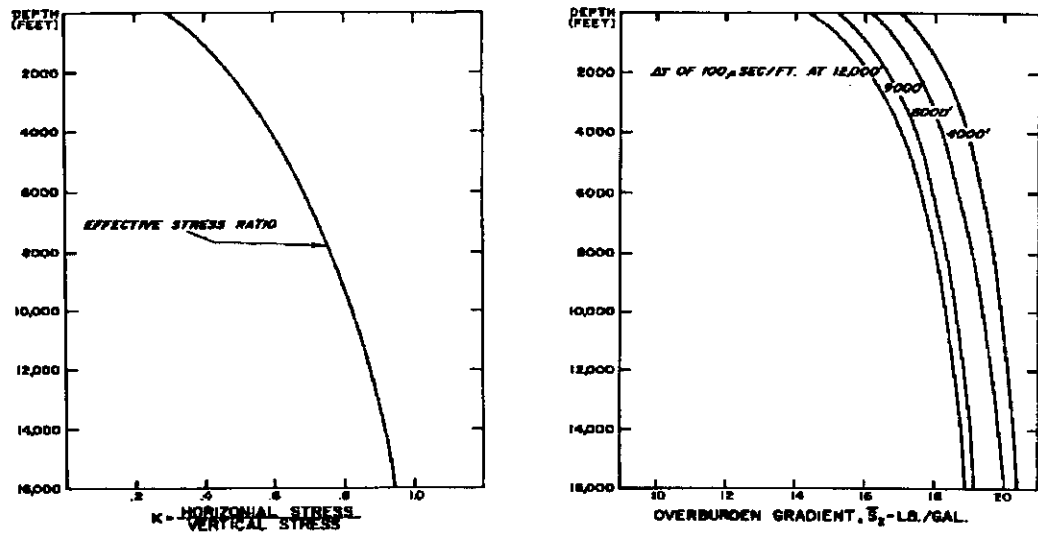


Fig. 13 -Pennebaker's (1968) stress ratio and overburden gradient curves.

3.1.4 Eaton

Eaton's method (1969) appears to have evolved from a misunderstanding of Hubbert & Willis' (1957) paper. As previously discussed, Hubbert & Willis used a soil mechanics relation involving the angle of internal friction for K, which for a 30° friction angle, comes out with $K = 0.33$. However, this represents a *lower bound* on the possible values for K.

A value of $K=0.33$ can also be obtained through an equation from elasticity theory that defines the horizontal compression that is generated when a formation squeezed vertically is prevented from elastically expanding laterally:

$$K = \frac{\nu}{1-\nu} \quad (15)$$

where ν is Poisson's ratio. Hubbert & Willis stress ratio of $K=0.33$ can be matched with Eq. 15 by setting $\nu = 0.25$. Eaton apparently concluded this is how Hubbert & Willis obtained their K value, and used this equation as the basis for his fracture gradient prediction method. And this method remains one of the most widely used approaches in the industry.

In applying this approach, it is crucial to realize that Eq. 15 cannot be applied too literally. Since sediments deform plastically when they are compacted, the amount of horizontal compression generated during burial is greater than elasticity theory would predict. Consequently, using "true" elastic Poisson's ratios in Eq. 15 can cause Eaton's method to significantly underestimate fracture gradients.

Dynamic Poisson's ratios calculated from shear and compressional velocity data can come out significantly higher than static values, particularly in shales. This is because the dynamic Poisson's ratio of a compressible, low permeability rock such as shale is dominated by pore water effects ($\nu=0.5$ for water). Therefore, while dynamic Poisson ratios may produce reasonable looking K values, the results very often have nothing to do with reality.

To make Eaton's method work, fictitious Poisson's ratios, backed out from leak-off test data must be used. First K is determined from Eq. 11, and then ν is calculated from the relation:

$$\nu = \frac{K}{1+K} \quad (16)$$

This is done at as many leak-off test points as possible, and then a ν vs depth relation is fit. In the absence of leak-off test data, Eaton & Eaton (1997) published two analytical relations for ν as a function of depth below mudline (TVD_{BML}):

Gulf Coast

for $0 \leq \text{TVD}_{\text{bml}} \leq 4,999.9$

$$\nu = -7.5 \times 10^{-9} \times (\text{TVD}_{\text{BML}})^2 + 8.0214286 \times 10^{-5} \times (\text{TVD}_{\text{BML}}) + 0.2007142857$$

for $5000 \leq \text{TVD}_{\text{bml}}$

$$\nu = -1.7728 \times 10^{-10} \times (\text{TVD}_{\text{BML}})^2 + 9.4748424 \times 10^{-6} \times (\text{TVD}_{\text{BML}}) + 0.3724340861 \quad (17)$$

Deep Water Gulf of Mexico

for $0 \leq \text{TVD}_{\text{bml}} \leq 4,999.9$

$$\nu = -6.089286 \times 10^{-9} \times (\text{TVD}_{\text{bml}})^2 + 5.7875 \times 10^{-5} \times (\text{TVD}_{\text{bml}}) + 0.3124642857$$

for $5000 \leq \text{TVD}_{\text{bml}}$

$$\nu = -1.882 \times 10^{-10} \times (\text{TVD}_{\text{bml}})^2 + 7.2947129 \times 10^{-6} \times (\text{TVD}_{\text{bml}}) + 0.4260341387 \quad (18)$$

In comparison to the Pennebaker method, which works directly with stress ratio, Eaton's method is considerably more cumbersome to apply. Poisson's ratios computed from effective stress ratios are used to calculate effective stress ratios. A lot of extra, unnecessary work. If calibrated with the same leak-off test data, the Pennebaker and Eaton approaches should produce the same results.

3.1.5 Christman

Christman's paper (1973) may be best remembered for its discussion on the effect of water depth on offshore fracture gradients. However, he also described two techniques he had developed for predicting stress ratios from offset well data. One approach was a Pennebaker-type stress ratio vs depth function. However, he also reported good success tying stress ratio to bulk density, as shown below.

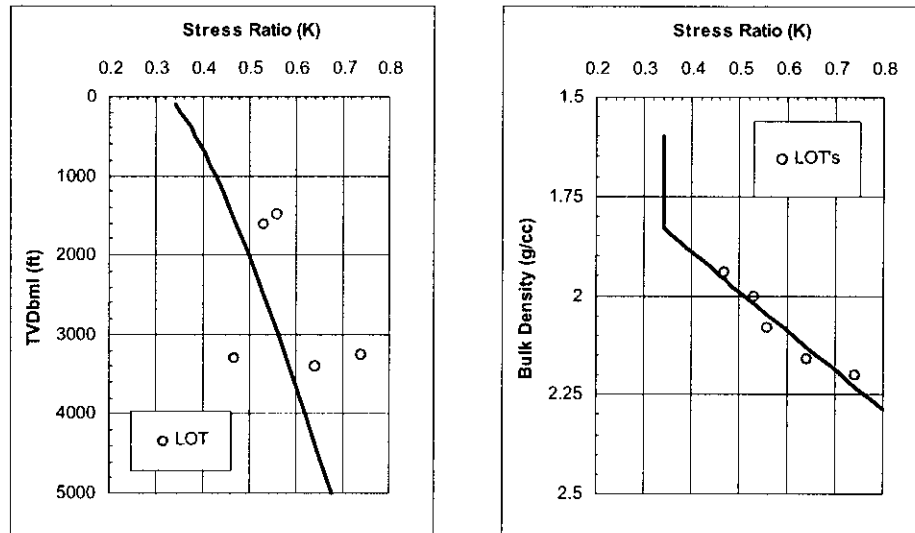


Fig. 14 - Christman's method (1973) for estimating stress ratios in the Santa Barbara Channel.

3.1.6 Pilkington

Pilkington (1978) used stress ratio data obtained from the papers of Matthews & Kelly (1967), Pennebaker (1968), Eaton (1969), and Christman (1973) to come up with an "average" stress ratio relation for Tertiary basins. In doing so, Pilkington adjusted Matthews & Kelly's stress ratio curve so that it would be applicable with Eaton's Gulf Coast overburden stress relation. He did this by requiring that at any give depth, the effective horizontal stress for normal pressure must be the same, whether calculated with a 1 psi/ft overburden gradient, or Eaton's relation. For a 0.465 psi/ft normal pressure gradient, this implies

$$K_{\text{Orig}} (1-0.465) * \text{TVD} = K_{\text{New}} (\text{OBG} - 0.465) * \text{TVD}$$

or

$$K_{\text{new}} = K_{\text{Orig}} \frac{.535}{\text{OBG} - 0.465} \quad (19)$$

where K_{Orig} is the original stress ratio at that depth, K_{new} is the new value, and OBG is the overburden gradient that would be calculated from Eaton's overburden stress relation.

Pilkington further found that his average effective stress ratio distribution could be expressed as the following functions of overburden stress gradient, in psi/ft:

for $\text{OBG} \leq 0.94$

$$K = 3.9 * \text{OBG} - 2.88$$

for $\text{OBG} > 0.94$

$$K = 3.2 * \text{OBG} - 2.224 \quad (20)$$

3.1.7 Daget & Parigot

Daget & Parigot (1979) recognized that the (OBG-PP) term in Eq. 10 could be expressed in terms of sonic travel time, overburden gradient, and normal pressure gradient through the Eaton equation (1975) for pore pressure estimation:

$$(\text{OBG-PPG}) = (\text{OBG-PPG}_N) \left(\frac{\Delta t_N}{\Delta t} \right)^E \quad (21)$$

where Δt is the measured interval transit time, Δt_N is the normal trend value at that depth, and E is the Eaton exponent, typically equal to 3. Eq. 10 and 21 then result in the following fracture gradient relation:

$$\text{FG} = \text{OBG} - (1-K)(\text{OBG-PPG}_N) \left(\frac{\Delta t_N}{\Delta t} \right)^E \quad (22)$$

They chose to define a new parameter “ ψ ”, where

$$\psi = (1-K) (\Delta t_N)^E \quad (23)$$

so that Eq. 22 can be re-written as:

$$\text{FG} = \text{OBG} - (\text{OBG-PPG}_N) \left(\frac{\psi}{(\Delta t)^E} \right) \quad (24)$$

Therefore, Daget & Parigot’s method centers around developing a relation for ψ as a function of depth. This approach combine pore pressure and fracture gradient estimation into one operation.

For calibration purposes, we need to know OBG, PPG_N , and Δt at each depth where the FG has been determined from leak-off tests or lost returns incidents. Eq. 24 can then be inverted to solve for the value of ψ at that depth, using the following equation:

$$\psi = \frac{(\text{OBG-FG})}{(\text{OBG-PPG}_N)} (\Delta t)^E \quad (25)$$

The ψ data points are then plotted versus depth, and fit with a curve. Daget & Parigot recommend a semi-log relation, of the form:

$$\ln(\psi) = A(\text{TVDbml}) + B \quad (26)$$

3.1.8 Daines

Daines (1982) proposed adding a second term to Eaton’s effective stress ratio relation:

$$K = \frac{\nu}{1-\nu} + \beta \quad (27)$$

where β is a lithology-independent parameter that is supposed to account for tectonic effects. Poisson’s ratio is obtained from a table of recommended values (see Tables 3a, 3b below), while β is backed out from leak-off tests using the following relation:

$$\beta = \frac{(FG-PPG)}{(OBG-PPG)} - \frac{v}{1-v} \quad (28)$$

where v corresponds to the lithology the LOT was performed in (typically shale).

In reality, Daines' " β " term in most cases is a correction factor that has to be introduced because he used real elastic Poisson's ratios to compute K , instead of fictitious ones. However, the bottom line is that he did figure out a way to make Eaton's method work. And Daines' Eq. 27 is intriguing, because it provides a way to take stress ratios determined from leak-off test data in one lithology, and predict what they would be in another. In other words, for lithologies "1" and "2", we require:

$$K_2 - \frac{v_2}{1-v_2} = K_1 - \frac{v_1}{1-v_1} = \beta \quad (29)$$

so

$$K_2 = K_1 + \frac{v_2}{1-v_2} - \frac{v_1}{1-v_1} \quad (30)$$

Lithology	v	Lithology	v
Clay, very wet	0.50	Limestone	
Clay	0.17	fine, micritic	0.28
Conglomerate	0.20	medium, calcarenitic porous	0.31
Dolomite	0.21	stylolitic	0.27
Siltstone	0.08	fossiliferous	0.09
Slate	0.13	bedded fossils	0.17
Tuff	0.34	shaley	0.17
Greywacke			
coarse	0.07		
fine	0.23		
medium	0.24		

Table 3a - Daines' suggested Poisson's ratios.

Lithology	v	Lithology	v
Sandstone		Shale	
coarse	0.05	calcareous	0.14
coarse, cemented	0.10	(<50%CaCo3)	
fine	0.03	dolomitic	0.28
very fine	0.04	siliceous	0.12
poorly sorted, clayey	0.06	silty (<70% silt)	0.17
fossiliferous	0.24	sandy (<70% sand)	0.12
	0.01	kerogenaceous	0.25

Table 3b- Daines' suggested Poisson's ratios - continued.

3.1.9 Brennan & Annis

Brennan & Annis (1984) developed a relation between the effective fracture gradient (FG-PPG), and the effective overburden gradient (OBG-PPG) for wells in the Western and Central Gulf of Mexico. They used leak-off tests from wells in water depths ranging from 50' up to 1200'. Their curve has the general form (see Fig. 15)

$$= -A X^2 + B X \quad (31)$$

where

Y = FG-PPG (psi/ft)

X = OBG-PPG (psi/ft)

For their data, Brennan & Annis found:

A = 1.40, B = 1.35 (gradients datumed to sea level)

Brennan & Annis used depth below sea level to compute gradients, so this must be accounted for when calculating fracturing gradients. First, depth below sea level is used to find an X value from the estimated overburden stress and pore pressure. A Y value is then calculated from Eq. 31. If the datum is sea level, the fracture gradient is simply

$$FG_{BSL} = PPG_{BSL} + Y \quad (32)$$

If the datum is the kelly bushing, the predicted fracture gradient is

$$FG_{RKB} = PPG_{RKB} + Y \frac{TVD_{BSL}}{TVD_{RKB}} \quad (33)$$

I have found that the Brennan & Annis relation can be applied over a wider range of water depths if all gradient are datumed to the mudline. The formulas for converting any gradient "GRD" (psi/ft.) from kelly bushing to mud line, and vice-versa, are as follows:

RKB to Mudline

$$GRD_{BML} = \frac{(TVD_{RKB} \times GRD_{RKB} - 0.444 \times WD)}{TVD_{BML}} \quad (34)$$

Mudline to RKB

$$GRD_{RKB} = \frac{(TVD_{BML} \times GRD_{BML} + 0.444 \times WD)}{TVD_{RKB}} \quad (35)$$

where WD is water depth. For X and Y datumed to mudline, the coefficients for Brennan & Annis' Gulf of Mexico data are:

$$A = 1.328, B = 1.323 \quad (\text{Gradients datumed to mudline})$$

Fig. 15 shows their data referenced to mudline. One aspect of Brennan & Annis' relation that makes it unique relative to most other fracture gradient methods is that it can predict fracture gradients higher than the overburden gradient.

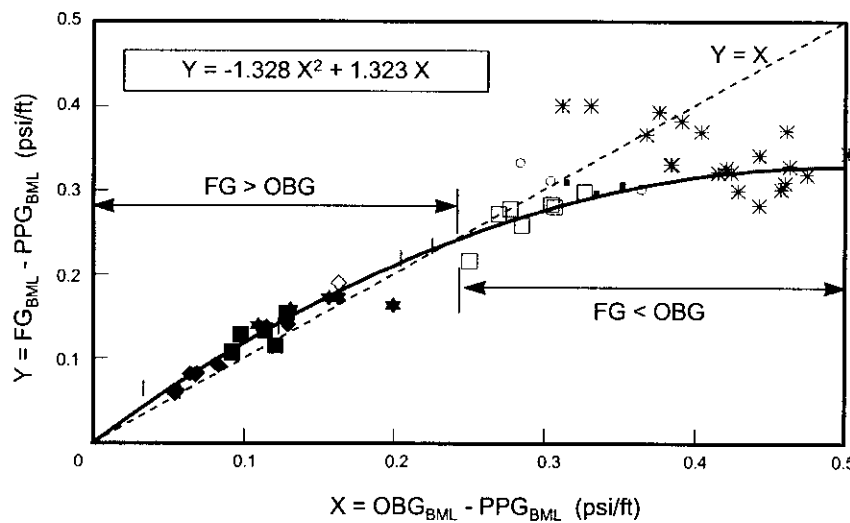


Fig. 15 -Gulf of Mexico effective fracture gradient vs effective overburden gradient relation; Brennan & Annis' data re-datumed to depth below mudline.

3.1.10 Zamora

Zamora (1989) presented the following set of generalized relations for estimating overburden stress and effective stress ratios:

Overburden Stress:

$$OBG \text{ (ppg)} = \frac{8.5 \times WD + (C_3 + AC_4)X(TVD_{BML})^{1+X}}{TVD_{RKB}} \quad (36)$$

Effective Stress Ratio:

$$K = M[1.0 - C_5 \exp(C_6 TVD_{BML})] \quad (37)$$

where WD is water depth, TVD_{BML} is true vertical depth below mudline (both in feet), A and M are locally calibrated, and parameters C_1 - C_6 , and X are listed below in Table 4.

Parameter	Value
C1	1.034
C2	0.03
C3	8.03
C4	0.232
C5	0.55
C6	-0.000134
X	0.075

Table 4 - Constants C_1 - C_6 , and X , for Zamora's method.

For the GOM, Zamora recommends a default M value of 1.0; for older formations, $M = 0.3$ - 0.5 is thought to be better. Zamora claims that $A = 4.0$ does a good job of matching Eaton's overburden stress relation. Expected ranges for A for different geologic ages are listed in Table 5.

Zamora also included sample "A" and "M" values for different parts of the U.S., which are summarized in Table 6.

A Range (MYA)	Geologic Age
0-5	Holocene - Pliocene
5-9	Miocene - Oligocene
9-10	Eocene - Paleocene
10-11	Cretaceous - Triassic
11-14	Permian - Older

Table 5 - Overburden stress coefficient "A" ranges by geologic age.

Area	A	M	Area	A	M
Alabama, Mobile Bay	6-7	1.0	New Mexico, northwest	10-11	0.45
Alaska	9-10	0.9	North Sea (Gullfaks)	7-10	1.0
Atlantic Coast (offshore)	9-10	0.7	Oklahoma	7-10	0.39
California (offshore)	6	1.0	Rocky Mountains	11	0.4
California (onshore)	7	1.0	Texas (Austin Chalk)	9	1.0
California (Sacramento)	8-9	1.0	Texas, north	12-13	0.4
Gulf Coast (Eaton equiv.)	4	1.0	Texas, south (offshore)	4-6	1.0
Louisiana (offshore)	3-5	1.0	Texas, south (onshore)	6-8	1.0
Mississippi (Smackover)	10.5	0.34	Texas, west	12-13	0.4

Table 6 - Sample "A" and "M" parameters for Zamora's method.

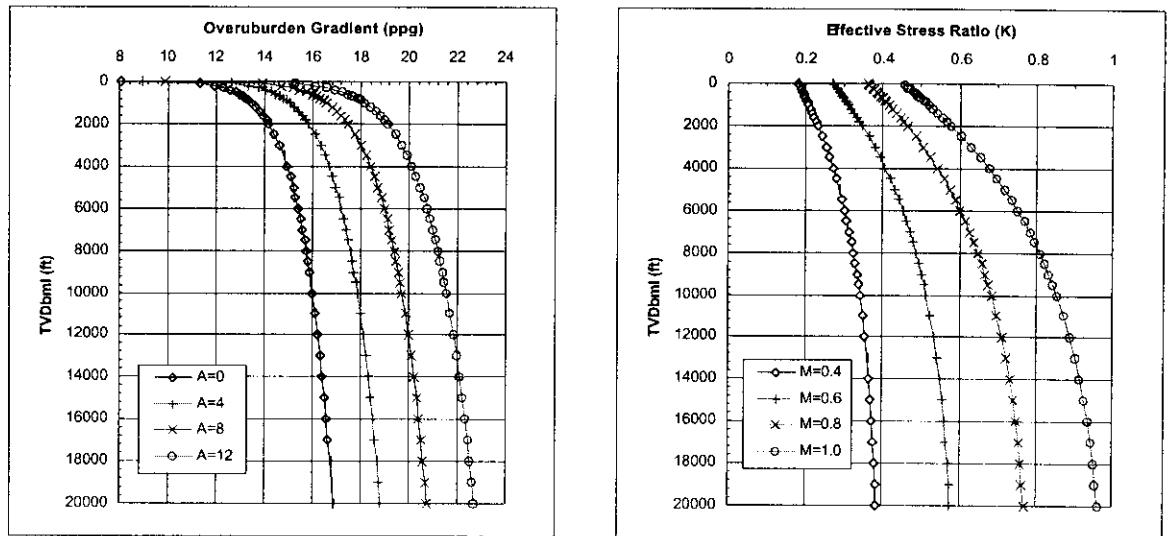


Fig. 16 - Example of Zamora's general relationships for overburden gradient, effective stress ratio. All quantities datumed to mud line.

3.1.11 Simmons & Rau

Simmons & Rau (1988) presented generic relations for estimating overburden stress and effective stress ratios in deepwater. Their method is based upon the idea that sediments at any given depth below mudline will be *more* compacted in deepwater than they would be in shallower water. To account for this effect, they introduce a factor called the *effective sediment depth* D_{eq} , which is calculated from water depth (WD) using either one of the following equations:

$$D_{eq} \text{ (ft)} = 1.489554 \times 10^{-5} + \frac{1}{\frac{1.911364}{WD} - \frac{2.703024}{WD^2}} \quad (38)$$

$$D_{eq} \text{ (ft)} = \frac{WD}{2} \quad (39)$$

D_{eq} is added to actual depth below mudline (TVD_{BML}) to obtain a new depth parameter called *effective sediment penetration depth* D_{eff} :

$$D_{eff} \text{ (ft)} = TVD_{BML} + D_{eq} \quad (40)$$

which is then used in the following relations for overburden stress (S_v) and effective stress ratio (K):

$$S_v \text{ (psi)} = 0.444 \text{ WD} + TVD_{BML} \times 0.8511934 \times \exp\left(\frac{(\ln(D_{eff}) - 6.206593)^2}{84.36084}\right) \quad (41)$$

$$K = 0.05329427 \times (0.999996)^{D_{eff}} \times (D_{eff})^{0.3006479} \quad (42)$$

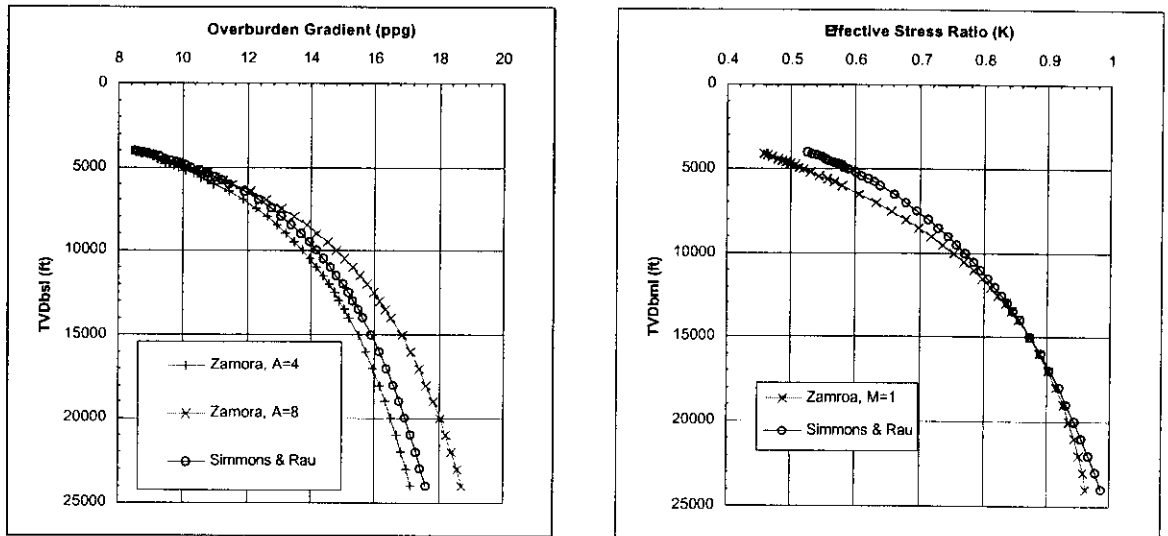


Fig. 17 - Comparison of Zamora's (1989) and Simmons and Rau's general relations for overburden gradient, effective stress ratio stress ratio. Assumed water depth of 4000'.

3.1.12 Singh & Emery

Singh & Emery's paper (1998) describes a method for predicting fracture gradients in depleted sands. Their approach consists of two parts. First, they present a way to estimate effective stress ratios in sands at virgin reservoir conditions from effective stress ratios determined in shales. They assume that K for any lithology can be written as the product of two factors:

$$K = K_C \left(\frac{v}{1-v} \right) \quad (43)$$

where v is Poisson's ratio, and K_C is a lithology-independent factor. At any given depth, sands and shales are both forced to satisfy the relation:

$$K_C = \frac{K_{shale}}{\left(\frac{v_{shale}}{1-v_{shale}} \right)} = \frac{K_{sand}}{\left(\frac{v_{sand}}{1-v_{sand}} \right)} \quad (44)$$

which means K_{sand} can be written in terms of K_{shale} , v_{sand} , and v_{shale} as follows:

$$K_{sand} = K_{shale} \left(\frac{v_{sand}}{1-v_{sand}} \right) \left(\frac{1-v_{shale}}{v_{shale}} \right) \quad (45)$$

They assume end member Poisson's ratios of $v_{qtz} = 0.125$ for clean sand, and $v_{shale} = 0.25$ for pure shale. For shaley sands, they compute v_{sand} from Gamma ray readings, using the relation:

$$v_{sand} = (1-f_{sh}) v_{qtz} + f_{sh} v_{shale} \quad (46)$$

with f_{sh} equal to:

$$f_{sh} = \frac{(GR - GR_{qtz})}{(GR_{shale} - GR_{qtz})} \quad (47)$$

Singh & Emery suggest values of 10 and 80 for GR_{qtz} and GR_{shale} , respectively.

The above relations are assumed to apply for sands at virgin reservoir conditions. The fracture gradient in drawn-down sands is determined using a depleted sand fracture gradient relation developed by Salz (1977), which can be written as:

$$FG_{depleted} = FG_{virgin} * \exp[-0.57 * (P_{initial} - P_{final})] \quad (48)$$

where $P_{initial}$ and P_{final} are the initial and final reservoir pressure gradients, in psi/ft.

3.1.13 Holbrook, Maggiori, & Hensley

Holbrook, Maggiori, & Hensley (1995) assume that K is related to fractional porosity ϕ by the simple relation:

$$K = (1 - \phi) \quad (49)$$

4 Hoop Stress Methods

The equations used by hoop stress methods fall into one of the three categories discussed in the section on fracture theories. For convenience, each case, and its associated equation for calculating the onset of wellbore fracturing are listed below:

Case I - Impermeable wellbore, permeable closed crack

$$P_w = 3 S_{MIN} - S_{MAX} - P_0 \quad (3)$$

Case II - Impermeable wellbore, impermeable closed crack

$$P_w = \frac{(3S_{MIN} - S_{MAX})}{2} \quad (4)$$

Case III - Permeable wellbore, permeable closed crack

$$P_w = \frac{(3S_{MIN} - S_{MAX} - 2\eta P_0)}{2(1-\eta)} \quad (7)$$

where

$$\eta = \frac{\alpha(1-2\nu)}{2(1-\nu)}, \quad \alpha = \left(1 - \frac{K}{K_G}\right)$$

ν is the "true" Poisson's ratio of the rock (not an Eaton value), $\alpha = 1 - K/K_G$, K is the bulk modulus of the dry rock, K_G is the bulk modulus of the rock grains, and S_{min} and S_{max} are the minimum and maximum in situ stresses that act perpendicular to the wellbore axis.

For $\eta = 0$:

$$P_w = \text{Eq. 4}$$

For $\alpha = 1$:

$$P_w = (1 - \nu) [2(S_{MIN} - P_0) - (S_{MAX} - S_{MIN})] + P_0 \quad (9)$$

4.1.1 Hubbert & Willis

Hubbert & Willis (1957) considered the pressure required to open both short and long cracks. Their long crack solution is Eq. 10. For short cracks, they assumed the wellbore and cracks were both impermeable (Eq. 3), which implies a fracture gradient of:

$$FG = \left(\frac{P_w}{TVD}\right) = \left(\frac{3S_{MIN} - S_{MAX}}{TVD}\right) - PPG \quad (50)$$

For vertical wells in a tectonically relaxed basin, $S_{MIN} = S_{MAX} =$ the in situ horizontal stress, S_u and

$$FG = 2 \left(\frac{S_h}{TVD}\right) - PPG \quad (51)$$

For horizontal wells in a tectonically relaxed basin, $S_{MIN} = S_h$, and $S_{MAX} =$ the overburden stress S_v , so:

$$FG = \left(\frac{3S_h - S_v}{TVD} \right) - PPG \quad (52)$$

4.1.2 Haimson & Fairhurst

Haimson & Fairhurst (1970) were the developers of Eq. 7, so for the most general case (permeable wellbore, permeable cracks), their fracture gradient relation would be:

$$FG = \frac{(3S_{MIN} - S_{MAX} - 2\eta P_0)}{2TVD(1-\eta)} \quad (53)$$

For vertical and horizontal wells in a tectonically relaxed environment,

Vertical Well

$$FG = \frac{(S_h - \eta P_0)}{TVD(1-\eta)} \quad (54a)$$

Horizontal Well

$$FG = \frac{2(S_h - \eta P_0) - (S_v - S_h)}{2TVD(1-\eta)} \quad (54b)$$

4.1.3 Bellotti & Giacca

For reservoir rocks (sands and limestones), Bellotti & Giacca (1978) compute fracture gradients by combining Haimson & Fairhurst's fracture pressure relations, the minimum stress equation (Eq. 10), and Eaton's relation for stress ratio (Eq. 15). Bellotti & Giacca considered two cases: 1) a non-penetrating drilling fluid (Eq. 4), and 2) a fully penetrating fluid with a highly compressible rock matrix (Eq. 9). They only addressed the case of a vertical wellbore in a tectonically relaxed environment. The resulting fracture gradient relations are:

Non-Penetrating Drilling Fluid (Eq. 4)

$$FG = \left(\frac{2\nu}{1-\nu} \right) (OBG - PPG) + PPG \quad (55)$$

Penetrating Drilling Fluid, Highly Compressible Rock (Eq. 9)

$$FG = 2\nu (OBG - PPG) + PPG \quad (56)$$

For what they called "plastic" formations (shales, marls, salt), they simply assumed:

$$FG = OBG \quad (57)$$

For clean sands, sandstones, and unfractured carbonates, Bellotti & Giacca use a value of 0.25 for ν . For shaley sands and sandstones, or deep limestones, the use $\nu = 0.28$. With exploratory wells, they recommend using Eq. 55, with $\nu = 0.25$, which results in a predicted fracture gradient of:

$$FG = 0.67 (OBG - PPG) + PPG \quad (58)$$

Eq. 56 is applied when drilling with water, or when drilling highly permeable formations.

4.1.4 Anderson, Ingram, & Zanier

Anderson, Ingram & Zanier (1973) tried to devise a fracture gradient relation that accounts for lithology changes. As a first step, they replaced the standard Terzaghi effective stress relation:

$$\sigma = S - P_0 \quad (59)$$

with Biot's relation:

$$\sigma = S - \alpha P_0 \quad (60)$$

where, as before, $\alpha = 1 - K/K_G$, K is the bulk modulus of the dry rock, and K_G is the bulk modulus of the rock grains.

This basically means that in any equation involving pore pressure, they replaced P_0 with αP_0 . For the case of a vertical well with equal horizontal stresses, their version of Eq. 3 (fracture pressure for an impermeable wellbore with impermeable cracks) is:

$$P_w = 2S_h - \alpha P_0 \quad (61)$$

Similarly, their equation for minimum stress is:

$$S_h = K(S_v - \alpha P_0) + \alpha P_0 \quad (62)$$

They combined Eqs. 61 and 62, with Eaton's relation for effective stress ratio (Eq. 15):

$$K = \frac{\nu}{1-\nu} \quad (15)$$

to obtain the following fracture gradient equation:

$$FG = \frac{2\nu}{1-\nu} OBG + \alpha \frac{1-3\nu}{1-\nu} PPG \quad (63)$$

The parameter α is assumed to equal the fractional density porosity:

$$\alpha = \phi_{\text{density}} \quad (64)$$

while Poisson's ratio ν is related to a *shale index* parameter "Ish", where

$$I_{sh} = \frac{\phi_{\text{sonic}} - \phi_{\text{density}}}{\phi_{\text{density}}} \quad (65)$$

and ϕ_{sonic} is sonic porosity. They did not specify how they calculate ϕ_{sonic} , but most likely it was with the time average equation:

$$\phi_{\text{sonic}} = \frac{\Delta t - \Delta t_{\text{matrix}}}{\Delta t_{\text{fluid}} - \Delta t_{\text{matrix}}} \quad (66)$$

The relation between ν and I_{sh} is obtained by fitting the equation:

$$\nu = A I_{sh} + B \quad (67)$$

through v , I_{sh} data points collected from leak-off tests and lost returns incidents, with I_{sh} calculated from sonic and density log data via Eq. 65, and v calculated from the relation:

$$v = \frac{FG - \alpha PPG}{FG + OBG - 3 \alpha PPG} \quad (68)$$

4.1.5 Aadnoy & Larsen

Aadnoy & Larsen (1987) introduce an additional term, called the *correlation coefficient* "A", into the fracture pressure relation for an impermeable wellbore with impermeable cracks (Eq. 3). For a vertical well with uniform horizontal stresses, their fracture gradient relation is:

$$FG = 2 GRD_h - PPG - A \quad (69)$$

where GRD_h is the horizontal stress gradient in ppg. The parameter "A" was introduced because Aadnoy & Larsen recognized that horizontal stresses backed out from leak-off test data using the original Eq. 3 often came out unreasonably low. The discussion in Section 2 would suggest that this is because Eq. 3 assumes all pre-existing cracks are short, and this is typically not the case.

Instead of using the stress ratio approach (Eq. 10) to define GRD_h , Aadnoy & Larsen consider GRD_h to be independent of pore pressure. They assume GRD_h can be found by simply shifting the overburden gradient curve laterally by a constant amount they call " K_1 ". In other words, their equation for GRD_h is:

$$GRD_h = OBG - K_1 \quad (70)$$

From Eq. 70, Eq. 69 can then be written as:

$$FG = 2 OBG - 2 K_1 - PPG - A \quad (71)$$

The constant K_1 is found by setting A equal to zero at the location of the leak-off test with the highest pore pressure gradient, and substituting known values for FG, OBG, PPG into Eq. 71:

$$K_1 = \frac{2 OBG - FG - PPG_{MAX}}{2} \quad (72)$$

The parameter "A" is assumed to be a linear function of pore pressure gradient:

$$A = a - b (PPG) \quad (73)$$

The A, PPG data required to fit this curve are obtained from additional leak-off tests, with A calculated from OBG, K_1 , PPG, and FG:

$$A = 2 OBG - 2 K_1 - PPG - FG \quad (74)$$

Once the parameters a, b, and K_1 have been established, the final form of the fracture gradient relation for vertical wells can be written as:

$$FG = 2 OBG - 2 K_1 - a - (1-b) PPG \quad (75)$$

According to Aadnoy & Larsen, Eq. 75 only applies for vertical wells. For deviated wells, they use the relation:

$$FG_{\gamma} = FG_0 + \frac{1}{3} (PPG - PPG^*) [\sin(\gamma)]^2 \quad (76)$$

where FG_0 is the fracture gradient for a vertical well, calculated from Eq. 75, FG_{γ} is the fracture gradient for a wellbore at an angle of γ degrees from vertical, and PPG^* is a constant parameter.

PPG^* is ideally backed out from Eq. 76 using leak-off data from a deviated well. If only vertical wells are available, Aadnoy and Larsen recommend taking the leak-off test where pore pressure is highest, and calculating PPG^* from Eq. 76 with γ set equal to 90° .

5 Direct Methods

As discussed in the Introduction, the methods classified as “direct” make no attempt to predict fracture gradients through any type of theoretical model. They simply correlate fracture pressure or fracture gradient to some other parameter. Five methods are discussed. Three (Breckels & van Eekelen, Rocha & Bourgoyne, and Barker) tie fracture gradient to depth. One (MacPherson & Berry) uses dynamic elastic moduli, while the fifth (Salz) links fracture gradient to pore pressure gradient.

Only the papers by Rocha & Bourgoyne, and Barker & Wood are based upon deepwater experience, so they may be most relevant to DEA 119. In particular, they discuss the observation that fracture gradients for deepwater Gulf of Mexico wells typically lie very close to the overburden gradient.

5.1.1 Rocha & Bourgoyne

Rocha & Bourgoyne (1996) defined a “pseudo-overburden pressure” relation, obtained by integrating densities calculated from an exponential porosity-depth function:

$$\phi = \phi_0 \exp(-K_{\phi} \text{TVD}_{\text{BML}}) \quad (77)$$

where ϕ is fractional porosity, TVD_{BML} is depth below mudline, and ϕ_0 , K_{ϕ} are parameters calibrated with leak-off tests. The pseudo-overburden pressure is found by substituting Eq. 77 into the equation for bulk density:

$$\rho = \rho_w \phi + \rho_G (1 - \phi) \quad (78)$$

and integrating, with ρ_F and ρ_G the bulk density of the pore fluid, and rock grains, respectively. This results in the following relation for overburden pressure:

$$S_0 \text{ (psi)} = 0.444 \text{ WD} + 0.4335 \rho_G \text{TVD}_{\text{BML}} - \frac{0.4335 (\rho_G - \rho_F) \phi_0}{K_{\phi}} [1 - \exp(-K_{\phi} \text{TVD}_{\text{BML}})] \quad (79)$$

Calibration has to be accomplished through a trial and error process. Initial values are picked for ϕ_0 and K_{ϕ} , and a pseudo-overburden stress is calculated at each leak-off test location. Rocha & Bourgoyne then convert each S_0 to a gradient, say G_0 , and they cross-plot:

$$G_0 = \frac{S_0}{TVD} \text{ vs FG}$$

where FG is the actual fracture gradient.

If the pseudo-overburden stress curve perfectly matches the fracture gradient data, the points will fall along a line that passes through the origin with a slope of 1. As a check, they fit their G_0 vs FG points with a power law relation:

$$= a \text{ FG}^b \tag{80}$$

If a and b both come out equal to one, then they have a perfect fit. If not, they tweak ϕ_0 and K_ϕ , re-calculate S_0 and G_0 , and re-plot and re-fit their G_0 , FG data. This process continues until the fit is satisfactory. Again, ϕ_0 and K_ϕ are the parameters they are really solving for; a and b are just used to check how good their match is with the fracture gradient data.

Table 7 lists the example ϕ_0 and K_ϕ values Rocha & Bourgoyne included in their paper.

Area	ϕ_0	K_ϕ
Mississippi Canyon, GOM	0.660	1.66×10^{-5}
Green Canyon, GOM	0.770	3.23×10^{-4}
Main Pass, GOM	0.565	9.90×10^{-8}
Ewing Bank, GOM	0.685	9.90×10^{-4}
Rio de Janeiro, Brazil	0.670	1.79×10^{-5}
Alba Field, Western Europe	0.555	9.90×10^{-8}

Table 7 - Example pseudo-overburden stress parameters.

5.1.2 Barker & Wood

Barker & Wood (1997) proposed a simplification of the Rocha & Bourgoyne (1996) method. Instead of trying to custom fit pseudo-overburden stress curves for different areas, Barker & Wood used over 50 leak-off tests from 20 Gulf of Mexico wells to develop one generic overburden gradient relation:

$$\text{OBG (PPG)} = \frac{8.55 \text{ WD} + 5.3 (\text{TVD}_{\text{BML}})^{1.1356}}{\text{TVD}_{\text{RKB}}} \tag{81}$$

Barker & Wood also observed that lost returns, and loss/gains problems usually occur when mud weights exceed 90% of the overburden gradient. In some cases, these problems occurred at mud weights less than the fracture gradient measured at the last casing shoe. Therefore, they recommend limiting mud weights in the deepwater to 90% of the overburden gradient.

Fig. 18 compares Barker & Wood's overburden gradient relation with curves computed using the equations of Zamora (1989), Simmons & Rau (1988), and Rocha & Bourgoyne. Water depth is assumed to be 4000'. The two curves shown for Zamora correspond to values of 4 and 8 for his parameter "A". The curves show for Rocha & Bourgoyne are their Mississippi Canyon and Green Canyon relations.

5.1.3 Breckels & van Eekelen

Breckels & van Eekelen's (1982) paper begins with an excellent review of the state of the art of fracture gradient prediction at that time. As in this report, they also expressed concern about Eaton's method, in particular: "... he writes $K=v/(1-v)$ and plots his results as a correlation of v with depth. This is an unnecessary and somewhat dangerous complication, because it might create the wrong impression that K also may be determined by measuring Poisson's ratio v on a core."

Although they were obviously aware of the minimum stress (stress ratio) approach for estimating fracture gradients, they opted to try to directly correlate minimum horizontal stress with depth. They were interested in determining the actual minimum stress, not leak-off pressures (see Fig. 1). Therefore, they tried to fit a lower bound to published leak-off test and fracture treatment data.

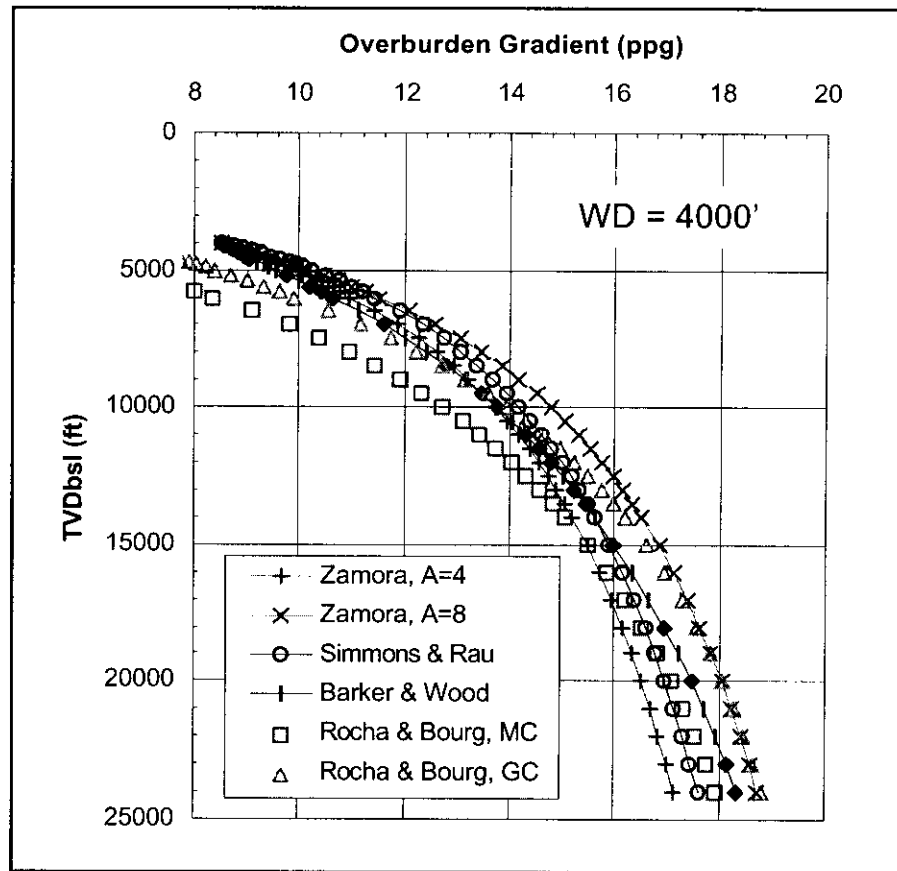


Fig. 18 -Comparison of the Zamora (1989), Simmons & Rau (1988), Rocha & Bourgoyne (1996), and Barker & Wood overburden gradient relations. Assumed water depth of 4000'. Rocha & Bourgoyne's curves for Mississippi Canyon and Green Canyon shown.

Breckels & van Eekelen ultimately concluded it was necessary to include pore pressure in their relations. They developed equations for the U. S. Gulf Coast, Venezuela, and Brunei, which are listed below: In these equations, depth is in feet, stress and pressure are in psi, P is the pore pressure, and P_N is normal pressure at that depth. The datum for depth was not specified, but most likely was sea level. Assuming these were predominately shallow water wells, the datum is not that critical an issue. However, if these relations are tried in deepwater, TVD should be treated as depth below mudline, and the hydrostatic pressure of the water column must be added to the S_{hmin} term.

U.S. Gulf Coast

For TVD \leq 11,500 ft.

$$S_{hmin} \text{ (psi)} = 0.197 \text{ (TVD)}^{1.145} + 0.46 \text{ (P} - P_N) \tag{82a}$$

For TVD > 11,500 ft.

$$S_{hmin} \text{ (psi)} = 0.197 \text{ (TVD)}^{1.145} + 0.46 (P - P_N) \quad (82b)$$

with normal pressure gradient = 0.465 psi/ft.

Venezuela

For 5,900 ft. < TVD < 9,200 ft.

$$S_{hmin} \text{ (psi)} = 0.210 \text{ (TVD)}^{1.145} + 0.56 (P - P_N) \quad (83)$$

with normal pressure gradient = 0.433 psi/ft.

Brunei

For TVD < 11,500 ft.

$$S_{hmin} \text{ (psi)} = 0.227 \text{ (TVD)}^{1.145} + 0.49(P - P_N) \quad (84)$$

with normal pressure gradient = 0.433 psi/ft.

5.1.4 MacPherson & Berry

MacPherson & Berry (1972) developed an X-Y relation for fracture pressure, where

$$X = \frac{\rho V^2}{S_v} \quad (85)$$

Y = fracture pressure in psi

and ρ is bulk density, V is compressional velocity, and S_v is overburden stress, in psi.

5.1.5 Salz

Salz (1972) was interested in predicting fracture propagation pressures in the Vicksburg formation in South Texas, both at virgin reservoir conditions, and after depletion. Unlike most fracture gradient prediction methods, Salz used initial shut-in pressures (ISIP) instead of leak-off pressures (see Fig. 1). He found that the fracture gradients in both virgin and depleted sands could be correlated to pore pressure gradient (PPG) through the equation:

$$FG = 0.57 \exp(0.57 \text{ PPG}) \quad (86)$$

where FG and PPG are both in psi/ft.

6 References

- Volterra, E. V., and Gaines, J. H., *Advanced Strength of Materials*, Prentice Hall, Inc., Englewood Cliffs, N. J., 1971, pg. 159.
- Hubbert, M. K., and Willis, D. G., "Mechanics of Hydraulic Fracturing", *AIME Petroleum Transactions*, Vol. 210, 1957, pp. 153-168.
- Detournay, E., and Carbonell, R., "Fracture mechanics analysis of the breakdown process in minifrac or leak-off tests", *Eurock '94*, Balkema Rotterdam, ISBN 90 541050x2, pp399-406.
- Abou-Sayed, A. S., Brechtel, C. E., and Clifton, R. J., "In Situ Stress Determination by Hydrofracturing: A Fracture Mechanics Approach", *J. Geophys. Res.*, 83 (B6), June 1978, pp 2851-2862.
- Rummel, F., "Fracture Mechanics Approach to Hydraulic Fracturing Stress Measurements", in *Fracture Mechanics of Rock*, Barry Kean Atkinson, ed., Academic Press, 1987, pp 217-239.
- Daneshy, A. A., Slusher, G. L., Cox, B. R., and Chisholm, P. T., "In-Situ Stress Measurements During Drilling", SPE 13227.
- Haimson, B., and Fairhurst, C., "In Situ Stress Determination At Great Depth By Means Of Hydraulic Fracturing", in *Rock Mechanics-Theory and Practice*, ed. By W. H. Somerton, Society of Mining Engrs., the American Institute of Mining, Metallurgical, and Petroleum Engrs., Inc., Salt Lake City, Utah, 1970, pp. 559-584.
- Eaton, B. A., "The Effect of Overburden Stress on Geopressure Prediction from Well Logs", *Journal of Petroleum Technology*, Aug., 1972, pp. 929-934.
- Biot, M. A., "Laboratory Experiments in Fracture Propagation", SPE 10377.
- Barenblatt, G. I., "On Certain Problems of the Theory of Elasticity That Arise in the Investigation of the Mechanisms of Hydraulic Rupture of an Oil-Bearing Layer", *Prikl. Mat. Mekh.*, Vol. 20, 1956, pp 475-486.
- Matthews, W. R., and Kelly, J., "How to predict formation pressure and fracture gradient", *The Oil and Gas Journal*, Feb. 20, 1967, pp. 92-106.
- Pennebaker, E. S., "An Engineering Interpretation of Seismic Data", SPE 2165.
- Eaton, B. A., "Fracture Gradient Prediction and Its Application in Oilfield Operations", *Journal of Petroleum Technology*, Oct., 1969, pp. 1353-1360.
- Eaton, B. A., and Eaton, T. L., "Fracture gradient prediction for the new generation", *World Oil*, Oct., 1997, pp. 93-100.
- Christman, S. A., "Offshore Fracture Gradients", *Journal of Petroleum Technology*, Aug., 1973, pp. 910-914.
- Pilkington, P. E., "Fracture Gradient Estimates In Tertiary Basins", *Petroleum Engineer International*, May, 1978, pp. 138-148.
- Daget, P., and Parigot, P., "Using log data to predict leak-off pressures", *World Oil*, Aug. 1, 1979.

- Daines, S. R., "Prediction of Fracture Pressures for Wildcat Wells", *Journal of Petroleum Technology*, April, 1982, pp. 863-872.
- Brennan, R. M., and Annis, M. R., "A New Fracture Gradient Prediction Technique That Shows Good Results in Gulf of Mexico Abnormal Pressures", SPE 13210.
- Simmons, E. L., and Rau, W. E., "Predicting Deepwater Fracture Pressures: A Proposal", SPE 18025.
- Zamora, M., "New Method Predicts Gradient Fracture", *Petroleum Engineer International*, Sept., 1989, pp. 38-47.
- Holbrook, P. W., Maggiori, D. A., and Hensley, R., "Real-Time Pore Pressure and Fracture-Pressure Determination in All Sedimentary Lithologies", *SPE Formation Evaluation*, Dec., 1995, pp. 215-222.
- Singh, B., and Emery, N., "Fracture Gradient Predictions In Depleted Sands In The Gulf Coast Sedimentary Basin", AADE Industry Forum on Pressure Regimes in Sedimentary Basins and Their Prediction, September 2-4, Lake Conroe, TX, 1998.
- Bellotti, P., and Giacca, D., "Pressure evaluation improves drilling performance", *Oil and Gas Journal*, Sept. 11, 1978.
- Anderson, R. A., Ingram, D. S., and Zanier, A. M., "Determining Fracture Pressure Gradients from Well Log", *Journal of Petroleum Technology*, Nov., 1973, pp. 1259-1268.
- Aadnoy, B. S., and Larsen, K., "Method for Fracture Gradient Prediction for Vertical and Inclined Boreholes", SPE 16695.
- Salz, B., "Relationship Between Fracture Propagation Pressure and Pore Pressure", SPE 6870.
- MacPherson, L. A., and Berry, L. N., "Prediction of Fracture Gradients from Log Derived Elastic Moduli", *The Log Analyst*, Sept.-Oct. 1972, pp. 12-19.
- Breckels, I. M., and van Eekelen, H. A. M., "Relationship Between Horizontal Stress and Depth in Sedimentary Basins", *Journal of Petroleum Technology*, Sept., 1982, pp. 2191-2199.
- Grauls, D. J., "Fracturing gradient, sonic compaction, and related to undercompaction pressure relationships in clays and shales", in *Rock at Great Depth*, Maury & Fourmaintraux, eds., 1990 Balkema, Rotterdam, ISBN 90 61919754, pp. 1543-1550.
- Barker, J. W., and Wood, T. D., "Estimating Shallow Below Mudline Deepwater Gulf of Mexico Fracture Gradients", *Houston AADE Chapter Annual Technical Forum*, April 2-3, 1997.
- Rocha, L. A., and Bourgoyne, A. T., "A New Simple Method To Estimate Fracture Pressure Gradient", *SPE Drilling & Completion*, Sept. 1996, pp. 153-159.
- Lambe, T. W., and Whitman, R., *Soil Mechanics*, John Wiley & Sons, 1969, ppg. 163-167.
- Eaton, B. A., "The Equation for Geopressure Prediction from Well Logs", SPE 5544, 1975.



KNOWLEDGE SYSTEMS, INC.

Pre-Drill Overburden Estimation

Steve Hobart

11/17/1999

CONFIDENTIAL

This report is provided to DEA Project 119 Project Participants under the terms of the DEA Project 119 Participation Agreement and is thereby subject to restrictions of confidentiality and non-disclosure to third parties.

DEA Project 119

Report No. 4

Corporate Offices

Knowledge Systems, Inc.
P. O. Box 1279
Stafford, Texas 77497-1279
Phone: 281-879-1400
Fax: 281-879-1499
E-mail: sales@knowsys.com

European Office

Knowledge Systems, Inc.
P.O. Box 274 Paradis
5856 BERGEN
Norway
Phone: +47 55 92 45 62
Fax: +47 55 92 45 62
E-mail: sales @knowsys.com

Please visit the Knowledge Systems' website at <http://www.knowsys.com>

Information in this document is subject to change without notice, and does not represent a commitment on the part of Knowledge Systems. The software described in this document is furnished under a license agreement or non-disclosure agreement. It is against the law to copy the software on any medium except as specifically allowed in the license or non-disclosure agreement.

© Copyright Knowledge Systems, 1989-2000. All rights reserved. *DrillWorks* is a registered trademark of Knowledge Systems, Inc. *PostScript* is a registered trademark of Adobe Systems, Inc. *Windows* is a trademark of Microsoft Corporation

Document Information

Title: Pre-Drill Overburden Estimation	
Description: DEA Project 119, Report #4	
Author(s): Steve Hobart	
Reviewer(s):	
Creation Date: 11/17/1999	Last Date Modified: 10/5/2000 9:43 AM
Approved By:	Approval Date:
Will be sent to:	
Sources Used: (can be other documents used as sources)	
Project Number:	Document Number: 2000-000002

Table of Contents

1	Introduction.....	1
1.1	Purpose	1
1.2	Scope.....	1
2	Units for overburden gradient.....	2
3	Calculation of overburden gradient	3
4	Sediments.....	5
5	Approaches to Pre-Drill Density and Overburden Estimation	6
5.1	Using Depth Only.....	6
5.1.1	Constant Value Overburden Gradient.....	6
5.1.2	Eaton’s Gulf Coast Overburden Gradient	6
5.1.3	Adaptation of Eaton’s Overburden Method to Other Regions.....	8
5.1.4	Simmons – Rau “Equivalent Depth” Technique	9
5.1.5	Bell’s Empirical Relation.....	10
5.1.6	Traugott’s Empirical Relation	10
5.1.7	Barker and Wood’s OBG Fit from Leak-off Test Data.....	10
5.1.8	John Jones’ Empirical Relation for Density of Deepwater Sediments.....	11
5.2	Combining Depth and Compaction Models.....	11
5.2.1	Athy’s Compaction Formula	12
5.2.2	Applying Athy’s Formula to Eaton’s Data for OBG Determination.....	12
5.2.3	Combining Athy’s and the Hubbert-Rubey Compaction Equations.....	14
5.2.3.1	Combining Athy’s with Other Compaction Equations	15
5.2.3.2	Athy and Baldwin-Butler Compaction Relations	15
5.2.3.3	Athy and Perloff-Baron Compaction Relations.....	16
5.2.4	Zamora’s Method – Factoring in the Age of the Rock.....	17
5.3	Density and OBG from Acoustic Data	17
5.3.1	Seismic Reflection Coefficient.....	17
5.3.2	Elastic Modulus.....	18
5.3.3	Gardner Equation.....	19
5.3.4	Pennebaker’s Transform	19
5.3.5	Bellotti – Giacca Transform.....	20
5.3.6	Early DEA-119 Velocity/Density Transform.....	20
5.3.7	Later DEA-119 Velocity/Density Transform.....	21
6	Results to This Point.....	23
6.1	Introduction.....	23
6.2	Methodology.....	23
6.3	Best Depth-only method	24
6.4	Best Acoustic method.....	25
6.5	Direct comparison of Gardner Method with Later DEA-119 Method	26
7	Conclusions.....	30
8	References.....	31
9	Appendix.....	34
9.1	On the Effect of Clay Diagenesis (Smectite to Illite) on the Density/Delta-T	
Crossplot		35
9.1.1	Geological model.....	36

9.1.2 Application of the integrated model 37
9.1.3 Method..... 38
9.1.4 References..... 39

1 Introduction

1.1 Purpose

The estimation of overburden stress is fundamental to both pore pressure estimation and fracture gradient estimation. The accuracy of these estimates, critical to well design, will be affected by the accuracy of the overburden estimate. The overburden stress at any given depth is a function of the density of the overlying sediments. Unfortunately, the density of the sediments cannot be reliably ascertained until they have been penetrated by the borehole and logged. This leads to the following paradox: in order to design the well properly, it is necessary to drill it first. Since this is a physical impossibility, exploratory well design must rely on overburden estimates based on indirect or empirical methods.

The purpose of this report is to document an investigation into methods for estimating overburden gradient for deep-water wells using the limited information available prior to drilling. Typically, the approaches used in the past have involved using depth alone as a basis for estimating sediment density or overburden stress or else using local seismic interval velocity data to provide an estimate of formation densities.

1.2 Scope

At the time of writing of this report, the bulk of the available deep-water logging data had been obtained from GDC, with comparatively little data from DEA 119 participants. The data comprise thirty-two deep-water wells with logging suites which include sonic (acoustic) transit time logs as well as density logs. In the absence of seismic interval velocity data from these wells, the assumption is made that any valid relationship between velocity and density obtained from well logs can be adapted for use in estimating density from seismic interval velocities.

The data obtained from GDC represent a cross-section of deep-water wells in the US Gulf of Mexico. The water depths range from 1015 feet to 7520 feet. The geographic range of the wells is a rough triangle from Viosca Knoll to Atwater Valley to East Breaks. Most of these wells were drilled in sediments that have spilled from the Mississippi-Atchafalaya river systems. A subset of twelve wells was selected in order to provide a fair sampling of the wells without biasing any quantitative conclusions due to an over-concentration of wells in a particular area. Empirical models developed using these wells were then tested against another set of representative wells in order to confirm the validity of the results.

Nevertheless, the restricted geographic range of these wells (US Gulf of Mexico) should be a cautionary note to those who may wish to apply the results of this study in other areas. On the other hand, these results are likely applicable to other Tertiary basins similar to the US Gulf of Mexico.

2 Units for overburden gradient

The overburden pressure is the stress created by the weight of the materials above the depth of interest. The overburden gradient is this stress divided by the vertical depth. The dimensions of stress are force per unit of area, or F/L^2 . The dimensions of depth are, of course, simply length, or L . Therefore, any measurement unit consistent with units F/L^3 can be appropriate for overburden gradient. Typical units of this form are: psi per foot and kilopascals per meter. With the assumption of a constant value for the acceleration due to gravity, mass density units such as pounds per US gallon (ppg), grams per cubic centimeter (g/cc) and kilograms per liter (kg/l) are also appropriate for overburden gradient as well. Specific gravity (SG), taking the density of water to be one g/cc, is also often used as a unit for overburden gradient.

The User-Defined Methods found in PREDICT provide a convenient means to convert from overburden stress to overburden gradient, from overburden gradient to overburden stress and to convert units between like kinds of quantities.

3 Calculation of overburden gradient

The calculation of the overburden gradient at any depth is, to a first approximation, rather straightforward. By summing the vertical stresses contributed by each layer of material above the depth of interest, the total stress is obtained. The vertical stress due to any layer is given by:

$$\sigma_{vi} = \rho_i h_i \quad (1)$$

Where: σ_{vi} vertical stress contributed by i-th layer
 ρ_i average weight density of the i-th layer
 h_i thickness of the i-th layer

The overburden gradient is derived by dividing the overburden stress by the vertical depth.

$$OBG = \sum_{i=1}^n \sigma_{vi} / Z \quad (2)$$

Where: σ_{vi} vertical stress contributed by i-th layer
 i index of material layer
 n number of material layers
 Z vertical depth (e.g. relative to rotary kelly bushing)

The air layer between the rotary table and the water line may be considered to have negligible density. The sea water layer down to the mud line has a density that falls in a very narrow range, depending on salinity and temperature. The salinity of seawater varies from about 32,000 ppm to 39,000 ppm. It may be less if there is a substantial plume of fresh water from a river. The water temperature generally decreases with depth down to about 40 degrees Fahrenheit at the mud-line, although many exceptions to this general rule do occur. The density of these waters may range from 1.02 to 1.03 g/cc. This is equivalent to a range of 8.51 to 8.59 pounds per gallon. Most informal sources consulted (i.e. on the Internet) list average seawater density as 1.027 g/cc (equivalent to 8.57 pounds per gallon). Although the variation in density is slight, the contribution of the water column to the total overburden in deep water increases as water depth increases. The variations may even be significant in shallow water flow and shallow fracture gradient determinations.

The value of Z, the depth relative to some reference point, must be chosen with some additional care in deepwater environments. The reason for this is that the use of overburden gradient as opposed to overburden stress is a concession to rig-site personnel who generally regard all pressure-related information in terms of equivalent mud density, for example in pounds per gallon. When the bell nipple and the rotary kelly bushing are within a few feet of each other, there is little error created when static bottom-hole pressure is calculated assuming a continuous fluid column all the way up to the rig's depth reference. When the mud returns are to the sea floor, as in riserless drilling, the use of the rotary kelly bushing elevation as the depth reference for pressure gradient calculation results in more significant errors. With current technology (1999), drilling in

each well eventually reaches the point where the mud return point and the well's depth reference are in the traditional proximity to each other that conventional calculations can be applied.

The form of the equations presented below is in keeping with the traditional paradigm of equivalencing fluid density and pressure gradients relative to the well's (i.e. driller's) depth reference.

4 Sediments

The term “deep-water” seems to have a meaning relative to the state-of-the-art of offshore drilling at the time the term is used. For example, for the purposes of the DEA-119 project, “deep-water” was defined, somewhat arbitrarily – based on a rough consensus as of early 1998, as water depths greater than 1500 feet.

In discussing sedimentological environments, a less artificial definition seems to be in order. A standard text (Krumbein and Sloss (1963)) defines a “bathyal environment”, which includes water depths from 600 to 13,500 feet. This would include all the well considered in this study. This text divides the bathyal environment into an “epibathyal zone”, extending to 3,600 feet and includes much of the outer slopes of the continental shelves, and a “mesobathyal environment” which includes the major part of the floor of ocean basins. Beyond the bathyal environment, Krumbein and Sloss define the “abyssal environment”, which extends to 21,000 feet of water and the “hadal environment” (from Hades?), which includes oceanic trenches.

A more recent text (Boggs (1995)) simply defines an oceanic zone, which includes the marine environment that extends between the continental shelf breaks. The average depth of the shelf break is said to be about 130 meters, or about 425 feet of water. The oceanic zone includes the continental slope, the continental rise, the abyssal plain, oceanic trenches and mid-ocean ridges. The following characterization of deep-water sediments is condensed from Boggs’ text.

Deep-water sediments may be divided into two broad (and sometimes overlapping) classes: terrigenous and pelagic. Terrigenous sediments are those transported from the continental shelf or shallower areas. These sediments may be transported by suspension in fresh-water river outflows, erosion by subsea currents, wind transport of fine particles, turbidity currents, slides and slumps. In some areas, volcanism and/or glacial transport may also contribute to sedimentation in the deep-water. Pelagic sediments are derived from materials originating apart from the influence of landforms. These include calcareous and siliceous oozes derived from the remains of plankton and pelagic clays.

The majority of the sediments penetrated by the wells in this study are presumed to consist of continental-type materials, although it is conceivable that at deeper depths there may be increasing amounts of pelagic materials.

5 Approaches to Pre-Drill Density and Overburden Estimation

There have been two main approaches to obtaining density or overburden data prior to drilling in exploratory areas. One approach disregards any contribution seismic data may make toward density estimation and uses depth as the sole input to create a regional correlation for either density or overburden gradient. The other approach attempts to create a usable relationship between density and either velocity or transit time. A third approach, based on an attempt to model bulk compressibility as a function of depth below mud-line, was developed and tested in the course of this project. However, it proved to be unsatisfactory for estimating formation densities from acoustic data.

5.1 Using Depth Only

The estimation of formation density or overburden gradient based solely on a depth criterion has been popular for several decades. The primary reason for this is simplicity: the algorithms are generally simple algebraic expressions and there is no requirement for other information such as seismic interval velocity in order to perform the calculation. Another reason for the popularity of depth-only methods is the advent of Gamma Ray/Resistivity MWD/LWD tools. Without density measurements to directly integrate for overburden stress, these methods can provide an estimate that can be used as a part of real-time pore pressure monitoring techniques.

5.1.1 Constant Value Overburden Gradient

Perhaps the earliest method of determining overburden gradients was the simplistic use of a constant gradient of 1.0 psi/ft. This corresponds to a density of 2.31 g/cc. In sandstone, this would be equivalent to an average porosity of 21 per cent. However, it was also early recognized that a constant overburden value can lead to grossly inaccurate pore pressure and fracture gradient estimations. This is particularly true in the offshore environment where the density of seawater must be averaged in with the density of the sediments (which themselves initially have quite low densities) and the water depth varies from well to well. This is why overlay techniques are not as successful in predicting pore pressures offshore.

5.1.2 Eaton's Gulf Coast Overburden Gradient

One of the earliest generalized overburden gradient formulations was based on a graph (Fig.1, below) prepared by Ben Eaton (1968). This graph plotted a composite overburden stress gradient against depth for normally compacted Gulf Coast formations. It was derived from an analysis of a composite of density log data from several Gulf Coast wells (Fig.1). Presumably, due to its antiquity, no deepwater wells were represented in Eaton's study.

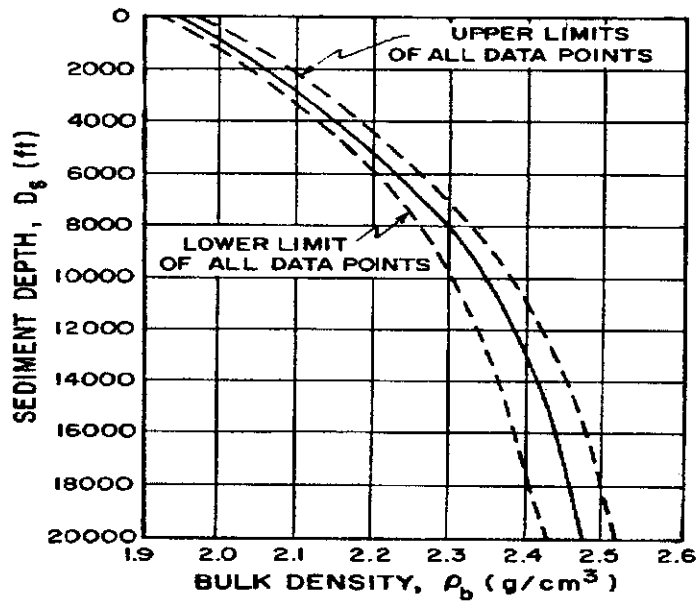


Fig.1 – Eaton’s composite Gulf Coast density data

To perform computer calculation of pore pressures using the Eaton overburden gradient curve it is necessary to represent the data in some kind of digital form. One means is to represent the data as a two-dimensional array of points of depth and overburden gradient. This is the basis for the “OBG: Louisiana-Texas (feet)” curve stored in the PREDICT software set of library curves.

Alternatively, it is reasonable to create an algebraic function of depth that yields values close to those of Eaton. While no examples of such an expression for the Gulf Coast were found, the formulas in the next section are representative of such a method. The discussion in section 5.2.2 concerns an application of Eaton’s density data to Athy’s compaction formula. The result of this combination is an expression that replicates the Eaton overburden data from 3,000 feet below the mud-line and deeper.

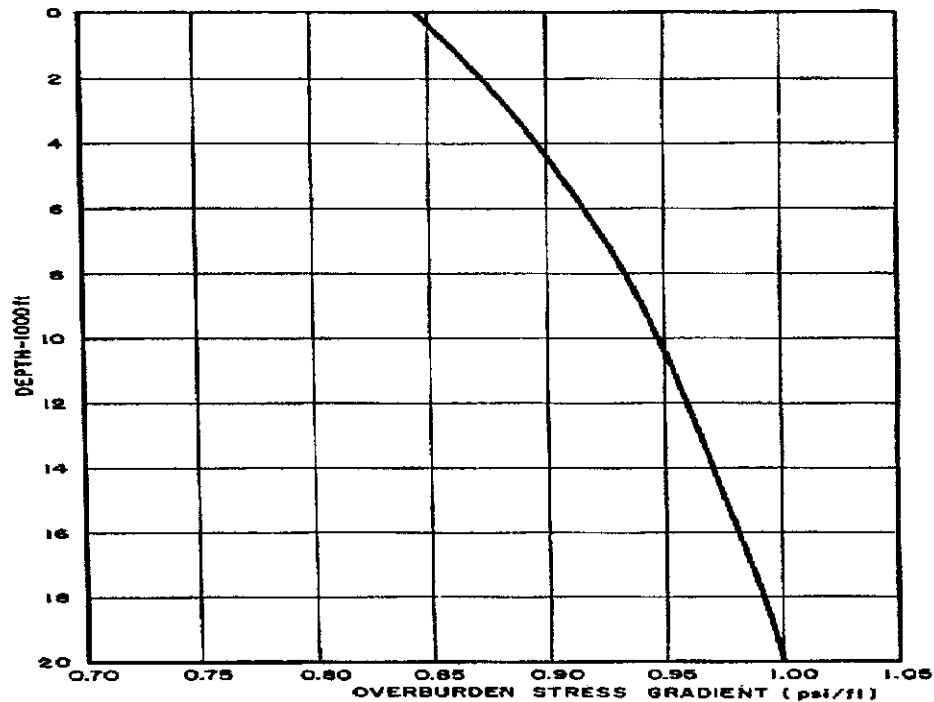


Fig. 2 – Eaton's overburden vs. depth relationship

5.1.3 Adaptation of Eaton's Overburden Method to Other Regions

Following Eaton's lead, algebraic expressions for OBG in other regional settings came into use. One example is the following expression for OBG in the Niger Delta. Although it was not originally intended for offshore applications, the following version has been adapted for that purpose:

$$\text{OBG} = (0.0133 \ln(D)^2 - 0.173 \ln(D) + 1.4335) D + 0.4335 \text{WD} \rho_w / Z \quad (4)$$

Where: OBG overburden gradient, psi/ft

D depth below mud-line, feet

WD water depth, feet

ρ_w sea water density, g/cc

Z true vertical depth (e.g. relative to RKB), feet

Another example was the derivation of an equation for the OBG in Statfjord Field in the North Sea by Aadnoy and Larsen (1987).

$$\text{OBG} = 19.5 - 1.21 \text{E-}3 D + 8.78 \text{E-}7 D^2 - 10.43 \text{E-}11 D^3 \quad (5)$$

Where: OBG overburden gradient, kPa / m

D depth, meters (Note: this equation has not been adjusted for water depth)

5.1.4 Simmons – Rau “Equivalent Depth” Technique

Simmons and Rau (1988) presented a method they called “The Modified Eaton Technique” to estimate overburden stress in “substantial water depths”, defined at the time to be water depths greater than 350 feet. The logic behind the technique seems to be fallacious in that it is based on the idea that the water column creates a “pre-stress” which contributes to the compaction of the sediments. This is contrary to the generally accepted Terzaghi’s soil compaction law (1943), which states that the stress due to the overburden is balanced by the pore fluid pressure and the grain-to-grain stress (equation (6)).

$$\sigma_{ovb} = p_f + \sigma_e \quad (6)$$

Where: σ_{ovb} overburden stress

p_f pore fluid pressure

σ_e grain-to-grain (“effective”) stress

Of course, all the terms in equation (6) could be divided by the depth to obtain an equally valid expression in terms of pressure gradients or equivalent mud weights.

Nevertheless, the technique Simmons and Rau presented is, at its foundation, an empirical relation that they found useful as an improvement over the then-current state-of-the-art for pre-drill estimates of fracture gradient in offshore environments. Due to its empirical foundation and the verification claimed for the technique, it was deemed worthy of inclusion on the DEA-119 study.

The first step in the Simmons-Rau technique is to establish an “equivalent sediment depth” that corresponds to the water depth of the well using either equation (7) or (8).

$$Deq = 0.00001489554 + 1 / (1.911364 / WD - 2.703024 / WD^2) \quad (7)$$

$$Deq = WD / 2 \quad (8)$$

Where: Deq “equivalent sediment depth”, feet

WD water depth, feet

The second step is to calculate the “effective sediment penetration depth” by adding the “equivalent sediment depth” of the water column to the depth below the mud-line:

$$Deff = Deq + D \quad (9)$$

Where: Deff “equivalent sediment penetration depth”, feet

Deq “equivalent sediment depth” from equation (7) or (8) above, feet

D depth below mud-line, feet

The third step in the Simmons-Rau technique is to determine the average overburden stress gradient at the “effective sediment penetration depth” using the following empirical relation:

$$\ln(Goba / 0.8511934) = (\ln Deff - 6.206593)^2 / 84.36084 \quad (10)$$

Where: ln Napierian (natural) logarithm function

Goba average overburden gradient, psi/ft

Deff “effective sediment penetration depth” from equation (9), feet

5.1.5 Bell’s Empirical Relation

This method was used by Tom Bryant in his "Dual Shale Pore Pressure Detection Technique" (1989). He attributed the algorithm to L.N. Bell as author of a 1969 Atlantic Richfield Drilling Manual. This method is an example of a polynomial fit. The form given below calculates the overburden gradient in units of psi/ft.

$$\text{OBG} = (0.444 \text{ WD} + \text{E D} + 2.64(10^{-5}) \text{ D}^2 - 1.97(10^{-9}) \text{ D}^3 + 6.6(10^{-14}) \text{ D}^4 - 5.94(10^{-19}) \text{ D}^5) / \text{Z} \quad (11)$$

Where: OBG overburden gradient, psi/ft
WD water depth, ft
D depth below mud-line, ft
Z true vertical depth (e.g. relative to RKB), feet

5.1.6 Traugott’s Empirical Relation

More recently, Martin Traugott (1997) introduced the following empirical equation to estimate overburden gradient based only on depth below the mud-line:

$$\text{OBG} = (8.5 \text{ WD} + (16.3 + (\text{D}/3125)**0.6) \text{ D}) / \text{Z} \quad (12)$$

Where: OBG overburden gradient, pounds per US gallon
D depth below mud-line, feet
WD water depth, feet
Z true vertical depth (e.g. relative to RKB), feet

Note that in this equation, the sea water density is given as 8.5 ppg and the mud-line density is given as 16.3 ppg. The 16.3 ppg mud-line density is consistent with Eaton’s average mud-line density of approximately 1.95 g/cc. Assuming that the average matrix density of deepwater sediments is 2.6 g/cc, this corresponds to a mud-line porosity of about 41 per cent. Indeed, it has been frequently found that density logs for DEA-119 deepwater wells do extrapolate to a mud-line density between 1.9 and 2.0 g/cc.

5.1.7 Barker and Wood’s OBG Fit from Leak-off Test Data

Barker and Wood (1997), assuming plastic deepwater formations, derived an expression for the cumulative average density from the mud-line to a depth of interest using leak-off test data from 70 deepwater wells. The essence of the plastic formation assumption is that the pressure required to open a fracture is equal to the overburden gradient. Eaton (1997) endorsed this means of obtaining OBG when applying his own approach for estimating fracture gradients in deepwater. When combined with the contribution of the overlying seawater (Barker and Woods suggest 8.55 ppg as the average sea water density for deepwater Gulf of Mexico wells.) the following expression results:

$$\text{OBG} = (8.55 \text{ WD} + 5.3 \text{ DBML}^{1.1356}) / Z \quad (13)$$

Where: OBG overburden gradient, pounds per US gallon
 D depth below mud-line, feet
 WD water depth, feet
 Z true vertical depth (e.g. relative to RKB), feet

5.1.8 John Jones' Empirical Relation for Density of Deepwater Sediments

Another strictly empirical means of obtaining an OBG Estimate using only depth comes courtesy of John Jones of Marathon Oil, Houston. The method employed is one of establishing an empirical equation for density for each of a series of depth ranges. The empirical equations were obtained using density data from both conventional density log data as well as data from site assessment borings. The resulting density profile is therefore more realistic than most for estimating near-mud-line densities. This profile can be used to obtain OBG using the methodology of equation (2) above.

For depths between the mud-line and 100 feet below the mud-line,

$$\rho = 1.47 + 0.0028 D - 0.0000033 D^2 \quad (14)$$

From 100 to 500 feet below the mud-line,

$$\rho = 1.6 + 0.0013 D - 0.00000132 D^2 \quad (15)$$

Between 500 and 8,000 feet below the mud-line,

$$\rho = 1.9 + 0.00006 D - 0.000,000,00106 D^2 \quad (16)$$

Beneath 8,000 feet below the mud-line,

$$\rho = 2.037 + 0.00004 D - 0.000,000,000,7 D^2 \quad (17)$$

For equations (14) through (17):

ρ formation density, g/cc
 D depth below mud-line, feet

5.2 Combining Depth and Compaction Models

The Simmons and Rau method, above, attempted to implicitly incorporate compaction effects into their model. Two widely known explicit models for compaction are presented in this section (Athy's and the Hubbert-Rubey Model), along with an empirical formula that deals with compaction by incorporating formation age in the model (Zamora's model).

5.2.1 Athy's Compaction Formula

In 1930, Athy published a study on Pennsylvanian and Permian shales in northern Oklahoma that led him to postulate the following relationship between porosity and depth of burial, i.e. a compaction equation:

$$\phi = \phi_0 e^{-kZ} \quad (18)$$

Where: ϕ porosity, fraction
 ϕ_0 mud-line (initial) porosity, fraction
 k compaction rate constant, feet⁻¹
 Z true vertical depth relative to mud-line, feet

This equation assumes that normal compaction has taken place and that no unconformities or faults have interrupted the burial profile.

The values of ϕ_0 and k for Athy's northern Oklahoma data are 0.48 and -4.33×10^{-4} ft⁻¹, respectively.

5.2.2 Applying Athy's Formula to Eaton's Data for OBG Determination

Using the average bulk density versus depth results obtained by Eaton (1968), it is possible to obtain a generic porosity versus depth profile for Gulf Coast sediments from which the Athy constants may be determined. This was done in the textbook "Applied Drilling Engineering" (1986), published by the Society of Petroleum Engineers. The constitutive equation for bulk density was applied to the Eaton data to estimate porosity:

$$\phi = (\rho_m - \rho_b) / (\rho_m - \rho_f) \quad (19)$$

Where: ϕ porosity, fraction
 ρ_m matrix density, g/cc
 ρ_b bulk density, g/cc
 ρ_f fluid density, g/cc

When the bulk density equation and Athy's equation are combined and applied to the calculation framework of equation (2) above, the following formula can be derived:

$$\text{OBG} = 19.25 (0.43345 (\rho_{sw} \text{WD} + \rho_m \text{D} - ((\rho_m - \rho_f) \phi_0 / k)(1 - e^{-kD}))) / Z \quad (20)$$

Where: 19.25 converts psi/ft to ppg
0.43345 converts g/cc to psi/ft
 ρ_{sw} sea water density, g/cc
WD water depth, feet
 ρ_m matrix (grain) density, g/cc
D depth below mud-line, feet

- ρ_f pore fluid density, g/cc
- ϕ_0 initial mud-line porosity, g/cc
- k Athy compaction constant, feet⁻¹
- Z true vertical depth (e.g. referenced to RKB), feet

Assuming the average matrix density to be 2.6 g/cc and the fluid density to be 1.074 g/cc, porosities were computed. A regression on the porosity data versus depth yielded a mud-line porosity, ϕ_0 , of 0.41 and a compaction constant, k , of 0.000085 ft⁻¹.

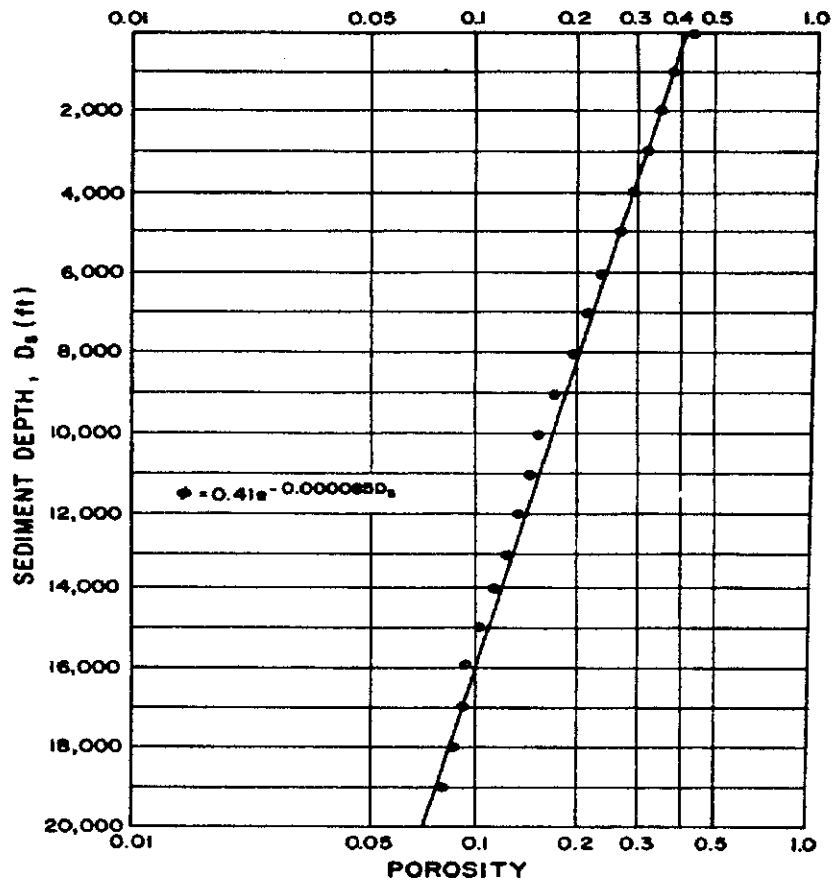


Fig.3 – Athy relation derived from Eaton’s Gulf Coast density data

If one were to assume the water depth to be negligible and $Z = D$, then equation (20) should yield an OBG profile very similar to Figure 1.

5.2.3 Combining Athy's and the Hubbert-Rubey Compaction Equations

The Hubbert-Rubey (1959) compaction equation is quite similar to the Athy compaction equation; however, it substitutes effective stress for the depth parameter used by Athy:

$$\phi = \phi_0 e^{-c\sigma} \quad (21)$$

Where: ϕ porosity, fraction
 ϕ_0 initial (mud-line) porosity, fraction
 c compaction constant

effective stress

It would seem reasonable to consider this an advancement over the Athy equation because depth in itself does not cause compaction. The vertical effective stress is the true cause of porosity reduction during compaction and depth is a convenient . Since this stress increases with depth, it can be seen that depth is merely a substitute parameter for vertical effective stress.

Since, according to Terzaghi's law (equation (7) above), the effective stress is equal to the overburden stress minus the pore pressure, we can substitute this into equation (21) to get:

$$\phi = \phi_0 e^{-c(OBG - PP)} \quad (22)$$

Where: ϕ porosity, fraction
 ϕ_0 initial (mud-line) porosity, fraction
 c compaction constant

OBP overburden pressure

PP pore pressure

Alixant and Desbrandes (1989) correctly observed that this approach could have been the first method to explicitly estimate pore pressure without the use of normal compaction trend lines. One Gulf of Mexico study, Eugene Island Block 331, obtained a value of 0.40 for ϕ_0 and 0.0368 Mpa^{-1} (Hart et al, 1995).

Comparing equation (22) with equation (18), it is clear that the two equations can be combined as follows:

$$c(OBP - PP) = k D \quad (23)$$

Where: c Hubbert-Rubey compaction constant, psi^{-1}
OBP overburden pressure, psi
PP pore pressure, psi
K Athy compaction constant, feet^{-1}
D depth below mud-line, feet

Rearranging the terms,

$$(OBP - PP) / D = k / c = A, \text{ a constant, psi/ft} \quad (24)$$

The implication of this result is that the effective stress is constant in normally compacted (normally pressured) sediments if both the Athy (1930) and the Hubbert-Rubey (1959) compaction equations are true. Since the overburden stress increases, the pore pressure must also increase. But if the pore pressure increases, then the assumption of normal compaction is violated. Therefore, both relationships cannot be true at the same time. It is beyond the scope of this study to further investigate this contradiction, but it may be noted that both compaction equations have their supporters in the industry and both have led to useful empirical techniques for geopressure estimation.

This concludes the consideration of depth alone as the means to estimate formation density or overburden gradient. The next section considers the use of pre-drill seismic interval velocity data (or equivalently, interval transit time) to estimate formation density or overburden gradient.

5.2.3.1 Combining Athy's with Other Compaction Equations

There are other compaction equations besides the Hubbert-Rubey (1959) one which relate porosity to vertical effective stress. When applied to estimating overburden stress, these combinations are only expected to be accurate when the formations are normally compacted and normally pressured. When these conditions are not met, the resulting overburden is expected to be too high. To apply these equations, knowledge of a pair of empirically derived constants is required.

5.2.3.2 Athy and Baldwin-Butler Compaction Relations

The Baldwin-Butler (1985) equation has been popularized by Phil Holbrook (1987 and since) and has also been used by Tom Bryant (1989) in his "Dual Shale" pore pressure technique. Following Holbrook's notation, the Baldwin-Butler equation considers effective stress to be a power law function of solidity as follows:

$$\sigma_e = \sigma_{\max} (1 - \phi)^\alpha \quad (25)$$

Where: σ_e effective stress

σ_{\max} a power law material constant, the stress at which porosity is reduced to zero porosity, fraction

α another power law material constant

When combined with Athy's (1930) law, the following expression for overburden stress in deepwater can be derived:

$$OB = \rho_{sw} WD + P + \sigma_{\max} (1 - \phi_o e^{-kD})^\alpha \quad (26)$$

Where: OB overburden pressure

ρ_{sw} sea water density

WD water depth

P pore fluid pressure

- σ_{\max} power law material constant
- ϕ_0 initial (mud-line) porosity, fraction
- k Athy compaction constant
- D depth below mud-line
- α power law material constant

Keeping in mind that Athy's (1930) law is only said to be valid for normally compacting sediments, and since pore pressure is not known *a priori*, the above expression may be useful for estimating an upper bound for overburden stress (i.e. assuming normal pore pressure, e.g. 8.7 ppg). However, the use of this overburden stress could result in excessively high calculated pore pressures and fracture gradients. Unlike the Hubbert-Rubey (1959) compaction law, the combination of Athy's (1930) law with the Baldwin-Butler (1985) relation does not lead to an obvious contradiction.

5.2.3.3 Athy and Perloff-Baron Compaction Relations

Yet another compaction equation relates the void ratio, $\phi / (1 - \phi)$, to effective stress. The pore pressure technique of Alixant and Desbrandes (1989) makes use of the following compaction equation attributed to Perloff and Baron (1976):

$$\sigma_e = 10^{(\phi / (1 - \phi) - b) / a} \quad (27)$$

- Where: σ_e effective stress
- porosity, fraction
- b constant
- a constant

As above, this expression can be combined with Athy's (1930) law to derive an expression that can be used to estimate overburden stress in deepwater environments:

$$OB = \rho_{sw} WD + P + 10^{(\phi / (1 - \phi) - b) / a} \quad (28)$$

- Where: OB overburden pressure
- ρ_{sw} sea water density
- WD water depth
- P pore fluid pressure
- porosity from Athy's law, $\phi = \phi_0 e^{-kz}$
- b constant
- a constant

As with the combination of Athy's (1930) law with the Baldwin-Butler (1985) equation, the calculated overburden is only expected to be accurate when the formations are normally compacted and normally pressured.

5.2.4 Zamora's Method – Factoring in the Age of the Rock

In an attempt to generalize the Eaton (1968) Gulf Coast overburden gradient for different basins and for offshore use, Zamora (1989) proposed the following formula:

$$OB = (8.5 WD + (8.03 + 0.232 A) D^{1.075}) / Z \quad (29)$$

Where: OB overburden gradient, ppg
WD water depth, feet
A a parameter dependent on the geologic age of the rock
D depth below mud-line, feet
Z true vertical depth (e.g. referenced to RKB), feet

The parameter, A, is dependent on the age of the rock according to the following table:

Holocene – Pliocene:	0 – 5
Miocene – Oligocene:	5 – 9
Eocene – Paleocene:	9 – 10
Cretaceous – Triassic:	10 – 11
Permian – Older:	11 – 14

Zamora noted that a value of 4 for A provides a good match to the Eaton Gulf Coast curve.

5.3 Density and OBG from Acoustic Data

Since pre-drill seismic data are often available, they can be used to provide information about the sediment layers. Physically, the propagation of a compressional wave through rock is directly related to the density in at least three distinct ways: through the seismic reflection coefficient (acoustic impedance), through the elastic modulus and through the porosity.

It might seem plausible to also consider using effective stress as a “common ground” between velocity and overburden gradient. On deeper reflection, it is clear that if velocity is used to determine overburden through an effective stress transform, using a normal pore pressure assumption, then when the resultant overburden stress is applied, the pore pressures will calculate to be (surprise!) normal.

Consequently, there is no point in try to estimate overburden from seismic interval transit times using an effective stress relationship. The reason for this is that when this overburden is used to calculate pore pressures, the resulting values will only reflect the pore pressures used to calculate the overburden. Obviously, this kind of circular reasoning will not facilitate the design of useful mud weight or casing programs.

5.3.1 Seismic Reflection Coefficient

The formula for the seismic reflection coefficient is given by:

$$R = (\rho_2 V_{p2} - \rho_1 V_{p1}) / (\rho_2 V_{p2} + \rho_1 V_{p1}) \quad (30)$$

Where: R seismic reflection coefficient
 ρ_1 density of layer 1
 V_{p1} compressional velocity in layer 1
 ρ_2 density of layer 2
 V_{p2} compressional velocity in layer 2

This formula could be algebraically solved for the density of the sediment in layer 2 if the velocities of the layers have been determined, the reflection coefficient between the layers has been established and the density of the layer 1 is known. For deepwater applications, the sea water column could be used as the first layer 1 to begin the process of establishing the densities in all subsequent layers. Unfortunately, neither the data nor the tools were available within the DEA-119 project for testing this approach.

5.3.2 Elastic Modulus

The velocity of a compressional wave is given by the following formula:

$$V = (E / \rho)^{0.5} \quad (31)$$

Where: V velocity
 E elastic modulus (Young's modulus)
 ρ density

This equation can be rearranged to solve for density in terms of velocity and elastic modulus:

$$\rho = E / V^2 \quad (32)$$

For the DEA-119 Project, a brief investigation was made into the possible use of elastic modulus as a means of obtaining density from velocity data. For twelve of the wells, a "log-value" elastic modulus was obtained by the following rearrangement of equation (30):

$$C = 1 / E = \Delta t^2 / \rho \quad (33)$$

Where: C compressibility, "log units", i.e. (microseconds per foot)² / (g/cc)
 E elastic modulus
 Δt acoustic transit time, microseconds per foot
 ρ bulk density, g/cc

The idea was to investigate whether a useful relation between the elastic modulus and depth below the mud-line could be obtained. If so, then velocity of transit time could be used to estimate formation density. Compressibilities were calculated for twelve DEA-119 wells distributed across the U.S. deepwater Gulf of Mexico and then averaged. The resulting average compressibility was used to calculate density as a function of acoustic

travel time. The result was a wildly varying curve that represented unrealistic density values.

5.3.3 Gardner Equation

By far, the most popular method for deriving density information from acoustic data is the Gardner (1974) equation. Part of the reason for this is its simplicity. There is no need for any additional inputs besides velocity. The equation has the form of a power law:

$$\rho = a V^b \quad (34)$$

- Where: ρ density, g/cc
a empirical coefficient, 0.23 was the original value
V velocity, feet per second
b empirical exponent, 0.25 was the original value

In practice the Gardner equation, with its original constants, has had a reputation for generally underestimating formation densities in offshore environments. This has been confirmed for most of the wells in this study. To correct the results of using the Gardner equation, some operators have locally calibrated the power law constants using available density log data. In some cases, it has been found that changing the coefficient to 0.25 has been sufficient to yield more accurate formation densities. Due to the magnitude of velocity values expressed in feet per second, Gardner's equation is more sensitive to changes in the exponent than to changes in the coefficient.

5.3.4 Pennebaker's Transform

Pennebaker (1968), one of the pioneers in pre-drill geopressure analysis from seismic data, published a method for pore pressure and fracture gradient analysis. One of the less utilized concepts in his paper was the idea of using the depth at which the interval transit time reached some compaction-related value to estimate overburden gradient. The criterion selected by Pennebaker was 100 μ sec/ft. In some respects this method is akin to Zamora's in that the resulting overburden gradient will be correlated with geologic age. The method probably has merit; however, Pennebaker's curves (Fig.3, below) have not yet been converted into an algorithm that can be readily tested with digital computer techniques.

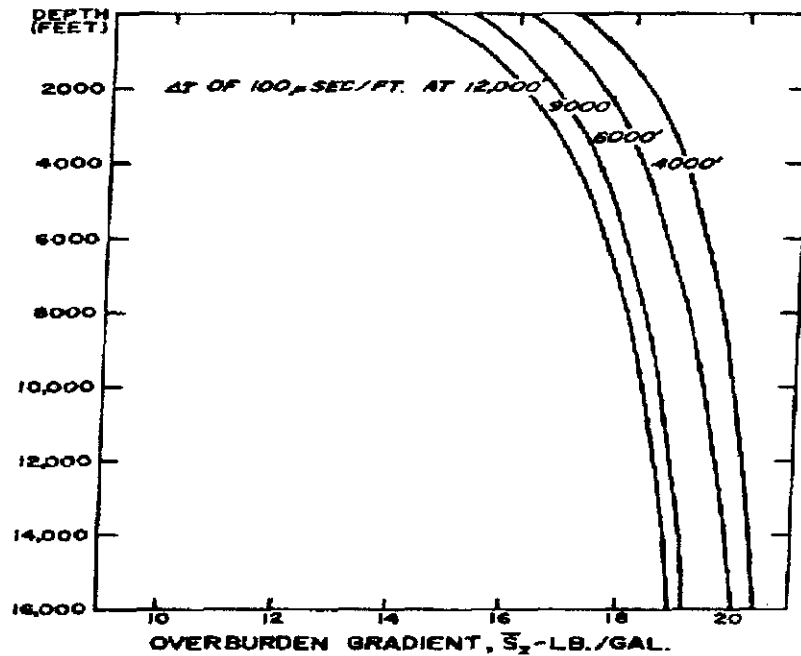


Fig.4 - Pennebaker's OBG Transform

5.3.5 Bellotti – Giacca Transform

This transform received wide attention due to the time and place it was published. It was published in 1978 as MWD tools were being introduced into commercial service and the need to establish overburden gradients in the absence of density logs was being increasingly appreciated. Furthermore, due to the fact that it was published in the Oil and Gas Journal gave it wide circulation. The constants used in the formula suggest that it has been optimized for a specific area (the Po Valley Basin in Italy), however the form of the equation may be applicable in other areas. The formula was published as follows:

$$\rho = 2.75 - 2.11 (\Delta t - 53) / (\Delta t + 200) \quad (35)$$

5.3.6 Early DEA-119 Velocity/Density Transform

This is not a generally available method for a velocity to density transform. It was produced by the collaboration of Nader Dutta and Steve Hobart in the early stages of the DEA-119 project. The essence of the method is the recognition that the smectite portion of shales undergoes a transformation into another clay called illite. This transformation is dependent on temperature and time ("cooking") and requires the presence of potassium, which is usually available in the pore waters. In this method, the transit time was taken as an indicator substitute for the degree of smectite/illite transformation. A more scientific approach would utilize a time-temperature history (assuming the data were available) to quantify the degree to which the transformation had completed. The details of such a method are laid out in working paper developed by Dutta and Hobart early in 1999 and presented as an Appendix. This ideal scientific approach requires that assumptions be made concerning initial smectite concentrations, burial rates, temperature gradients and

chemical kinetics constants and was considered to be too complex for general use, even if the constants could be accurately determined.

The simplified method was an improvement over the Gardner Method, but has since been superceded by the Later DEA-119 Velocity/Density Transform.

The formulas used in the Early DEA-119 Velocity/Density Transform created three linear equation for estimating density from transit time. These equation were suggested by inspection of crossplots of delta-t and density data from the earliest wells submitted to the DEA_119 project.

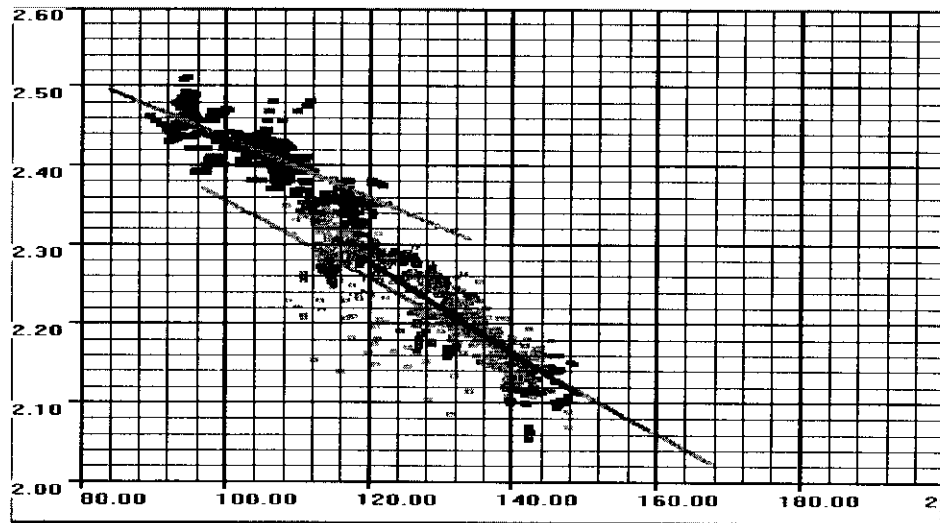


Fig.5 – Delta-T/Density crossplot suggests possible clay diagenesis effect

The formulas were written in a form conducive to utilizing sonic logs, i.e. in terms of transit times rather than velocities. The reason for this was that sufficient seismic data had not been available at the time the transform was developed, but wireline logging data had become available. The three equations are for three distinct ranges of Δt :

$$\text{For } \Delta t > 130 \mu\text{sec/ft:} \quad \rho = (-0.00516) \Delta t + 2.922 \quad (36)$$

$$\text{For } 100 \leq \Delta t \leq 130 \mu\text{sec/ft:} \quad \rho = (-0.008) \Delta t + 3.24 \quad (37)$$

$$\text{For } \Delta t < 100 \mu\text{sec/ft:} \quad \rho = (-0.00381) \Delta t + 2.81568 \quad (38)$$

5.3.7 Later DEA-119 Velocity/Density Transform

This transform is, as of this report, the one which best transforms acoustic velocity data into formation density. The transform was created by combining two simple components: the constitutive equation for bulk density and the porosity transform developed by Raiga-Clemenceau *et al.* (1986) for obtaining porosity from acoustic log measurements. With apologies to Mr. Raiga-Clemenceau and his colleagues, this acoustic porosity transform will be referred to as simply the Raiga equation to facilitate discussion.

The constitutive equation for bulk density is a simple average of the densities of the rock constituents weighted by the bulk volumes of each material. For a binary mixture of a single mineral and a single fluid:

$$\rho_b = \phi \rho_f + (1 - \phi) \rho_m \quad (39)$$

Where: ρ_b bulk density

porosity

ρ_f fluid density

ρ_m matrix density

When solved for porosity, the equation becomes:

$$\phi = (\rho_m - \rho_b) / (\rho_m - \rho_f) \quad (40)$$

The Raiga equation, also known as the acoustic formation factor equation after its similarity to Archie's (1942) resistivity equation is as follows:

$$\phi = 1 - (\Delta t_m / \Delta t)^{1/x} \quad (41)$$

Where: ϕ porosity

Δt_m transit time of matrix material

Δt transit time of formation

x an empirical exponent dependent on the matrix material

Using porosity as the common parameter, the two equations can be combined and solved for bulk density in terms of acoustic transit time and material properties:

$$\rho_b = \rho_f + (\rho_m - \rho_f) (\Delta t_m / \Delta t)^{1/x} \quad (42)$$

For the wells studied to date, the following parameters have been useful in synthesizing density data from acoustic logs: $\rho_f = 1.03$ g/cc, $\rho_m = 2.60$, $\Delta t_m = 67.054$ and $x = 2.19$. The matrix travel time and the exponent, x, were obtained from references to a work by Issler (1992) wherein these parameters were attributed to shale.

It should be noted that other (older) velocity to porosity transforms, such as the Wyllie (1956) or Raymer-Gardner-Hunt (1980), could have been coupled to the constitutive bulk density equation in the same manner. This was not been done for this study.

6 Results to This Point

6.1 Introduction

At this time, November 1999, insufficient seismic interval velocity data have been collected to test the various acoustic methods for obtaining density estimates for deriving local pre-drill overburden gradients. Hopefully, this data will be forthcoming and will permit this study to reach its intended objective. Nevertheless, a preliminary study and comparison of several of the above referenced methods has been conducted and is discussed below.

6.2 Methodology

At the time this study was conducted, the bulk of the available DEA-119 well data consisted of public domain wireline logging data obtained from GDC. Data from thirty-two deepwater wells from across the Gulf of Mexico had been collected and analyzed. Of these thirty-two wells, twelve were selected to provide a wide geographic sweep and to try to avoid creating a geographic bias. The water depths for these wells range from 1220 feet to 7520 feet. Full analyses have since been conducted on the remainder of the wells (including wells submitted by other participants) and have confirmed the overall conclusions reached from the initial study.

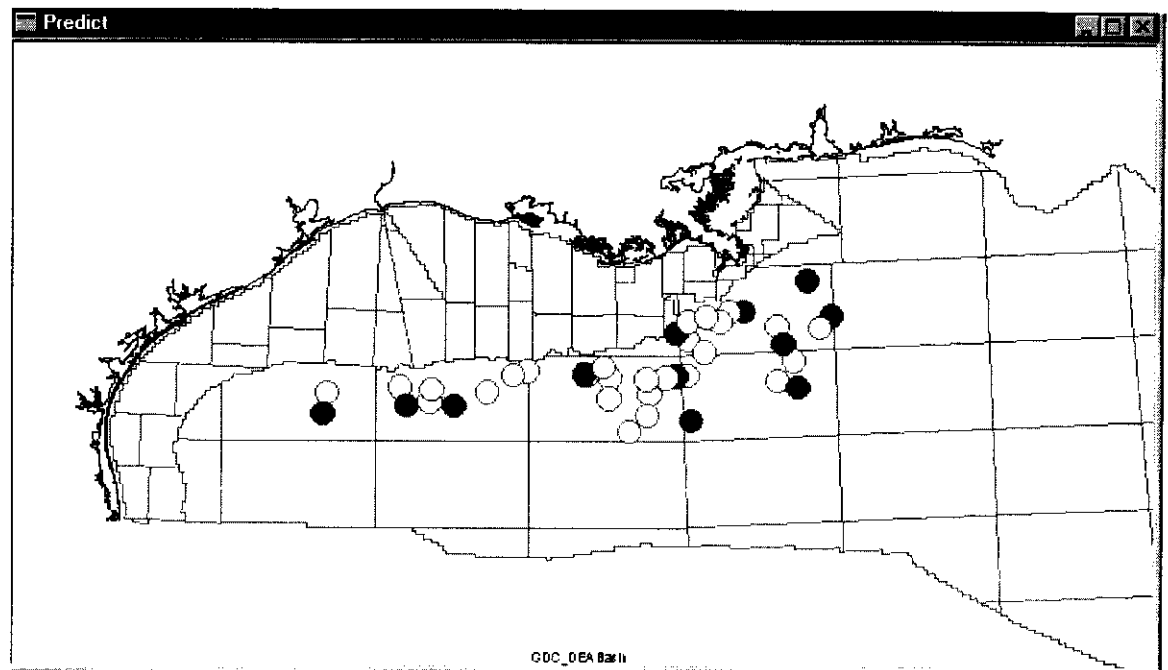


Fig.6 - Subset of wells for preliminary OBG study

The data provided by GDC was in LAS format. It included curves indicating “bad hole flags” for both density and sonic data. The “bad hole flag” data, density and sonic log data were imported into the DrillWorks/PREDICT program for analysis. The density and

sonic log data were filtered to remove data from depths in which either log was tagged with the “bad hole flag”.

The comparison of the depth-based methods involved first calculating an average density curve relative to depth below the mud-line for the twelve study wells. This average density was then integrated to obtain an overburden gradient, interpolating linearly from 2000 feet below the mud-line to an assumed a mud-line density of 1.95 g/cc. The Jones and Barker methods were also converted from density to overburden gradient using the same assumptions. The algorithms for the Bell, Simmons-Rau and Traugott methods were computed from the mud-line, as well. The original Eaton (1968) Gulf Coast overburden gradient was plotted alongside the previously mentioned curves for comparison purposes.

The comparison of velocity-to-density methods involved estimating formation density using various methods and creating a “density difference” dataset for each method. This density difference was constructed by subtracting the density obtained from each of the studied methods from the filtered wireline bulk density log. The mean value of this density difference curve was used to rank the accuracy of the various methods tested.

6.3 Best Depth-only method

Among the algorithms tested, the one provided by John Jones of Marathon for calculating density as a function of depth created an overburden gradient with the least difference from the one produced using the average of the density log readings in the subject wells.

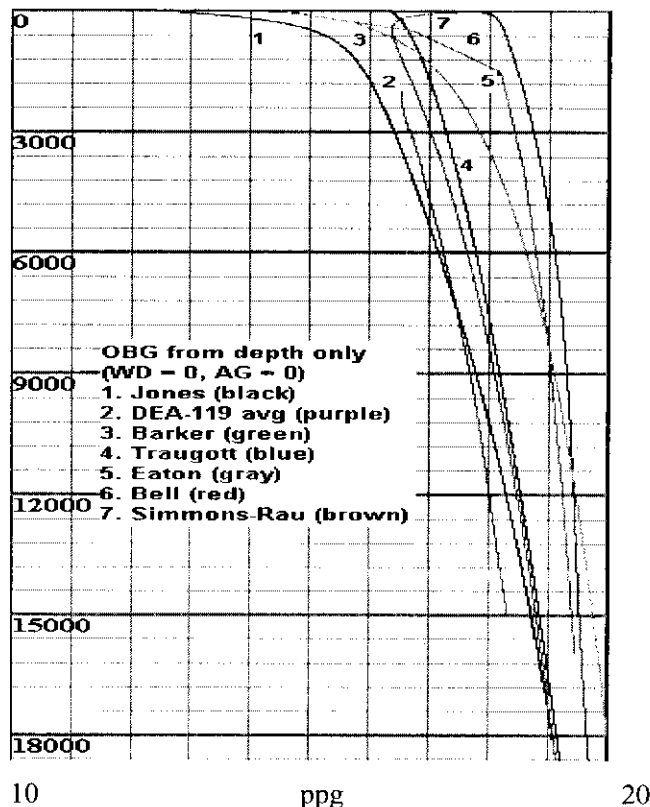


Fig.7 – OBG from depth below mud-line

It is feasible to modify the Jones algorithm to create a better fit to the DEA-119 data, however the findings shown in Fig.7 below indicate that no depth-only method can be used with confidence without data from near-by control wells. The reason for this is the range of density data encountered in these wells. The Eaton data (Fig.1, above) have a maximum spread of about 0.1 g/cc between the minimum and maximum densities encountered. For just the twelve wells analyzed, the variation in densities is over 0.2 g/cc over the interval 2910 to 12700 feet below the mud-line. Obviously, this kind of variation in actual densities could lead to serious errors in overburden estimation. Therefore, it is recommended to use the site-specific seismic interval velocity data to estimate densities for overburden gradient calculation.

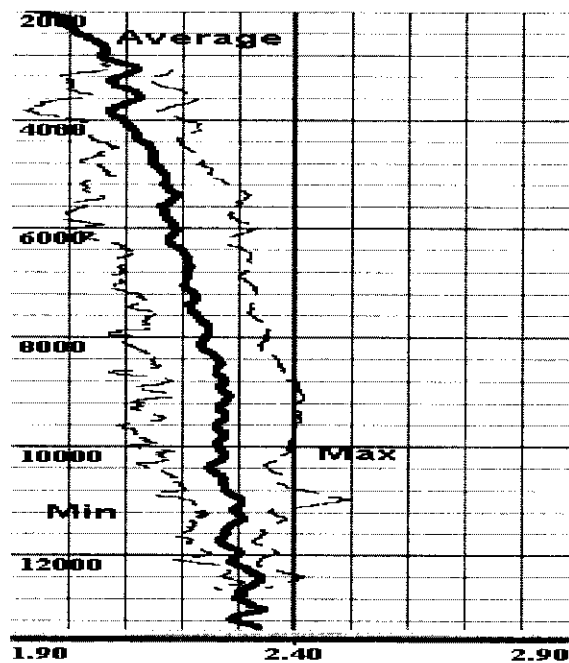


Fig.8 – Range of density data for 12 DEA-119 wells

6.4 Best Acoustic method

As mentioned above, two new algorithms have been developed so far in the course of the DEA-119 study. The best one by far is the one called the “Later DEA-119 Velocity/Density Transform” based on the Raiga-Clemenceau (1986) equation using Issler’s (1992) constants, an average matrix density of 2.6 g/cc and a fluid density of 1.03 g/cc. This method was the best in eight of the twelve representative wells selected, producing the least mean difference between actual density data and density predicted from the new transform. In only two of the wells did another method yield a smaller standard deviation in the difference between actual and predicted density.

Of the four wells in which the new method was not the best, two were the most westerly wells. In these, the Gardner method produced the best results. This suggests that a regional calibration of the constants could improve the results, as would be expected

when there may be a difference in source rocks or other geological parameters. Overall however, the Gardner method did not fare well: the actual density data averaged higher than the Gardner prediction by 0.040 g/cc, being higher in eleven of the twelve wells. In contrast, the new method produced average densities that were too low in seven of the twelve wells, with an average difference of 0.0037 g/cc.

An attempt was made to find the best-fit coefficient and exponent for the Gardner equation for each of the twelve wells in this study. The results were surprising. Although the average values of the best-fit coefficient (0.230) and exponent (0.261) were close to the originally published values, (0.23 and 0.25, respectively), the range of these parameters was considerable. The range for the coefficient was 0.098 to 0.448 with a standard deviation of 0.106. The range for the exponent was 0.178 to 0.348, with a standard deviation of 0.047. In the two wells in which the Gardner was the best method, one had a coefficient and exponent of 0.399 and 0.190, respectively (East Breaks 688) which is a considerable deviation from the standard values. The other well (Garden Banks 581) had values of 0.248 and 0.240 as the best-fit coefficient and exponent, which are close to the published values.

In the very deepest well, the Traugott algorithm (a depth-only method) produced the best match to actual density. However, the standard deviation for the difference between actual and predicted densities was greatest of the methods tested. The new method was second best in this well, surpassing the other acoustic-based methods.

In the other well, the "Earlier DEA-119 Velocity/Density Transform" was the best. This was the only one in which it was known that the analyzed data were sub-salt. This is too small a sample to be conclusive, but this correlation perhaps ought to be investigated further.

6.5 Direct comparison of Gardner Method with Later DEA-119 Method

Since one of the objectives of the DEA-119 project is to seek improvements to existing methodologies, this section will focus on a comparison of the best DEA-119 method produced so far with the existing, default, industry standard, the Gardner Method. The following table contains three columns. The first column identifies the block from which the study well was taken. The second column contains the result of subtracting the Gardner-derived density from the actual wireline density ("bad hole" data excluded). The third column contains a similar calculation performed on density data derived from the Later DEA-119 transform.

	<u>Gardner</u>	<u>Later DEA-119</u>
MC546	0.021	-0.016
AV575	0.038	0.001
GC260	0.044	0.007
GC235	0.036	0.001
MC211	0.085	0.049
MC706	0.028	-0.009
GB581	-0.011	-0.049
AV471	0.028	-0.009
MC657	0.059	0.022
EB688	0.017	-0.019
GB594	0.05	0.013
MC952	0.047	0.011
-----	-----	-----
Average	0.036833	0.000166667

Table 1 – Mean differences from wireline density

As can be seen, in eleven of the twelve representative sample wells, the Gardner Method underestimated the formation densities using wireline sonic data. This supports the general consensus that the Gardner Method underestimates densities. In contrast, the new method underestimated the densities in roughly half of the wells, seven out of twelve. Of these twelve wells, the Gardner Method did a better job of estimating densities in only two, the GB581 and EB688 wells. These are the two most westerly wells in the sample, which suggests that a further investigation into the influence of geographic location is warranted.

The GC235 well has statistics which match fairly well with the average statistics, as can be seen from the above table. To get a visual feel for the significance of the differences between the methods, the following plot is presented.

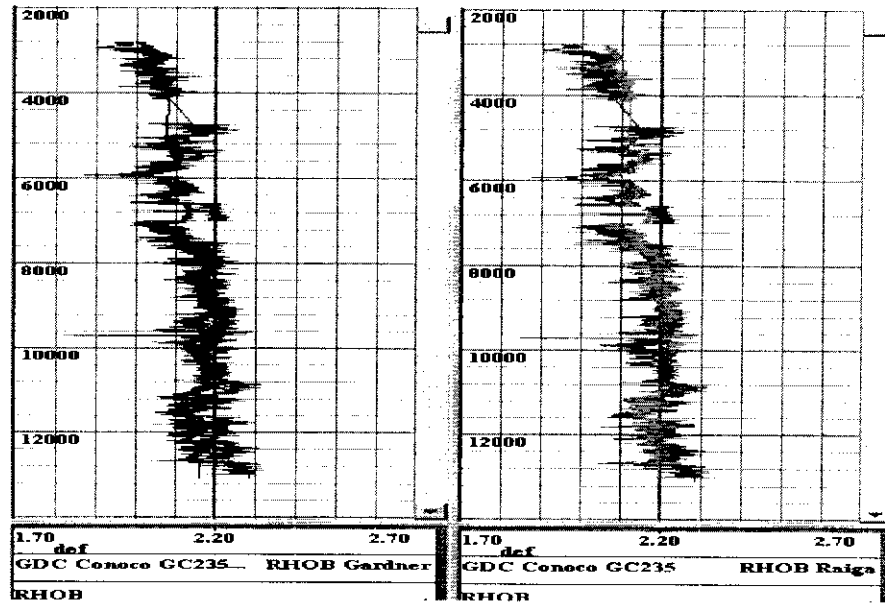


Fig. 9 – Comparison of Gardner and Later DEA-119 methods with actual density logs. Well is representative of study wells.

Being that the object of this study is to determine the best method for estimating overburden gradient before drilling, it is appropriate to include another plot which shows, on average, what the expected difference between overburdens should be when using the two methods. At 10,000 feet below the mud-line, i.e. at a depth of 11,792 feet in this well, the Later DEA-119 overburden gradient is 0.25 ppg “heavier” than the overburden gradient obtained using the Gardner-derived densities.

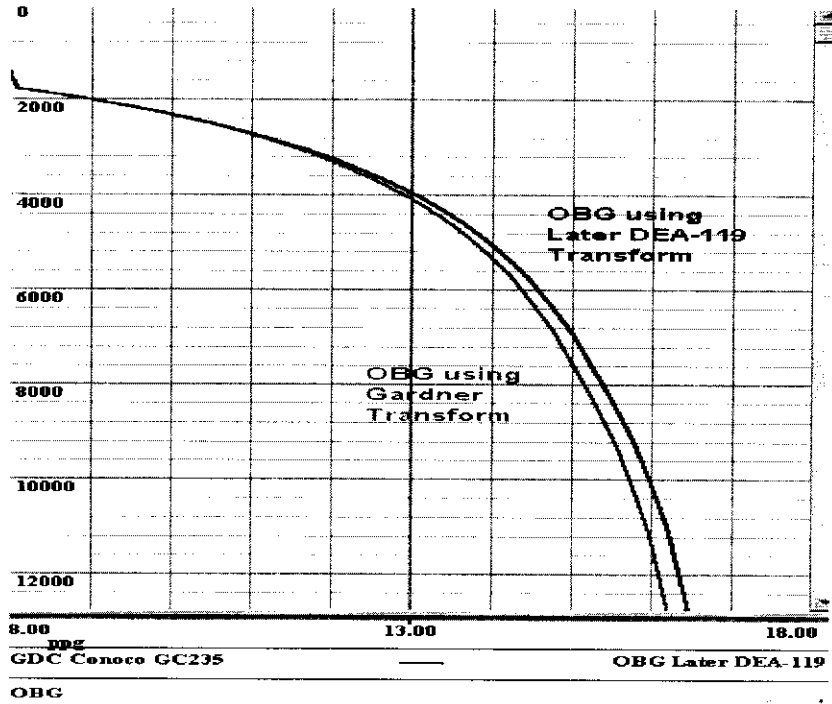


Fig. 10 – Comparison of overburden gradients from Gardner and Later DEA-119 methods.

7 Conclusions

It should also be noted that the above results were obtained using wireline sonic log data in the absence of actual seismic interval velocity data. Without being able to test these algorithms against actual seismic interval velocities, it can only be presumed that these conclusions will be valid for seismic data as well.

Preliminarily, however, it can be concluded that the Later DEA-119 transform provides the best means of converting acoustic log data into synthetic density logs that can be integrated to provide overburden gradient estimates for pore pressure and fracture gradient calculations. The Gardner method has been shown to generally underestimate densities and all depth-only methods are suspect because of the variability in deepwater formation densities. This conclusion has been supported by the subsequent geopressure analyses performed on the remainder of the DEA-119 well data collected to this point, however a statistical analysis of this larger body of data has not been completed.

There is scope for further work in this investigation. Foremost is the necessity of apply these transforms to actual seismic interval velocity, of which very little has been received at this time. In addition, the reliability of the statistics may be enhanced somewhat by including all of the DEA-119 wells, however this increases the risk of introducing geographical bias into the results. This suggest, in turn that the role of geographic location should also be investigated with respect to choice of method and/or parameter selection. It is also possible that an as yet uninvestigated technique could provide an even better acoustic data-to-density transform, although a review of Table 1 suggests that any future improvement would be quite marginal.

8 References

Note: Asterisk indicates reference for which the original document was not available at the time of this report.

Aadnoy, B.S., and Larsen, K., 1987, "Method for Fracture Gradient Prediction for Vertical and Inclined Boreholes", SPE 16695, presented at 62nd Annual Technical Conference and Exhibition of the Society of Petroleum Engineers, Dallas, Texas, September 27 – 30, 1987.

Alixant, J-L., and Desbrandes, R., 1989, "A New Approach to Real-Time Pore Pressure Evaluation", SPE 19336, presented at the SPE Eastern Regional Meeting, Morgantown, West Virginia, October 24 – 27, 1989.

* Archie, G.E., 1942, "The Electrical Resistivity Log as an Aid in Determining Some Reservoir Characteristics", Transactions of the AIME, Volume 146, pp.54 – 62.

Athy, L.F., 1930, "Density, porosity, and compaction of sedimentary rocks", *Bulletin of the American Association of Petroleum Geologists*, volume 14, pp. 1 – 24.

* Baldwin, B, and Butler, C.O., 1985, "Compaction Curves", *American Association of Petroleum Geologists Bulletin*, Volume 69, April 1985, pp.622 – 626.

Barker, J.W., and Wood, T.D., 1997, "Estimating shallow below mud-line deepwater Gulf of Mexico fracture gradients", Presented at the Houston AADE Chapter Annual Technical Forum, April 2-3, 1997. (An adaptation of this presentation can be found in the August 1998 *Deepwater Technology* supplement to *World Oil* magazine, page 51.)

* Bell, L.N., 1969, Atlantic Richfield Drilling Manual.

Bellotti, P., and Giacca, D., 1978, "Pressure Evaluation Improves Drilling Program", *The Oil and Gas Journal*, September 11, 1978, pp. 76 – 85.

Boggs, Sam, Jr., 1995, Principles of Sedimentology and Stratigraphy, 2nd ed., Prentice-Hall, New Jersey, 774 p.

Bourgoyne, A.T., Chenvert, M.E., Millhelm, K.K., and Young, F.S., Jr., 1986, Applied Drilling Engineering, SPE Textbook Series, Volume 2, Society of Petroleum Engineers, Richardson, Texas, 502 p.

Bryant, T., 1989, "A Dual Shale Pore Pressure Detection Technique", SPE/IADC 18714, 1989 Drilling Conference, New Orleans, Louisiana, February 28 – March 3, 1989.

Christman, S.A., 1972, "Offshore Fracture Gradients", SPE 4133, 47th Annual Fall Meeting of the Society of Petroleum Engineers of AIME, San Antonio, Texas, Oct. 8 – 11, 1972.

Dobrin, M.B., 1976, Introduction to Geophysical Prospecting, 3rd ed., McGraw-Hill, Inc., New York, 630 p.

Eaton, B. A., 1968, "Fracture Gradient Prediction and Its Application in Oilfield Applications", SPE 2163. SPE 43rd Annual Fall Meeting, Houston, Texas, Sept.29 – Oct.2, 1968.

Eaton, B.A., and Eaton, T.L., 1997, "Fracture gradient prediction for the new generation", *World Oil*, October 1997, pp. 93 – 100.

* Gardner, G.H.F., Gardner, L.W., and Gregory, A.R., 1974, "Formation Velocity and Density – The diagnostic basis for stratigraphic traps", *Geophysics*, Volume 39, Number 6, pp. 2085 – 2095.

Hart, B.S., Flemings, P.B., and Deshpande, A., 1995, "Porosity and Pressure: Role of Compaction Disequilibrium in the Development of Geopressures in a Gulf Coast Pleistocene Basin", *Geology*, Volume 23, pp. 45-48. Available at <http://hydro.geosc.psu.edu/Papers/Hart/pressure.html>

Holbrook, P.W., and Hauck, M.L., 1987, "A Petrophysical-Mechanical Math Model for Real-Time Pore Pressure/Fracture Gradient Prediction", SPE 16666, 62nd Annual Technical Conference and Exhibition, Dallas, Texas, September 27 – 30, 1987.

* Issler, D.R., 1992, "A New Approach to Shale Compaction and Stratigraphic Restoration, Beaufort-Mackenzie Basin and Mackenzie Corridor, Northern Canada", *American Association of Petroleum Geologists Bulletin*, Volume 76, number 8, pp. 1170 – 1189.

Jones, John, 1999, personal communication. Used by permission.

Krumbein, W.C., and Sloss, L.L., 1963, Stratigraphy and Sedimentation, 2nd ed., W.H. Freeman and Company, San Francisco, 660 p.

Magara, K., 1978, Compaction and Fluid Migration – Practical Petroleum Geology, Elsevier Scientific Publishing Company, New York, 319 p.

Pennebaker, E.S., 1968, "An Engineering Interpretation of Seismic Data", SPE 2165, 43rd Annual Fall Meeting of the Society of Petroleum Engineers of AIME, Houston, Texas, Sept. 29 – Oct 2, 1968.

* Perloff, W.H., and Baron, W., 1976, Soil Mechanics Principles and Applications, John Wiley and Sons

Raiga-Clemenceau, J., Martin, J.P., and Nicoletis, S., 1986, "The Concept of Acoustic Formation Factor for More Accurate Porosity Determination from Sonic Transit Time Data", SPWLA 27th Annual Logging Symposium Transactions, Paper G, June 9 – 13, 1986.

Raymer, L.L., Hunt, E.R., and Gardner, J.S., 1980, "An Improved Sonic Transit Time-to-Porosity Transform", SPWLA 21st Annual Logging Symposium Transactions, Paper P, July 8 – 11, 1980.

* Rubey, W.W., and Hubbert, M.K., 1959, "Overthrust belt in geosynclinal area of western Wyoming in light of fluid pressure hypothesis, 2: Role of fluid pressure in mechanics of overthrust faulting", *Geological Society of America Bulletin*, v. 70, pp.167 – 205.

Stump, B.B., Flemings, P.B., Finkbeiner, T., and Zoback, M.D., 1998, "Pressure Differences Between Overpressured Sands and Bounding Shales of the Eugene Island 330 Field (Offshore Louisiana, U.S.A.) with Implications for Fluid Flow Induced by Sediment Loading", Proceedings of the Workshop on Overpressures in Petroleum Exploration, Pau, France, April 7 – 8, 1998.

- * Terzaghi, K., 1943, Theoretical Soil Mechanics, John Wiley and Sons, New York City.
- Traugott, M.O., 1997, "Pore/fracture pressure determinations in deep water", *World Oil – Deepwater Technology Supplement*, August 1997, pp. 68 – 70.
- * Wyllie, M.R.J., Gregory, A.R., and Gardner, L.W., 1956, "Elastic Wave Velocities in Heterogeneous and Porous Media", *Geophysics*, Volume 21, number 1, pp.41-70.
- Zamora, M., 1989, "New Method Predicts Gradient Fracture" (*sic*), *Petroleum Engineer International*, September 1989, pp. 38 – 47.

9 Appendix

“On the Effect of Clay Diagenesis (Smectite to Illite) on the Density/Delta-T Crossplot”

The following short paper is appended to show another possible approach to estimating density from velocity, taking into account the possible effect of clay diagenesis on such a transform. This short paper was to provide a scientific foundation for the Early DEA-119 method, which was supplanted by the much more accurate Later DEA-119 method. It remains feasible that with accurate information regarding sedimentation rates, temperature gradients and chemical reaction constants that this model could provide the basis for an even better transform. The bulk of the included science pertaining to clay diagenesis was provided by Nader Dutta, a consultant for the DEA-119 project in early 1999. Steve Hobart of Knowledge Systems, Inc., performed the remainder of the work.

9.1 On the Effect of Clay Diagenesis (Smectite to Illite) on the Density/Delta-T Crossplot

By: Nader Dutta and Steve Hobart for the DEA-119 Project

Basic physical principles and mathematical modeling

Physical Principles

The rate of change in the number of moles of smectite in a sediment is proportional to the number of moles remaining.

$$dN/dt = -K N$$

Where: N number of moles of smectite
 t time
 K proportionality constant

The Arrhenius equation for the rate of a chemical reaction is assumed to be adequate to model the smectite illite transformation.

$$K = A e^{-E/RT}$$

Where: K rate constant
 A frequency factor
 e base of natural logarithms
 E activation energy
 R gas constant in appropriate units
 T temperature in degrees Kelvin

The two equations can be combined as follows:

$$dN/dt = -N A e^{-E/RT}$$

The inflection point in the transformation occurs at the point of maximum change in the transformation rate.

$$dN/dt \Big|_{\max} \quad \text{occurs at} \quad d/dt (dN/dt) = 0$$

Differentiation of (3) yields:

$$d/dt (dN/dt) = -A e^{-E/RT} dN/dt + (-NA (d(e^{-E/RT})/dt))$$

$$d/dt (dN/dt) = -A [e^{-E/RT} dN/dt + N e^{-E/RT} d(-E/RT)/dt]$$

$$d/dt (dN/dt) = -A e^{-E/RT} [dN/dt + (-NE/R (d(T^{-1})/dt))]$$

$$d/dt (dN/dt) = -A e^{-E/RT} [dN/dt - (NE/R) (-1/T^2) (dT/dt)]$$

Since the expression is equal to zero at the inflection point and since neither A nor $e^{-E/RT}$ are equal to zero:

$$0 = dN/dt + NE/RT^2 dT/dt$$

$$dN / dt = - NE / RT^2 dT / dt$$

Substitution of equation (3) in the left side of (10) yields:

$$- N A e^{-E/RT} = - NE / RT^2 dT / dt$$

$$e^{E/RT} = (E / RA) T^{-2} dT / dt$$

Various values for the activation energy for the conversion of synthetic beidellite to a mixed layer smectite- illite:

$$E = 19.6 \pm 3.6 \text{ kilocalorie per mole} \quad \text{Eberl and Hower (1976)}$$

$$E = 19.3 \pm 0.7 \text{ kilocalorie per mole} \quad \text{Dutta (1987)}$$

Various values for the frequency factor:

$$A = 2 \text{ sec}^{-1} \quad \text{Eberl and Hower (1976)}$$

$$A = 1 - 10 \text{ sec}^{-1} \quad \text{Eberl (1980) quoted by Domenico \& Palciauskas}$$

$$A = 0.4 \times 10^5 \text{ yr}^{-1} \quad \text{Dutta (1987)}$$

$$!!! 0.4 \times 10^5 \text{ yr}^{-1} = 0.0013 \text{ sec}^{-1}$$

9.1.1 Geological model

There is an average rate of growth, ω , for a basin. This rate is expressed as number of feet of sediment per year. This will be a positive number if the rate of accretion is greater than the combination of the rate of subsidence (compaction) and the rate of erosion. A simplified model says that the depth of a given formation is equal to the average rate of basin growth times the number of years (age) the elapsed since the deposition of the formation sediments.

$$Z = \omega t$$

Where: Z true vertical depth of the formation

average basin growth rate

t age of the formation

The temperature of a sediment increases with depth. A simplified model for the temperature of a formation equates it to the average surface temperature plus the depth times a geothermal gradient:

$$T = T_s + G Z$$

Where: T temperature of the formation

T_s average surface temperature (mudline temperature for deepwater)

G geothermal gradient in degrees per unit depth

Z true vertical depth below surface temperature depth reference

Substituting equations (13) into equation (14):

$$T = T_s + G \omega t$$

Assuming the average surface temperature has remained constant (more valid for deepwater than elsewhere), it may be noted that the term $(G \omega)$ is the rate of temperature increase. This leads to the derivative:

$$dT / dt = G \omega$$

Integration of the Geological and Phase Transformation Models

Substitution into equation (12) yields:

$$e^{-E/RT} = (E / RA) T^{-2} G \omega$$

Recalling that T is the temperature at which the transformation rate from smectite to illite is at a maximum, we designate this temperature as T_m . Taking logarithms of both sides of equation (17) we get:

$$E / RT_m = \ln (ART_m^{-2} / G\omega E)$$

This is equation (16) in the article by Domenico and Palciauskas. Since there is no analytical solution, an iterative method must be used. Rearranging the terms of equation (17) above, we are seeking the value of T_m where the following expression is true:

$$e^{-E/RT_m} - (G\omega E / RA) T_m^{-2} = 0$$

The Newton-Raphson method, also known as *regula falsi* (or the method of false position), may be used to converge on a value for T_m . The algorithm convergence is based on the following series:

$$x_{n+1} = x_n - F(x_n) / F'(x_n)$$

Dispensing with the m subscript for T_m , this becomes for $F(T) = e^{-E/RT} - (G\omega E / RA) T^{-2}$ (equation 19 above):

$$T_{n+1} = T_n - (e^{-E/RT_n} - (G\omega E / RA) T_n^{-2}) / ((-E/RT_n^{-2}) (e^{-E/RT_n}) + 2 (G\omega E / RA) T_n^{-3})$$

Equation (21) may be iterated as many times as necessary until the absolute value of the difference between T_n and T_{n+1} is smaller than some pre-selected value, say 0.1 degrees.

9.1.2 Application of the integrated model

To use the model certain physical constants must be known or assumed. Nader suggests the following (for a one significant digit accuracy):

E	19.3	kilocalorie / mole
A	0.4×10^{-5}	/ year
R	0.002	kilocalorie / mole / degree Celsius
G	5.6×10^{-3}	degrees Celsius per foot
ω	0.001 to 0.005	feet / year

To facilitate computations, a table was constructed:

T (degC)	T (degK)	E/RT (degK)	$\ln[(RA/EG\omega) T^2]_{\omega=0.001}$
80	353	27.34	25.25

100 373 25.87 25.357 (?)

$$RA/EG\omega = (2) (10^{-3}) (4.0) (10^4) / (19.3) (5.6) (10^{-3}) (10^{-3}) = 7.4 \times 10^5$$

We have determined that there are three regions on the $\Delta t - \rho$ crossplot:

A region in which the original smectite concentration remains virtually constant but compaction process dominates the $\Delta t - \rho$ relationship. This occurs at lower temperatures or with higher sedimentation rates, basically the smectite can be considered as "uncooked". This is modeled with a linear relation.

A region in which all the smectite has converted (been "cooked") into illite, modeled with a different linear relation.

A region of transition between the two above regions

For sake of discussion, the linear model for the "uncooked" sediment will be designated as follows:

$$\rho_1 = a_1 + b_1 \Delta t$$

Likewise the "cooked" sediment will be modeled as follows:

$$\rho_2 = a_2 + b_2 \Delta t$$

The transition zone can be modeled taking into account the degree of transformation that has taken place:

$$\rho_3 = \rho_1 I(t) + \rho_2 [1 - I(t)]$$

Where:

$$(25) \quad I(t) = \exp\left(-\int_{0,t} A e^{-E/RT(t')} dt'\right)$$

$$\text{As: } t \rightarrow 0, \quad \dot{I}(t) \rightarrow 1, \quad \rho \rightarrow \rho_1$$

$$\text{As: } t \rightarrow \infty, \quad \dot{I}(t) \rightarrow 0, \quad \rho \rightarrow \rho_2$$

The integration of equation (25) can be performed if the burial history is known, namely the $T(t)$ function. For uniform burial, equation (15) can be assumed.

Logging data suggest that the minimum Δt for which equation (22) is valid is greater than the maximum Δt for which equation (23) is valid. Also, the maximum ρ for which equation (22) is valid is less than the minimum ρ for which equation (23) is valid.

9.1.3 Method

Steps:

Edit the Δt and ρ_b logs as necessary. The caliper and Delta-Rho curves may be used to identify questionable Density log data. The Sonic log should be edited to remove cycle-skipping.

Smooth the Δt and ρ_b logs. The smoothing should be a moving, depth-based filter with an averaging length sufficient to eliminate any reversals. A smoothing interval of at least 500 feet or more may be needed.

Assign a surface / mudline temperature, $T_s = 40$ degF Assume a simple (uniform) geothermal gradient, G : $T = GZ + T_s$

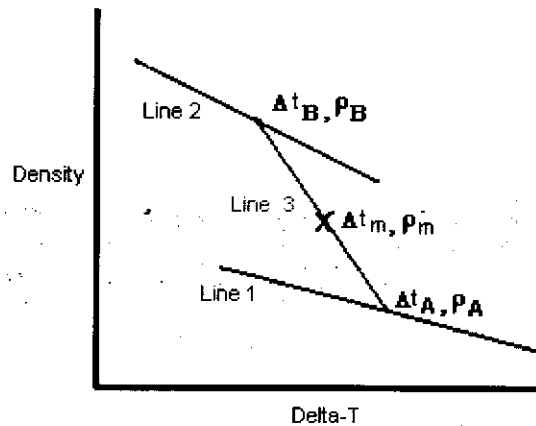
Assume a uniform burial rate: $\omega = 1 - 5$ feet / 1000 years

Find T_m by solving: $E / RT_m = \ln (ART_m^2 / G\omega E)$

Convert to degF

Compute depth $Z = Z_m$, where $T = T_m$: $Z_m = (T_m - T_s) / G$

Use smoothed data to find $\rho = \rho_m$ and $\Delta t = \Delta t_m$ at $Z = Z_m$



(Note: Point A is defined at $Z = Z_A$ where $T = 175$ degF.)

Obtain slope and intercept of Line 3 (from points A and m)

Find intersection of Line 3 with Line 2, for ρ_B and Δt_B .

9.1.4 References

Domenico, P.A., Palciauskas, V.V., 1988, The generation and dissipation of abnormal fluid pressures in active depositional environments in The Geology of North America Volume O-2, Hydrogeology, The Geological Society of America, pp. 435-445.

Dutta, N.C., IFP book (1987) (pp.567-596)

Eberl, D., Hower, J., 1976, Kinetics of illite formation: Geological Society of America Bulletin, v.87, pp. 1326-1330.



KNOWLEDGE SYSTEMS, INC.

Velocity - Effective Stress Relations

Steve Hobart

3/30/1999

CONFIDENTIAL

*This report is provided to **DEA Project 119** Project Participants under the terms of the DEA Project 119 Participation Agreement and is thereby subject to restrictions of confidentiality and non-disclosure to third parties.*

DEA Project 119

Report No. 5

Corporate Offices

Knowledge Systems, Inc.
P. O. Box 1279
Stafford, Texas 77497-1279
Phone: 281-879-1400
Fax: 281-879-1499
E-mail: sales@knowsys.com

European Office

Knowledge Systems, Inc.
P.O. Box 274 Paradis
5856 BERGEN
Norway
Phone: +47 55 92 45 62
Fax: +47 55 92 45 62
E-mail: sales @knowsys.com

Please visit the Knowledge Systems' website at <http://www.knowsys.com>

Information in this document is subject to change without notice, and does not represent a commitment on the part of Knowledge Systems. The software described in this document is furnished under a license agreement or non-disclosure agreement. It is against the law to copy the software on any medium except as specifically allowed in the license or non-disclosure agreement.

© Copyright Knowledge Systems, 1989-2000. All rights reserved. *DrillWorks* is a registered trademark of Knowledge Systems, Inc. *PostScript* is a registered trademark of Adobe Systems, Inc. *Windows* is a trademark of Microsoft Corporation

Document Information

Title: Velocity - Effective Stress Relations	
Description: DEA 119, Report No. 5	
Author(s): Steve Hobart	
Reviewer(s):	
Creation Date: 10/5/2000 9:45 AM	Last Date Modified: 10/5/2000 9:45 AM
Approved By:	Approval Date:
Will be sent to:	
Sources Used: (can be other documents used as sources)	
Project Number:	Document Number: 2000-000003

Table of Contents

1	Velocity/Effective Stress Relations	1
2	Direct Relations	2
2.1	Eaton (actually a trend-line method)	2
2.2	Baker-Hughes	2
2.3	Bellotti & Giacca (O&G Journal, 21Aug 1978, pp.47-52)	2
2.4	Bowers ("virgin curve")	2
2.5	Hamouz & Mueller	3
2.6	Hart, Flemings & Deshpande	3
3	Velocity/Porosity – Porosity/Effective Stress Relations	4
3.1	Velocity/Porosity Relations	4
3.1.1	Wyllie et al.	4
3.1.2	Bellotti & Giacca	4
3.1.3	Raymer-Gardner-Hunt (1)	4
3.1.4	Raymer-Gardner-Hunt (2)	4
3.1.5	Raiga-Clemenceau et al	4
3.1.6	Amoco	5
3.1.7	Gardner-Gardner-Gregory + Density Equation	5
3.1.8	Meese's Logarithmic Time-Average Equation	5
3.2	Porosity/Effective Stress Relations	5
3.2.1	Rubey-Hubbert	5
3.2.2	Perloff-Baron (Alixant)	5
3.2.3	$\phi = (R_i - I_c \log_{10}(\sigma)) / (1 + R_i - I_c \log_{10}(\sigma))$ Baldwin-Butler (Holbrook & Bryant)	6
3.2.4	Audet	6
3.2.5	Atkinson-Aplin	6
3.2.6	Terzaghi	6
3.2.7	Palciauskas and Domenico	7
3.2.8	On the Fundamental Equivalence of the Perloff-Baron, Audet and Atkinson Formulas	7
3.3	Porosity/Depth Relations	7
3.3.1	Athy	7
3.3.2	Amoco	7
3.3.3	Revil – Cathles	7
4	More Complete Models	9
4.1	Introduction	9
4.2	Amoco (Traugott)	9
4.3	Gassmann	9
4.4	Eberhart-Phillips et al	9
4.5	Hobart extension of Holbrook	9
5	References	10

1 Velocity/Effective Stress Relations

There are three possible ways to approach effective stress calculation using velocity (or transit time) data: (1) direct methods which directly calculate effective stress from velocity; (2) indirect methods that combine a velocity-porosity relation with a porosity-effective stress relation; and (3) trend-line methods (e.g. Eaton's or the Equivalent Depth methods).

Since the accuracy of a trend-line method relies, in large part, on the placement of the normal compaction trend-line by the user, these methods will not be considered further.

The direct and indirect methods can be re-written to create a "normal compaction trend-line" for velocity or transit time by assuming the effective stress to be "normal", i.e. $\sigma = \sigma_{\text{normal}}$ = normal hydrostatic stress, and then solving for the velocity or transit time. This value could then be used in place of V_{NORM} in the Eaton equation (see section 3.1). This procedure has already been done using the Bowers' velocity-effective stress relation. The irony of employing these methods to create a "normal line" is that, if it is assumed that a relation is sufficiently accurate to generate a normal compaction line, why not consider sufficiently accurate to estimate effective stress and pore pressure? For this reason, the application of these relations to construct a "normal compaction trend" for use with the Eaton or Equivalent Depth method will also not be considered.

2 Direct Relations

2.1 Eaton (actually a trend-line method)

$$\sigma = \sigma_{\text{NORM}} (V / V_{\text{NORM}})^3$$

2.2 Baker-Hughes

$$V_p = 930.4 \sigma_e^{0.374}$$

(Note: This is a simple power law relation between stress and velocity. The units involved are not

yet known.)

Solving for σ

$$\sigma_e = V_p^{2.2638} / 86622200$$

2.3 Bellotti & Giacca (O&G Journal, 21Aug 1978, pp.47-52)

$$V_{\text{sh}} = V_{\text{ma}} \sigma / (A\sigma + B) + V_{\text{min}}$$

V_{sh} velocity in shale

V_{ma} matrix velocity, published as 7000 m/s

V_{min} minimum soil velocity, published as 1500 m/s

effective stress, $\sigma_{\text{overburden}} - \sigma_{\text{pore pressure}}$

A constant

B constant

Solving for σ

$$\sigma = B (V_{\text{sh}} - V_{\text{min}}) / [V_{\text{ma}} - A (V_{\text{sh}} - V_{\text{min}})]$$

2.4 Bowers ("virgin curve")

$$V = V_f + A \sigma^B$$

V_f fluid velocity, e.g. 5000 ft/sec

Gulf Coast values for constants: A = 4.4567 B = 0.8168

Deepwater values for constants: A = 28.3711 B = 0.6207

Central North Sea (Tertiary shales): A = 2.8746 B = 0.9037

Solving for σ (psi)

$$\sigma = [(V - V_f) / A]^{1/B}$$

2.5 Hamouz & Mueller

$$\text{Log}(\Delta t - \Delta t_{mx}) = A - B\sigma$$

$$(\Delta t - \Delta t_{mx}) = A 10^{-B\sigma}$$

$$\sigma = (A - \log_{10}(\Delta t - \Delta t_{mx})) / B$$

Δt_{mx} 65 microseconds per foot

A 2.2120

B 1.50×10^{-4}

In terms of velocity:

$$\sigma = (A - 6 \log_{10}((1 / V) - (1 / V_{mx}))) / B$$

Where: V velocity in feet per second

2.6 Hart, Flemings & Deshpande

This method is a combination of the Raiga-Clemenceau porosity equation with the Rubey-Hubbert equation.

$$V = V_m (1 - \phi_0 e^{-\eta\sigma})^x$$

V_m 14925

ϕ_0 0.409

2.36×10^{-4}

x 2.19

$$\sigma = (1 / \eta) \ln (\phi_0 / (1 - (V / V_m)^{1/x}))$$

Where: η Athy compaction constant

ϕ_0 mudline porosity

V velocity

V_m matrix velocity

x Issler exponent for shale in Raiga-Clemenceau et al porosity equation

3 Velocity/Porosity – Porosity/Effective Stress Relations

3.1 Velocity/Porosity Relations

3.1.1 Wyllie et al

Time-average equation

$$\Delta t = \phi \Delta t_f + (1 - \phi) \Delta t_m$$

$$\phi = (\Delta t_m - \Delta t) / (\Delta t_m - \Delta t_f) \text{ or } (\Delta t - \Delta t_m) / (\Delta t_f - \Delta t_m)$$

In terms of velocities:

$$\phi = ((1 / V_m) - (1 / V)) / ((1 / V_m) - (1 / V_f))$$

3.1.2 Bellotti & Giacca

$$\phi = 1.228 (\Delta t - \Delta t_m) / (\Delta t + \Delta t_f)$$

In terms of velocities:

$$\phi = 1.228 ((1 / V) - (1 / V_m)) / ((1 / V) + (1 / V_f))$$

or

$$\phi = 1.228 (V_f (V_m - V)) / (V_m (V + V_f))$$

3.1.3 Raymer-Gardner-Hunt (1)

$$\phi = -\alpha - (\alpha^2 + (\Delta t_m / \Delta t) - 1)^{1/2}$$

$$\text{Where: } \alpha = (\Delta t_m / (2 \Delta t_f)) - 1$$

In terms of velocities:

$$\phi = -\alpha - (\alpha^2 + (V / V_m) - 1)^{1/2}$$

$$\text{Where: } \alpha = (V_f / (2 V_m)) - 1$$

3.1.4 Raymer-Gardner-Hunt (2)

3.1.5 Raiga-Clemenceau et al

Acoustic Formation Factor

$$\phi = 1 - (\Delta t_m / \Delta t)^{1/x}$$

In terms of velocity:

$$\phi = 1 - (V / V_m)^{1/x}$$

3.1.6 Amoco

$$\phi = (43 / \Delta t_m) (1 - \Delta t / \Delta t_m)$$

In terms of velocity (feet per second):

$$\phi = 0.000043 V_m (1 - V_m / V)$$

3.1.7 Gardner-Gardner-Gregory + Density Equation

$$\rho = 0.23 V^{0.25}$$

$$\rho = \phi \rho_f + (1 - \phi) \rho_m$$

$$\phi = (\rho_m - 0.23 V^{0.25}) / (\rho_m - \rho_f)$$

3.1.8 Meese's Logarithmic Time-Average Equation

$$\ln(\Delta t) = \ln(\Delta t_m) (1 - \phi) + \ln(\Delta t_f) \phi$$

Solving for ϕ :

$$\phi = [(\ln(\Delta t) - \ln(\Delta t_m)) / [\ln(\Delta t_f) - \ln(\Delta t_m)]] \quad \text{or}$$

$$\phi = \ln(\Delta t / \Delta t_m) / \ln(\Delta t_f / \Delta t_m)$$

In terms of velocity:

$$\phi = \ln(V_m / V) / \ln(V_m / V_f)$$

3.2 Porosity/Effective Stress Relations

3.2.1 Rubey-Hubbart

$$\phi = \phi_o e^{-c\sigma}$$

$$\sigma = \ln(\phi_o / \phi) / c$$

3.2.2 Perloff-Baron (Alixant)

$$\sigma = 10^{((R - R_i) / (-I_c))}$$

R = void ratio, i.e. $[\phi / (1 - \phi)]$

R_i: void ratio reference state (3.84)

I_c: stress state dependent compaction constant (1.1)

3.2.3 $\phi = (R_i - I_c \log_{10}(\sigma)) / (1 + R_i - I_c \log_{10}(\sigma))$ Baldwin-Butler (Holbrook & Bryant)

$$\sigma = \sigma_{\max} (1 - \phi)^\alpha$$

$$\phi = 1 - (\sigma / \sigma_{\max})^{1/\alpha}$$

3.2.4 Audet

$$\text{Log}_{10}(\sigma / \sigma_{100}) = (r_{100} - r) / C$$

$$\sigma = \sigma_{100} 10^{(r_{100} - r)/C}$$

effective stress

σ_{100} a reference value of effective stress, in this case 100 kPa

r void ratio = $\phi / (1 - \phi)$

r_{100} void ratio at 100 kPa effective stress

C compaction coefficient

$$\phi = (C \log_{10}(\sigma / \sigma_{100}) - r_{100}) / (1 + C \log_{10}(\sigma / \sigma_{100}) - r_{100})$$

3.2.5 Atkinson-Aplin

Atkinson

$$\text{Ln}(\sigma / \sigma_{100}) = (r_{100} - r) / \beta$$

σ_{100} effective stress at 100 kPa

r void ratio

r_{100} voidratio at 100 kPa

β compression coefficient

Aplin (using Burland's data)

$$r_{100} = 0.3417 + 3.745 \beta + 3.224 \beta^2$$

β is reasonably modeled as a linear relationship with clay particle content (Aplin et al)

$$\sigma = \sigma_{100} e^{(r_{100} - r)/\beta}$$

3.2.6 Terzaghi

Attributed to Terzaghi in GRI-97/0266: Topical Report Number 2 (April 1, 1996 – March 1, 1998): “Sediment Loading and Resulting Pressure Differences Between Overpressured Sands and Bounding Shales of the Eugene Island 330 Field (Offshore Louisiana)” by Beth B. Stump and Peter B. Flemings, Pennsylvania State University, for the Gas Research Institute, contract number 5095-260-3558.

Equation (5) of the report:

$$\phi = 1 - (\phi_0 \sigma_v^{c/2 (2.2303)})$$

$$\sigma_v = e^{(4.606/c) \ln((1 - \phi) / \phi_0)}$$

3.2.7 Palciauskas and Domenico

$$\phi = 1 - \phi_0 e^{\beta \sigma}$$

$$\sigma = (-1 / \beta) \ln((1 - \phi) / \phi_0)$$

3.2.8 On the Fundamental Equivalence of the Perloff-Baron, Audet and Atkinson Formulas

All three formulas reduce to the same fundamental form:

$$R = A \ln(\sigma) + B \text{ or } \sigma = e^{(R - B)/A}$$

Where: R = void ratio = $\phi / (1 - \phi)$
 effective stress

Perloff-Baron

$$A = -I_c / \ln(10)$$

$$B = R_i$$

Audet

$$A = -C / \ln(10)$$

$$B = C \log_{10}(\sigma_{100}) + r_{100}$$

Atkinson

$$A = -\beta$$

$$B = \beta \ln(\sigma_{100}) + r_{100}$$

3.3 Porosity/Depth Relations

3.3.1 Athy

$$\phi = \phi_i e^{-kz}$$

3.3.2 Amoco

$$\phi = 0.41 - (D - W - A) / 45,455$$

3.3.3 Revil – Cathles

Solidity model

$$\phi = 1 - (1 - \phi_0) \exp(z / z_c)$$

porosity at depth z, hydrostatic pressure (normal compaction)

ϕ_0 “non-compactional” porosity (i.e. at mud-line)

z vertical depth of burial

z_0 characteristic depth defined by

$$1 / z_0 = \phi_0 (\rho_g - \rho_f) g \beta$$

where: ρ_g grain density

ρ_f density of pore fluid

g gravitational acceleration constant

“long-term compressibility”

$$\beta = -(1 / \phi_0)(d\phi / d\sigma_{\text{eff}})$$

$$\sigma_{\text{eff}} = \sigma - p$$

total confining stress

p pore pressure

OR

$$\sigma_{\text{eff}} = P - p$$

P lithostatic (overburden) stress

4 More Complete Models

4.1 Introduction

These models require more information than the above methods. Generally, they extend the relation between velocity and effective stress to include varying lithological composition. As such they are not appropriate for pre-drill seismic pore pressure estimation because these lithological factors cannot be known in advance.

4.2 Amoco (Traugott)

$$\Delta t_m = 95[(O - P)(D - W - A)]^{-0.05} + 15 V_{sh}$$

4.3 Gassmann

4.4 Eberhart-Phillips et al

$$V_p = 5.77 - 6.94 \phi - 1.73 C^{0.5} + 0.446 (P_e - e^{-16.7 P_e})$$

V_p compressional velocity, km/s

ϕ porosity, fraction

C clay content, fraction

P_e effective pressure, kbar

4.5 Hobart extension of Holbrook

A derivation of a bi-mineral model. The basic Holbrook model is identical to the Baldwin-Butler formula.

5 References

- Aplin, A.C., Yang, Y., Hansen, S., 1995, Assessment of β , the compression coefficient of mudstones and its relationship with detailed lithology. *Marine and Petroleum Geology*, v.12, p.955-963.
- Atkinson, J., 1993, *An introduction to the mechanics of soils and foundations*. McGraw-Hill, London.
- Audet, D.M., 1996, Compaction and overpressuring in Pleistocene sediments on the Louisiana Shelf, Gulf of Mexico: *Marine and Petroleum Geology*, v.13, p.467-474.
- Bowers, G.L., 1994, Pore pressure estimation from velocity data: accounting for overpressure mechanisms besides undercompaction: *Proceedings of the 1994 IADC/SPE Drilling Conference*, Dallas, Texas, p.515-530.
- Bowers, G.L., 1999, *State of the Art in Pore Pressure Estimation*, DEA-119 Report No.1
- Burland, J.B., 1990, On the compressibility and shear strength of natural clays. *Geotechnique*, v.40, p.329-378.
- Issler, D.R., 1992, A new approach to shale compaction and stratigraphic restoration, Beaufort-Mackenzie basin and Mackenzie Corridor, northern Canada: *American Association of Petroleum Geologists Bulletin*, v.76, no.8, p.1170-1189.
- Stump, B.B., Flemings, P.B., Finkbeiner, T., Zoback, M.D., 1998, Pressure Differences Between Overpressured Sands and Bounding Shales of the Eugene Island 330 field (Offshore Louisiana, U.S.A.) with Implications for Fluid Flow Induced by Sediment Loading, *Proceedings of the 1998 Overpressures in Petroleum Exploration Workshop*, Pau, France.